MORPHOSTRUCTURAL AND PALEO-SEISMIC ANALYSIS OF FAULT INTERACTIONS IN THE OXFORD–CUST–ASHLEY FAULT SYSTEM, CANTERBURY

A thesis submitted in partial fulfilment of the requirements

for the Degree of Master of Science in Geology

in the University of Canterbury

by Luke E. Mahon

University of Canterbury

July, 2015

Frontispiece

View southwest from the highpoint of the western arm of the Cust Anticline showing the subtle geomorphic feature (arrow) that is documented as an active fault in this study.

Abstract

This study investigates evidence for linkages and fault interactions centred on the Cust Anticline in Northwest Canterbury between Starvation Hill to the southwest and the Ashley and Loburn faults to the northeast. An integrated programme of geologic, geomorphic, paleo-seismic and geophysical analyses was undertaken owing to a lack of surface exposures and difficulty in distinguishing active tectonic features from fluvial and/or aeolian features across the low-relief Canterbury Plains.

LiDAR analysis identified surface expression of several previously unrecognised active fault traces across the low-relief aggradation surfaces of the Canterbury Plains. Their presence is consistent with predictions of a fault relay exploiting the structural mesh across the region. This is characterised by interactions of northeast-striking contractional faults and a series of re-activating inherited Late Cretaceous normal faults, the latter now functioning as E–W-striking dextral transpressive faults. LiDAR also allowed for detailed analysis of the surface expression of individual faults and folds across the Cust Anticline contractional restraining bend, which is evolving as a pop-up structure within the newly established dextral shear system that is exploiting the inherited, now re-activated, basement fault zone. Paleo-seismic trenches were located on the crest of the western arm of the Cust Anticline and across a previously unrecognised E–W-striking fault trace, immediately southwest of the steeply plunging Cust Anticline termination. These studies confirmed the location and structural style of north-northeast-striking faults and an E–W-striking fault associated with the development of this structural culmination. A review of available industry seismic reflection lines emphasised the presence of a series of common structural styles having the same underlying structural drivers but with varying degrees of development and expression, both in the seismic profiles and in surface elevations across the study area. Based on LiDAR surface mapping and preliminary re-analysis of industry seismic reflection data, four fault zones are identified across the restraining bend structural culminations, which together form the proposed Oxford–Cust–Ashley Fault System.

The 2010–2012 Canterbury Earthquake Sequence showed many similarities to the structural pattern established across the Oxford–Cust–Ashley Fault System, emphasising the importance of identification and characterization of presently hidden fault sources, and the understanding of fault network linkages, in order to improve constraints on earthquake source potential. Improved understanding of potentially-interactive fault sources in Northwest Canterbury, with the potential for combined initial fault rupture and spatial and temporal rupture propagation across this fault system, can be used in probabilistic seismic hazard analysis for the region, which is essential for the suitability and sustainability of future social and economic development.

Acknowledgements

The following people and organisations provided support for this thesis.

- Funding was made available from the EQC Capability fund (E 5713) at the Department of Geological Sciences, University of Canterbury, as well as the Mason Trust.
- I was supported by a University of Canterbury Masters Scholarship, and a Hastie Research Grant from the Geological Society of New Zealand.
- I acknowledge the Waimakariri District Council and Environment Canterbury (Ecan) for providing the LiDAR to Dr Brendan Duffy.
- My supervisors, Professor Jarg Pettinga, Dr Brendan Duffy, Professor Andy Nicol, provided great guidance and reviews of the research and support when the project took many different directions during the 12 months. Dr Brendan Duffy gave me expert guidance and training in the field.
- I was grateful to be able to have discussions with Mrs Jocelyn Campbell at the Elliotts Road paleo-seismic site, as well as at other times during the year.
- Dr David Nobes provided assistance very early on during the project with the initial GPR setup and training in how to process the data.
- I am extremely grateful to all the landowners for allowing me access to their land for all aspects of the work, in particular to: Togs Ensor, Noel and Audrey Miles, Dallas Grant, Graham and Lorraine Robinson, and Alan Hawker.
- Ross Mitchelmore Contracting and their staff were excellent, and very helpful at the paleo-seismic trench sites.
- I am grateful to Dr Mike Finnemore and staff at Southern Geophysical Ltd during the HRR survey at Chapmans Boundary Road, both for their time and equipment. Also for the use of the GPR unit from Southern Geophysical Ltd.
- The technical staff at the Department of Geological Sciences, University of Canterbury, was great. Matt Cockcroft provided fantastic support during the collection of GPR data and HRR data and for all geophysical requirements. I also would like to thank Cathy Higgins and Sacha Baldwin-Cunningham for logistical support, Dr Kerry Swanson for guidance using the scanning electron microscope, and Dr Anekant Wandres.
- Finally, this whole venture would not have been possible without the support and understanding of my family, and particularly my son, Arthur.

Table of contents

Table of figures

Table of tables

Chapter 1. Introduction

1.1. Introduction

The structural styles of active earth deformation observed across the Northwest Canterbury Plains are characterised by the complex interactions of re-activated inherited E–W-striking faults, now accommodating oblique strike-slip, with newly developed relays of northeast-striking thrust faults and associated thrust propagated anticlines (Campbell et al., 2012). These evolving and interacting structures have been propagating south-eastwards during the Quaternary, progressively widening the active plate boundary zone.

The importance of identification and characterization of presently-hidden fault sources and the understanding of fault network linkages is a critical issue in light of the 2010–2012 Canterbury Earthquake Sequence, in which multiple fault segments ruptured in close succession (e.g. Gledhill et al., 2011; Holden et al., 2011; Beavan et al., 2012; Bradley, 2012; Elliott et al., 2012; Quigley et al., 2012; Duffy et al., 2013; Syracuse et al., 2013). The sequence, which commenced with the Darfield Earthquake (M7.1) on 4 September, 2010, involved up to 6–8 faults and initiated from the previously unknown blind, reverse Charing Cross Fault, passing onto strike-slip and oblique-normal fault segments with the subsequent triggering of another blind, oblique-reverse fault rupture five months later within the sequence (i.e. Christchurch Earthquake of 22 February, 2011). Such combined fault ruptures propagating both spatially and temporally through a fault network, as exemplified by the 2010–2012 Canterbury Earthquake Sequence, highlights how a structural mesh of oblique strike-slip E–W-striking faults and northeast-striking thrust faults operates within the active tectonic setting of the present-day transpressional plate boundary margin. It provided the motivation for this project in a geographically adjacent and equivalent setting, but with better surface expression of structurally-driven activity, where linkages between known faults and presently-hidden fault sources could be directly investigated using surficial geological and geomorphological mapping techniques.

The study area selected for this project is centred on the Cust Anticline, located in the northwest part of the Canterbury Plains, as it represents an emergent and laterally propagating structural high that has developed in response to Late Cenozoic hybrid deformation including both strike-slip re-activation of the inherited E–W-striking normal fault zone of Late Cretaceous–Paleogene age and a more recent relay of thrust faulting (Campbell et al., 2012). The Cust Anticline is positioned to be part of a more elongate network of fault interactions between the established

E–W-striking Ashley and Loburn fault zone to the northeast, and the poorly known E–W-striking fault zone defining the south margin of Starvation Hill near Oxford to the southwest. This provides a more evolved analogue of the recently intensely studied Greendale Fault network involved in the 2010–2012 Canterbury Earthquake Sequence.

Although previous work has been undertaken in the vicinity of the study area used for this project, these earlier studies were focussed on individual faults rather than fault systems (e.g. Sisson et al., 2001; Estrada, 2003). Previous paleo-seismic investigations in North Canterbury have shown interaction and re-activation of inherited E–W-striking faults such as the Boby's Creek Fault (Nicol, 1993), and trenching across the Ashley and Loburn faults has established a paleo-seismic history of multiple ground ruptures within the Late Quaternary (Sisson et al., 2001). However, there is a lack of paleo-seismic data south of the Ashley River where these faults are likely to be linked through a fault relay to the southwest, via the Cust Anticline and Starvation Hill to the Southern Alps foothills rangefront. This fault relay, that has developed surface expression through a series of inferred contractional pop-up structures at restraining step-overs and bends in the dextral shear system along the re-activated inherited basement fault zone, is not clearly documented southwest of the previously defined Ashley Fault Zone. Finally, although industry seismic reflection lines have shown the presence of Late Cretaceous E–W-striking re-activated normal faults with possible linkages to more recently developed thrust faults (Jongens et al., 1999; Ghisetti & Sibson, 2012; Jongens et al., 2012), and E–W-striking faults are inferred from gravity data (Davy et al., 2012), it has so far been difficult to reconcile the seismic reflection data with geomorphic surface expression across this region.

This thesis investigates morphostructural and paleo-seismic evidence for linkages and fault interactions within the area centred on the Cust Anticline structure, between Starvation Hill to the southwest and the Ashley and Loburn faults to the northeast. Extensive LiDAR and industry seismic reflection lines provide significant datasets for this project to investigate the geometry and kinematics of active tectonic structures. Combined, these datasets were complementary across the field area where there were both areas of obvious topographic expression of northeast-striking faults and fold structures (i.e. western arm of the Cust Anticline) and very subtle topographic expression of active tectonic features in close proximity to, and across the flat aggradation surfaces between, these structural culminations (i.e. Cust River aggradation surface southwest of the Cust Anticline). An integrated programme of geologic, geomorphic, paleo-seismic and geophysical analyses were carried out for this study owing to the lack of surface

exposures across the Cust Anticline and the difficulty in distinguishing active tectonic features from fluvial and/or aeolian features across the low-relief topography of the Canterbury Plains.

East–west-striking fault segments potentially extend over 35–40 km from the rangefront west of Oxford, via Starvation Hill and the Cust Anticline, to the eastern location of the Ashley Fault surface trace. Hence a further, more detailed appraisal of this region, centred on the Cust Anticline, with respect to fault linkages between the Ashley, Loburn, Cust and Starvation Hill faults is appropriate given the recent earthquake activity associated with the nearby Greendale and other faults. Improved understanding of potentially-interactive fault sources and the potential for combined initial fault rupture and spatial and temporal rupture propagation along this fault network, immediately north of the Waimakariri River, in future large earthquake events is important given its proximity to Christchurch and other regional centres such as Rangiora, Kaiapoi and Oxford. The results of this study will improve constraints on earthquake source potential in the Canterbury region with consequent improvements in probabilistic seismic hazard analysis, essential for the suitability and sustainability of future social and economic development.

1.2. Objectives of this thesis

This thesis will focus on understanding the spatial interactions of the Starvation Hill, Cust, Ashley and Loburn faults, with particular emphasis on the Cust Anticline, and includes the following aims:

- To develop a detailed structural geomorphic understanding of the area encompassing the Cust Anticline in order to document and characterize the geomorphic expression of fault-driven structures and establish their interactions. This is based on LiDAR interpretation to semi-quantify deformation and landscape response and geomorphic field mapping to ground-truth the LiDAR.
- To use combined geomorphic and geophysical techniques to establish constraints on location and extent of structures mapped in the LiDAR analysis. This may include the use of ground-penetrating radar (GPR) and high resolution reflection (HRR) seismic surveys of the shallow subsurface.
- To attempt to establish the paleo-seismic history of faults associated with the north-northeast-trending western arm of the Cust Anticline using trenches and radiocarbon and/or optically stimulated luminescence (OSL) dating.

- To establish improved age constraints, based on subsurface OSL dating rather than surface ages, for deformed and undeformed surfaces.
- To re-analyse the relevant industry seismic reflection data for the area in order to correlate the geometry and kinematics of faulting and folding at the surface with the subsurface structural geology of the study area.
- To develop a model for the development of the Cust Anticline structure in relation to the established fault network interactions for the area between the Ashley and Loburn faults to the northeast and the Starvation Hill faults to the southwest.

1.3. Thesis format

Chapter 1 provides an introduction to the objectives of the thesis and a summary of the active tectonic setting across the region.

Chapter 2 outlines the study area for this project and the geomorphic and active tectonic features within this area. It also provides background information on the study methods used and the reasons these were adopted.

Chapter 3 details the extensive qualitative and quantitative LiDAR analysis across the study area within six selected areas between Starvation Hill and the Ashley and Loburn faults, with particular emphasis on the western arm of the Cust Anticline.

Chapter 4 presents the stratigraphic and tectonic interpretations of the paleo-seismic studies at the Elliotts Road and Glews Road sites, as well as related analysis and dating results.

Chapter 5 provides an interpretation of the relevant North Canterbury industry seismic reflection lines and relates the structures displacing the top of Oligocene marker horizon with surface structures identified and quantified across the study area by the use of LiDAR. (Further information is given in Appendix 1.)

Chapter 6 presents an overall interpretation and a model of the potential interactions and linkages between the Ashley and Loburn faults to the northeast, through the Cust Anticline to Starvation Hill to the southwest, with respect to the kinematics and geometry of active tectonic faulting and folding across this region of the Northwest Canterbury Plains.

Appendix 2 details the results of a high resolution reflection seismic line undertaken in the very initial stages of this thesis across a potential E–W-striking fault trace at the southern temination of the Springbank Fault. Although this survey does not directly relate to the final conclusions of the thesis, the results are archived for future reference.

1.4. The South Island tectonic setting

The emergent landmass of the South Island forms part of the proposed continent of Zealandia which, although mostly submerged, represents the 7th largest continental lithospheric block on Earth (Mortimer & Campbell, 2014). The South Island straddles the Australian–Pacific plate boundary zone, with opposite dipping offshore subduction zones to the northeast and southwest linked by the Marlborough Fault Zone and the Alpine Fault (e.g. Litchfield et al., 2014). To the northeast of the South Island (Figure 1.1) the oceanic Pacific plate obliquely subducts under the continental Australian plate at the westward dipping Hikurangi subduction zone (initiated ≈25 Ma during Oligocene–Miocene) that extends southward from the Kermadec Arc along the offshore eastern North Island to the Hikurangi Plateau/Chatham Rise margin east of the South Island near Kaikoura (e.g. Pettinga et al., 2001; Reyners & Robertson, 2004; Nicol et al., 2007; Litchfield et al., 2014). To the southwest of the South Island the Puysegur subduction zone (initiated ≈5 Ma during the Pliocene) is facing to the east. Here the oceanic Australian plate is subducting obliquely north-eastward under the continental Pacific plate (e.g. Smith & Davey, 1984; LeBrun et al., 2000; Reyners & Webb, 2002; Barnes et al., 2005). These two oppositely facing subduction zones are linked by what is often described as a trench–trench transform fault system including the Marlborough Fault Zone and linking into the Alpine Fault (e.g. Reyners & Cowan, 1993; Wallace et al., 2007; Litchfield et al., 2014).

The Alpine Fault, initiated in the mid-Cenozoic, now extends for about 450 km along the western Southern Alps rangefront and accommodates oblique continental–continental crustal convergence (e.g. Stirling et al., 2001; Sutherland et al., 2006). The slip on the Alpine Fault is indicated to be around 27 +/- 5 mm/yr strike-slip and around 5–10 mm/yr reverse dip-slip (Berryman et al., 1992; Norris & Cooper, 2001; Sutherland et al., 2006). The slip along the Alpine Fault is therefore transpressive dextral strike-slip although it is complexly segmented into oblique thrust regions and sub-vertical dextral tear-faults of parallel strike to the modern plate convergence vector in the near surface (Norris et al., 1990; Berryman et al., 1992).

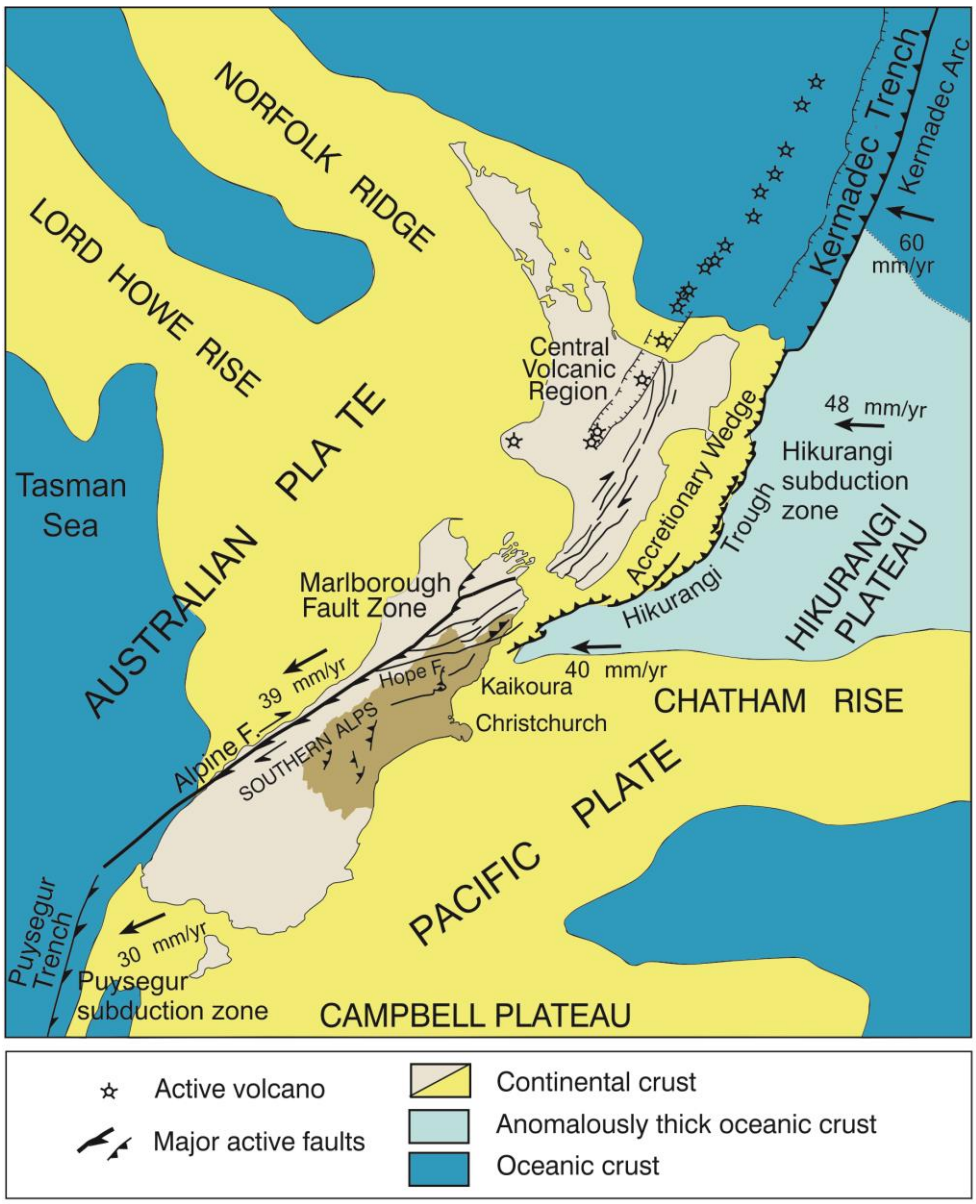

Figure 1.1. The main features of the obliquely convergent Australian–Pacific plate boundary zone across the continent of Zealandia (modified from Pettinga et al., 2001). The relative plate vector rates of convergence are indicated in mm/yr (Wallace et al., 2007). The Canterbury region is indicated by dark brown shading.

1.5. Relative plate motion slip-rates

Relative convergence rates (Figure 1.1) decrease north to south along the plate boundary margin decreasing from >60 mm/yr within the northern Kermadecs to between 48–39 mm/yr through New Zealand (e.g. Beaven et al., 2002; Wallace et al., 2007; DeMets et al., 2010; Litchfield et al., 2014). The relative plate motion is around 40 mm/yr around the Chatham Rise and Hikurangi Plateau margin offshore of Canterbury (e.g. Pettinga et al, 2001; Stirling et al., 2008; Wallace et al., 2012; Litchfield et al., 2014).

Around 75% of motion along the South Island onshore plate boundary is accommodated by the Alpine Fault (e.g. Norris & Cooper, 2001; Sutherland et al., 2006; Wallace et al., 2007). Oblique plate motion is also accommodated across the Southern Alps and through the Marlborough Fault Zone where a significant amount of the motion is accommodated by the main strike-slip Marlborough faults (i.e. Wairau, Awatere, Clarence and Hope faults) at dextral slip-rates ranging from 5–27 mm/yr (Langridge et al., 2003). The remaining component of oblique plate motion is distributed across the Canterbury region mainly by reverse and strike-slip faults with much lower slip-rates (Pettinga et al., 2001; Wallace et al., 2007; Reyners et al., 2013). Many individual regional faults have slip-rates of the order of 0.1 mm/yr but can range up to about 3.5 mm/yr (i.e. Porters Pass Fault; Howard et al., 2005). However, slip-rates on many structures are poorly constrained due to the limited number of absolute ages available from paleo-seismological studies across the region (e.g. Pettinga et al., 2001; Litchfield et al., 2014). Interpretation of GPS surface velocities indicate that in Canterbury slip-rates two or three times greater than those estimated from geological studies may be present east of the Alpine Fault with perhaps 6–8 mm/yr slip on the Porters Pass–Amberley Fault Zone (Wallace et al., 2007). Cumulative net slip-rates generally decrease in the Canterbury region from northwest to southeast away from the rangefront foothills with lowest rates recorded on the submarine faults offshore (e.g. Barnes et al., 1998; Litchfield et al., 2014).

Using interpreted GPS, geological and seismological data, models to describe active faulting within defined regions across New Zealand have been developed (Wallace et al., 2007; Litchfield et al., 2014) and are useful to refine probabilistic seismic hazard models (e.g. Stirling et al., 2002; Stirling et al., 2012).

1.6. Canterbury regional tectonics

Within this plate tectonic framework the South Island continental transpression zone is responsible for the active tectonic styles of deformation and kinematics observed in the Canterbury region.

1.6.1. Thrust wedge model

The Alpine Fault dips eastward (Figure 1.2A) and projects at depth (probably becoming more listric) beneath the Southern Alps, linking to an inferred low to mid-crustal detachment (Norris et al., 1990; Reyners & Cowan, 1993; Pettinga et al., 2001; Stein et al., 2007; Norris & Toy, 2014).

Furthermore, the location of the south and west margins of the Hikurangi Plateau with respect to the Chatham Rise also influences the present-day subduction of the E–W-converging Pacific and Australian plates (Reyners et al., 2011). The crustal delamination within the oblique continental transpression zone of the South Island has been studied using 3D seismic velocity models (e.g. Eberhart-Phillips et al., 2010; Eberhart-Phillips & Reyners, 2012). Subduction of the Hikurangi Plateau below the central South Island, where there is no leading edge oceanic crust, is therefore achieved by delamination whereby there is subduction of the lower crust of the Hikurangi Plateau and exhumation of the upper crust of the Hikurangi Plateau along the Alpine Fault (Reyners et al., 2011). This crustal delamination associated with the projected Alpine Fault and the southwestern subducting margins of the Hikurangi Plateau clearly influences the active tectonics and deformation styles in the Canterbury eastern foothills of the Southern Alps (Figure 1.2B; Reyners et al., 2013).

North of the Rakaia River this ductile, mid-crustal seismic detachment zone, which separates the lower crust from the upper brittle crust at about 12 km depth beneath the Canterbury Plains, has been inferred from earthquake focal mechanisms (Cowan, 1992; Reyners & Cowan, 1993; Pettinga et al., 1998; Reyners et al., 2013). Within the upper crustal zone many faults are inherited and are complexly segmented. They are sub-optimal in terms of their orientation with respect to the present-day plate boundary motion and regional stress field. These inherited structures are characterised by more variable slip which does not reflect translation parallel to the underlying plate motion (Pettinga & Wise, 1994; Pettinga et al., 2001).

Southeast-facing thrust faults are propagating from the basal décollement and accommodating contraction (e.g. Bannister et al., 2006; Campbell et al., 2012). The thrust fault blocks are further shortened by synthetic and antithetic back-thrusts forming a series of fault-bounded topographic ridges and ranges (e.g. Cox & Sutherland, 2007; Campbell et al., 2012). Therefore, faulting within this upper crustal zone reflects regional spatial and volume constraints of adjacent blocks driving the overall tectonic architecture of the eastern foothills of the Southern Alps and the Canterbury Plains (e.g. Pettinga et al., 2001; Litchfield et al., 2014).

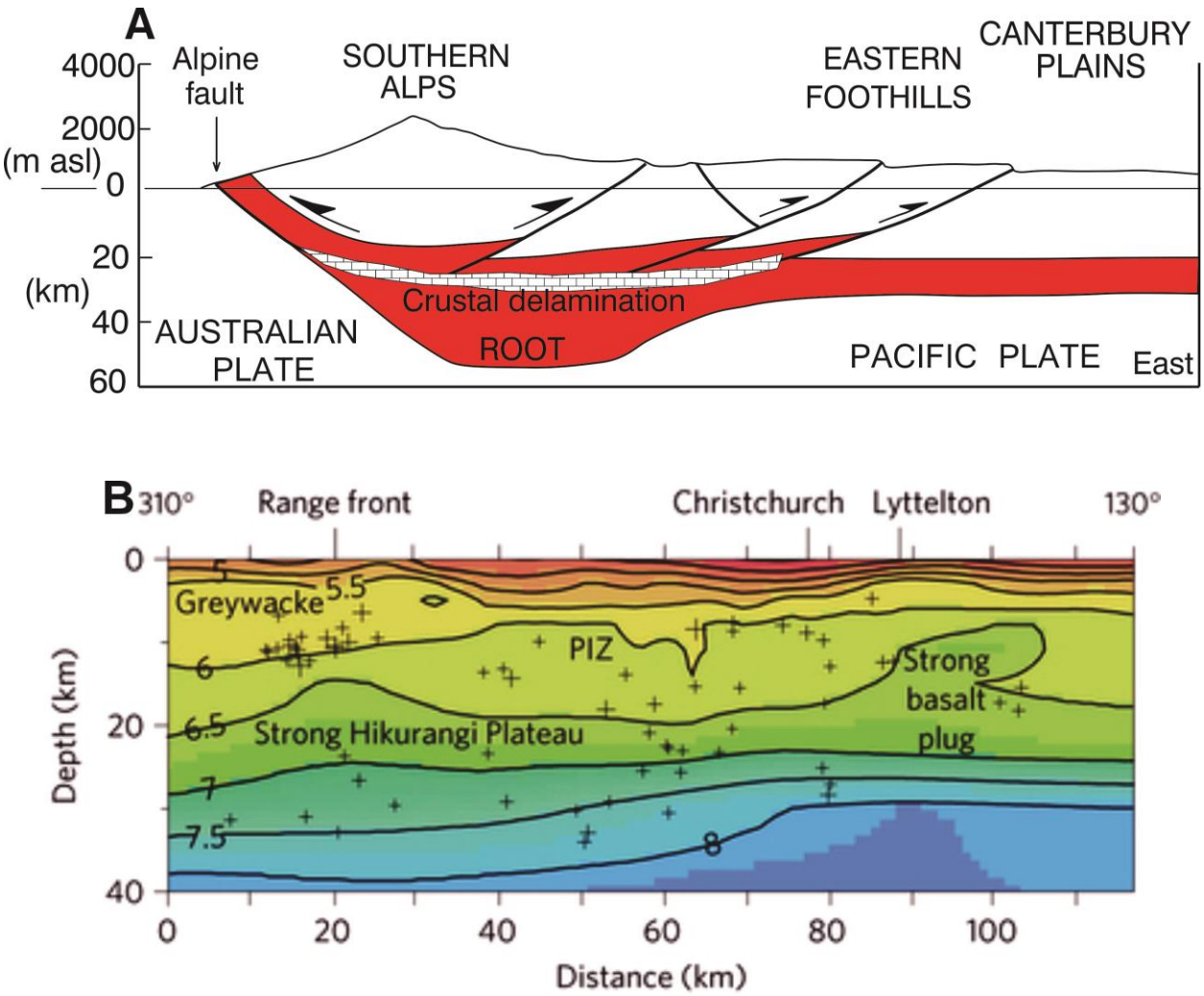

Figure 1.2. A: Schematic diagram of the two-sided wedge model representing the oblique continent–continent collision zone of the Australia–Pacific plate boundary across the central South Island (modified from Pettinga et al., 2001). Crustal delamination is indicated at mid to lower crustal levels and the red shading represents lower crustal rocks. The scale changes from above to below sea-level. B: A depth section of the P-wave velocity model normal to the plate boundary and through Lyttelton volcano. Velocity contours are in kilometres per second and interpreted geological units are shown, with PIZ denoting the approximately 100-Myr-old plate interface zone. Plus symbols are small earthquakes within 30 km of the section from 2001 until just before the 3 September 2010 Darfield earthquake. These illustrate that brittle deformation occurs throughout the Hikurangi Plateau the edge of which forms the Alpine Fault at depth. An active décollement is present at about 11 km depth where the plateau subducts beneath the range front. (Source: Reyners et al., 2013)

1.6.2. Structural style of faulting and folding in Canterbury

The inherited E–W-striking fault fabric of Late Cretaceous and Lower Tertiary normal faults is progressively being re-activated and overprinted by active earth deformation in the eastern foothills and beneath the northwest sector of the Canterbury Plains, and is linked in turn beneath the plains into the offshore faults documented in Pegasus Bay (Barnes et al., 2011; Ghisetti & Sibson, 2012; Ristau et al., 2013).

Active tectonics of the Canterbury region reflects a transition from newly developed fault-zones accommodating upper crustal deformation of the eastern foothill ranges of the Southern Alps to early stage re-activation of the inherited normal fault fabric beneath the Canterbury Plains linked by thrust faults relaying deformation between E–W-trending fault segments via a series of topographic steps. Overall, deformation reflects complex strain partitioning in the upper crust (e.g. Jongens et al., 1999; Campbell et al., 2012; Pettinga et al., 2014). The ongoing active tectonics of the northern and central Canterbury Plains is thus characterised by the complex interactions of re-activated inherited E–W-striking faults now accommodating oblique strike-slip with northeast-striking thrust faults and associated thrust propagated anticlines accommodating regional shortening perpendicular to the maximum regional shortening direction (Sibson et al., 2011; Campbell et al., 2012). This mesh of active tectonic structures, extending eastwards from the Southern Alps and eastern foothills, accommodates the relative plate motion transfer between the Hikurangi trench and the continent–continent collision along the Alpine Fault, through active earth deformation within the Late Cenozoic gravels and subsequently deposited Quaternary sediments.

The thrust fault blocks become less evolved southeastwards from the rangefront through a series of less emergent but tectonically similar structures. A similar but largely concealed structure was revealed for the complex fault interactions associated with the co-seismic daylighting of the Greendale Fault observed in 2010 (e.g. Beaven et al., 2012; Quigley et al., 2012). Less evolved, early stage fault propagation folds are more dominant in accommodating the early phases of shortening compared to emergent faults. Therefore, folding becomes more important geomorphologically in identifying these structures. The two-sided deforming wedge model based on delamination at lower to mid-crustal levels (Reyners & Cowan, 1993) has been invoked to provide a better fundamental understanding of the prolonged seismic activity associated with the Canterbury Earthquake Sequence of 2010–12 (Reyners et al., 2013).

1.6.3. Canterbury regional stress regime

The wide zone of active earth deformation present within the Canterbury region due to the southward transition from subduction to continent–continent oblique collision of the tectonic plates is reflected in the overall regional stress regime (Pettinga et al., 2001; Stirling et al., 2008; Ghisetti & Sibson, 2012). The Canterbury region inferred horizontal maximum compressive stress orientation is σ_1 = 115 +/- 5° (Sibson et al., 2011; Ghisetti & Sibson, 2012). Spatially,

levels of tectonic activity vary throughout Canterbury reflecting the relative effects and proximity of the Alpine Fault deformation zone, the Marlborough Fault transfer zone and the presence of offshore–onshore fault projections. The present regional stress regime influences both the re-activated older Cretaceous–Paleogene normal structures and the younger Paleogene and Quaternary layers beneath the Canterbury Plains (e.g. Campbell et al., 2012; Ghisetti & Sibson, 2012; Litchfield et al., 2014).

1.6.4. Regional fault kinematics and geometry

The northeast-striking thrust faults and associated fault propagation folds are Late Cenozoic structures evolving beneath the North Canterbury Plains, and are documented in seismic reflection data of upper Cretaceous–Tertiary 'cover' sequence sedimentary strata (Jongens et al., 2012). The north to northeast trending Late Cenozoic structures are mainly accommodating oblique thrusting associated with the plate convergence, while strike-slip along the inherited E–W-striking structures is facilitating associated slip transfer in response to the regional stress regime (Campbell et al., 2012; Ghisetti & Sibson, 2012).

The contractional North Canterbury fault zones (Litchfield et al., 2014) are therefore characterised by a range of fault zone orientations and slip types, although there is a predominance of northeast-striking thrust faults overprinting and linked to E–W-striking re-activated oblique strike-slip faults (Campbell et al., 2012; Ghisetti & Sibson, 2012). Many of these fault zones are likely to be upward projections from the mid-crustal detachment as indicated by microseismicity measurements (Reyners & Cowan, 1993). Fault zones further west within the Canterbury region become more predominantly transpressional with complex interactions and transfers between the northeast-striking fault zones and the reactivated E–W-striking faults due to the present plate boundary tectonic stress regime (Campbell et al., 2012; Ghisetti & Sibson., 2012).

Fault zone lengths range from short (<10 km) to up to 90 km (Porters Pass–Amberley Fault Zone). However, the complexity of the fault network in the Canterbury region means that many segmented faults are highly interactive forming significant fault networks and transfers as was highlighted by the complexity of the ruptures associated with the 2010–2012 Canterbury Earthquake Sequence (e.g. Beavan et al., 2012).

Active fault zones in the eastern parts of the region are relatively youthful, less than 1 Ma (e.g. Pettinga et al., 2001; Litchfield et al., 2014). This indicates that the plate boundary deformation is widening, encroaching into the region and migrating southeast including into the offshore Pegasus Bay region (Barnes et al., 2011), as observed from the progressive re-activation of structures associated with active faulting. Onshore, two-end members of this process are represented by the Cust Anticline, which is a significantly evolved structure in the northwest of the Canterbury Plains, and the recently emergent and previously concealed Greendale Fault network structure southeast of the study area of this project (e.g. Campbell et al., 2012; Quigley et al., 2012; Duffy et al., 2013).

1.7. Offshore versus onshore faulting in Canterbury

Offshore Canterbury, south of the Hikurangi trench, the Pacific plate crust changes from anomalously thickened oceanic crust to thinned continental crust along the E–W strike of the northern margin of the Chatham Rise (Figure 1.1). Late Cretaceous–Eocene rifting and extension has created E–W-striking, south-dipping steep normal faults in the Torlesse basement (Barnes, 1994). The active tectonic deformation of the Hikurangi Plateau margin is progressively overprinting these structures with contractional deformation beneath the continental shelf. Further north the offshore Canterbury faults consist of reverse and thrust zones verging eastward and probably splaying upwards from the Hikurangi subduction zone (Barnes et al., 1998; Barnes et al., 2011; Wallace et al., 2012). However, in Pegasus Bay, seismic reflection data indicates that offshore E–W-striking Late Cretaceous faults have documented projections to the onshore region and form similar southwest–northeast-trending relays (Barnes et al., 2011). It has been shown that many of the projected east-striking onshore faults have deeper Late Cretaceous structural projections (Ghisetti & Sibson, 2012). These Late Cretaceous–Eocene normal faults have a dominant easterly trend and some faults may remain active with normal displacement in the offshore regions along the Chatham Rise northern slope (Barnes et al., 2011).

Although inherited E–W-striking Chatham Rise faults likely extend into the onshore Canterbury Plains area, surface evidence for contractional inversion of structures is rare (Ghisetti & Sibson, 2012). Inversion is indicated by change from normal to reverse faulting, domal uplift, inversion of basement and synrift deposits, asymmetric folding of cover, as well as uplift and erosion of Pliocene–Quaternary gravels. Onshore these faults are regularly spaced E–W-trending, re-activated Late Cretaceous–Lower Tertiary normal faults. They are dextral-transpressive and form

associated tear-faults throughout the region (e.g. Campbell et al., 2012). The transpressive inversion of a regional Cretaceous normal fault was first shown on the Birch Fault (Nicol, 1993) and subsurface E–W-striking faults in the Ashley River region indicate contractional inversion during the Pliocene and Quaternary (Jongens et al., 2012). The recent activity on the Hororata and Greendale faults and associated structures also revealed the significance of co-seismic re-activation of these faults in the Canterbury region (e.g. Campbell et al., 2012; Quigley et al., 2012).

Therefore, the eastward expansion of the Southern Alps plate boundary deformation zone across the North Canterbury Plains is interfering with the propagation of a westward converging belt of structures associated with the onshore propagation of thrust fault deformation of the southern end of the Hikurangi subduction zone (Wallace et al., 2007). The latter becomes less important south of the Ashley River and Waipara Basin (Campbell et al., 2012). At a broad regional level these two opposing onshore and offshore propagating thrust systems are involved in generating rising anticline structures and fault-related topography across the Canterbury Plains (e.g. Campbell et al., 2012). However, the complex nature of faulting beneath the Canterbury Plains may also involve new faults not seen in the basement and left-lateral NW–SE orientated faults may form conjugates with the reactivated E–W-striking right-lateral faults (Ghisetti & Sibson, 2012). New fault splays linking older inherited segments are also likely.

1.8. Gravity anomalies

Gravity and magnetic data across Canterbury reveal distinct lineaments oriented broadly NE–SW and E–W and are probably related to basement structure (Davy et al., 2012). Many of these gravity anomaly lineaments correspond to known fault traces such as the E–W-striking trace of the Ashley Fault and the northeast-striking Springbank Fault. A large positive gravity anomaly occurs at, and southwest of, the location of the Cust Anticline west of the Springbank Fault (Figure 1.3). The offshore faults in Pegasus Bay that strike broadly east to east-northeast (Barnes et al., 2011) are likely to be extensions of the onshore faults and fault zones seen in the gravity and magnetic anomaly measurements north of Christchurch (Davy et al., 2012).

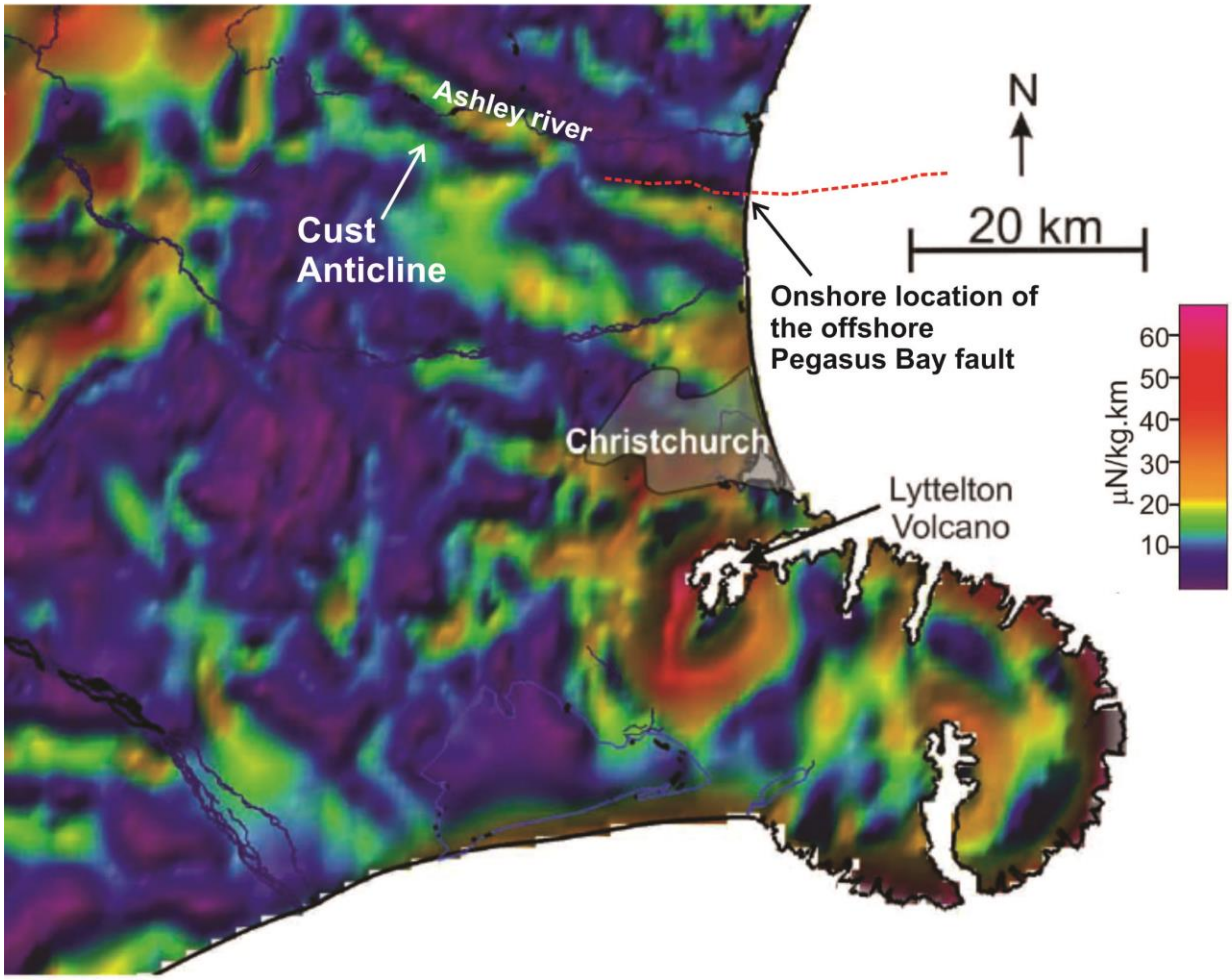

Figure 1.3. Map of Bouguer gravity anomalies (modified from Davy et al., 2012). The location of the Cust Anticline which is in the centre of the study area is indicated and shows the presence of gravity anomaly highs around this area. Also indicated is the onshore projection of the Pegasus Bay Fault (Barnes et al., 2011).

1.9. Summary of North Canterbury active tectonics

Pre-existing faults have a strong influence on the active tectonic geometry and spatial distribution of active earth deformation in present-day New Zealand (e.g. Nicol & Van Dissen, 2002). In North Canterbury northeast-striking structures are accommodating contractional deformation during Miocene to Quaternary times, but there is also a component of transpressive dextral slip on east-striking faults which are exploiting inherited normal faults now being re-activated (Campbell et al., 2012). These inherited Late Cretaceous–Eocene faults represent a deeper structural fabric beneath North Canterbury (Jongens et al., 2012). In North Canterbury, the location of surface traces of E–W-striking faults have been shown to have a close association and interaction with adjacent thrust faults and their associated emerging anticlines (e.g. Nicol & Campbell, 2001; Litchfield et al., 2003; Campbell et al., 2012).

The transpressional E–W-striking faults lead to structural inversion along the pre-existing Late Cretaceous–Eocene normal fault zones, but often only show surface geomorphic expression and Late Quaternary displacements where closely associated with linking faults and folds of the northeast thrust (contractional) system. The E–W-striking re-activated dextral transpressive slip structures do not appear to propagate to the surface independent of the dominant northeast-striking contractional structures. This implies that they truncate the folds and thrust segments and provide links that facilitate displacement transfer in the thrust front and are not simply controlled by the regional stress (Campbell et al., 2012; Ghisetti & Sibson, 2012).

Many remnant visible E–W-striking traces are therefore limited to the projected ends of the northeast-striking folds and thrusts and are often relatively short. They do not always extend far beyond the controlling influence of the associated northeast-striking thrust transfer faults and often have variations along their length in terms of both net displacement and slip orientation (Campbell et al., 2012). The east-striking faults are probably acting co-seismically with the thrust faults and therefore activity on associated strike-slip faults can record and document co-seismic activity on the associated thrust system (Campbell et al., 2012). This was highlighted by the series of interactive fault ruptures associated with the 4 September, 2010, Darfield Earthquake, and the subsequent Canterbury Earthquake Sequence (Sibson et al., 2011; Campbell et al., 2012; Ghisetti & Sibson, 2012; Jongens et al., 2012).

1.10. Active tectonic hazards within the Canterbury region

The Canterbury region has been divided into structural domains (based on the neotectonic style, geometry and deformation rates) with respect to determining earthquake-related hazard (Pettinga et al., 2001; Stirling et al., 2008). The study area for this project is within domain 3, which is broadly part of the Porters Pass–Amberley Fault Zone (PPAFZ) along the Southern Alps foothills and the western rangefront of the Canterbury Plains. Within this zone there is a mesh of east-northeast-trending strike-slip transfer faults and oblique thrusts and reverse faults and folds (Figure 1.4).

However, hazard interpretations are also influenced by active tectonics throughout the entire Canterbury region, especially the surrounding areas such as the North Canterbury fold and thrust belt of domain 4 that extends southwest of Kaikoura through the northeast onshore region of Canterbury and southeast offshore across the continental Canterbury shelf. This zone is defined

by thrust faults and asymmetric folds due to oblique plate convergence and a change to continent–continent collision west of the Chatham Rise. Interestingly, in domain 7 much of the deformation is hidden below the Quaternary gravels of the Canterbury Plains. However, recent events on structures (i.e. Greendale Fault) within the Canterbury Plains zone have emphasised how these daylighting structures are similar to the more evolved structures in the Northwest Canterbury Plains. This is despite this zone being the furthest distance from the Australian and Pacific plate boundary and defined as a region with very low rates of deformation (Figure 1.4).

Within the study area of this project E–W-trending fault segments potentially extend over 35–40 km from the rangefront west of Oxford via Starvation Hill, the Cust Anticline to the location of the Ashley Fault (e.g. Campbell et al., 2012; Barrell & Begg, 2013). Although individual faults have been studied throughout this area (e.g. Sisson et al., 2001; Estrada, 2003) an improved understanding of potentially-interactive fault sources and the potential for combined initial fault rupture and spatial and temporal propagation along fault networks across this region is important given the recent events associated with the Canterbury Earthquake Sequence. This study, centred on the Cust Anticline, is in close proximity to Christchurch as well as other regional centres such as Rangiora, Kaiapoi and Oxford. Therefore, the outcomes of this study will provide improved constraints on seismic source potential in the Canterbury region, with consequent improvements in probabilistic seismic hazard analysis with respect to future seismic events which is essential for the sustainability of future social and economic development.

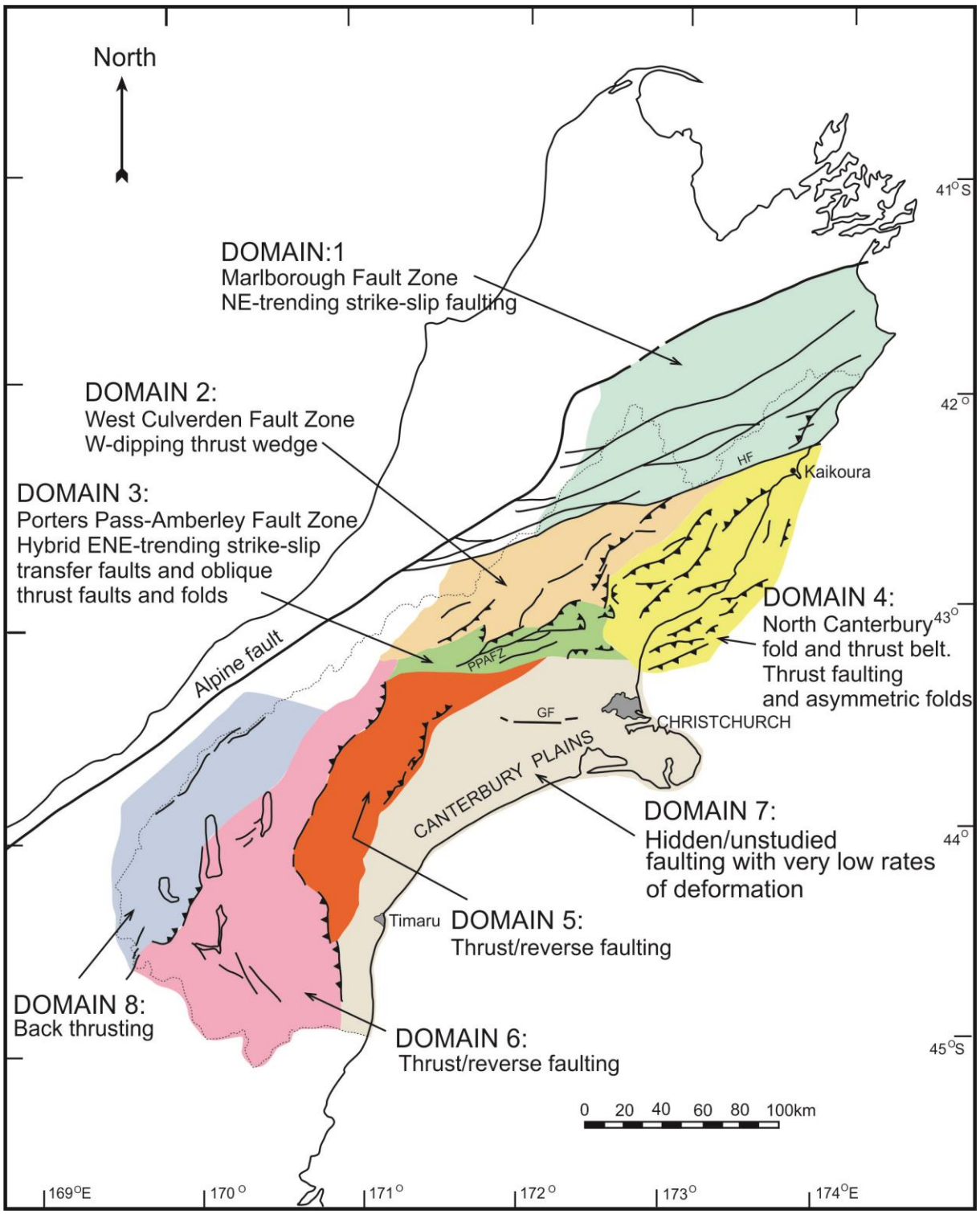

Figure 1.4. Summary map for the structural domains for the Canterbury region (domains 1-8). (modified from Pettinga et al., 2001). The study area for this project is within North Canterbury which is part of domain 3. [PPAFZ = Porters Pass–Amberley Fault Zone; GF = Greendale Fault]

Chapter 2. Study area and methodology

2.1. Study area overview

The study area is centred on the Cust Anticline which is located in North Canterbury between the Cust River to the south and the Ashley River to the north (Figure 2.1). The LiDAR analysis (Chapter 3) although centred on the Cust Anticline also covered other sections of the study area, which extended ~30 km east from Oxford and ~15 km north–south from the Ashley River to the Eyre River. The township of Oxford is situated 14 km to the west of the Cust Anticline and the small village of Cust is 4 km south of the anticline. The study area is ~40 km northwest of Christchurch (Figure 2.1).

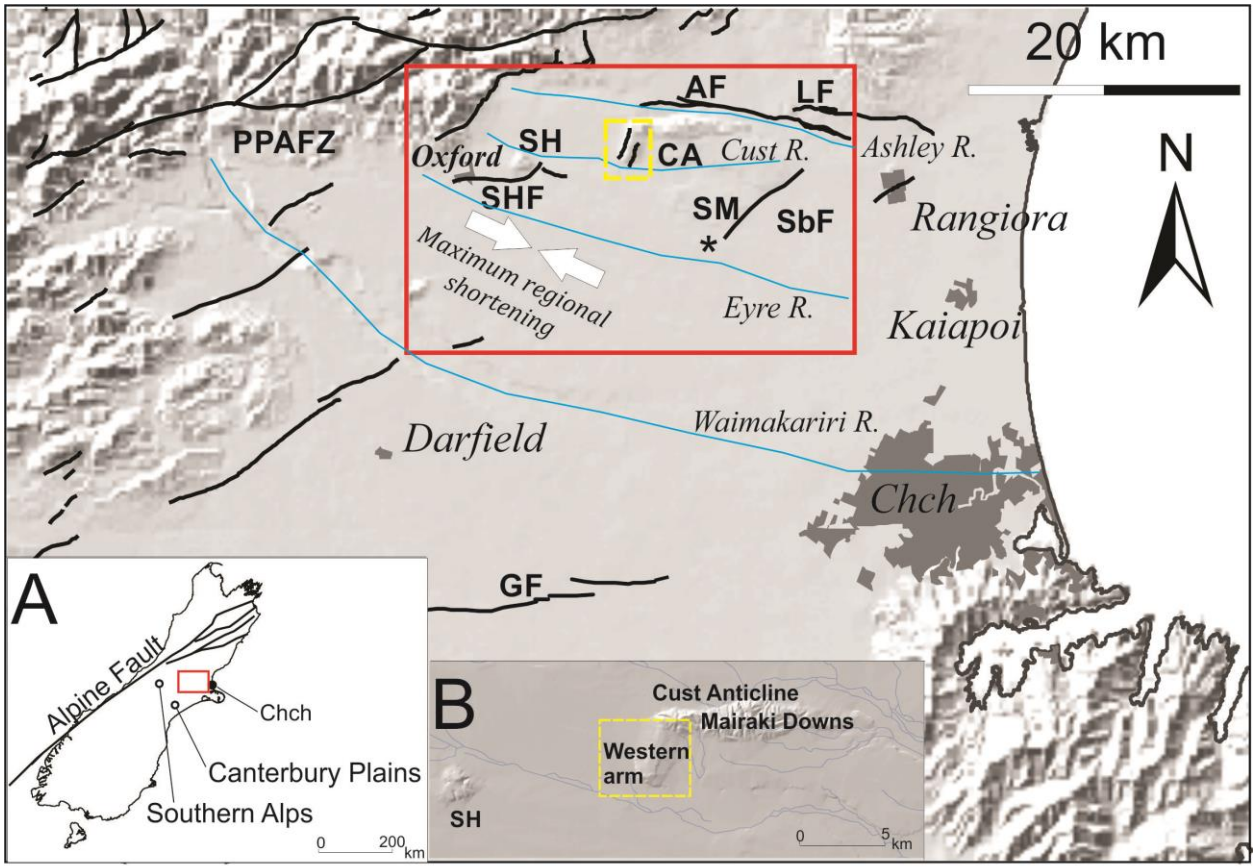

Figure 2.1. Location of field area. The field area is located within the red box and extends about 30 km east of Oxford and north–south between the Ashley and Eyre rivers. The asterisk indicates the approximate location for the high resolution reflection seismic line (Appendix 2). Inset A: Regional context for the field area with respect to the South Island. Inset B: Hillshade image of the Cust Anticline indicating the L-shape of the anticline due to the E–W-trending and north-northeast-trending sections. The yellow dotted box indicates the location for the paleo-seismic studies and geophysical surveys centred across the north-northeast-trending western arm of the Cust Anticline. [PPAFZ = Porters Pass–Amberley Fault Zone; SHF = Starvation Hill Fault; AF = Ashley Faults; LF = Loburn Fault; SbF = Springbank Fault; GF Greendale Fault; CA = Cust Anticline; SH = Starvation Hill; SM = Springbank Monocline/Cust Downlands; ChCh = Christchurch]. Known active (i.e. Late Quaternary) faults are based on GNS Science QMAP Geology of the Christchurch Area (Forsyth et al., 2008). Maximum regional shortening direction is from Sibson et al., (2011). Figure modified from Duffy et al., (2013).

Paleo-seismic and geophysical investigations for this project (Chapter 4) were focussed on the western arm of the Cust Anticline and the northern floodplain of the Cust River immediately to the southwest of the Cust Anticline (Figure 2.1B). This was in order to establish links between the north-northeast-striking faults across the western arm of the Cust Anticline and the less well known E–W-striking fault extending from the Cust Anticline to Starvation Hill to the southwest. A series of industry seismic reflection surveys were located across the study area and were also utilised (Chapter 5). During preliminary investigations for this project a high resolution seismic reflection survey line was obtained along Chapmans Boundary Road southeast of the Springbank Monocline ~8 km southeast of the western arm of the Cust Anticline. This was to follow-up on an ambiguous E–W-striking scarp, located on the LiDAR, at the southern termination of the Springbank Fault and to try to conclude some uncertainties for the location of this fault termination from previous work (Estrada, 2003). Although this survey does not directly relate to the Cust Anticline or the final conclusions of this thesis the results are briefly presented and discussed in Appendix 2.

2.2. Rivers in the study area

2.2.1. The Ashley River

The Ashley River, which flows north of the Cust Anticline, is a significant river draining the Canterbury foothills. It initially flows out of the foothills in a southeast direction before flowing eastward around the northern margin of the Cust Anticline. The course of the Ashley River, north of Rangiora, is a consequence of the tectonic growth of the Cust Anticline which diverted the Ashley River flow from its former course to the southeast where the present Cust River flows (Cowan, 1992; Sisson et al., 2001; Estrada, 2003). The Ashley River is now entrenched in its present drainage by the presence of the Cust Anticline and is continuing to erode the anticline's northern margin over time. Erosion of this northern margin could also indicate that the Ashley River is cutting southward due to being trapped in a fault angle depression across this location.

2.2.2. The Cust River

The present-day Cust River is underfit as previously this valley accommodated the flow of the much more substantial Ashley River during and prior to the last glacial maximum about 20,000 years ago (Cowan, 1992). The aggradation surface for the Cust River corresponds to the deposition of the Burnham (27–14 ka) Formation (Wilson, 1989). The Cust River is likely to mark the northernmost extent of the Waimakariri Fan aggradation surface. The Cust River drains

the eastern foothills immediately north of Oxford township and flows in a southeast direction north of Starvation Hill and then around the southern termination of the western arm of the Cust Anticline. It then flows through a constructed drainage south of Rangiora into the Waimakariri River near the township of Kaiapoi. River channel gradients can be useful indicators of surrounding tectonic deformation underlying Quaternary surfaces (Holbrook & Schumm, 1999; Burbank & Anderson, 2001). Morphometric analysis of the Cust River has indicated tectonic perturbation of the Cust River as it flows around the southern termination of the Cust Anticline around the 150 m topographic contour (Estrada, 2003).

2.2.3. The Eyre River

The Eyre River drains from the Canterbury foothills and flows in a southeast direction past the town of Oxford then south of Starvation Hill and across the Canterbury Plains before being diverted into the Waimakariri River near Eyreton. Flow in the Eyre River can often be intermittent in the summer months. Although the Eyre River is further to the south from the southern termination of the Cust Anticline beneath the Cust River a broad zone of deformation below the Quaternary aggradation surfaces of the Eyre River, based on stream gradient morphometric river analysis, was observed within this region of the Canterbury Plains southwest of the Cust Anticline (Estrada, 2003).

2.2.4. The Waimakariri River

The Waimakariri River is a major river draining the Southern Alps and flows in wide braided channels, along the southwest edge of the field area, to the sea at Kaiapoi. Both the Cust and the Eyre rivers, which only drain from the eastern foothills, flow into the larger eastward flowing Waimakariri River before it reaches the coast. Morphometric analysis indicated that the Waimakariri River is also responding to active tectonics (Estrada, 2003).

2.3. Geology within the study area

Most of the study area is of very low-relief and covered by Late Pleistocene and Holocene deposits made up of numerous depositional surfaces related to cycles of fluvial aggradation and degradation, associated with processes related to the Quaternary glaciation cycles (Forsyth et al., 2008). The Canterbury Plains are formed by coalescing alluvial fans consisting of thick sequences of gravel deposited by the major rivers that drain and emerge from the Southern Alps

(i.e. Waimakariri River). Gravel deposition is further enhanced by the larger rivers (i.e. Ashley River) that emerge from the Canterbury foothills (Forsyth et al., 2008; Barrell & Begg, 2013).

The topographic highs within the study area include the Cust Anticline, Mairaki Downs, Starvation Hill and the Springbank Monocline/Cust Downlands (Figure 2.1). The exposed geology at scattered outcrops at these locations within the study area has been reported in other studies (Starvation Hill: May, (2004); Springbank Monocline: Estrada, (2003); Porters Pass Fault Zone: Cowan, (1992); Howard, (2001); Mairaki Downs: Cowan, (1992); Cowan et al., 1996) and has been incorporated into the Christchurch QMAP (Forsyth et al., 2008).

The field locations for the paleo-seismic and geophysical fieldwork of this study had no outcrops of Cenozoic cover or Mesozoic basement rocks however, the geology underlying the Cust Anticline has been documented and logged within the Arcadia-1 well drilled by Indo-Pacific (located at E1547252, N5208457) just north of Summerhill Road (Indo-Pacific Energy, 2000). This information has been used to interpret the numerous Indo-Pacific (IP) seismic reflection survey lines in North Canterbury (Jongens, 1999; Jongens et al., 2012).

The sequence logged in the Arcadia-1 well was an unusually thick (about 1200 m) Late Cretaceous–Paleogene sequence compared to other parts of the Canterbury Plains region (Jongens et al., 2012). The Arcadia-1 well passed through ~40 m of surface gravels followed by ~144 m of Plio–Pleistocene Kowai Formation gravel. A 111-m section of Starvation Hill basalts (Miocene) were encountered above a thin marker section of Oligocene limestone at about 300 m below ground level. A further 800 m of Paleogene sediments were then logged before Paleogene Broken River Formation with Cretaceous basement greywacke was identified at the base of the well which ended at about 1475 m below ground level (Indo-Pacific Energy, 2000). This logged sequence was used to create the cross-section of the western arm of the Cust Anticline produced as part of the Christchurch Area 1:250,000 QMAP (Forsyth et al., 2008).

2.3.1. Geological units

In general the geological units of the Canterbury Plains consist of basement rocks (Permian to Lower Cretaceous), Paleogene–Neogene cover sequences (about 85 Ma to 1 Ma) and unconsolidated Quaternary sediments (1 Ma to present).

2.3.2. Basement rocks (Permian to lower Cretaceous)

The Mesozoic basement rocks of North Canterbury comprise the Torlesse Supergroup (alternating indurated sandstones and argillite known as greywacke) and are made up of the Rakaia and Pahau terranes which are separated by the Esk Head Belt (Bradshaw, 1989; Browne et al., 2012). There are also some volcanic rock units within the upper section of the basement sequence. These are identified, within the Arcadia-1 well log, as the Mt Somers Volcanics which were formed at the initial stages of extension along the previously convergent Gondwana margin (Browne et al., 2012).

2.3.3. Cover sequence (Late Cretaceous to Pliocene)

The basement rocks are overlain by a Paleogene sequence including Oligocene limestone and Miocene sequences. This Paleogene sequence is made up of significant thicknesses of sedimentary strata of both marine and terrestrial origin including coal measures, quartz sands, gravelly conglomerates and limestones. The Plio–Pleistocene Kowai Formation is predominantly comprised of gravels which outcrop extensively in the Mairaki Downs area of the Cust Anticline.

2.3.4. Quaternary deposits

The distribution of Late Quaternary deposits, formed during glacial and interglacial periods over the last 200,000 years, is a result of fluctuating climate cycles during this period as well as uplift and erosion caused by active tectonics across the region (Browne et al., 2012; Barrell 2013; Barrell & Begg, 2013). During this time, transgression and regression of the coastline resulted in interfingering of swamp, beach, estuary and lagoon deposits with the alluvial fan gravels especially eastward towards the coast (Brown & Wilson, 1988; Forsyth et al., 2008).

During glacial periods the rivers carry larger volumes of eroded sediments from the Southern Alps which they deposit as outwash deposits forming aggradational surfaces (Wilson, 1989; Forsyth et al., 2008). Conversely during interglacial periods the rivers cut down into these earlier aggradation deposits in response to reduced bedload detritus. Subsequent fluvial aggradation and degradation cycles create successive deposits and associated fluvial surfaces which make up the Late Quaternary surficial units. Quaternary river bed and river terrace landforms so formed during the glacial/interglacial cycles may be affected by subsequent tectonic activity resulting in progressively evolving tectonic geomorphic landforms. These relatively young geomorphic

surfaces may be overlain or onlapped by subsequent Late Quaternary deposits, potentially providing age constraint for activity on Late Pleistocene and Holocene active faults and folds.

Loess deposits, accumulated in the Late Quaternary as wind borne river derived silt deposits, overlying the cover sequences are common on higher surfaces and terraces within the study area, and range from decimetre to several metres in thickness. Loess ages have been determined using luminescence chronology at a site located on the Springbank Monocline about 8 km southeast of the western arm of the Cust Anticline (Berger et al., 2001). Three samples were dated at this location giving resultant ages of the units as 73 +/- 13 ka, 41 +/- 5 ka and 27 +/- 3 ka, oldest to youngest respectively (Berger et al., 2001; Estrada, 2003).

The five main Late Quaternary formations associated with glacial advances are from oldest to youngest: the Hororata (uncertain age), Woodlands (150 ka), Windwhistle (70–40 ka), Burnham (27–15 ka) and Springston (within the last 14 ka) formations (Browne & Field, 1985). The last glacial maximum was around 20 ka and ended about 18 ka with sea-level 120 m lower than present day (Alloway et al., 2007; Forsyth et al., 2008; Barrell & Begg, 2013). Sea level was last at the same height as today about 125 ka (Lambeck & Chappell, 2001).

Within the study area the river terrace aggradation surfaces generally correspond to Windwhistle and Burnham formations depending upon the elevation from the present river channel (Wilson, 1989). The higher surfaces mapped on Starvation Hill that are not underlain by volcanics are of inferred Woodlands Formation (Wilson,1989; May, 2004). The Cust Anticline consists of older tectonically deformed surfaces contrasting with the low-level surfaces of the present-day river terraces and plains. The older east-striking Mairaki Downs section of the Cust Anticline is underlain by Plio–Pleistocene Kowai Formation and there is extensive thick loess cover in many places. The western arm of the Cust Anticline is considered to be Hororata Formation on the higher elevations and Woodlands Formation on the lower elevations (Wilson, 1989) where a former Ashley River channel was located. Interestingly, the southern termination of the western arm of the Cust Anticline, before it steeply plunges beneath the Cust River has also been labelled as Kowai Formation (Wilson 1989). Alternatively the Quaternary surface deposits of the western arm of Cust Anticline are mapped as middle Quaternary alluvium on the Christchurch QMAP and Quaternary sediments are further differentiated by age and mode of deposition as required (Forsyth et al., 2008).

2.4. Tectonic structural culminations within the study area

2.4.1. The Cust Anticline

The Cust Anticline (Figure 2.2) is the most topographically emergent structure in the North Canterbury Plains. It increases in elevation westward for about 8 km along the south side of the Ashley River to the highpoint of 283 m of the Mairaki Downs (about 150 m above the south bank of the Ashley River). The anticline is a combination of E–W-trending and north-northeast-trending fault related folds and forms a doubly plunging periclinal structure (Campbell et al., 2012).

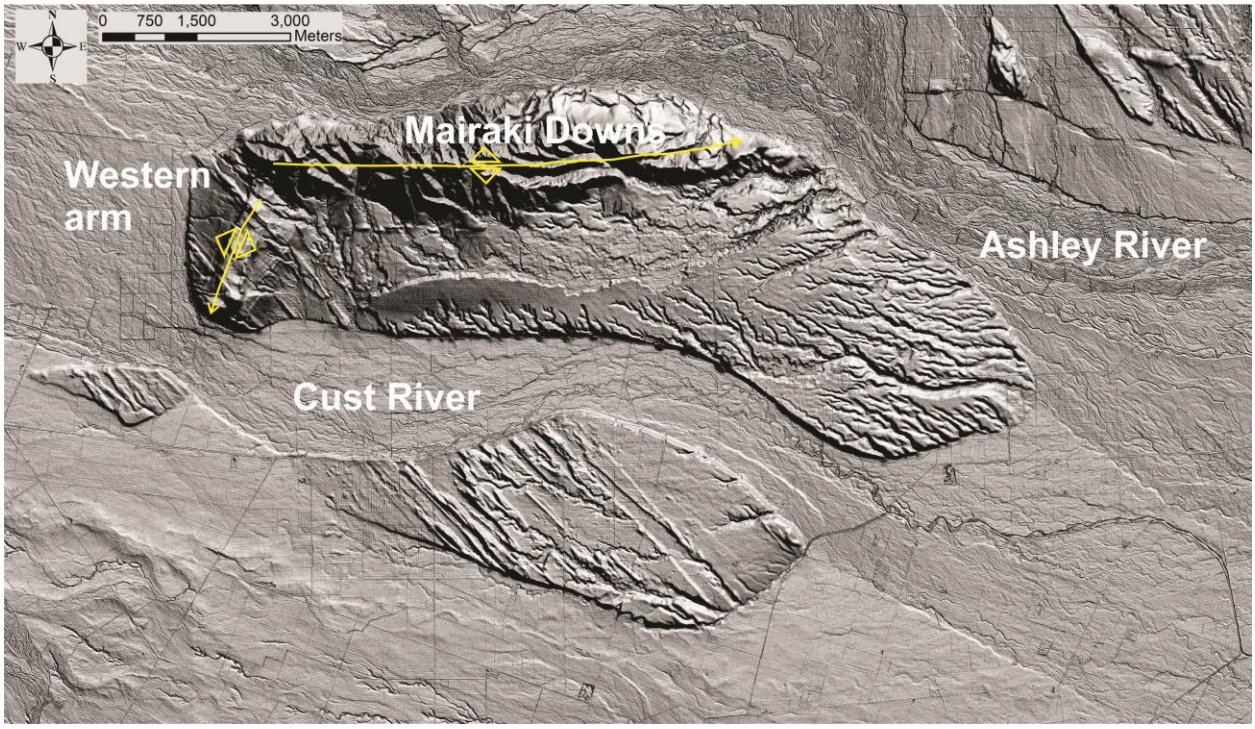

Figure 2.2. Vertically exaggerated (20x) hillshade LiDAR image of the doubly plunging L-shaped Cust Anticline emergent between the Ashley River and the Cust River. LiDAR map at 1:70,000. The image indicates the E–W-trending older anticline structure of the Mairaki Downs and the north-northeast-trending anticline of the younger western arm of the Cust Anticline. The plunging anticline fold axis are indicated by yellow arrows. Paleo-aggradation surfaces can be seen crossing the western arm of the Cust Anticline and also along the southern margin of the Mairaki Downs.

The L-shape of the Cust Anticline is the result of the intersection of a north-northeast-trending anticline at the younger western end with the older, E–W-trending Mairaki Downs anticline. Interaction between re-activated E–W-striking Late Cretaceous basement faults and the thrusts associated with the principal horizontal compression direction (115 +/- 5°) is responsible for the change of the structural trends of this feature (Campbell et al., 2012; Ghisetti & Sibson, 2012). The younger north-northeast-trending western arm of the Cust Anticline projects ~2.5 km southwards before plunging steeply beneath the present-day antecedent Cust River channel (Figure 2.2). There is no surface expression of the anticline across the Cust River channel and

the anticline does not appear to continue southwest beyond the river. However, there are older uplifted southeast-trending paleo-aggradation surfaces of the Ashley River across the western arm of the Cust Anticline and on the southern margin of the Mairaki Downs (Figure 2.2).

2.4.2. Starvation Hill

The Cust River plain west of the Cust Anticline has an eastward depositional gradient and these aggradation surfaces extend west to Starvation Hill, interpreted as a structural uplift consisting of Paleogene volcanic rocks, east of Oxford township and about 1 km south of the present Cust River drainage (Figure 2.1). Starvation Hill is elevated 85 m above the surrounding plains and is a dual hinged anticline with two directions of folding consisting of broadly northerly and easterly trending axes (May, 2004). The higher surface is underlain by volcanic basaltic sediments and the western slopes are of Woodlands Formation (Wilson, 1989).

2.4.3. Springbank Monocline and Cust Downlands

This area is located between the Cust and Eyre rivers (Figure 2.1). They are loess covered surfaces that rise about 20 m above the surrounding Springston Formation aggradation surface of the plains. The uplifted topography is much more subtle when compared to the Cust Anticline, however, it reflects the northeast-trending monocline associated with the hanging wall of the Springbank blind thrust fault located within industry seismic reflection lines (Jongens, 1999; Estrada, 2003).

2.5. Active faults located within the study area and surrounds

The low-relief Canterbury Plains are covered in Pliocene–Quaternary sediments, up to 500 m or more thick in places (Wilson, 1985; Browne et al., 2014). However, there is a structural mesh beneath the Canterbury Plains that consists of inherited E–W-striking Late Cretaceous normal structures, that are being re-activated as strike-slip faults, overprinted and linked by younger blind to emerging northeast-striking thrust fault propagating structures often expressed by growing asymmetric anticlines at the surface (Forsyth et al., 2008;. Dorn et al., 2010a; Campbell et al., 2012; Ghisetti & Sibson., 2012). Active faults are defined as having undergone at least one ground surface deforming fault rupture in the last 125,000 years or two ruptures in the last 500,000 years (Kerr et al., 2003; Barrell & Begg, 2013). The locations of active faults and folds from the GNS Science 1:250,000 Canterbury QMAP (Forsyth et al., 2008) are indicated in

Figure 2.3. This study aims to provide more detail of the E–W-striking and northeast-striking faults and folds associated with the tectonic structural culminations across this area.

2.5.1. The Porters Pass–Amberley Fault Zone

This fault zone includes a significant number of strike-slip fault traces that accommodate dextral transpressive shear and may be an evolving structure of the southward migrating Marlborough strike-slip fault zone (Cowan, 1992; Howard et al., 2005; Campbell et al., 2012). The Porters Pass–Amberley Fault Zone (PPAFZ) extends along the east flank of the Torlesse Range, southwest of the study area, and progressively steps across the Mount Oxford and Mount Grey rangefronts to near the Waipara River mouth. Although this fault zone is not within the study area for this project (Figure 2.1) the degree of active earth deformation in North Canterbury during the Quaternary appears to decrease away from the active rangefront faults of the Porters Pass–Amberley Fault Zone, expanding southeastward through the more recently evolving contractional structures (Cowan et al., 1996; Campbell et al., 2012).

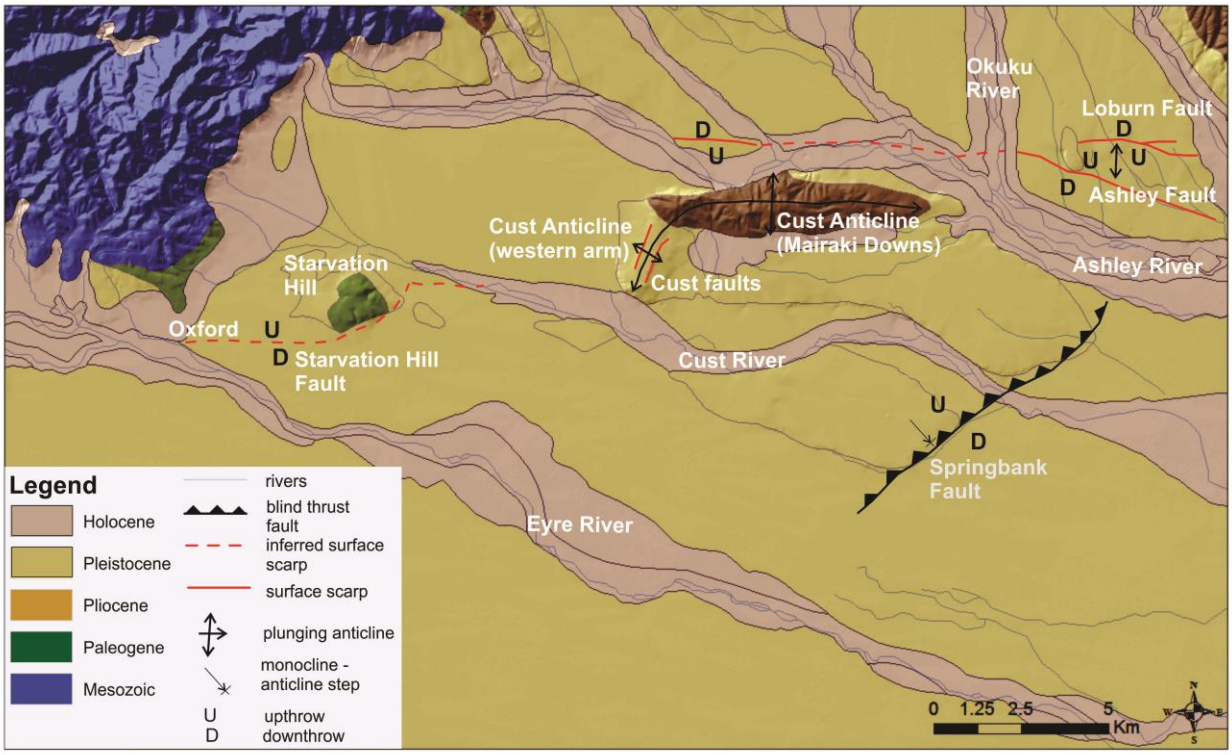

Figure 2.3. Synoptic geology and selected active faults and folds within the study area. The image includes the locations of known active (i.e. Late Quaternary) faults and folds, relevant to the study area, based on GNS Science QMAP Geology of the Christchurch Area (Forsyth et al., 2008). Geology is based on GNS Science QMAP data sets (Cox and Barrell, 2007). [Holocene and Pleistocene consist of undifferentiated fluvial gravel deposits; Pliocene represents Kowai Formation; Mesozoic consists of Torlesse supergroup composite basement terrain].

2.5.2. Cust Anticline faults (north-northeast-trending arm)

The north-northeast-trending western arm of the Cust Anticline is controlled by north-northeast-striking faults on either side of this asymmetric uplifted structure (Figure 2.3). The north-northeast-striking fault with surface expression on the eastern limb of the western arm of the Cust Anticline has previously been called the Cust Fault (Cowan, 1992). However, no detailed studies of this fault have been undertaken. There is also a north-northeast-striking fault scarp on the western limb of the fold (Forsyth et al., 2008; Barrell & Begg, 2013). This fault appears to be of similar strike and length to the eastern fault. Both these faults structurally bound the upper crestal anticline surface. These two faults of similar throw but opposing direction on either side of the anticlinal fold axis are both mapped as active faults on QMAP (Forsyth et al., 2008) and have recently been classified as definite faults (Barrell & Begg, 2013).

The western arm of the Cust Anticline has been attributed to fault-propagated folding as part of a backthrust fault mechanism off the nearby Springbank thrust fault to the southeast (Jongens et al., 1999; Estrada, 2003; Campbell et al., 2012). This backthrust was attributed by these authors as fault-bend folding initiated off the point where the Springbank Fault ramps up from a mid-crustal basal detachment structure (Estrada, 2003). A more recent interpretation considers the surface expression of the north-northeast striking faults to be due to shallow, subsidiary tensional normal faults due to the anticlinal warp (Barrell & Begg, 2013) however, this would not account for the emergence of the asymmetric western arm of the Cust Anticline which is clearly a significant tectonic structural culmination within the North Canterbury Plains.

2.5.3. Ashley and Loburn faults

These E–W-striking faults located north of the Ashley River, have obvious topographic expression and displace Late Quaternary river channels and associated terraces between the Okuku and Makerikeri rivers (Figure 2.3). The northern scarp is named the Loburn Fault, and the more recently active southern scarp is named the Ashley Fault (Sisson et al., 2001; Barrell & Begg, 2013; Barrell & Van Dissen, 2014). While slip evidence based on surface geomorphic expression remains poorly constrained, analysis of the faults as a whole suggests transpressive dextral strike-slip with apparent offset for the Ashley Fault being south-side down east of the Okuku River while the related Loburn Fault is north-side down (Sisson et al., 2001; Forsyth et al., 2008). Thus the low-relief topographic ‘high’ between these faults is inferred to represent a transpressional uplift. Oblique strike-slip kinematics might be expected along this fault zone given its strike direction relative to the present regional tectonic shortening direction of 115°

(Ghisetti & Sibson, 2012) and the Ashley Fault has been interpreted as a re-activated Late Cretaceous–Paleogene normal fault (Jongens et al., 2012).

West of the Okuku River the projected strike of the Ashley Fault is inferred to cross the active floodplains of the Ashley River north of the escarpment of the E–W-trending Mairaki Downs and a possible monocline has been suggested to extend southwest of the Ashley River parallel to the north-northeast-striking Cust Anticline fold axis (Barrell & Begg, 2013). A section of the inferred Ashley Fault across a small terrace on the northern side of the Ashley River indicates an upthrow to the south. Projection of an E–W-striking south-dipping fault plane west from the junction of the Ashley and Loburn fault traces would place the Cust Anticline in the hanging wall of the wider Ashley Fault Zone (Sisson, 1999; Campbell et al., 2012). Although Late Cenozoic deformation on the Ashley Fault has probably mainly transferred southwest to the Cust Anticline there may be some deformation transfer west onto the Glentui Fault Zone therefore, the relationship between the Ashley Fault and the Cust Anticline remains unresolved. (Jongens et al., 2012; Barrell & Begg, 2013).

2.5.4. Starvation Hill Fault

This poorly constrained E–W-striking fault is inferred on QMAP as a possible link across the aggradation surfaces between Starvation Hill and the southwest tip of the Cust Anticline (Figure 2.3; Forsyth et al., 2008). However, confirmation of this inferred fault and any extension towards the Cust Anticline has not been clearly documented prior to this study. An E–W-striking topographic step upthrown to the north, extending from Oxford township towards Starvation Hill has been inferred, however, although this scarp is likely to be tectonic it could also have some fluvial modification by present-day channels and paleo-channels of the Eyre River (Barrell & Begg, 2013). The structural culmination of Starvation Hill is likely to be tectonically formed, however, inferred faults directly northeast and southwest of Starvation Hill are poorly constrained.

2.5.5. Springbank Fault

The Springbank Fault is ~8 km southeast of the north-northeast-trending western arm of the Cust Anticline and forms the southeast edge of the uplifted Cust Downlands (Estrada, 2003). The fault, which terminates in near-surface Pliocene Kowai Formation gravel units, is a northeast-striking, northwest-dipping blind thrust fault with fault-propagated monocline reflectors in the

top 0.5 km of the subsurface (Jongens et al., 2012; Campbell et al., 2012). There is a southeast-facing monocline surface displacement (~20 m uplift) of the elevated Late Quaternary gravel river terraces (Estrada, 2003).

2.6. Study methods used in this thesis

2.6.1. LiDAR analysis

Light detection and ranging (LiDAR) is a remote sensing method that can provide very accurate, high resolution 3D data. Airborne LiDAR uses pulsed laser light, that is scanned from side to side as the aircraft and source fly over an area, to measure distances to the Earth's surface. An extremely high number of points can be measured per second. The laser beam is reflected back to the LiDAR sensor when it hits an object and the time interval between the pulse leaving the system and its return to the LiDAR sensor is measured. The time interval measurements are converted to distances and corrected with respect to the position (using onboard GPS units) and orientation (using inertia measurement units) of the aircraft. A high density and extremely accurate point cloud of x, y and z (latitude, longitude and altitude) co-ordinates is then used to generate very precise three dimensional information which can generate high resolution digital terrain models (DTMs) of the Earth's surface morphology.

LiDAR datasets can allow significantly large areas to be mapped and quantitatively analysed. Furthermore, the extensive and high resolution DTMs generated from LiDAR datasets can be used to quantify geomorphic expression of active tectonic processes in comparison to the geomorphic expression of fluvial or aerial processes (Roering et al., 2013). Rivers are useful for distinguishing tectonic events where channel offsets and topographic gradients cannot be attributed to the ongoing fluvial processes of the river (Holbrook & Schumm, 1999; Burbank & Anderson, 2011). The high resolution of LiDAR datasets can potentially determine paleo-channel directions and very subtle tectonic geomorphic features such as fault scarps which might not be evident using field mapping alone.

In areas of relatively flat, weakly deformed Quaternary surfaces, such as the Canterbury Plains, where there are no outcrops or significant topography to give clear expression of fault traces LiDAR can be very useful. Across the Canterbury Plains active faults can cause very subtle topographic expressions across landforms developed by Quaternary fluvial processes. However, very young landforms may also conceal active faults by post-dating the last rupture event that

may have occurred on a fault. LiDAR analysis has been used to interpret active and inferred tectonic traces and fault induced folding, and to give a relative age of the last offset, from Quaternary landscape surfaces (Barrell & Begg, 2013; Barrell & van Dissen, 2014) and has also been effectively used in active tectonic studies in New Zealand (Barth et al., 2012; Langridge et al., 2014) and elsewhere especially California (Hudnut et al., 2002; Prentice et al., 2009; Gold et al., 2013; Gold et al., 2014).

The geomorphic interpretation in this study utilised a 2-m resolution LiDAR dataset that was surveyed for the Waimakariri District Council in 2005 and provided for this study by Environment Canterbury. The initial dataset required interpretation and computation from the raw data files. For the second dataset this had been performed already and the relevant tiles within the study area were mosaicked in ArcGIS and overlain across aerial photos for presentation and analysis. The LiDAR DTMs were interpreted using vertically exaggerated hillshade models (up to 20x) and slope maps. Quantification and profiles from the results of the LiDAR interpretation across the study area are presented in Chapter 3.

2.6.2. Paleo-seismic investigations

Trench excavation is a significant part of any paleo-seismic study to investigate faulting and folding affecting near surface deposits. Trenching thus provides information about the stratigraphy, structure and age of the near surface units to determine paleo-earthquake displacement and recurrence as well as long-term folding rates (McCalpin, 2009). Two trenches were excavated in this study. The first was located against a topographically well-defined scarp on the crest of the north-northeast-trending western arm of the Cust Anticline. The second trench was located across a fault scarp immediately to the southwest of the Cust Anticline. Both trenches were located perpendicular to the strike of the fault trace. At the completion of each trench they were back-filled close to their original condition.

The trenches were excavated using a 13 tonne digger and the soil was initially removed and laid to one side while the trench fill below the soil was excavated and placed on the other side. The conditions of the subsurface (saturation and type of material) dictated the requirements of each trench in terms of benching, wall height and other considerations. The stratigraphic and tectonic interpretation of these trenches and specific details of each site are presented in Chapter 4.

The trench walls were cleaned and prepared once the excavation was complete. The walls were gridded using string and levels into one-metre grids along the length and depth of the trench. The locations of beds, units and other stratigraphic horizons were marked using coloured tape and nails before logging commenced. Logging was performed at a scale of 1:10 using graph paper overlaid with plastic mylar sheets. Contacts were measured using tapes and transferred to the log systematically from one end of the trench to the other. The walls of the trenches were also photographed as a secondary record of the trench characteristics. The trench logs were digitised and processed in ArcGIS.

During the initial reconnaissance of the trench, before logging, sample locations for possible dating were determined. These were marked on the logs. Preliminary interpretations of areas of interest were also marked on the logs. Samples for optically stimulation luminescence (OSL) dating were taken using stainless steel tubes hammered into the dating location and then removed and bagged in light proof material for subsequent processing. Radiocarbon samples were collected and labelled in plastic bags. Radiocarbon samples were sent to the University of Waikato radiocarbon dating laboratory and the OSL samples were sent to Victoria University, Wellington.

2.6.3. Optically Stimulated Luminescence dating method

This is a form of geochronology that measures the energy of photons being released and is a useful technique for dating Quaternary sediments. It is especially applicable for sediments up to 100,000 years old and therefore goes beyond the range available for radiocarbon dating. The calculated age is the time since the last exposure to sunlight. Sunlight before deposition and burial bleaches the luminescence signal and resets the time clock. Windblown sediments such as loess are likely to have been zeroed before burial. The age is determined by evicting with light stimulation the stored ionizing radiation which has been absorbed by the crystal lattice of the sediments during burial. The radiation is released as luminescence. During dating the radiation dose received by the sample since being zeroed and the dose rate experienced during the accumulation burial period is quantified.

2.6.4. Radiocarbon dating method

Radiocarbon is formed when high energy cosmic rays collide with nitrogen nuclei in the atmosphere to form ^{14}C which then forms CO_2. The CO_2 is incorporated into plant matter

through photosynthesis. When the plant dies ^{14}C is no longer being fixed from the environment and provides a clock that can be used for dating of the material. Dating is performed by measuring the amount of ^{14}C in the sample and calculating the time elapsed since it was in equilibrium with the surrounding environment. Ideally sample material used for radiocarbon dating of tectonic events was deposited when it was young and therefore the radiocarbon content will reflect the time of deposition for a sediment layer. It is important to make sure that the material for dating is not affected or contaminated by carbon from transported, reworked older or younger material or by rootlets from surface vegetation.

2.6.5. Ground penetrating radar (GPR)

Ground penetrating radar uses electro-magnetic waves to determine the change in electrical properties of the subsurface (Davis & Annan, 1989; Milsom & Eriksen, 2011; Nobes, 2011). The general GPR setup (Figure 2.4) involves two antennas: one transmits radio-frequency EM pulses and the second receives reflected pulses from the subsurface layers or structures located beneath and near to the antennas (as well as the direct air waves and upper ground surface waves). The lower the frequency of the radar antenna the greater the depth of penetration but lower frequency antenna are larger. The time of a returning signal (two-way travel time) is converted to the depth of the structure by knowing the radar subsurface velocity. This gives a cross-sectional representation, based on the subsurface physical properties, of the subsurface structure and stratigraphy over the survey area.

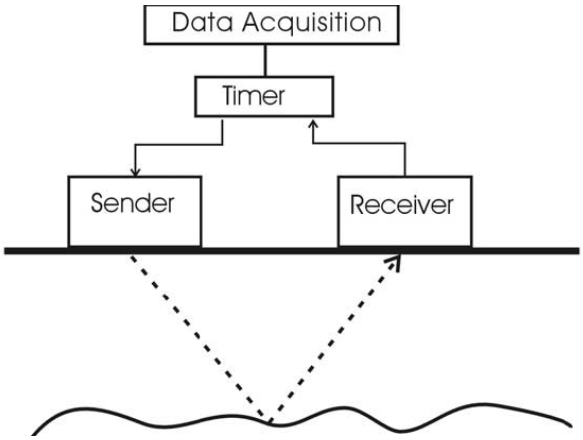

Figure 2.4. Ground penetrating radar acquisition setup. An electro-magnetic wave is transmitted below the surface which is reflected at an interface and detected by the receiving antenna. The timing of the signal between sending and receiving is recorded and saved for subsequent analysis. (source: Jaedicke, 2003).

GPR surveys were undertaken at numerous locations throughout the study area. Surveys were performed as initial reconnaissance to determine the suitability of sites for paleo-seismic studies.

They were also undertaken post-trenching to complement the data obtained at the paleo-seismic sites and to collect information at these sites beyond the location of the trench.

Surveys involved the use of two different GPR systems (Figure 2.5). Initial surveys were undertaken using a Sensors and Software PulseEKKO system utilising 100 MHz antennas. However, due to limitations in the PulseEKKO processing software and also reliability issues later surveys used a GSSI 200 MHz shielded antenna courtesy of Dr Mike Finnemore of Southern Geophysical Ltd, Christchurch. This compact system was especially useful along the confined space of the base of the paleo-seismic trenches. Ground penetrating radar results will be presented in Chapter 4 in conjunction with the trench interpretations.

Figure 2.5. Diagrams of the GPR equipment used in the surveys. The PulseEKKO system is indicated on the left and the GSSI system on the right.

2.6.6. High resolution reflection (HRR) seismic surveys

Seismic reflection surveys are an effective way of imaging layered subsurface geology using acoustic energy sound waves transmitted through vibration of the rock mass and near surface unconsolidated deposits (Milsom & Eriksen, 2011). The low energy waves are approximately elastic and generally leave the rock mass unchanged. P-waves (which travel as a series of compressions and rarefactions) have the highest velocity of any of the possible wave motions generated and are also known as primary waves.

A HRR survey was obtained along the length of Chapmans Boundary Road across a potential E–W-striking fault scarp observed on the LiDAR that was inferred to be an indication of the southern termination of the Springbank Fault. Although this survey is not directly related to the

Cust Anticline or the final conclusions of this thesis it nevertheless fits with the idea of determining the locations of E–W-striking tear-faults associated with northeast-striking thrust faults across the Canterbury Plains. The seismic survey results are presented in Appendix 2.

2.6.7. Re-analysis of industry seismic lines

A comprehensive series of industry seismic reflection surveys have been run within the main study area of this project during 1998–2000 (Indo-Pacific Energy 2000; Jongens, 1999). However, these surveys were more focussed on the deeper structures and therefore were not specifically designed to interpret the top few hundred metres of stratigraphy. Faulting and folding of the deeper units will be analysed in comparison to the surface expression observed using the LiDAR, and augmented by surface mapping, to determine the kinematics and geometry of faulting and folding across the region. This will involve a desktop study of digitised seismic survey lines within the area and is presented in Chapter 5.

The above study methods provided an integrated programme of geologic, geomorphic, paleo-seismic and geophysical analyses across the study area. This was necessary due to the lack of surface exposures and difficulty in distinguishing active tectonic features from fluvial and/or aeolian features across the low-relief Canterbury Plains. It also enabled the results of targeted paleo-seismic trenches and geophysical surveys located around the western arm of the Cust Anticline to be integrated across the larger study area so as to develop a model of fault linkages between the tectonic structural culminations. This would not have been possible, within the time frame of this study and due to access issues, without the LiDAR and industry seismic reflection lines.

Chapter 3. Tectonic geomorphology from LiDAR interpretation

3.1. Introduction to the LiDAR dataset

The geomorphic interpretation for the field area was made using a high resolution LiDAR dataset surveyed for the Waimakariri District Council in 2005. This dataset was flown at a resolution of 2 m and the relevant tiles within the study area were mosaicked in ArcGIS and overlaid across other layers, including aerial photos, for analysis and presentation. The processed LiDAR digital terrain maps were interpreted using vertically exaggerated hillshade models (up to 20x) and slope maps applied to the processed datasets. Ground truthing of the LiDAR interpretation was performed across the western arm of the Cust Anticline, but was dependent upon land access in some areas.

3.2. Fault and fold geomorphic interpretation

The study area has been divided into sections for qualitative and quantitative LiDAR analysis with respect to the structural culminations within the fault network between Starvation Hill, the Cust Anticline and the Ashley and Loburn area (Figure 3.1). These sections from west to east are: area 1 Oxford to Starvation Hill; area 2 Starvation Hill to Cust Anticline; area 3 Glews Road paleo-seismic site; area 4 north-northeast-trending western arm of the Cust Anticline; area 5 E–W-trending Cust Anticline (Mairaki Downs); area 6 northeast of the Cust Anticline.

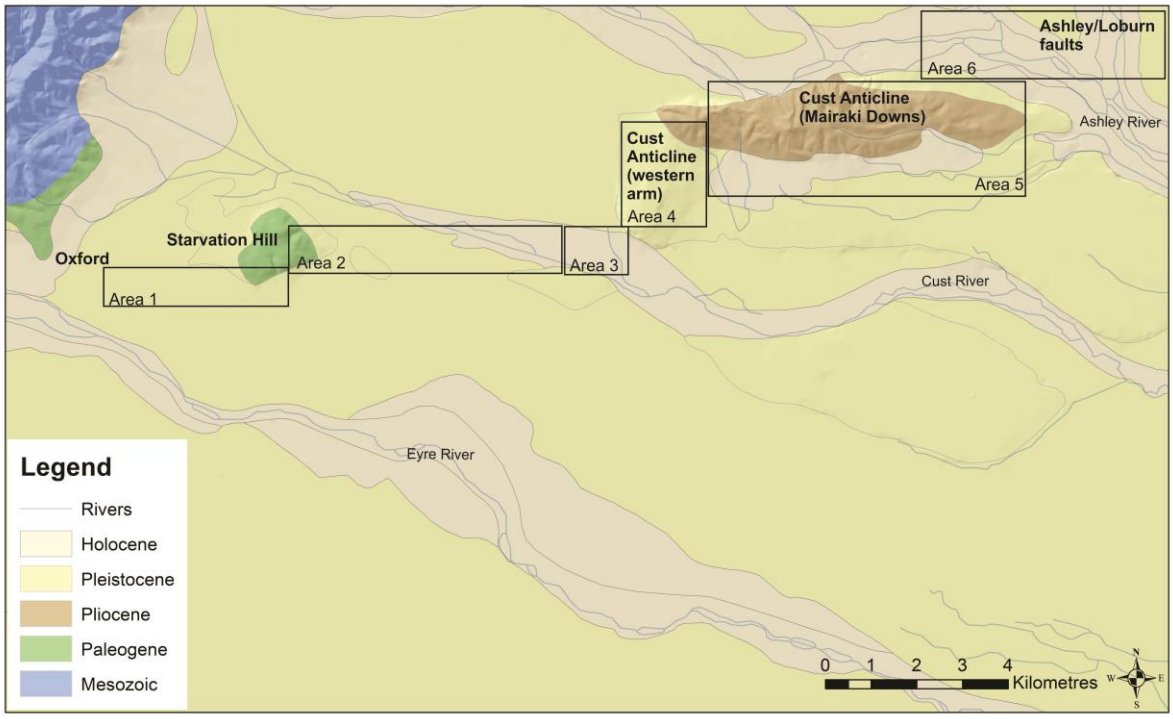

Figure 3.1.Map of the study area locations for LiDAR tectonic geomorphology interpretation. Geology is based on GNS Science QMAP data sets (Cox and Barrell, 2007). [Holocene and Pleistocene consist of undifferentiated fluvial gravel deposits; Pliocene represents Kowai Formation; Mesozoic consists of Torlesse supergroup composite basement terrain].

3.2.1. Area 1: Oxford to Starvation Hill

East of Oxford township and west of Starvation Hill a distinct 3.75 km E–W-striking, south-facing fault scarp is upthrown to the north with a scarp height that varies from around 1 m to a maximum of around 2.5 m (Figure 3.2A). The scarp height appears to increase eastwards towards Starvation Hill as seen in a comparison of the top profile with the lower profile in Figure 3.2A. These E–W-striking fault traces run sub-parallel to the overall southeast paleo-channel flow direction across the aggradation surface between the Eyre River to the south of Starvation Hill and the much smaller Cust River to the north. The age of this aggradation surface, across which the fault trace is located, is considered to be on the boundary between the Windwhistle (70–40 ka) and Burnham (27–15 ka) Formations (Wilson, 1989).

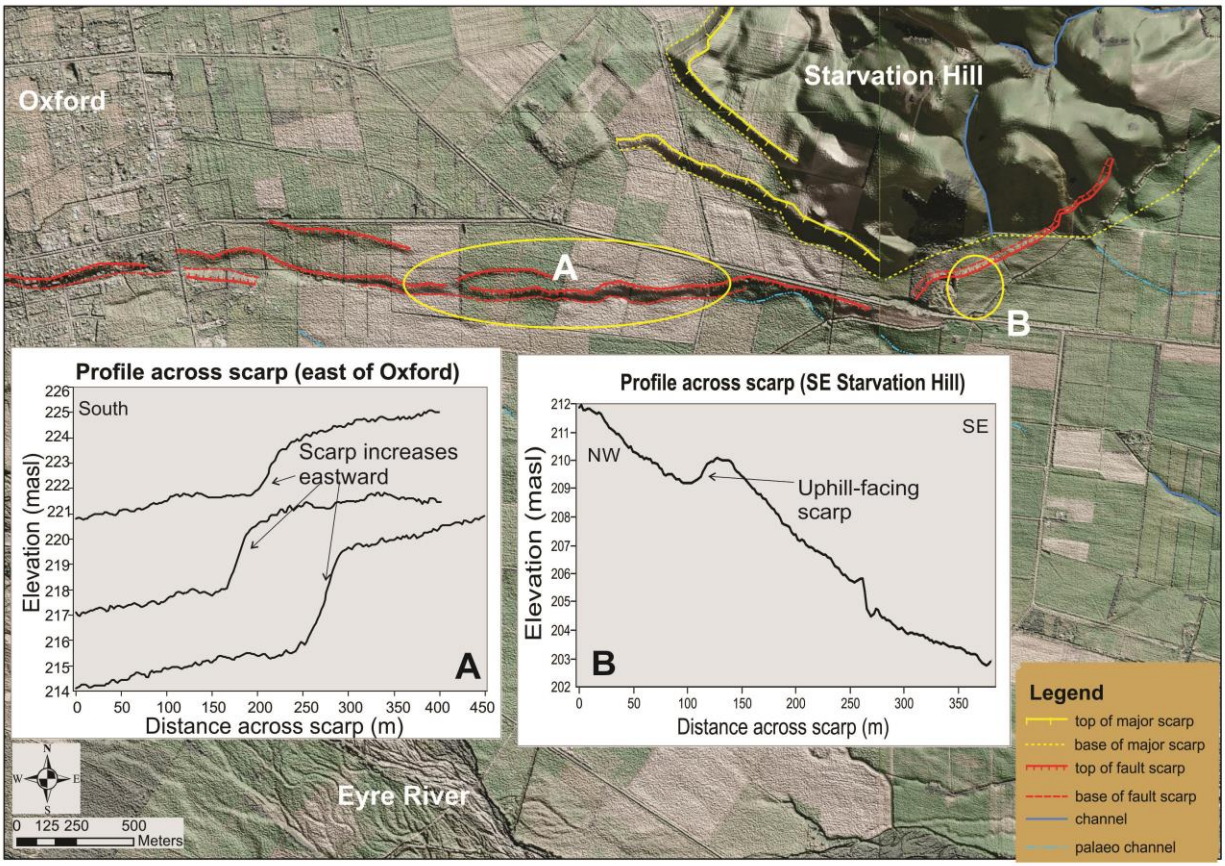

Figure 3.2. Area 1: Oxford to Starvation Hill. LiDAR image at scale of 1:18,000 with vertical exaggeration 20x. Inset A: Profiles perpendicular to the E–W strike of the scarp at three locations indicating offset surfaces sloping gently to the south and also downthrown to the south side of the fault. Note that the scarp height increases eastwards towards Starvation Hill as indicated by comparing the top profile with the lower profile. Inset B: Profile perpendicular to the scarp across the southeast-facing slopes of Starvation Hill indicating an uphill-facing scarp offsetting the southeast-facing slope of the hill.

Starvation Hill is elevated about 85 m above the surrounding plains and is a dual hinged anticline with two directions of folding suggestive of the interaction of more than one active fault during its formation (May, 2004). The higher surface is underlain by basaltic volcaniclastic sediments

and the western slopes are underlain by late penultimate glaciation gravels of Woodlands Formation of ~150,000 years before present (Wilson, 1989). Starvation Hill is about 1 km south of the present Cust River. The E–W-striking fault trace (Figure 3.2) is located <1 km north of the Eyre River near Oxford and about 2.5 km north of the Eyre River near Starvation Hill which emphasises the E–W strike of the fault trace compared with the general southeast flow direction of the rivers on the paleo-aggradation surface. Therefore, although there are no definitive features that cross-cut the inferred fault trace the implication for this feature as one that is tectonically formed is reasonably conclusive.

The E–W-striking fault trace does not appear to continue beyond the southern tip of the Starvation Hill terraces. Instead a trace appears to trend northeast for about 1.1 km across the southeast terraces of Starvation Hill. This section of the trace manifests as an uphill-facing scarp, about 1–1.5 m high, across the southeast-facing slope (Figure 3.2B). There is more tilt on the offset surface compared to the higher surface above the scarp suggesting there to be some progressive rotation of this uphill-facing scarp. The LiDAR does not reveal the trace to extend across the entire southeast-facing slope. The scarp height decreases slightly to the northeast and the trace disappears within the older and more incised hill slopes where it passes from surficial gravel units to bedrock. These two fault traces around Starvation Hill are probably not directly equivalent as suggested by the change in throw as well as the change in strike, however, they likely rupture syn-kinematically.

3.2.2. Area 2: Starvation Hill to Cust Anticline

The northeast extent of Starvation Hill, on the southern side of the Cust River, lies directly west of the southern extent of the Cust Anticline, on the northern side of the Cust River (Figure 3.3). A discontinuous 6 km-long E–W-striking fault trace extends between these two structural culminations. However, the surface trace is not geomorphically continuous across the LiDAR image and was also not able to be traced continuously during ground mapping.

The Cust River flows southeast across this fault trace, being north of the fault trace near Starvation Hill and south of the trace at the Cust Anticline. There is a 2–3 m terrace riser from the present Cust River bed to the aggradation surface surrounding the slopes of Starvation Hill. The fault trace has varying expression depending upon its location within the present floodplain surfaces of the Cust River (Figure 3.3, locations 2–4) or on the higher aggradation surfaces to the

west (Figure 3.3, location 1). An E–W-striking fold axis, shown on QMAP as an extension of the Cust Anticline westwards towards Starvation Hill, is not evident from the LiDAR maps. At best the Cust River and the associated aggradation surface on its southern side show a very subtle 1–2 m of warping throughout this region.

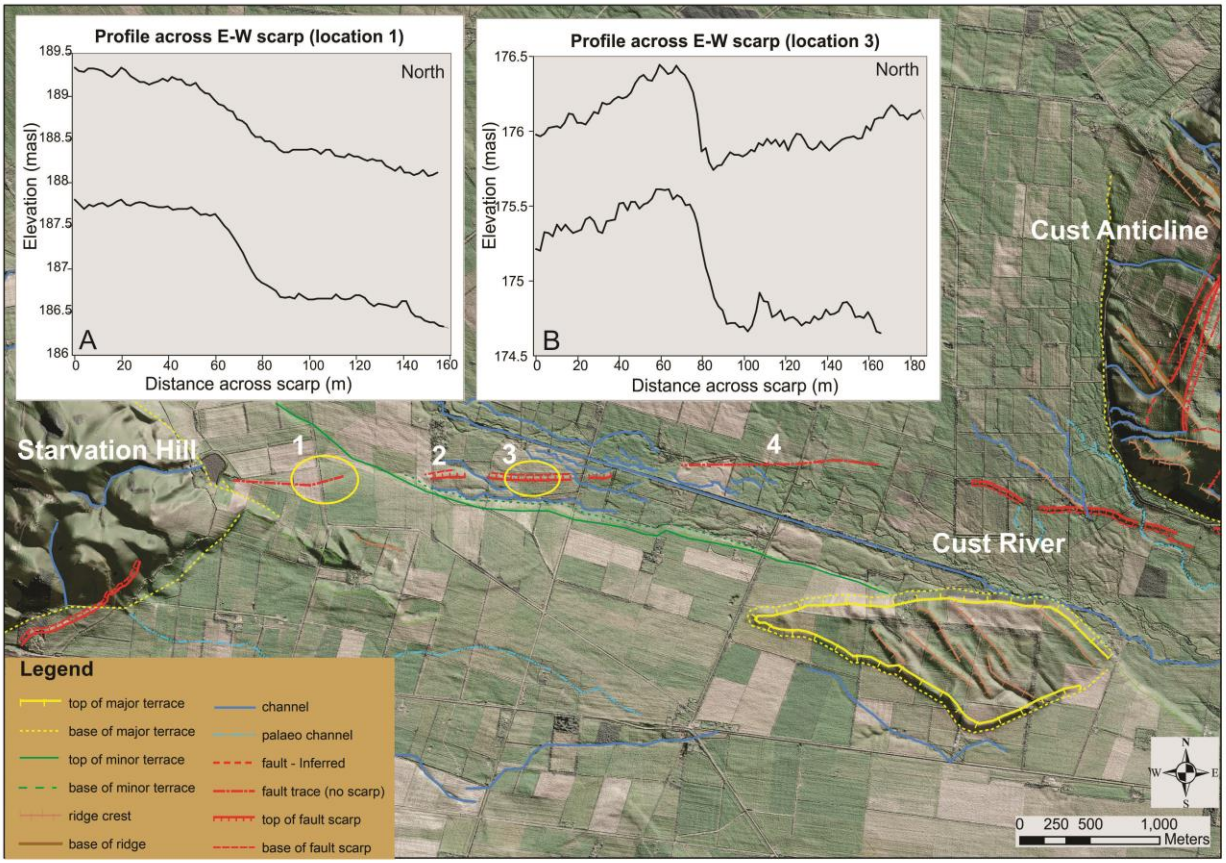

Figure 3.3. Area 2: Starvation Hill to Cust Anticline. LiDAR image at scale of 1:30,000 with vertical exaggeration 20x. Inset A: Profiles perpendicular to the E–W strike of the scarp across the higher aggradation surface east from Starvation Hill indicating offset surfaces downthrown to the north side of the inferred fault (location 1). Inset B: Profiles perpendicular to the scarp (location 3) on the lower aggradation surface of the Cust River floodplain indicating offset surfaces sloping gently to the south and downthrown to the north.

The fault trace at location 1 extends E–W about 900 m across the aggradation surface (Windwhistle Formation) from Starvation Hill. Although geomorphic surface expression of this trace is subtle the LiDAR indicates the scarp height to be between 0.5–1 m and upthrown to the south (Figure 3.3A). While the surface lineament could be fluvial in origin, given the general E–W strike of the inferred fault trace across the surface as well as the general southeast direction of the Cust River terraces and paleo-drainage channels, it is reasonable to infer this to be expression of a fault at an acute angle to the present, and paleo-channel, flow directions across the plains. The expression of this E–W-striking fault trace relay becomes more evident as it projects eastward towards the southwest termination of the western arm of the Cust Anticline.

A more distinct E–W-striking scarp offsets the lower terrace (Springston Formation) within the present floodplain of the Cust River (Figure 3.3, locations 2 and 3). The scarp is sub-parallel to the continuation of the east-southeast-striking terrace riser of the southern bank of the Cust River and is upthrown on the south side of the scarp (Figure 3.3B). The Cust River is diverted within an irrigation channel east of this location. However, southeast flowing paleo-channels show a decreased channel gradient across the scarp indicating that the scarp has affected but not defeated the flow of channels across it. A similar example of this effect was shown on the western segment of the Greendale Fault where numerous old channels passing through the scarp were re-occupied by the river (Duffy et al., 2013).

On the northern side of the present Cust River channel an indistinct E–W-striking trace (Figure 3.3, location 4) continues across the extensively reworked farm surfaces within the floodplain. On its own the inferred trace at location 4 would be difficult to justify as tectonic related, however, it forms a direct continuation and relay link between localities 1–3 (Figure 3.3) and the Glews Road paleo-seismic site (Section 3.2.3 and Chapter 4). LiDAR profiles across this location indicate that there is a very shallow slope to the north but no significant offset compared to the locations (1–3) further west. Therefore, it could represent a transition between the segments of the trace (upthrown to the south) west towards Starvation Hill and the segments of the trace (upthrown to the north) east towards the emergent western arm of the Cust Anticline.

3.2.3. Area 3: Glews Road paleo-seismic site

Immediately to the southwest of the Cust Anticline the E–W-striking fault trace from Starvation Hill becomes geomorphically more distinct across the swampy low-lying ground within the floodplain on the northern side of the present Cust River channel (Figure 3.4). This aggradation surface is mapped as Burnham Formation (27–15 ka; Wilson, 1989). Within this section the trace shows a definite, but eroded scarp, generally striking E–W, that steps through a series of short east-southeast-striking segments to curve around the uplifted topography of the north-northeast-trending western arm of the Cust Anticline. The scarp, which offsets the Burnham aggradation surface, is upthrown to the north throughout this section. Parallel LiDAR profiles along the top and base of the scarp indicate that the scarp height is, on average, slightly less than 1 m at the western end, increasing to a scarp height around 1.25–1.5 m through the central section and then decreasing in geomorphic expression at the eastern termination. This can also be seen by comparing the top to lower perpendicular profiles shown in the insets of Figure 3.4.

There are no geomorphic piercing points, observed on the LiDAR, along the entire fault trace between Starvation Hill and the Cust Anticline that substantiate and quantify any unequivocal strike-slip component. However, aspects of the fault trace geomorphology outlined below infer the presence of an oblique strike-slip component on the fault. This might also be expected given the orientation of the fault trace with respect to the present tectonic stress regime and the observations made on nearby faults such as the Ashley and Loburn faults to the northeast and the recently active Greendale Fault southeast of the Waimakariri River.

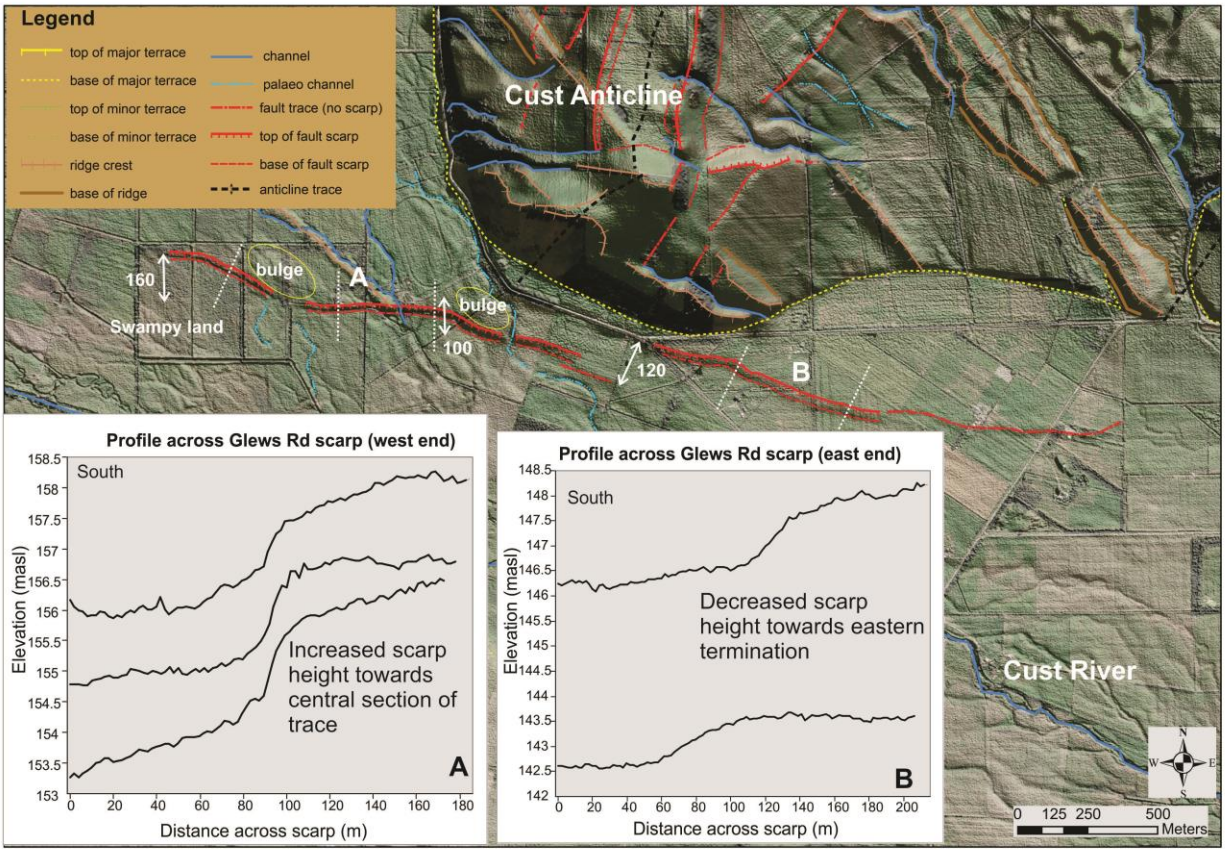

Figure 3.4. Area 3: Glews Road paleo-seismic location. LiDAR image at scale of 1:15,000 with vertical exaggeration 20x. Inset A: Profiles perpendicular to the E–W strike of the scarp at three locations across the western end of the fault trace. The offset surfaces slope gently to the south and are downthrown to the south side of the fault. Inset B: Profiles perpendicular to the scarp across the eastern end of the fault trace east of the left-step in the trace, indicating minor-offset surfaces sloping gently to the south and downthrown to the south. Profile locations are indicated by dotted white lines.

Initially the western end of this fault scarp has the geometry of a wingcrack structure that strikes east-southeast, for a length of around 400 m with an offset of 160 m, and leads into a 525 m long E–W-striking segment (Figure 3.4). A wingcrack structure is due to tensile growth at the tip of a shear zone, oriented parallel to the applied σ_1 compression, and is formed during fault growth or re-activation (Fossen, 2010). Alternatively, this initial east-southeast-striking segment could simply represent a right-bend between these two E–W-striking segments, due to oblique strike-

slip, with the western-most segment not having an extended surface representation in this location.

Either of these structures indicate that this fault has a component of strike-slip along its trace. Immediately adjacent to this right-bend there is a bulge and zone of warped ground surface deformation within the upthrown side which is also consistent with an element of strike-slip along the fault trace (Figure 3.4). The formation of a bulge at this location is in response to a very weak left-bend with respect to the slip direction and is further evidence for oblique strike-slip being the sense of this fault. The parallel LiDAR profiles along the top and base of the scarp also indicated that the scarp height was more indistinct near the location of the bulge. These effects at bends along strike-slip faults in relation to rupture directivity and segmentation were documented by Sibson (1989) and have been recorded along the Glynn Wye fault trace releasing bend in North Canterbury (Cowan, 1990). Similar geomorphology was also shown at the western end of the Greendale Fault, at the Waterford releasing bend, and was due to small-scale oppositely-stepping segments within the apex of the overall bend (Duffy et al., 2013).

The scarp continues east for about 525 m to another east-southeast-striking right-bend across an offset of about 100 m (Figure 3.4). Again the LiDAR reveals a bulge on the northern side of this step, although it is less distinct and was not so clearly observed in the field. After another 430 m the scarp appears to die out and step-left about 120 m onto a less prominent scarp. This scarp trace does not overlap with the end of the previous trace and continues for about 850 m east-southeast before becoming indistinct in the landscape. However, it can be traced indistinctly for a further 800 m on the LiDAR image.

3.2.4. Area 4: The western arm of the Cust Anticline

The north-northeast-trending western arm of the Cust Anticline extends for about 2.5 km between the southern termination of the plunging anticline at the Cust River and the western end of the E–W-trending Mairaki Downs section of the Cust Anticline (Figure 3.5). Faulting and folding accounts for the uplift of the western arm of the Cust Anticline and this is manifest at the surface by 2–3 prominent fault traces and numerous minor traces associated with the anticline and crestal structural depression (these faults are discussed in detail in the following sub-sections).

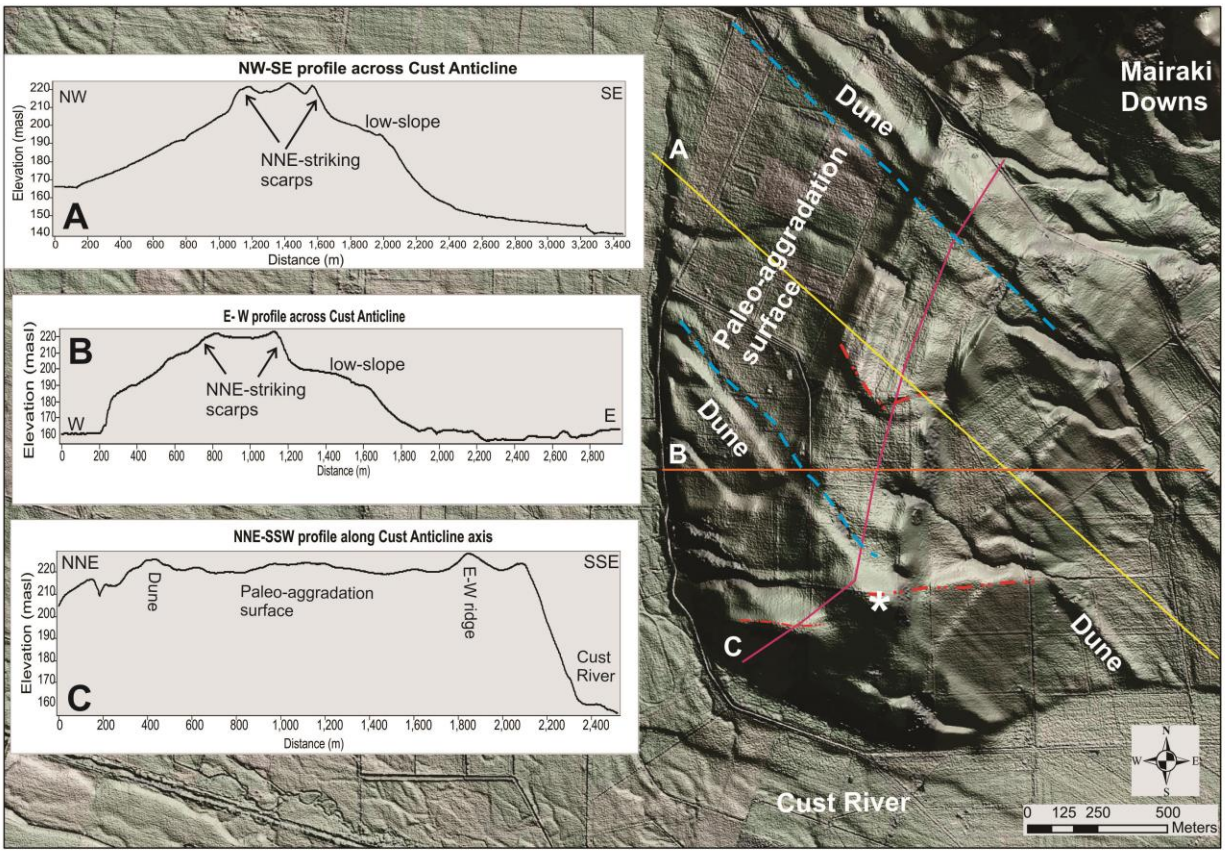

Figure 3.5. Area 4: Western arm of the Cust Anticline. LiDAR image at scale of 1:15,000 with vertical exaggeration 20x. Inset A: NW–SE profile across the fold axis of the anticline indicating the asymmetry of the anticline and the location of the crestal scarps. Inset B: E–W profile across the western arm of the Cust Anticline indicating the low-slope break on the eastern anticline limb. Inset C: Profile along the north-northeast-striking fold axis showing the constant elevation along the anticline and the steeply plunging termination to the south. In the main image the highpoint (indicated by *) is located about 500 m north of the anticline termination along an E–W-striking ridge crest (dashed red line) The substantial main paleo-aggradation surface is outlined by blue-dashed lines and a curved scarp within the crest of this surface by the dashed-red line.

A NW–SE profile across the anticline indicates that the topographic elevation of the anticline crest is about 60 m above the surrounding plains on the northwest side and about 70–80 m on the southeast side (Figure 3.5A). The crest of the anticline is characterised by a structural depression bounded by north-northeast-striking fault scarps. These eastern and western crestal scarps are separated by ~250 m at the southern end of the anticline and this increases up to around 300 m northwards consistent with the plunging nature of the anticline to the south. Furthermore, the anticline profile is asymmetric with a shallower dipping west-northwest-facing limb and a steeper dipping southeast-facing limb. The west-northwest limb has a constant topographic limb dip of ~2.5–3° towards 290° below the fault scarp. In contrast there is a 300-m wide low-slope zone, below the fault scarp, before the steeper section of the southeast limb which has a topographic limb dip of ~7–9° towards 130°. However, these surface dips do not necessarily equate to the dip of the underlying older strata which would reflect the fault propagated folding of the older units below the surface cover. An E–W profile across the Cust Anticline further

highlights this low-slope break on the southeast limb of the anticline compared to the slope of the western limb (Figure 3.5B). This low-slope zone could represent a zone of shallow flexural-slip faulting in the footwall syncline of a thrust fault controlling the eastern scarp which will be further discussed later in this section.

The north-northeast-trending profile along the anticline axis remains at a relatively constant elevation between 205–227 m above sea-level (Figure 3.5C). The western arm of the Cust Anticline, where it intersects with the E–W-trending Mairaki Downs section, decreases slightly in elevation from the relatively constant elevation along the fold. Southwards along this profile there are two shallow basin-like depressions separated by a curved eroded scarp that strikes east-northeast towards the eastern fault scarp and northwest towards the western fault scarp (Figure 3.5, red-dashed line). The inferred highpoint of the anticline fold axis (227 m) is around 500 m north of the steeply plunging anticline termination into the Cust River northern floodplain. This corresponds to an east-striking ridge (Figure 3.5). The anticline axis changes to a more southwest direction at this highpoint along with a left-step in the location of this ridge.

There is a broad southeast-trending paleo-aggradation surface across the western arm of the Cust Anticline. This is inferred to represent where former channels of the ancestral Ashley River flowed southeast around the now uplifted area south of the E–W-trending, older Mairaki Downs section of the Cust Anticline (Cowan, 1992). As the younger north-northeast-trending western arm of the Cust Anticline was uplifted the Ashley River channels likely slipped-off this surface to the south. Eventually, the Ashley River was defeated from flowing south of the Cust Anticline and became relocated and confined to its present position north of the Cust Anticline structure (Cowan, 1992; Estrada, 2003). The present channel-flow of the southeast flowing Cust River, to the south of the anticline, is therefore significantly undersize compared to the previously combined Ashley and Cust rivers that would have flowed across this floodplain.

There are also prominent southeast-striking linear paleo-dune ridges, on the edges of the main paleo-aggradation surface across the anticline, that intersect the north-northeast-striking eastern and western fault scarps (Figure 3.5). These scarps are the prominent faults that cross-cut the paleo-aggradation surface and the southeast-striking dune structures across the anticline. The southern dune feature is truncated by the E–W-striking ridge associated with the anticline highpoint and a similar dune feature is located at the eastern termination of this E–W-striking ridge. The northern dune feature is continuous across the entire fold (Figure 3.5). Augering of

the southern dune feature confirmed there to be ~3.3 m of silty loess above gravels below the dune surface. The loess deposition above the gravels at a location off the dune, towards the centre of the structural depression between the western and eastern scarps, was only ~1.5 m. This indicates that this feature was a linear dune-like feature as the loess cover is not constant between the sites. Therefore, the loess does not simply drape across and reflect the underlying gravel-surface topography between the western and eastern scarps. Similar paleo-dune features with strong northwest–southeast alignment have been recorded across the nearby Springbank structure to the southeast (Estrada, 2003), and on the south margin of the Waimakariri River further south from the study area.

E–W-striking fault trace

A prominent E–W-striking ridge cuts across the anticline about 500 m from its southern termination and is the highpoint of the north-northeast-trending western arm of the Cust Anticline. North of this ridge the anticline is of relatively constant elevation and south of this ridge elevation decreases sharply and is inferred to reflect the steep plunge of the western arm of the Cust Anticline structure towards its southern termination (Figure 3.5C).

This E–W-striking ridge could represent a terrace edge, nested within the uplifted and folded structure of the anticline, of an ancestral channel at the southern edge of the paleo-aggradation surface of the ancestral Ashley River immediately north of the ridge. Interestingly, this scarp is parallel to, and of the same polarity as a co-linear channel edge south of the Mairaki Downs further east (Figure 3.10B). However, an inferred E–W-striking fault could also be considered as a viable explanation and is the preferred interpretation. This inferred E–W-striking fault trace truncates the uplifted southeast-trending paleo-aggradation surface and also cross-cuts the southeast-trending dune structure at this location (Figure 3.6). This would indicate that this inferred fault is younger than the paleo-aggradation surface, and possibly developed co-evally with the dune structure. This fault and associated topographic ridge has elevation change of about 7 m above the height of the crest of the dune and about 10 m above the level of the crestal depression on its northern side. Furthermore, the inferred E–W-striking fault appears to truncate the north-northeast-striking fault scarp that extends along the western edge of the anticline. However, the north-northeast-striking fault trace on the eastern side of the anticline appears to cross-cut this inferred E–W-striking fault on the LiDAR (Figure 3.6).

Profiles along the top and base of the inferred E–W-striking scarp do not show any significant elevation displacement changes along their length eastwards from the crest of the anticline indicating that the scarp height is approximately the same elevation both sides of the north-northeast-striking eastern scarp (Figure 3.6A). This is consistent with this being an E–W-striking fault trace, rather than the cumulative displacement of different age surfaces of a river channel terrace edge offset by the north-northeast-striking fault. Interestingly, the height of the north-northeast-striking scarp on the eastern crest of the anticline is approximately the same elevation both north and south of the inferred E–W-striking scarp and there is no substantial lateral offset of the E–W-striking scarp by the north-northeast-striking scarp and vice-versa. However, there is apparent vertical offset of this E–W-striking scarp (Figure 3.6A). Therefore, although it is difficult to give relative ages based on the geomorphic evidence this could indicate that the E–W-striking fault is older than the north-northeast-striking crestal faults although it is likely that the E–W-striking fault trace is coevally active with the main north-northeast-striking faults.

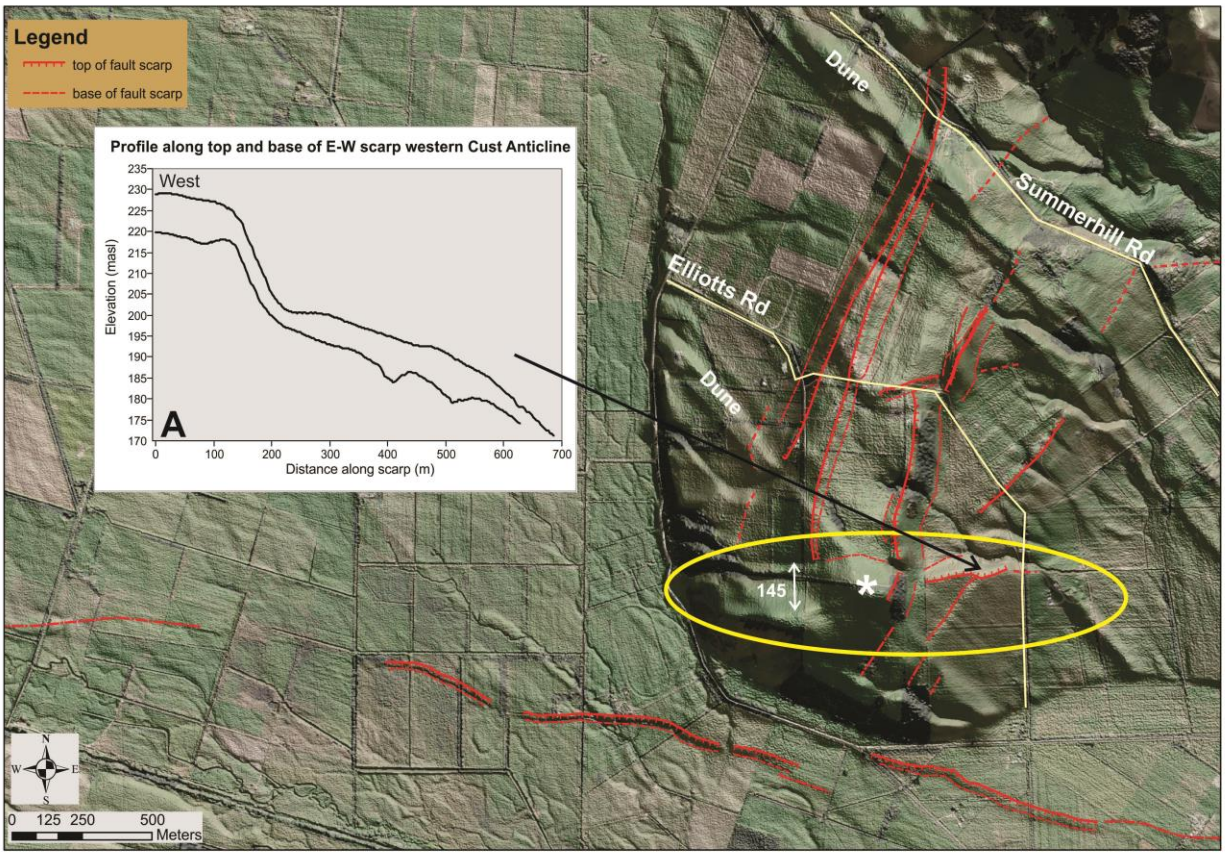

Figure 3.6. Area 4: Western arm of the Cust Anticline - E–W-striking fault trace. LiDAR image at scale of 1:15,000 with vertical exaggeration 20x. The anticline highpoint is indicated by the asterisk along with a left-step in the ridge crest location. Inset A: Profile along the top and bottom of the scarp, east of the highpoint, indicating constant displacement along its length.

The southern section of the western arm of the Cust Anticline has been mapped as Kowai Formation (Pliocene), the same unit which also underlies the older Mairaki Downs section of the

anticline (Wilson, 1989). The Arcadia-1 industry well also confirmed this stratigraphy (Indo-Pacific Energy, 2000). This area of Kowai Formation approximately coincides with the section of the western arm of the Cust Anticline south of this inferred E–W-striking fault ridge (Figure 3.6). Therefore, uplift along this E–W-striking fault could account for the presence of the older Pliocene Kowai Formation unit to the south of this ridge and the younger Plio-Pleistocene Hororata and Woodlands Formations to the north of the ridge as mapped by Wilson (1989). Alternatively, the Hororata Formation to the north of the ridge could simply represent part of a channel or could be a veneer of loess and fluvial material, deposited across the surface during more recent glacial advances. However, there is no other confirmation of these ages available.

The westward projection of this inferred E–W-striking fault and associated topographic ridge across the anticline crest appears to left-step by about 145 m around the location of the highpoint of the anticline (Figure 3.6). Although there is no direct evidence from the LiDAR, this inferred fault may extend westward and step-over onto the fault traces, outlined in the previous section, that extend westwards across to Starvation Hill. However, the E–W-striking scarp is ‘down’ to the north at this location which is inconsistent with the throw at the Glews Road paleo-seismic site (Section 3.2.3). Finally, while there appears to be mainly vertical movement on this fault a dextral transpressive slip component could be responsible in part for the apparent southwest rotation of the anticlinal axis at this location.

North-northeast-striking western scarp

The north-northeast-striking western scarp is about 1.5 km in length (Figure 3.7). The western scarp can be traced continuously along its length, cross-cutting the southeast-trending dune structure parallel to, and slightly south of, Summerhill Road. There is a relatively wide deformation ridge associated with the western scarp with the more significant west-northwest-facing scarp (height ~10−12 m) associated with the fault trace along the western edge of the anticline crest and a much more gentle east-southeast-facing scarp (height ~2.5 m) associated with the crestal structural depression (Figure 3.7C). The distance between these two scarps increases southward along the fault trace where south of Elliotts Road the main west-northwest-facing scarp dies out against the southeast-trending dune feature at this location while the deformation ridge bounding the western side of the crestal structural depression continues towards the inferred E–W-striking fault scarp (Figure 3.7).

Parallel elevation profiles, along the top and base of the length of the west-northwest-facing fault scarp indicate two distinct displacement heights with a stepwise displacement change across the southeast-trending dune structure near Summerhill Road (Figure 3.7A). North of this dune feature the displacement along the fault is about 8 m and this increases to between 10–11 m south of this feature (Figure 3.7B). This stepwise change in scarp height from north to south across the dune ridge could indicate that the surface to the north of the dune is younger and that the surface to the north was active as a younger paleo-channel after the higher aggradation surface to the south was abandoned. There is some evidence from LiDAR profiles, parallel to the fault across this section, and from ground-mapping, that this area north of the dune ridge was active as a channel that is no longer antecedent.

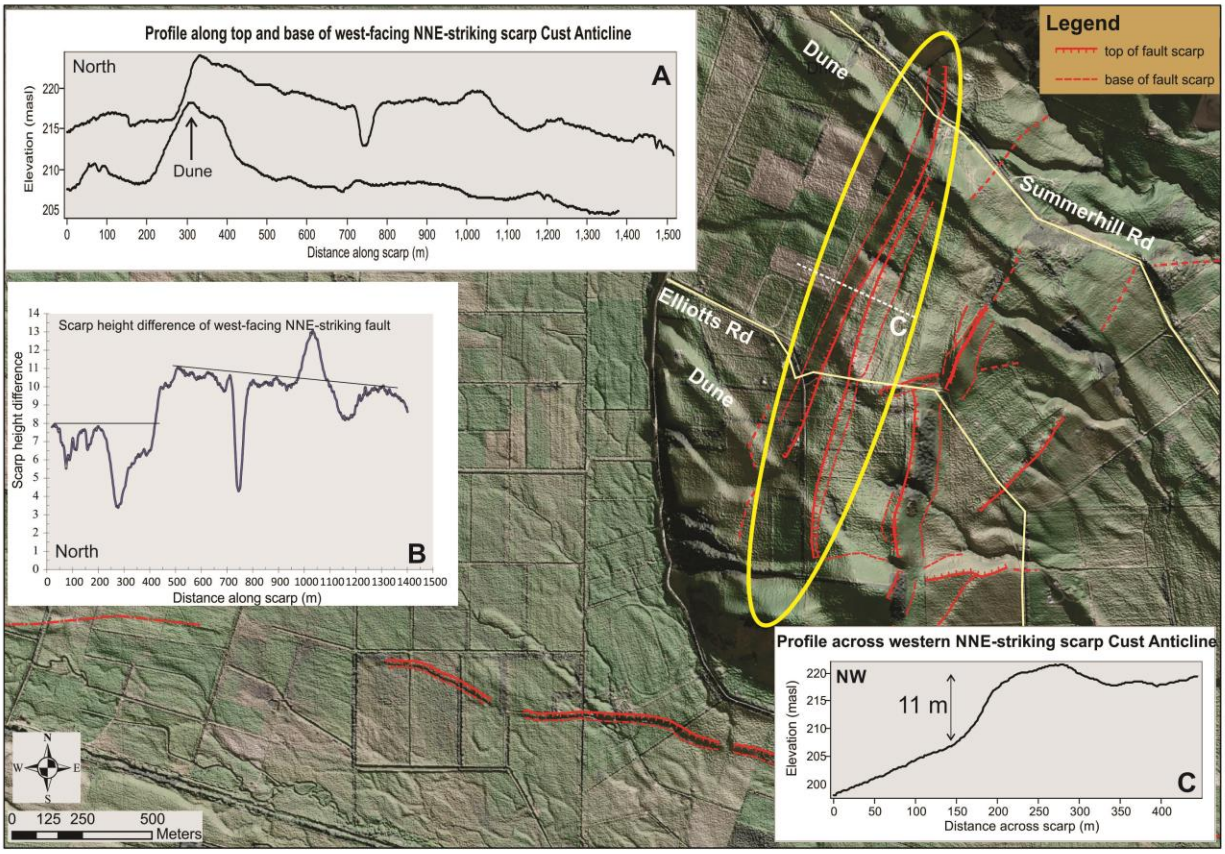

Figure 3.7. Area 4: Western arm of the Cust Anticline - north-northeast-striking western limb fault. LiDAR image at scale of 1:15,000 with vertical exaggeration 20x. The fault scarp faces west-northwest. Inset A: Parallel profiles along the top and base of the scarp indicate a stepwise decrease in the scarp height across the northern dune structure. Inset B: The difference between the top and base profiles along the scarp further indicating the stepwise change in scarp height to the north-northeast. Inset C: Profiles perpendicular to the scarp had a similar shape along the length of this fault. There is a relatively wide deformation ridge associated with the western scarp with a much more significant north-northwest-facing scarp and a much less significant south-southeast-facing scarp. The location for this profile is indicated by the white dotted line.

The stepwise decrease in displacement across the dune could also indicate interaction with a cross-cutting fault. This north-northeast-striking fault trace appears to terminate within the

region where the Cust Anticline changes regional strike from NNE–SSW to E–W. Although there is no obvious E–W-striking fault trace cross-cutting this scarp at this northern tip location the change in scarp height and its apparent termination indicates there could be interaction with the E–W-striking fault trace that is indicated south of the Mairaki Downs and which is discussed in area 5 (Section 3.2.5).

North-northeast-striking eastern scarp

The north-northeast-striking eastern scarp is a composite scarp that steps right at Elliotts Road (Figure 3.8). This eastern fault scarp, of similar length to the western fault scarp, does not appear to cross-cut the northern dune structure although subtle LiDAR expression indicates it continues to the dune's location. However, this fault does cross-cut, and vertically displaces, the E–W-striking scarp that is coincident with the highpoint on the south end of the anticline as discussed previously.

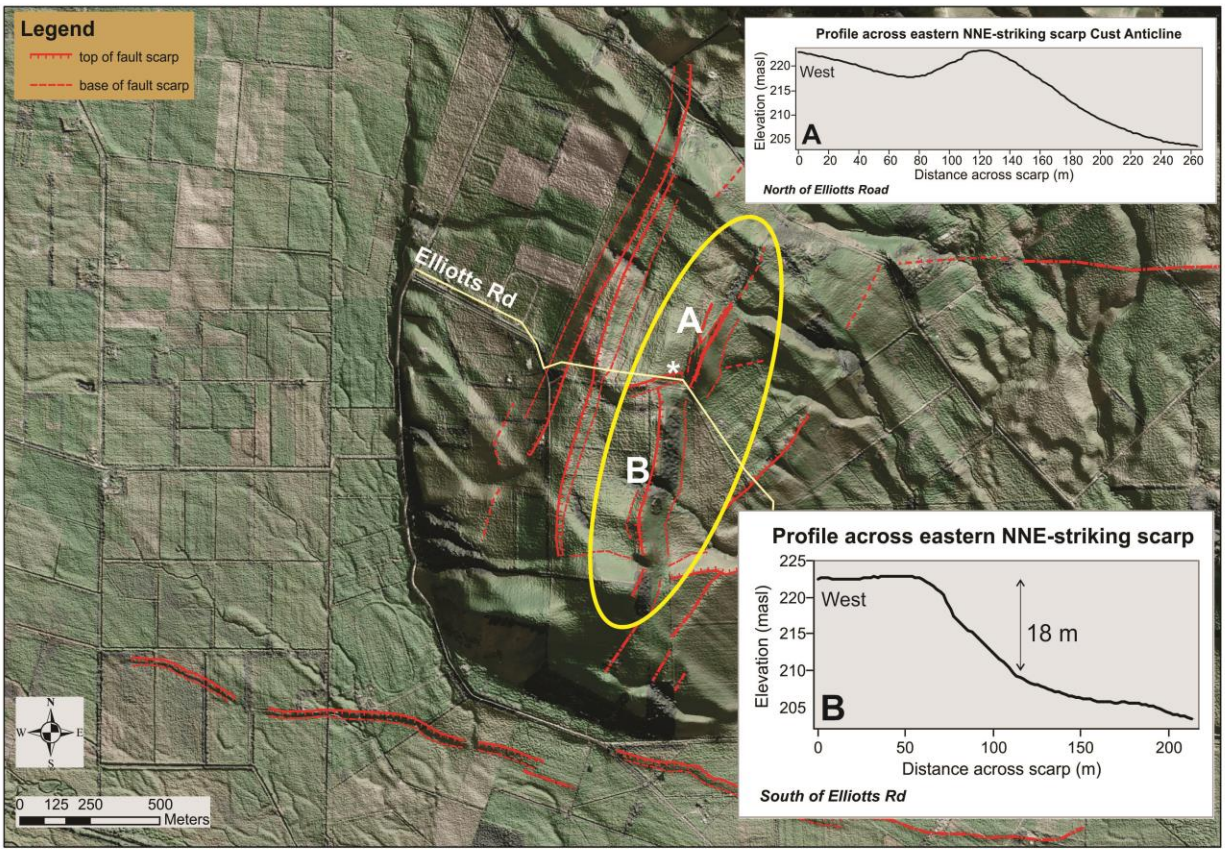

Figure 3.8. Area 4: Western arm of the Cust Anticline - north-northeast-striking eastern limb fault. LiDAR image at scale of 1:15,000 with vertical exaggeration 20x. The throw of the fault diminishes towards the north-northeast termination of the fault. The scarp height and the scarp profile perpendicular to the fault changes with location. Inset A: Scarp profiles north of Elliotts Road indicate a broad flexure ridge across the fault. Inset B: Scarp profiles south of Elliotts Road indicate a more clearly defined east-southeast-facing scarp. The location of the inferred right-stepover is indicated by a white asterisk in the main image.

The scarp profile and scarp height of this fault trace changes north–south around the location of Elliotts Road. Profiles perpendicular to the fault scarp north of Elliotts Road indicate a broad flexural ridge rather than a more characteristic sharply defined profile typical of Late Quaternary fault scarps (Figure 3.8A). Although this scarp forms a distinctive topographic feature on the eastern crest of the anticline the profile suggests that this fault may not have a high fault rupture recurrence rate in the Late Quaternary therefore forming a degraded scarp modified by erosion, slopewash and the scarp apron. The scarp height gradually increases, from its northern termination, along the trace southwards towards Elliotts Road. South of Elliotts Road the scarp height is relatively constant at ~16–18 m and profiles perpendicular across the fault define a significant southeast-facing scarp (Figure 3.8B). The height of the scarp at this location indicates that although the fault may not be very active overall this fault has a relatively long history.

The change in the scarp profile along this fault occurs at the location of a right-step on the north-northeast-striking eastern scarp which coincides with offset by an inferred east-northeast-striking fault trace sub-parallel and crossing Elliotts Road (Figure 3.8). The LiDAR expression of this secondary inferred fault trace is up to 500 m long and continues both east and west of the step-over location, being more clearly defined west of the main scarp, across the anticline crest. The apparent lateral offset of the north-northeast-striking fault is ~80 m. Interestingly, the structural depression along the anticline crest between the north-northeast-striking crestal faults is more pronounced to the north and less marked to the south of this stepover. Therefore, this inferred secondary fault could be accommodating partitioning between different styles of deformation along the eastern crest. This inferred fault scarp, sub-parallel to Elliotts Road, that offsets the eastern fault trace does not appear to offset the western north-northeast-striking fault. Therefore, it is likely forming part of a stepover affecting the eastern fault only, perhaps confined to structural complexity within the eastern fault anticline limb, or reflect a near-surface fault-driven strain partitioning or displacement transfer.

Flexural-slip faults

On the southeast limb of the anticline there are several minor lineaments across the low-slope area (Figure 3.9). On the LiDAR these are identified as shallow uphill-facing scarps of <0.5 m. The apparent curve of these lineaments across the topography of the southeast limb of the anticline indicates that they likely dip to the east. The lineaments across this low-slope zone could represent an area of shallow flexural-slip faulting, parallel to the strike of bedding, in the footwall syncline of a thrust fault (Yeats et al., 1997). Examples of flexural-slip faulting have

been shown associated with thrust faulting of the Inangahua earthquake (Anderson et al., 1994) and in other similar tectonic settings elsewhere in New Zealand (Yeats, 2000; Nicol & Nathan, 2001).

Although there is good evidence, from seismic reflection data at depth, for thrust faulting controlling the north-northeast-striking eastern scarp of the western arm of the Cust Anticline, in the present-day regional tectonic stress regime the location of this fault with respect to the surface is not clear. Therefore, it cannot be concluded that these nearby subtle lineaments are definitely due to flexural-slip faulting without further investigation. Alternatively, these lineaments may simply be resistant strata across the southeast limb where the shallow scarps have formed parallel to the strike of the folded bedding below the surficial cover deposits and are apparent in this region as a result of the asymmetric anticline limb topography. Ground penetrating radar profiles across this region, performed during the field work for the study, were not able to provide any further clarification.

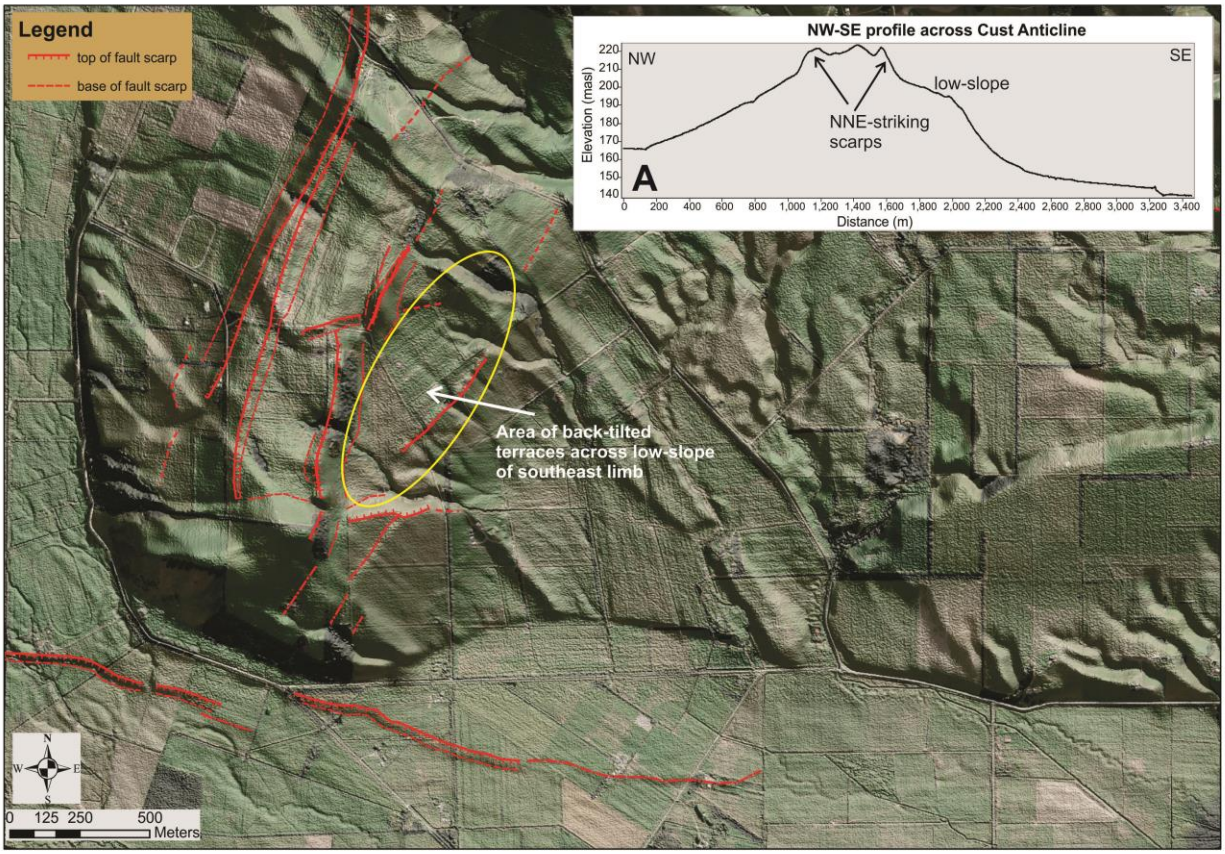

Figure 3.9. Area 4: Western arm of the Cust Anticline - low-slope zone of southeast limb. LiDAR image at scale of 1:15,000, vertical exaggeration 20x. Inset A: NW–SE profile across the western arm of the Cust Anticline. There are low-relief back-tilted terraces across this section with shallow, eroded low-relief uphill-facing scarps.

Summary of structures of western arm of Cust Anticline

LiDAR interpretation and field mapping across the western arm of the Cust Anticline indicates a broad paleo-aggradation surface across which former Ashley River channels were located. The former course of the Ashley River was eventually defeated across this surface by the progressive tectonic structural emergence of the western arm of the Cust Anticline. However, there is little evidence for progressive slip-off to the southwest and the anticline crest remains at constant elevation for most of its length before it plunges steeply at its southern end. The uplifted paleo-aggradation surface is truncated by an inferred E–W-striking fault that has resulted in an uplifted section at the southern end of the anticline before its steeply plunging termination into the northern floodplain of the present-day Cust River. The paleo-aggradation surface is also cross-cut and vertically offset by the north-northeast-striking western and eastern fault scarps which have resulted in significant throw of the crestal surface of the emerging anticline. The throw and length of these north-northeast-striking faults is similar but oppositely-facing. Slip on both the north-northeast-striking western and eastern faults along the crest of the anticline appears to be syndepositional with the dune structures across the older paleo-aggradation surface. These dunes are likely to have surface ages that are similar to the surface ages obtained for dune structures on the nearby Springbank Monocline surface (Estrada, 2003).

Based on the LiDAR interpretation of the surface fault geomorphology it is difficult to determine any relative chronology of faulting development for the north-northeast-trending western arm of the Cust Anticline. There are no consistent differences in scarp height, or any clear lateral offsets, of either north-northeast-striking scarp with respect to the inferred E–W-striking scarp. However, there is apparent vertical offset of the E–W-striking scarp by the eastern crestal fault which could indicate that this E–W-striking fault is older than the north-northeast-striking crestal faults. However, all of these faults are probably kinematically linked by stepovers and sub-parallel secondary faults such as the inferred east-northeast-striking scarp across Elliotts Road that cross-cuts the north-northeast-striking eastern fault scarp. This is to be expected with the development of the anticline in response to the present-day tectonic stress regime across the Northwest Canterbury Plains. Therefore, fold growth will be accompanied by progressive shortening and the development of associated conjugate fault sets, cutting obliquely across the anticline fold axis, will accommodate extension parallel to the axial trace. Although there are no outcrops within the study area where such structures might be able to be measured complex shallow fault sets have been associated with thrust propagated folding in other similar settings (e.g. McCalpin, 2009).

The north-northeast-striking structures are consistent with their interpretation as a stepover relay between the E–W-striking faults both to the southwest and the northeast of the western arm of the Cust Anticline. The E–W-striking Glews Road Fault (Section 3.2.3., area 3) in the Cust River floodplain immediately to the southwest of the anticline most likely ruptures co-evally with the north-northeast-striking crestal structures. Dextral shear, between E–W-striking faults immediately northeast and southwest of the north-northeast-trending anticline, may also have caused some rotation of the fault block forming the western arm of the Cust Anticline although there is very little evidence for this from the LiDAR analysis.

3.2.5. Area 5: E–W-trending Cust Anticline - Mairaki Downs

There is evidence on the LiDAR for an E–W-striking fault trace south of the Mairaki Downs on the northern edge of a former Ashley River channel (Figure 3.10). Drainage of the slopes of the Mairaki Downs show offsets consistent with a dextral strike-slip component to this inferred fault trace. Furthermore, a series of pressure ridges along the fault trace indicate possible surface rupture of the trace across younger landslide features and surfaces that overprint the more dissected relict channel surface (Figure 3.10A).

Westward this fault trace likely extends across the highly dissected surfaces towards the intersection of the northern termination of the north-northeast-striking fault scarps of the western arm of the Cust Anticline around Summerhill Road (Figure 3.10). Kinematically this E–W-striking fault should extend into the corner where the Cust Anticline abruptly changes trend from E–W to NNE–SSW. However, the E–W strike-slip component at this location might be transferred to contractional deformation on the coincident thrust faults driving up the adjacent north-northeast-striking western arm Cust Anticline structures, effectively dissipating the dextral-slip geomorphic evidence and expression of this trace.

The highly dissected topography across the southern slopes of the Mairaki Downs also makes it difficult to define any surface trace of this fault lineament further east across the ancestral Ashley River channel towards the eastern termination of the plunging E–W-trending Cust Anticline. This prominent paleo-channel has been tilted as well as uplifted as a consequence of the emergence of the Mairaki Downs section of the Cust Anticline (Figure 3.10B). Although an inferred fault is indicated on the Canterbury QMAP (Forsyth et al., 2008) extending from the

northern side of the Mairaki Downs southeast across the plunging eastern termination of the Cust Anticline there is no LiDAR surface geomorphology to confirm any tectonic structures further east of this inferred surface trace.

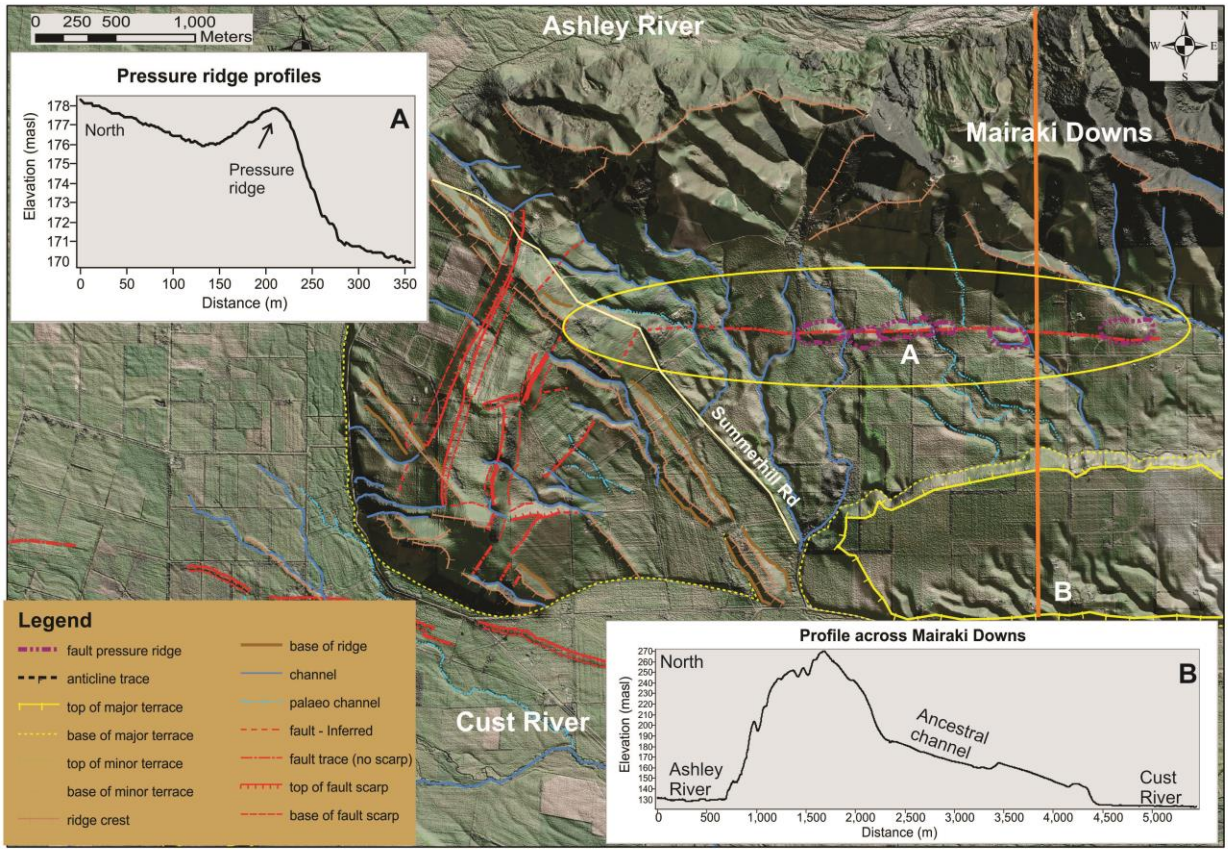

Figure 3.10. Area 5: E–W-trending Cust Anticline (Mairaki Downs). LiDAR image at scale of 1:30,000 with vertical exaggeration 20x. Inset A: A perpendicular profile across one of the pressure ridge structures indicating offset of the south-facing slope. Inset B: N–S profile across the Mairaki Downs indicating asymmetry of the present E–W-trending Cust Anticline due to erosion of the northern limb by the Ashley River. An ancestral channel of the Ashley River is evident across the south-facing slope south of the Mairaki Downs.

3.2.6. Area 6: Northeast of the Cust Anticline

Northeast of the Mairaki Downs on the north side of the Ashley River the Ashley and Loburn faults are traced across the river terraces east of the Okuku River with the northern scarp being the Loburn Fault and the southern scarp being the Ashley Fault (Figure 3.11). Although this area was not studied in detail in this project it has been well documented by previous geomorphic and paleo-seismic studies (Sisson et al., 2001) and by LiDAR profiling (Barrell & Van Dissen, 2014). East of the Okuku River the offset along the Ashley Fault is south-side down while the Loburn Fault is upthrown to the south in this location creating an emerging low-relief uplifted deformation zone (incipient structural inversion) between the two scarps. West of the Okuku River the projected strike of the Ashley Fault is inferred to cross the active floodplains of the

Ashley River north of the Mairaki Downs and an inferred trace from this projection across a small terrace indicates a fault trace north-side down at this location (Figure 3.11).

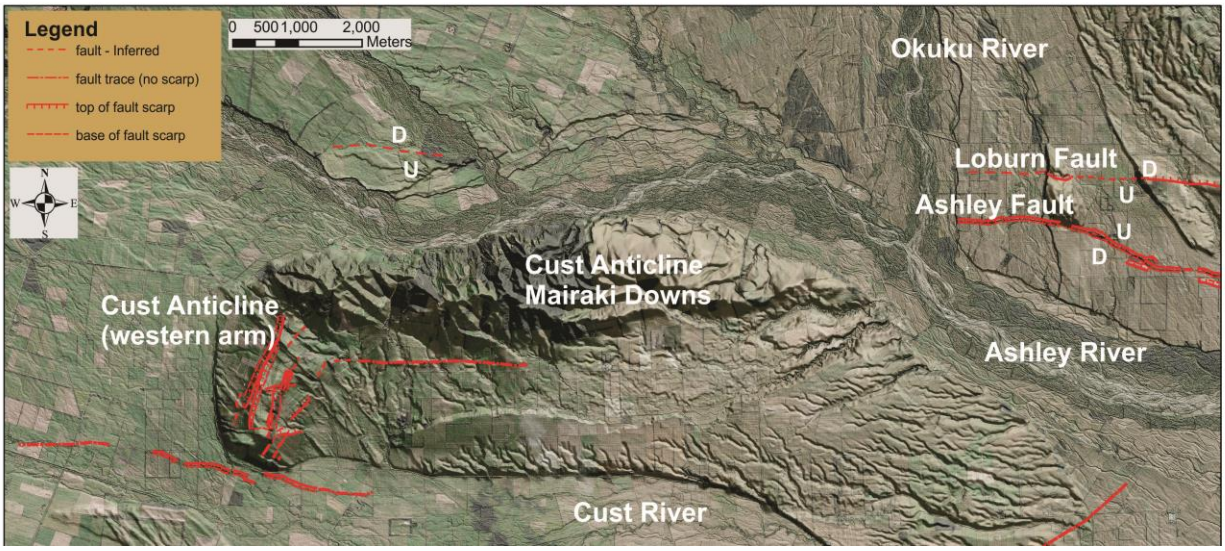

Figure 3.11. The location of the Ashley and Loburn surface faults (east of the Okuku River) northeast of the E−W-trending section of the Cust Anticline Mairaki Downs. LiDAR image at scale 1:65,000, vertical exaggeration 20x.

3.3. Summary of LiDAR interpretation

This chapter has utilised the LiDAR dataset made available for the area of North Canterbury north of the Waimakariri River. Combined with field observations at selected locations the active tectonic geomorphic expression of fault-driven structures has been detailed for the area east of Oxford around the structural culminations of Starvation Hill and the Cust Anticline and across the flat aggradation surfaces of the plains in between these topographic highs. Particular emphasis has been given to the LiDAR interpretation of the north-northeast-trending western arm of the Cust Anticline and the area immediately southwest and northeast of this region as these areas were also the subject of further detailed paleo-seismic and geophysical studies as part of this project (Chapter 4). However, deformation and landscape responses to active earth deformation across the entire study area have been described and quantified in order to establish the geometry and extent of evidence for tectonic activity associated with the surface landforms. These will be compared to structures established at depth on industry seismic lines for the area (Chapter 5).

The LiDAR interpretation has confirmed a series of E–W-striking faults between and bounding these structural culminations that are linked by north-northeast-striking faults across or around the topographic highs. These are clearly representative of the style of active earth deformation observed across the Northwest Canterbury Plains which is characterised by complex interactions

of re-activated, inherited E–W-striking faults now accommodating oblique strike-slip with northeast-striking thrust faults and associated thrust propagated anticlines (Campbell et al., 2012). This is also consistent with these structural culminations (Starvation Hill, Cust Anticline, Ashley-Loburn) being inferred to form a series of contractional pop-up structures at restraining stepovers in the newly evolving dextral shear system along the inherited re-activated basement fault zone.

The Cust Anticline is part of an elongate network of fault interactions between the established E–W-striking Ashley and Loburn fault system to the northeast and the less well-known E-W-striking fault zone defining the south margin of Starvation Hill near Oxford to the southwest (Figure 3.12). The north-northeast-striking structures are consistent with their interpretation as a stepover relay between the E–W-striking faults both to the southwest and the northeast of the western arm of the Cust Anticline. These E–W-striking faults are consistent with dextral transpressional re-activation of the inherited normal faults whereby the western arm of the Cust Anticline forms a ramp inversion structure between the Ashley/Loburn fault zone to the northeast and the Glews Road structure (Section 3.2.3., area 3, and Chapter 4) to the southwest of the Cust Anticline. Effectively this is an upper crustal scale stepover between the major dextral E–W-striking faults, whereby the Cust Anticline is a large restraining stepover forming a pop-up structure that reflects the complex interaction between the re-activated E–W-striking faults and the north-northeast-striking faults across its doubly plunging L-shaped structure. The Mairaki Downs section is interpreted as an early-stage contractional zone between two E–W-striking fault strands with significant overlap, whereas the western arm of the Cust Anticline is a late-stage broader stepover where E–W-striking faults have less overlap (this will be further discussed in Chapter 6).

The distance between the inferred E–W-striking fault south of the Mairaki Downs section of the Cust Anticline and the E–W-striking Ashley Fault trace east of the Okuku River is about 2 km (Figure 3.12). Similarly the N–S distance between the inferred E–W-striking trace south of the Mairaki Downs and the eastern end of the Glews Road trace is also about 2 km. Interestingly, the northeast-striking Springbank Fault projects south of the Ashley River across the eastern edge of the Springbank Monocline towards the Eyre River (Estrada, 2003). The Springbank Fault appears to be a longer, northeast-striking structure compared to the north-northeast-striking structures along the anticline crest of the western arm of the Cust Anticline and is likely to be a frontal thrust structure associated with the leading edge of a regional thrust block above the mid-

crustal décollement. The Cust Anticline is a structural culmination within such a regional block. However, any relationship of the Springbank Fault to the north-northeast-striking faults of the western arm of the Cust Anticline, which are about 6 km northwest of the Springbank Fault structure, have not been clearly determined.

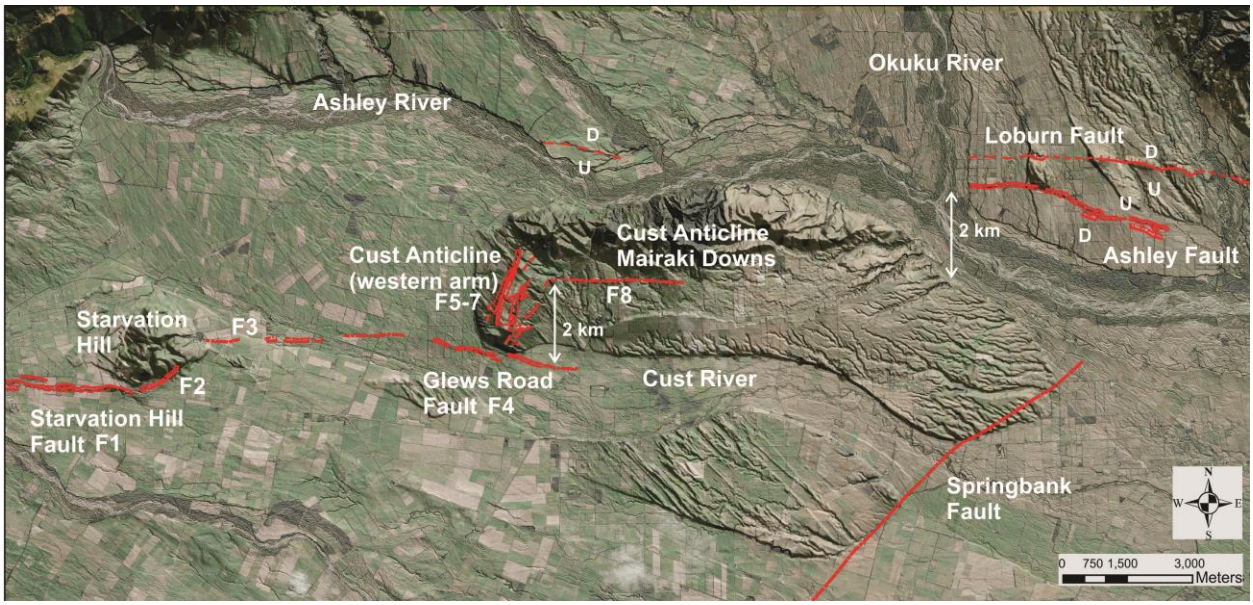

Figure 3.12. Summary of fault traces across areas 1–6. LiDAR image at scale of 1:100,000 with vertical exaggeration 20x. The summarised faults that will be discussed in the paleo-seismic and seismic chapters are labelled F1–F8. The Ashley and Loburn faults, the inferred E–W-striking fault south of the Mairaki Downs and the E–W-striking fault southwest of the western arm of the Cust Anticline are each separated by about 2 km.

In summary the LiDAR analysis has confirmed the presence of (Figure 3.12):

- An E–W-striking fault trace between Oxford and the southern apex of Starvation Hill (F1).
- A northeast-striking fault trace across the southeast-facing slopes of Starvation Hill (F2).
- An E–W-striking, non-continuous fault trace (F3) from Starvation Hill towards the southern termination of the western arm of the Cust Anticline across the Cust River floodplain (this trace was not detailed before this study).
- A definite E–W-striking fault trace (F4) immediately southwest of the Cust Anticline which was first discovered in this study and for which detailed paleo-seismic and geophysical results are presented in Chapter 4 (Glews Road site).
- Two north-northeast-striking crestal faults (western fault F5; eastern fault F6) truncated by an inferred E–W-striking fault (F7), as well as numerous minor faults, on the uplifted western arm of the Cust Anticline. These faults are indicative of this north-northeast-trending section of the Cust Anticline being a ramp inversion structure between E–W-

striking structures to the northeast and southwest. A paleo-seismic trench across the F6 scarp is presented in Chapter 4 (Elliotts Rd site).

- A low-slope area on the southeast limb of the western arm of the Cust Anticline where potential flexural-slip type faults may be located.
- An E–W-striking fault trace (F8) at the western end of the E–W-trending section of the Cust Anticline along the southern margin of the Mairaki Downs.
- The E–W-striking Ashley Fault and Loburn Fault east of the Okuku River.

A further synthesis of these structures will be presented in Chapter 6.

Chapter 4. Paleo-seismic studies

The LiDAR interpretation detected and quantified the fault characteristics of the north-northeast-trending western arm of the Cust Anticline and also discovered new multiple fault traces immediately to the southwest of the steeply plunging termination of the Cust Anticline at the Cust River (Figure 4.1 and also Chapter 3). Both the north-northeast-striking fault traces and the east-striking fault trace underpin the active tectonic deformation of the western arm of the Cust Anticline and led to the selection of two paleo-seismic trench sites for investigation (Figure 4.1). This chapter outlines the sites and the stratigraphic and tectonic interpretations from each of the trenches as well as the results of dating from materials collected.

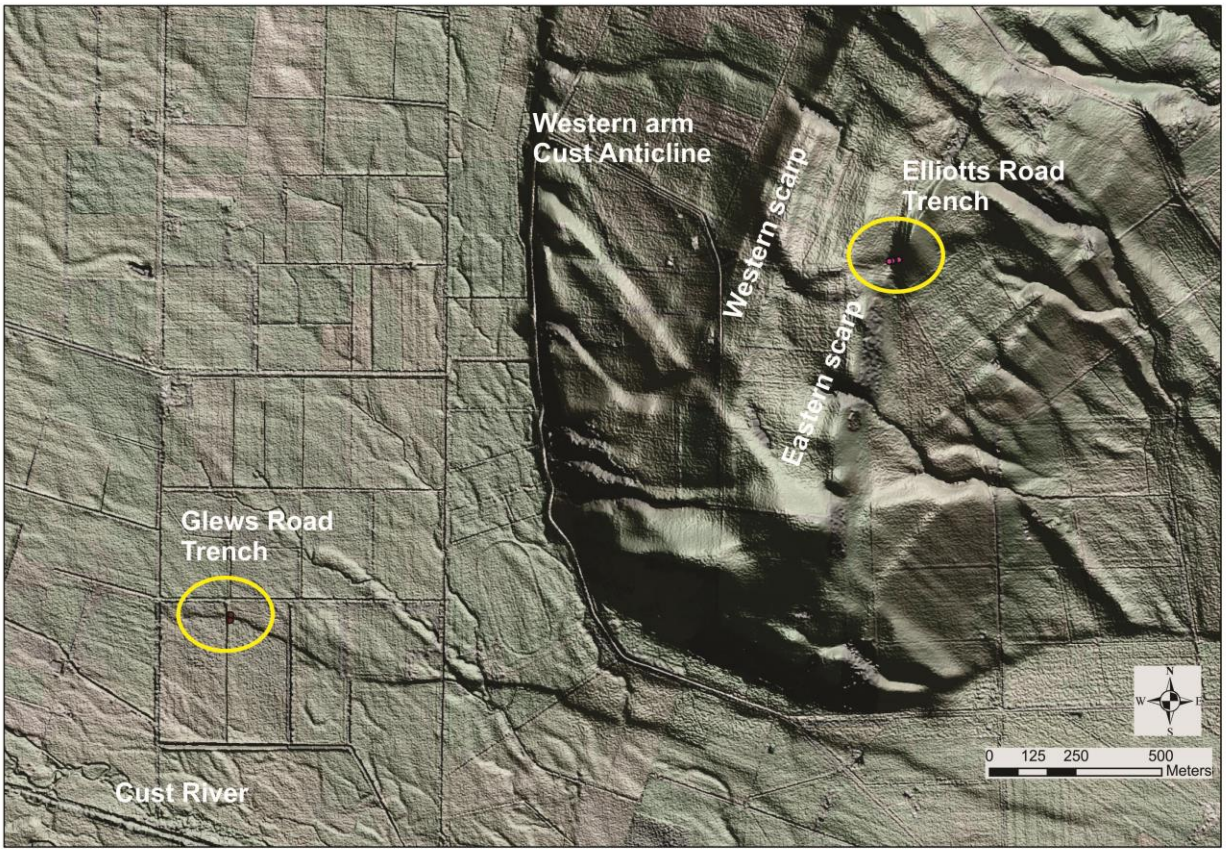

Figure 4.1. Location of the paleo-seismic study sites. LiDAR image 1:12,000 with vertical exaggeration 20x. The Elliotts Road site was located across the north-northeast-striking eastern scarp on the top of the anticline. The Glews Road site was located on an E–W-striking scarp to the southwest of the plunging termination of the anticline.

4.1. Elliotts Road trench

4.1.1. Trench location

The trench was located on the eastern scarp (north-northeast-striking) of a structural depression on the crest of the western arm of the Cust Anticline. (Figure 4.2). The trench location (E1546933 N5207739) was positioned across the centre of the fault trace rather than being

placed towards either end. Although this scarp does not exhibit a typical sharp fault-trace profile, it nevertheless forms a very distinctive topographic feature on the crestal zone of the anticline and along with the western scarp creates the distinctive structural depression, across the anticline axis, between the two north-northeast-striking western and eastern scarps (Chapter 3, Figure 3.5). The scarp height is ~4.5 m at this location and the width of the scarp across the uplifted surface is ~40 m (Figure 4.3). The surface slope angle of the trench site is around 6°. The trench was located perpendicular to the scarp (striking east) and extended from the scarp base as high up to the scarp crest as was possible (Figure 4.3B). The 27-m long trench encompassed approximately 3 vertical m of the scarp face. The west end of the trench extended into a swampy area that had formed at the base of this scarp, where the drainage along this side of the scarp had been ponded (Figure 4.3A).

Figure 4.2. Scarp location of the Elliotts Road trench on the crest of the western arm of the Cust Anticline. LiDAR image 1:8,000 with vertical exaggeration 20x. The trench is located on the north-northeast-striking eastern crestal scarp. Inset: an aerial photo of the scarp location on the western face of the fault scarp.

The trench was excavated to a depth of 1.5 m along its entire length. A further 1.5 m depth was excavated in the central 5 m of the trench, where a discordant clay unit cropped out in the base of the trench about half way along (at the 13-m location). For the upper section of the trench (depth 1.5 m) the walls were very similar on both the north and south sides. Therefore, it was decided to

extensively log only the north wall which included the deep central region. The south wall was not excavated to the 3-m depth in the central part of the trench.

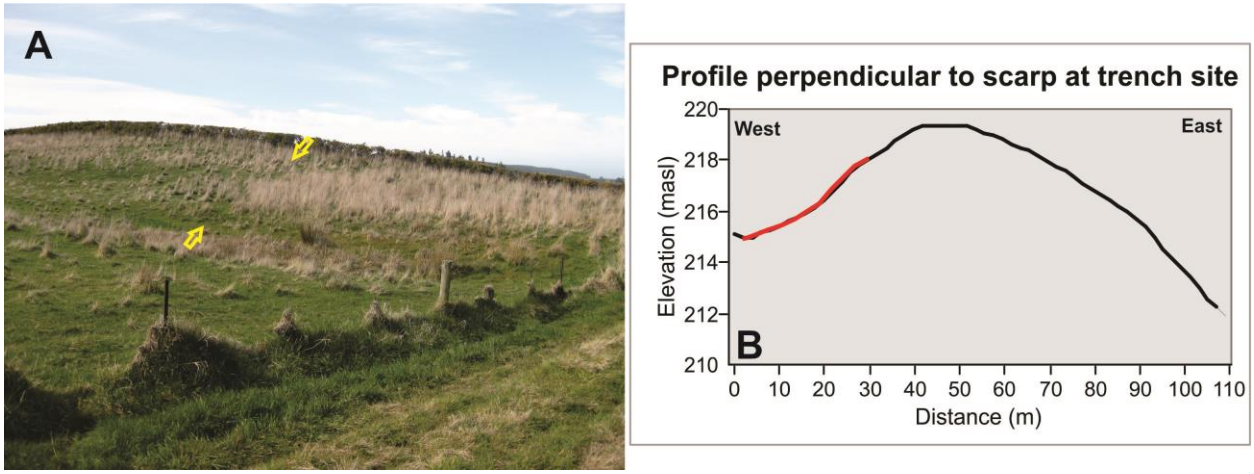

Figure 4.3. Elliotts Road scarp profile. A. Photo of the western face of the scarp. Note that the scarp varies in elevation along the scarp crest. The trench location is indicated between the yellow arrows. B. Perpendicular scarp profile from the LiDAR DTM. Although the fault scarp is a significant feature of the landscape it has a broad profile rather than a sharp characteristic profile typical of Late Quaternary fault scarps. The location of the trench is indicated by the red trace.

4.1.2. Stratigraphy interpretation

The stratigraphic units in the trench can be divided into three packages (Figure 4.4). Firstly, the oldest units (1–3) in the base of the central part of the trench. These are unconformably overlain by a second set of units (5–8) which are mainly on the east side of the trench. The youngest set of units (9–11), on the west side of the trench, overlay unconformably units 5–8 and are themselves overlain (inferred unconformably) by the youngest gravel unit (12) and the pedological soil A-horizon (13).

In the central 3-m-deep region of the trench (Figure 4.5), between 9.5 m and 14.5 m, three vertically oriented beds were observed which were the oldest stratigraphic units in the trench. The largest and oldest was a 1.3-m-wide organic clay unit (1) that extended up to about 1.2 m from the base of the central trench. This layer had unidentifiable organic remnants within the clay, however, these were considered likely to be too old for reliable radiocarbon dating. An oriented sample from this layer was obtained for scanning electron microscope analysis of potential shearing fabric and this will be discussed in Section 4.1.6.

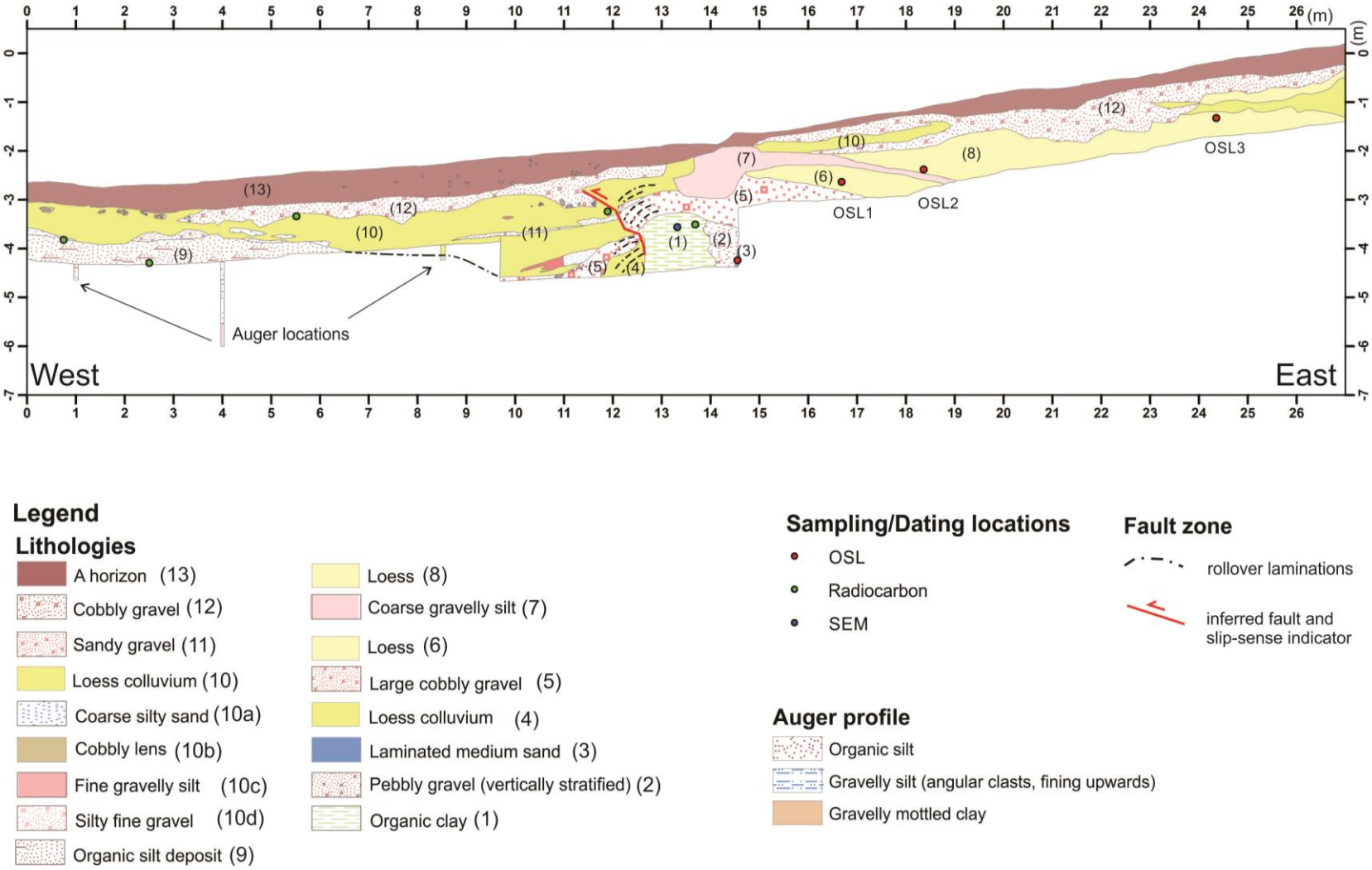

Figure 4.4. North wall of Elliotts Road trench. The oldest units (1–3) are located in the base of the central part of the trench and are overlain by the second oldest package (5–8) on the upthrown, east end of the trench. The youngest units (9–11) are located at the western end of the trench and are overlain by a cap of the youngest gravel unit (12) and present-day soils (13).

A conformable, 60-cm-wide, gravel layer (2) overlies the clay layer at the 14 m grid line. Crudely stratified, highly weathered pebbles indicate that the bed is vertical. The stratification indicates a fluvial origin for this gravel deposition and there was no indication of faulting within the limited exposure. A small exposure of laminated sand (3) overlies the stratified gravel layer about 2 m below the trench surface on the eastern edge of the central section at about the 14.5 m location. This sand layer was very saturated and formed a conduit for the water table to seep through at this location, producing about a litre per minute of seepage. This laminated medium sand layer was also vertical as confirmed by the presence of downward flowing ripple cross-laminations (way up indication to the east) striking perpendicular across the trench.

Although these three layers extended across the trench floor they could not be mapped in detail on the south side due to collapse of the south wall of the central trench during excavation. These vertically oriented beds are unconformably overlain by the subsequent stratigraphy of the trench.

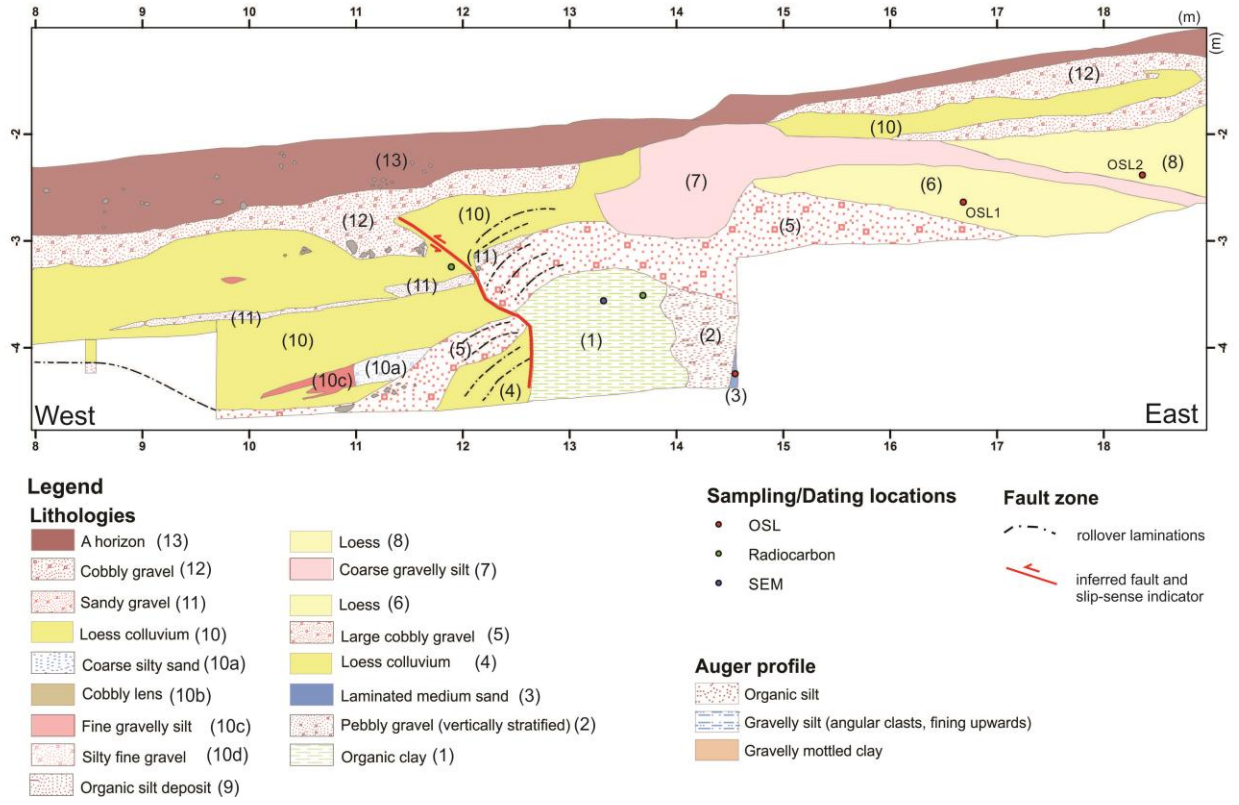

Figure 4.5. Elliotts Road trench – central section. This central section of the trench indicates a fault propagating up from the base of the clay unit (1). Note the vertical orientation of beds 1–3 and eastward-dipping unconformable growth strata (5–8). Uppermost strata (10–13) dip west. The fault trace is indicated by the red line and arrows.

A small unit of loess colluvium (4), which contained angular granule-size greywacke fragments, is present adjacent to the organic clay unit on its west side and this is in fault contact with the

clay unit. The overlying large cobbly gravel layer (5) is draped over the older vertical beds (1–3) and is inferred to represent an unconformable contact here and with the loess colluvium unit (4). This gravel unit (5) is exposed as a thin layer along the bottom of the central pit of the trench from location 9.5 to 11 m before extending above the trench floor at a moderate westward dip and across the vertical beds (Figure 4.5). The gravel unit (5) dips eastward across the vertical units on the east side of the central pit and disappears into the trench floor around trench location 17 m. On the west side of the vertical clay bed where it is relatively unconstrained by the upthrown scarp this gravel unit is sheared and offset by a fault. There is also some roll-over distortion of this unit, and moderately-defined laminations within this gravel unit, and the loess colluvium, on both sides of the offset.

On the east side of the trench (Figure 4.6) the loess deposition (6, 8) and coarse gravelly silt (7) is stratigraphically conformable and forms a package of sediments above the large cobbly gravel unit (5) that likely pre-dates the rupture of the cobbly gravel unit along the zone of shearing. These loess deposits (6, 8) are texturally different (no gravel fragments) to any of the loess colluvium units on the west side of the trench. Optically stimulated luminescence (OSL) samples of these loess sediments were submitted for dating. The slight variation within the loess unit at the far east end of the trench (location 24–27 m), with respect to the presence of gravel fragments, may represent mixing of colluvium from higher up the scarp during the ongoing loess deposition, possibly in response to a tectonic event. The loess colluvium lens (10), at location 15–19 m, within the highest stratigraphic cobbly gravel (12) east of the fault shear zone may be related to the more extensive unit of similar composition (10) across the fault zone further west along the trench, although the amount of gravel fragments appeared less extensive in the unit to the east. The exact interpretation of the trench units below the pedological soil A-horizon (13) was difficult to distinguish between location 13.5–15 m due to the height and extent of the trench wall, however, unit 10 is not in stratigraphic sequence with respect to the lower package of units (5–8) on the east side of the trench (Figure 4.5).

The dips of the loess and coarse gravelly silt layers on the east side of the trench become shallower towards the east, indicative of these being growth strata against the vertical beds due to episodic tectonic uplift of the vertical beds. Ground penetrating radar (GPR) surveys along the eastern trench (location 16–24 m) indicated that these units extended at least a further 1.5 m below the trench floor towards a lower boundary layer and confirmed the decreasing dips of these beds (Figure 4.7).

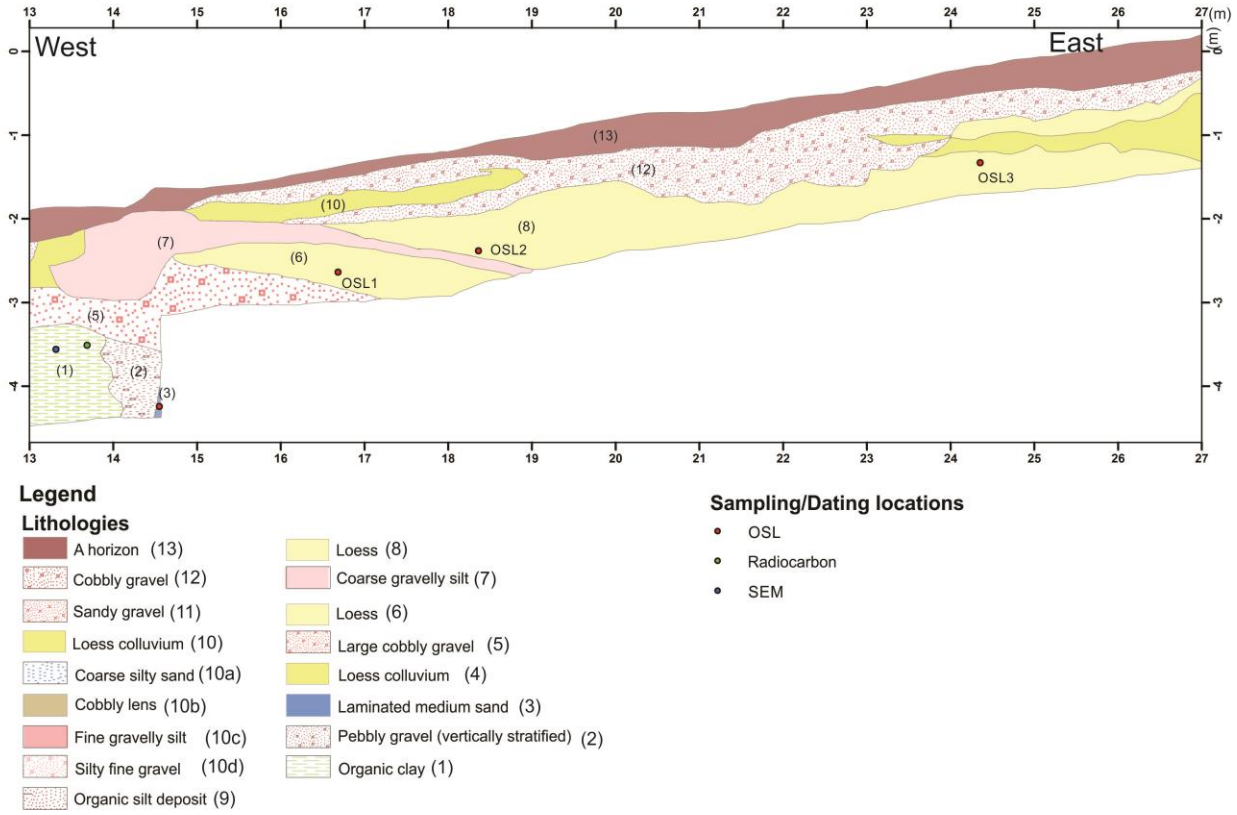

Figure 4.6. Elliotts Road trench – east end. The gravel and loess units (5–8) are inferred to represent an unconformable contact across units 1–3 and form growth strata dipping to the east. The youngest gravel (12) is unconformable across units 5–8 and overlies the younger units (9–11 not shown) on the western side of the trench.

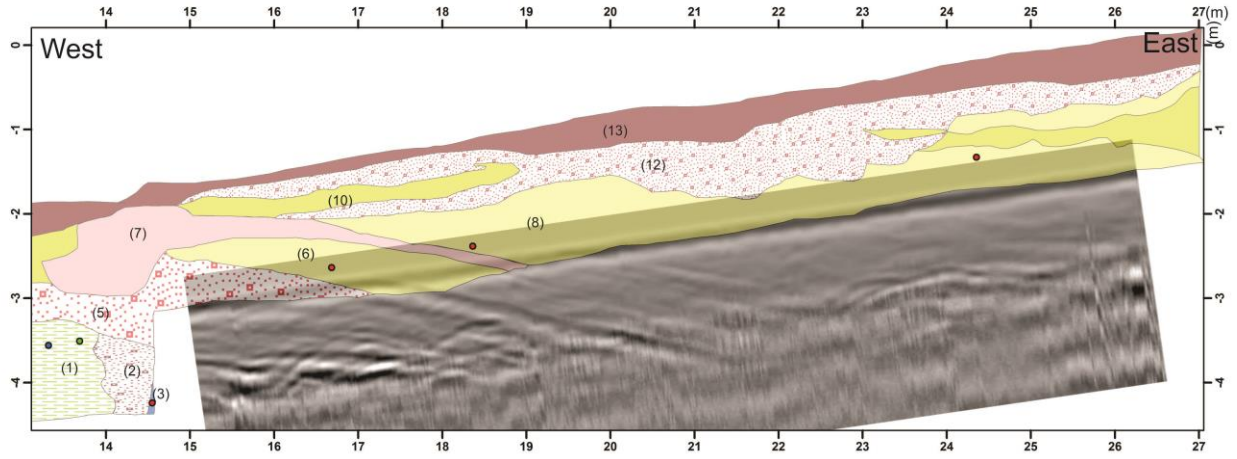

Figure 4.7. Elliotts Road trench – east end with GPR. Stratigraphic units are as indicated in Figure 4.6. The GPR profile confirms the dip direction and extension of the loess and gravel units down to a deeper bounding layer.

The organic silt deposit (9) to the west of the trench centre (Figure 4.8) is shown from augering to extend below the floor of the trench down another 1.25 m, through lenses of cobbly silts, into a lower layer of mottled very wet clay (base of auger 1.9 m below trench floor). Therefore, on

the west side of the trench the loess colluvium and sandy gravel layers (10, 11) are underlain by organic silt deposits. Given their stratigraphic location these organic silts could uncomformably overlie at depth the sheared and displaced large cobbly gravel layer (5).

The ongoing deposition of the unconformable loess colluvium unit (10) on top of the displaced large cobbly gravel (west side) is interbedded with fine gravelly silts as well as smaller lenses of sandy gravels, silty sands and silty fine gravels (10a–10d) which may represent local influxes of material into this topographically lower region associated with the scarp, away from the fault plane (Figure 4.8). All of these lenses are probably not associated with tectonic events and some may represent the effects of alluvial processes.

The loess colluvium is substantially thicker on the west side of the trench with only a thin lenticular layer of loess colluvium, within the highest stratigraphic gravel unit, on the east side of the trench between 15–19 m along the trench. The gravel nature of the loess colluvium was less marked on the east side of the trench compared to the west side. Loess was not observed on the west side of the trench.

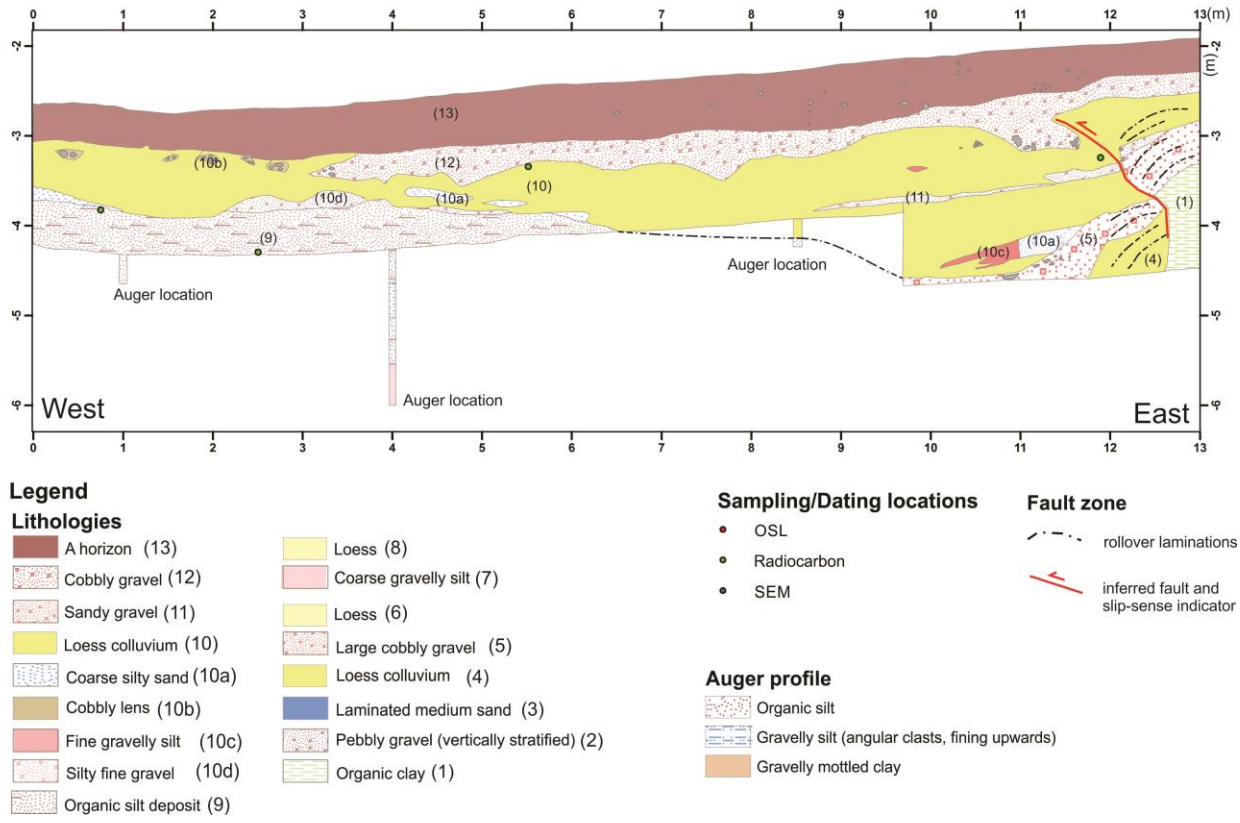

Figure 4.8. Elliotts Road trench – west end. Units 9–12 represent the youngest package of sediments in the trench stratigraphy.

A thin sandy gravel (11), at trench location 9–12 m, within the main loess colluvium layer (10) also appears to have been disrupted and may represent a younger displacement event within this fault zone. The uppermost cobbly gravel (12) could represent colluvial deposition however its exact genesis is uncertain. The fault zone does not obviously cause any offset within this unit although, interestingly, this gravel layer is thicker on the west side of the underlying projected shear zone (Figure 4.8). The entire stratigraphic sequence is unconformable with the modern pedological soil A-horizon (13) which is draped across all the older layers and thickens on the western, downthrown side of the trench.

4.1.3. Auger interpretation

Initial augering at the trench site, before trench excavation, has been interpreted and located on the western end of the trench log (Figures 4.4 and 4.8). These locations correspond to trench locations at around 1 m and 8.5 m and complement the auger obtained from the trench floor at location 4.5 m. The auger location at 1 m indicated three main units which corresponded to the relative depths of the A-horizon, loess colluvium and organic clay observed in the trench. No gravel units were found at this location. The auger location at 4.5 m confirmed that the organic clay extended well below the trench floor and was interspersed with gravelly silt before becoming a gravelly mottled clay at depth. The auger location at 8.5 m indicated an upper unit that corresponded with the observed relative depths of the A-horizon followed by a silty gravel unit that corresponded with the loess colluvium unit. No significant gravel unit was found during augering at this location although similar locations near this site could not be augered due to the presence of subsurface gravel lenses. The auger at this location also indicated that the loess colluvium extended for a further 0.2 m below the trench floor and overlays an organic clay. The augering and trenching clearly indicate that the loess colluvium thickens towards the fault, from <1 m up to ~2 m beyond trench location 6.5 m. An auger location at approximately trench location 20 m intersected only the soil A-horizon and impenetrable gravel, probably unit 12, at 35 cm below the surface.

4.1.4. Tectonic context of trench site and interpretation

The north-northeast-trending, south-plunging western arm of the Cust Anticline is located at the western end of the east-trending older section of the Mairaki Downs (Figure 4.9; see also Figure 3.12). On the north side of the Ashley River, to the northeast of the Cust Anticline, are the Ashley and Loburn faults. An inferred E–W-striking fault trace on the south side of the Mairaki

Downs (LiDAR fault F8) extends westwards, to the location of the change of strike from E–W to NE–SE of the Cust Anticline, and appears to intersect where the north-northeast-striking eastern and western fault scarps (LiDAR faults F5, F6) die out. Southwest of the steeply plunging termination of the Cust Anticline, on the north side of the Cust River, an E–W-striking fault trace is located (LiDAR fault F4) which is the site of the second trenching study discussed in Section 4.2. The distance between these E–W-striking fault traces is about 2 km at each left stepover from the northeast to the southwest across the Cust Anticline (Figure 4.9). This indicates that the Cust Anticline has developed as a restraining stepover as the E–W transpressive strike-slip faults relay across various splays at depth in the subsurface. The western arm of the Cust Anticline structure is driven by reverse faults offsetting Paleogene, Cretaceous and Torlesse basement units at depth (Chapter 5). Interestingly, the seismic reflection data also indicate that the Oligocene strata are downdropped in the centre of the western arm of the Cust Anticline most likely due to Late Pleistocene–Holocene faulting and folding.

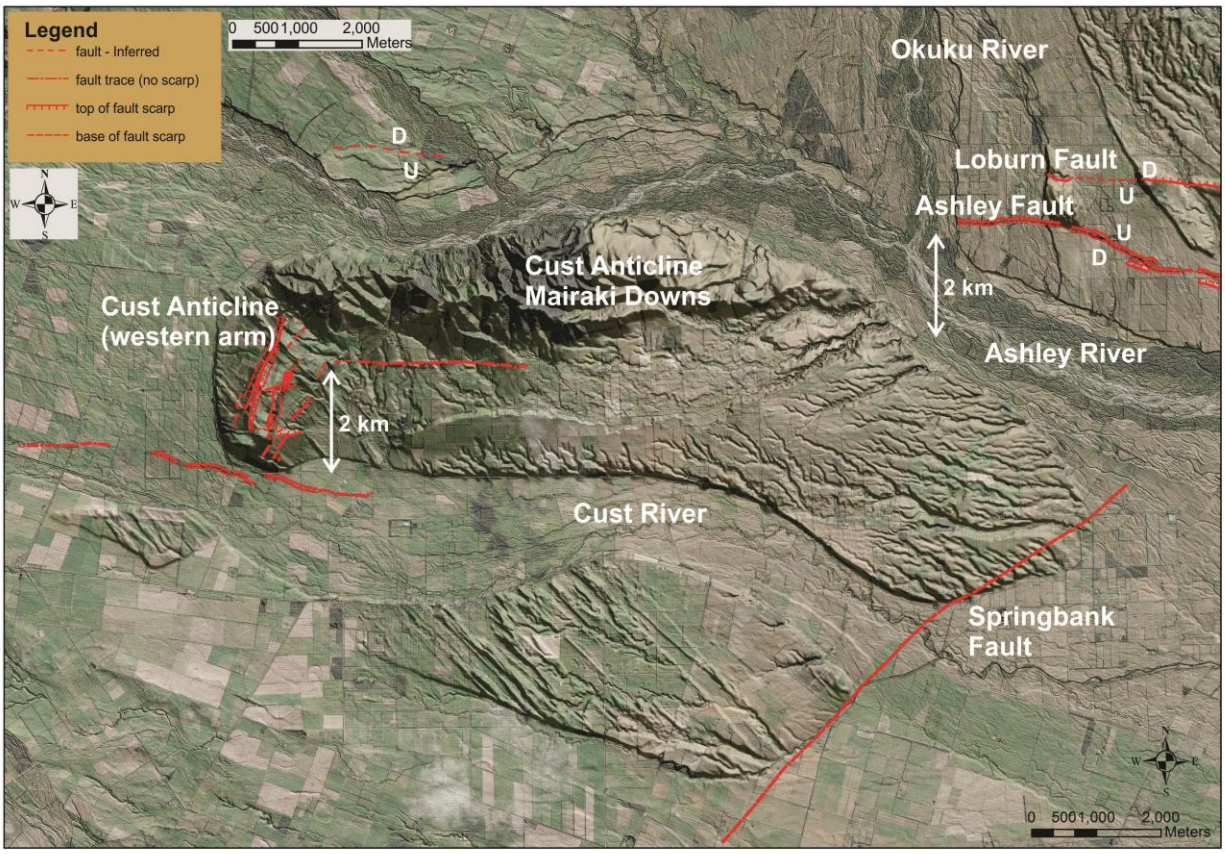

Figure 4.9. Location of known and inferred faults across the Cust Anticline region. These have been determined from previous studies as well as the LiDAR interpretation discussed in Chapter 3 and shown in Figure 3.12.

The development of the western arm of the Cust Anticline has been driven by a combination of folding and thrust faulting within the Quaternary units in response to re-activated E–W-striking faults in basement and cover sequence units and newly developed north-northeast-striking thrust

faults. The trench is located within the hanging wall of a deeper bounding reverse fault but the stratigraphy within the trench itself indicates the presence of distributed shear on shallow Late Pleistocene–Holocene near-surface faults within units significantly younger than the stratigraphically oldest units (Plio–Pleistocene) within the trench. Therefore, the eastern and western north-northeast-striking faults, that are responsible for the crestal structural depression apparent across the western arm of the Cust Anticline, could be shallow non-seismogenic faults, related to the fault propagated folding and structural contraction of older units in response to seismogenic fault rupture of the major thrust faults bounding the western arm of the Cust Anticline. Flexural-slip faulting within the near surface may also be present but would likely only extend into the subsurface a few hundred metres.

The organic clay, stratified gravel and laminated sand (1–3) would have originally been laid down horizontally and have subsequently been tilted into a vertical orientation. This could be due to reverse motion on a deeper blind fault causing a fault propagated anticlinal fold of these layers within the hanging wall. The relative amount of tectonic activity must have been substantial, or occurred over a significant length of time, to result in tilting to the vertical. The vertical orientation of these beds most likely facilitates ongoing vertical shearing along these bedding planes during subsequent tectonic events within the present regional stress regime. Although there was no indication of shearing upon excavation between the clay and stratified gravel units the relative height of the clay unit to the gravel unit and the upwards extensional shape of the clay unit suggests that the clay is probably acting like a diapiric intrusion during tectonic events.

The vertical orientation of the oldest three units (1–3) within the trench is therefore likely due to significant thrust propagated folding. Within the trench the dip of the beds to the east (6–8) indicate growth strata in response to more recent folding and faulting events. The dip of the loess and gravel layers slightly reduces eastward away from the vertical units indicating that the subsequent sedimentation rate was greater than the uplift rate during deposition of the growth strata. As the vertical units are pre-growth strata then the unconformity (between units 1–3 and units 5–8), created by erosion of the vertical beds, could represent the onset of folding of the growth strata, however evidence from the trench with regards to the age and length of this unconformity is equivocal. Ongoing vertical intrusion of the older units may also have affected the dip of the growth strata.

The younger Late Pleistocene–Holocene deposits (9–12) appear to be draped across the highpoint created by the vertically tilted beds (1–3) and the eastern trench units (5–8) and become thicker further west from the fault displacement zone. The A-horizon also becomes thicker westward along the trench wall. The organic silt at the base of this sequence, in the west side of the trench, likely represents swamp deposits associated with the anticlinal structure created by the rotated and vertically tilted beds and ongoing uplift of the topographic scarp.

The fragmented-granular nature of the loess colluvium within the youngest package of units may be due to disrupted fine gravels being incorporated downslope of the scarp subsequent or during an event. The relative age of the loess colluvium on the west side of the trench will be younger than the loess on the east side of the trench given the unconformity between the loess and large cobbly gravel units (5–8) with the overlying series of units (9–12).

Two possible tectonic displacement events indicate reverse displacement along an east-dipping distributed shear zone. This trace displaces the unconformable gravel unit (5) overlying the vertically tilted units and also displaces a younger shallower dipping thinner gravel unit (11) within the ongoing loess colluvium deposition (10). The displacement amount of the deeper gravel unit is greater than the shallower gravel lens (which indicates the possibility of there being two events recorded on the older gravel unit). Therefore, the tectonic events displace the large cobbly gravel unit (5), that is uncomformable above the vertical beds, as well as the loess colluvium sediments (10) and the gravel unit (11) within the loess colluvium.

The distributed shear zone continues up to the base of the stratigraphically highest gravel unit (12). This upper gravel unit appears to be draped across the displacement zone and is thicker on the west side of the trace due to movement of the gravels into this area of increased depositional accommodation. However, the fault trace does not appear to displace the highest gravel unit (12).

4.1.5. Radiocarbon and OSL dating

Radiocarbon material for dating was sparse within the loess colluvium and gravel layers of this trench. The oldest organic clay unit (1) had organic material up to a few centimetres present within it, however, this layer was considered too old for radiocarbon dating purposes. An oriented sample of this clay was collected for scanning electron microscope (SEM) analysis of shear fabric and the organic components were also investigated using the SEM (Section 4.1.6).

Some radiocarbon material (organic matter sieved from the soil) was located within the main loess colluvium unit (10) just above the displaced thin layer of silty fine gravel (11) near the displacement zone (Figure 4.4). This sample was submitted for radiocarbon dating as it could represent an age for recent faulting events that displaced the unconformable cobbly gravel unit (5) overlying the vertical beds and the fine gravel unit (11) within this loess colluvium. These faulting events must have occurred after the middle package of units (5–8) were deposited which indicates that the shearing only localised on the clay recently, since it is was overturned. Any further constraints on the timing of these faulting events could not be obtained due to the lack of organic material within the trench.

The results of the radiocarbon dating were equivocal. The age for the sample, representing an age of recent faulting events, was 975 +/- 23 yrs BP. This age is relatively young for a recent faulting event within this trench as the scarp profile and evidence from the trench does not necessarily indicate a tectonic event as recent as this. Therefore, perhaps this radiocarbon material was not in situ but contained contaminated organics from surface layers. If the organic material was in situ it suggests that there was a significant time period for the development of the unconformity between the middle package of units on the east side of the trench and the youngest package of units on the west side. Alternatively, it suggests that the thickness of the youngest package of units might be greater than what was observed in the trench, or that there are other units, missing within the stratigraphy, that are not represented due to erosion on the upthrown side of the scarp. Although augering indicates that the organic silt extends below the trench, neither of these explanations could be further tested from the data, and therefore the timing of any recent tectonic events remains poorly constrained.

OSL dating samples were obtained from the loess units (6, 8) on the east side of the trench (Figure 4.4). These samples should provide an age of deposition for these units. The oldest age (location 16.5 m) should represent an age for the onset of deposition of the lowest loess unit. The third sample (location 24 m) would give an average age of deposition of the loess unit that lies below the unconformity with the higher stratigraphic units on the west side of the trench.

The age of the OSL samples were dated as between 61–91 ka (Table 1). This indicates that the age for the loess deposition decreased with higher stratigraphy although the error bars for the

ages would indicate that the age difference could be essentially zero up to around 20 ka from the base to the top of the loess units. The middle sample (91.1 ka) is significantly higher than either of the two bounding samples.

One reason for an excessively older age is due to incomplete bleaching prior to deposition however, this is unlikely for windblown loess material. Although the water content in a sample can reduce the dose rate (and increase the age), the time of collection was the same and so even though the sample sites were wet when the trench was opened and then dried out before collection this was a constant factor for all samples and should not have had a differential effect on the middle sample over the others. Furthermore, there was very little chance that any significant light exposure occurred during sampling to reduce the dose for either the top (OSL3) or base (OSL1) loess samples and thus return a younger than expected age for these samples.

Field code	a-value	Water content (%)	Equivalent dose (Gy)	Dose rate (Gy/ka)	Luminescence age (ka)
OSL1	0.05 +/- 0.02	20.4	279.99 +/- 5.00	3.96 +/- 0.30	70.7 +/- 5.4
OSL2	0.05 +/- 0.02	20.4	337.95 +/- 4.52	3.71 +/- 0.29	91.1 +/- 7.2
OSL3	0.05 +/- 0.02	18.3	218.16 +/- 3.97	3.57 +/- 0.28	61.1 +/- 4.8

Table 4.1. OSL results from the Elliotts Road trench.

Interestingly, both the OSL1 and OSL2 samples have equal water contents. However, the oldest sample (OSL2) has the highest, not the lowest dose of the two samples, and so maybe some contamination increased the dose in the middle sample. The most likely explanation is that the weathered gravels (7) were too close to the second sample and that some of this gravel material was incorporating older material into the middle sample and enhancing the dose.

Given the above explanations it is likely that the younger ages (61–71 ka) are realistic ages for the loess deposition. These ages correspond with the early Otiran glaciation (Barrell, 2013) which corresponds to the marine isotope stage 4 (Ehlers et al., 2011). The older age of 91 ka (MIS5b) is also within a relative glacial period. However, the glacial time period from120–80 ka was on average not as cold as the period from 75–20 ka and a recent report has considered this period to perhaps be part of the last interglacial (Barrell, 2013). Significant loess deposition occurs during glaciation periods and is not associated with interglacial periods. Therefore, the

second package of sediments, unconformably above the three oldest vertical units, are likely of an age range between 61–71 ka which corresponds to the timing of the last significant glacial period in Quaternary New Zealand stratigraphy.

4.1.6. Scanning electron microscope analysis

An oriented sample of the clay unit (1) was obtained for analysis under the scanning electron microscope in order to determine if there was any evidence for vertical shearing within the fabric of the material. Three small pieces from the top, middle and lower part of the sample were mounted maintaining their orientation markers. They were dehydrated slowly up to 75% before microscopy. During this process it was important to try not to create any artefacts from the processing that could mimic any shearing fabric.

Overall there was no convincing evidence of a shearing fabric within the samples although it is possible that the long axis of some of the individual clay particles and detrital mineral grains had an alignment oriented north-northeast with respect to the orientation of the sample. Microscopy did confirm the presence of plant material and residual organics within this clay unit. The plant material present, although quite fragmented, appeared to be woody tissues that were not related to present-day material and that were in situ and unlikely to be remnants filtered down from somewhere else. There was also some possible evidence of broken clay particles being infilled with organics along northeast-oriented lineations.

An interesting observation of the samples under the SEM was that the grains and particles were often ‘infilled’ by a very fine grained enveloping material (or coating) as if some sort of mesh had flowed around everything. This effect was quite pervasive throughout the mounted samples and appeared as if it could have been injected through and encapsulated around the clay particles and then precipitated out over time. It did not appear to be a processing issue with the samples. This could represent an effect due to squeezing and intrusion of material through this clay unit during periods of high stress and pressure associated with tectonic events.

4.1.7. Elliotts Road trench summary

This paleo-seismic trench site, on the crest of the western arm of the Cust Anticline, resulted in a useful structural interpretation of the eastern crestal fault scarp and established that the

subsurface units span a significant period of the Quaternary. The presence of the older, vertically oriented, Pliocene units established the presence of a long standing blind fault that has had considerable activity during the Late Quaternary to cause the fault propagated folding into a vertical orientation of these older units.

Unconformably above the vertical beds is a second set of units, with OSL ages of between 71–61 ka for the base and top of the loess packages respectively, that were likely deposited during the early Otiran glaciation (Barrell, 2013). The second (middle) package of units is overlain by the youngest package of units which are unconformable with respect to the middle package. The Kowai Formation and underlying Miocene strata and Oligocene limestone units have similar amounts of folding, revealed by the seismic reflection profile here, indicating that the folding is probably all post-Kowai Formation (Pliocene) deposition (Chapter 5). As the vertical units (oldest package) within the trench are pre-growth strata (middle package: loess and gravels of east side of trench) then the angular unconformity above these oldest units may represent the onset of folding of the growth strata. However, the relatively shallow dips of the loess units in the trench may indicate that they have simply been draped across existing folded and uplifted topography. Furthermore, there may be older gravel packages not revealed within the trench; these might be indicative of folding deformation and ongoing uplift over a longer time period. Therefore, the OSL ages from these units, while representative of when these loess units were laid down, are not necessarily unequivocally representative of when subsequent folding and uplift was initiated with respect to the older vertically tilted Pliocene units.

The age of the paleo-aggradation surface across the western arm of the Cust Anticline (consisting of Pliocene Kowai Formation gravels) is uncertain but has previously been considered to be older than the subsurface loess ages obtained in this study. This surface has been suggested to be as old as the third-to-most-recent ice age ending about 250,000 years ago (Barrel & Begg, 2013). However, this would give very slow uplift rates associated with this structure for the 50–60 m of surface elevation of the western arm of the Cust Anticline, and therefore provides a minimum uplift rate. For the loess ages obtained (71–61 ka) from the trench, using a fold amplitude of around 50 m, a maximum uplift rate of ~0.7–0.82 mm/yr is calculated, assuming that no uplift above the Canterbury Plains datum had previously occurred. Although similar uplift rates have been shown elsewhere in North Canterbury (e.g. Nicol et al., 1994; Litchfield et al., 2014) the inability to constrain the timing of the unconformity above the oldest units in the trench and correlate this with regional interpretations makes this much higher uplift

rate across the western arm of the Cust Anticline somewhat speculative. Uplift rates on the nearby Springbank Monocline surface have been considered between 0.1–0.22 mm/yr using surface ages ranging from 250,000 years (Barrell & Begg, 2013) to slightly less than 100,000 years (Estrada, 2003), respectively. Therefore, an uplift rate between 0.2 and 0.7 mm/yr is likely, however, further constraints on the age of the older vertical units within the stratigraphy and the age of obvious surface structures (i.e. the paleo-dunes) would be necessary to accurately constrain uplift rates of the western arm of the Cust Anticline above the Canterbury Plains datum.

During the deposition of the youngest package of units there has been at least one and possibly two tectonic events within a distributed reverse sense shear zone that extends from the base of the vertical clay units to below the present-day youngest stratigraphic gravel unit. The most recent co-seismic rupture events likely involve both vertical bedding-parallel slip on the upturned older beds along with reverse shear within the younger near-surface units. A lack of datable material and the single radiocarbon date obtained from within units associated with these offsets did not allow timing of these events to be highly constrained, however, given the scarp profile the fault is not considered to be highly active. Furthermore, the displacements in the trench were relatively small (10's cm) and therefore these small displacements could be hidden at the surface by the topography of the scarp.

The structural and stratigraphic interpretation of the trench, along with the subsurface ages, provide a framework for the present-day active tectonics of the western arm of the Cust Anticline and constrains the relationship of the crestal faults with the geomorphology observed across the western and eastern limbs of the anticline both on the LiDAR and in the field. However, the complexity of the trench and the equivocal results from dating highlight further questions that need to be investigated.

4.2. Glews Road trench

The second paleo-seismic site is located to the southwest of the western arm of the Cust Anticline at the projected eastern end of the fault trace between Starvation Hill and the Cust Anticline (Figure 4.10). This fault trace has not previously been documented in any publications, and was first identified using the LiDAR interpretation as discussed in Chapter 3. Ground penetrating radar (GPR) surveys and auger profiles were performed prior to trenching to confirm the scarp was due to faulting and not fluvial processes. The eventual trench site was chosen to maximise the chances of fault location in an undisturbed setting and was also based on access and landowner consent.

4.2.1. Trench location

The trench was located across an E–W-striking, south-facing scarp that was upthrown to the north (E1545040, N5206721). The overall length of the visible fault trace is approximately 3.2 km, extending westwards from the steeply plunging termination of the western arm of the Cust Anticline across the abandoned terraces on the north side of the Cust River. The trench was located within a swampy paddock towards the western tip of this fault scarp (Figure 4.10). Augering of the fault scarp to confirm this paleo-seismic location prior to trenching was performed 180 m east of the trench location and will be discussed subsequently in Section 4.2.5.

The trench was excavated perpendicular (N–S) across the scarp to a depth of around 1.5 m and benched on the western side. The trench location meant that the gravels were saturated and therefore the trench walls were unstable, even during excavation. At the base of the trench on the northern end a spring was unearthed and contributed to the instability, owing to the high volumes of water that were constantly filling the trench. Along the eastern trench wall the region around the fault deformation zone was more unstable than wall locations away from this zone confirming the tectonic disturbance near the fault. The fault deformation zone began collapsing by the end of the first day and overnight the east wall had significantly slumped but the west wall (benched) remained intact until the third day.

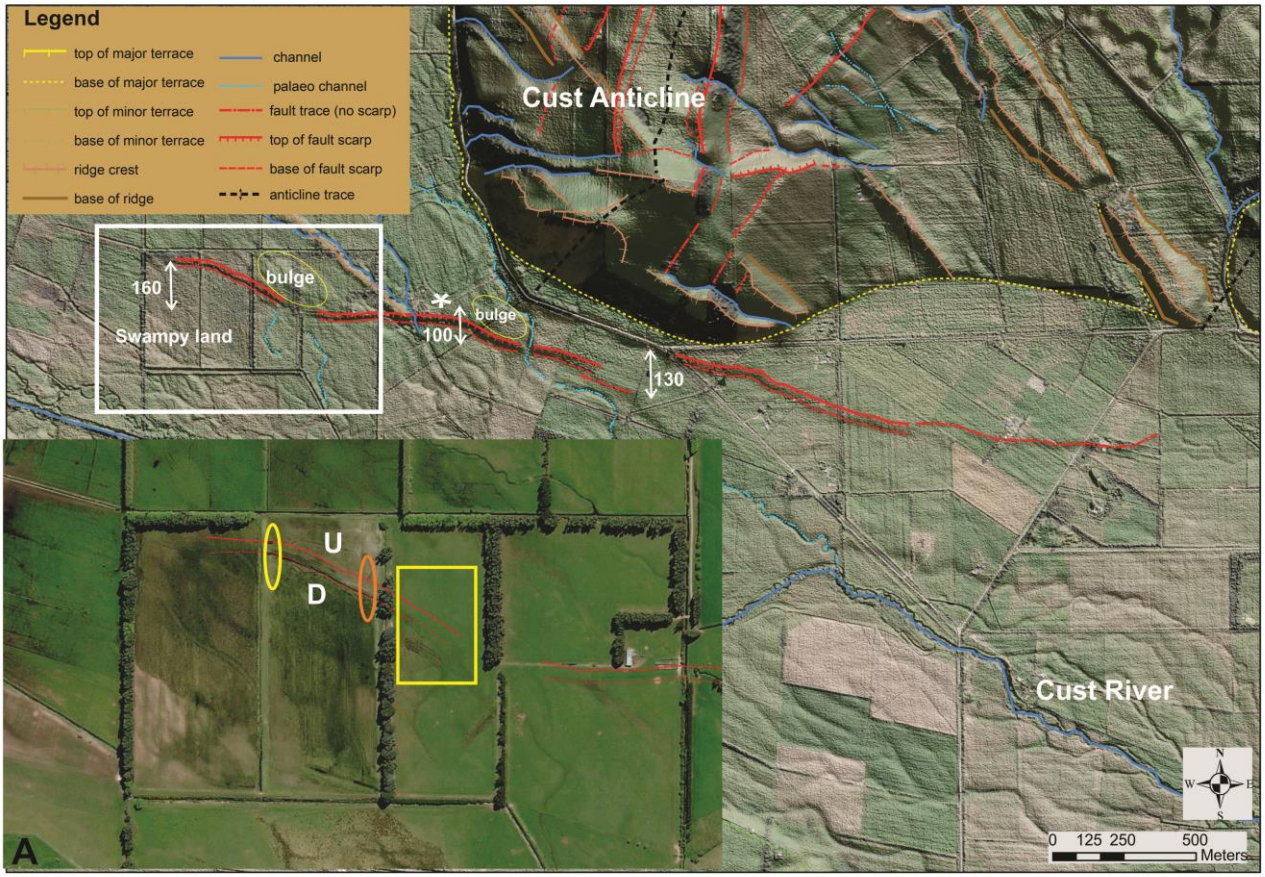

Figure 4.10. Glews Road paleo-seismic trench location. LiDAR image at scale of 1:15,000 with vertical exaggeration 20x. The white box in the main image indicates the site in relation to the fault trace southwest of the Cust Anticline. The fault trace detail is described in Chapter 3. Inset A: aerial photo image of the site located within the white box indicating the swampy ground associated with the downthrown side of the fault scarp. The yellow ellipse is the trench location, the orange ellipse is the augering location, the yellow rectangle is the location used for GPR surveys. The white star in the main image indicates the initial reconnaissance GPR site pre-trenching.

4.2.2. Stratigraphic interpretation

The east wall of the trench is shown in Figure 4.11 and the legend indicates the stratigraphic units from oldest (1) to youngest (8). At the north end of the trench (location 1–7 m) there are four different gravel deposits (1–4). The oldest gravel unit (1) is a clast supported large cobble, sandy gravel that is gradational with the gravel unit above. Within the stratified sandy cobbly gravel unit (2) there are sand lenses (2a) which are gradational within the layer 2 gravels and may be representative of a fluvial depositional environment. A similar sand lens deposit was also present on the west side of the trench but was disrupted by the cut-bench (Figure 4.12). The second youngest stratified pebbly sandy gravel unit (3) is gradational with the youngest sandy pebbly gravel unit (4) which is imbricated to the east (tilt to west), also indicative of a fluvial origin.

Therefore, multiple depositional events are represented within the stratigraphy north of the fault deformation zone which is located in the trench between the grid points 7–8 m. Subsequent to their deposition these gravel layers (1–4) have been offset by faulting whereby across the fault younger gravels (4) to the south are adjacent to older gravels (1) to the north. On the south side of the fault zone none of the three older gravels (1–3) found north of the fault are visible within the depth of the trench. Only the uppermost gravel layer (4) is represented south of the fault zone. The relative depth of the uppermost gravel unit cannot be determined south of the fault zone as it is parallel to and forms the trench floor.

The fault is located between trench locations 7–8 m and is a relatively steeply dipping fault plane with the youngest gravels (4) draped across this zone. There is clear evidence for the imbricated pebbles of the youngest unit being affected by roll-over into the fault zone with the pebbles having a more vertical orientation. The deformation within the fault zone was confirmed by careful excavation across the fault zone on the west wall (Figure 4.12) which remained more stable until the second and third days. The trench walls within the fault zone were significantly unstable compared to the gravels north of the fault zone and the peats and clays south of the fault zone which is a testament to the crushed and deformed nature of the gravels, due to the shearing, within the fault zone.

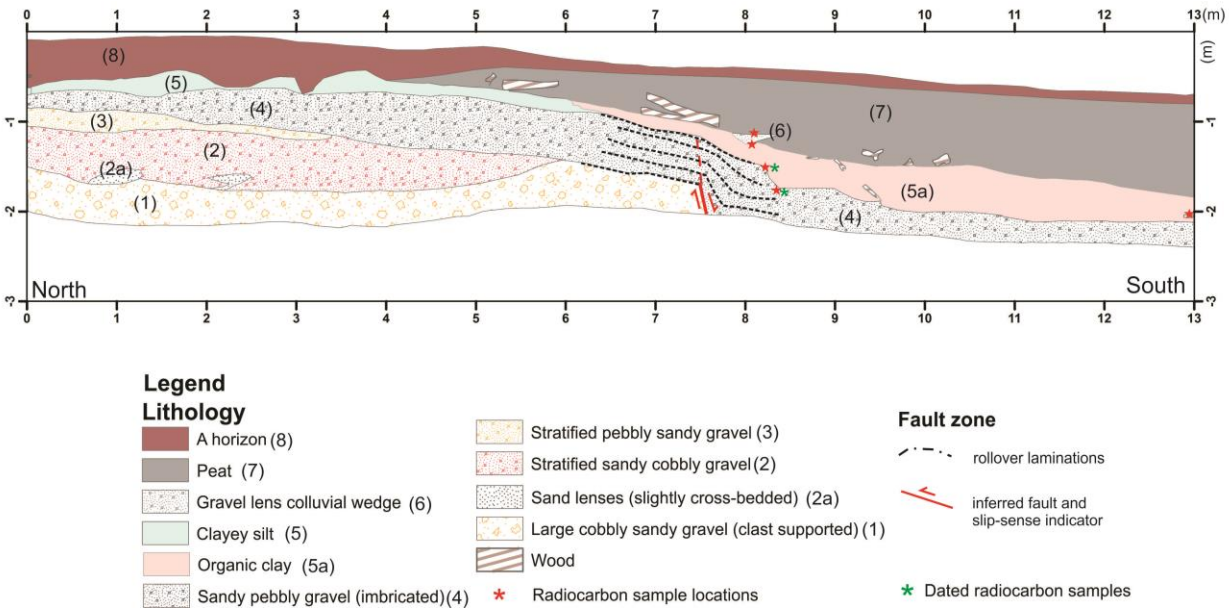

Figure 4.11. Glews Road trench site – east wall. The normal fault trace (red) offsets younger gravels against older gravels and is inferred to extend up through the youngest gravel layer over which the upper stratigraphy is draped.

The gravel units (1–4) are overlain unconformably by swamp deposits (5a, 7) accommodated within the downthrown region of the fault zone and by clayey silts (5) within the upthrown

region (Figure 4.11). The clayey silt has peat infilled worm burrows, up to 2 cm diameter, and small cracks. Layers 5 and 5a are laterally gradational across the fault zone. The clayey silt unit (5) directly above the youngest gravel unit is of relatively uniform thickness up to about trench location 6 m. Between 6 and 7 m, the clayey silt texture grades into a more rich organic clay unit (5a) and thickens across the fault zone where the organic clay south of the fault zone is three times the thickness of the clayey silt north of the fault zone. The organic clay (5a) on the downthrown side of the fault corresponds to the stratigraphically lowest buried swamp deposits which are associated with a faulting event within the underlying gravel units.

At the top of this organic clay layer (5a) and below the overlying peat layer (7) is a small colluvial wedge of pebbly gravel (6), at location 7.8–8.4 m and depth 1.2 m, on the downthrown side of the fault. This wedge of gravel appears to be in situ. However, it is relatively small compared to the thickness of the overlying peat and is not present on both sides of the trench which may be due to some erosion of this gravel unit before subsequent peat deposition. Alternatively, this gravel wedge could have been dragged up by tree fall associated with the presence of the large logs located at the interface between the organic clay layer (5a) and the peat layer (7) above.

The youngest peat layer (7) begins about the 4 m mark along the trench and also thickens considerably as it drapes across the fault deformation zone and onto the downthrown side of the fault. The thickness of the peat increases from about 0.45 m at the 7 m location immediately north of the fault zone to about 0.65 m just beyond the fault zone and up to 0.9 m thick at the 11 m location which is well within the downthrown region of the trench wall. The thickness change and location of the peat indicate an association with the last tectonic event.

There are many fallen tree logs and large roots within the base of this peat layer, many of which are draped across the fault zone. It is possible that these trees could have fallen and landed on the organic clay layer and then subsequently been covered in the peat. Therefore, they may be related to tree fall in response to a tectonic event that occurred between the deposition of two layers.

Finally, the A-horizon is also draped across the fault deformation zone and appears to be thicker on the upthrown side of the fault and less developed on top of the peat on the downthrown side. The A-horizon is a dry, blocky peaty topsoil.

The stability of the east wall did not allow any further face-logging after the first day. Furthermore, the stability of the east wall did not allow for any significant removal of material within the fault zone without creating a significant hazard from collapse. Therefore, the west wall was logged within the central section of the trench in order to confirm the findings indicated on the east wall. The logged section of the west wall corresponded to trench locations between 5.5–8.5 m with reference to the east wall. A bench supported this wall at a depth of about 1.1 m from the trench surface. Similar units (1–8) were logged on the west wall (Figure 4.12).

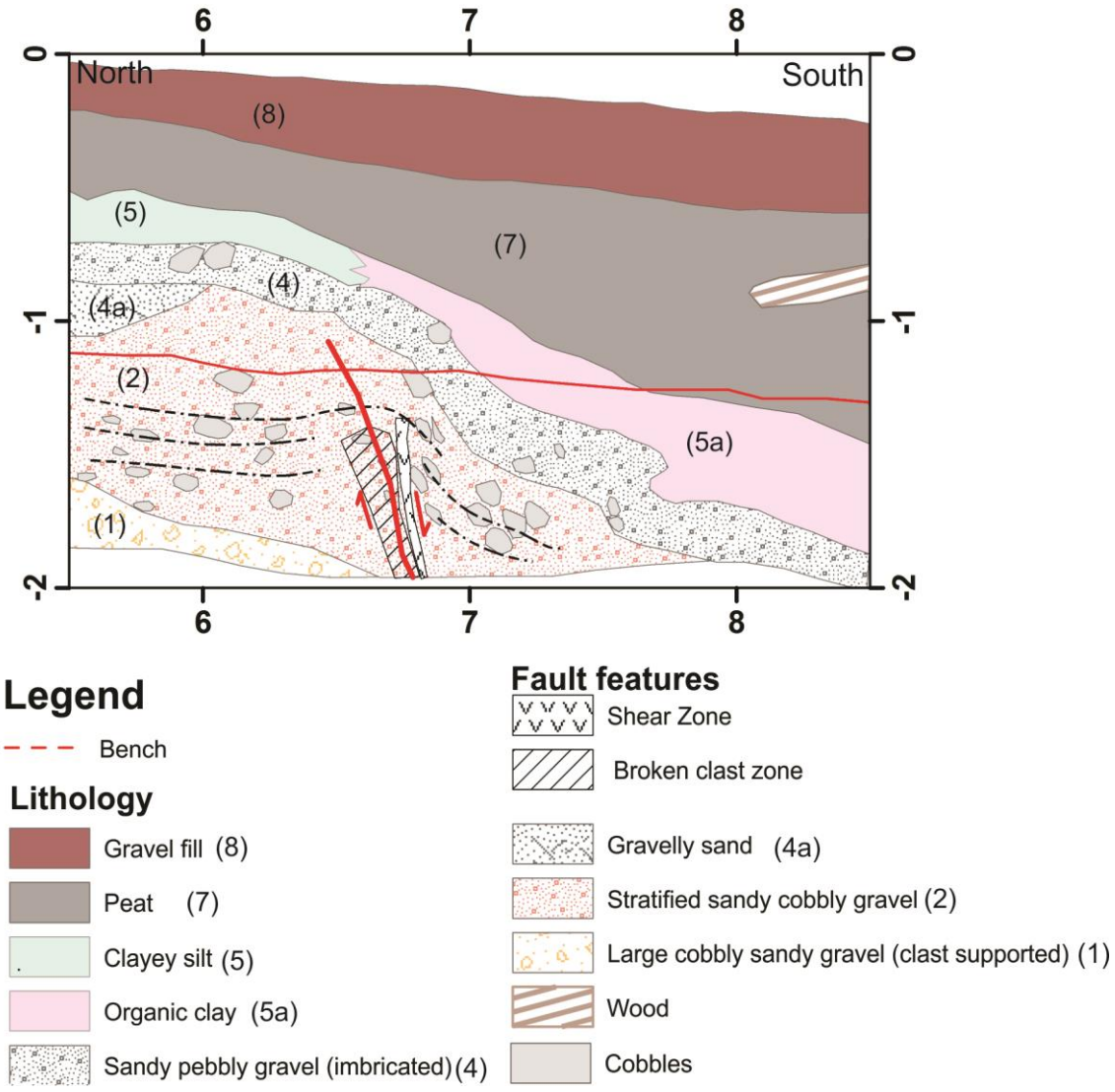

Figure 4.12. Glews Road trench site – west wall. The trench-log for the west wall has been inverted to match the corresponding locations with the view of the east wall. The normal fault trace and deformation shear zone is located within the stratified sandy cobbly gravel unit over which the upper stratigraphy is draped.

The oldest layer within the stratigraphy of the west wall was the large cobbly gravel unit (1) which disappeared into the trench floor at trench location 6.5 m just before the fault deformation zone. Within the west wall the fault deformation zone was within the second oldest gravel unit (2) where there was a significant zone of broken clasts, rotated vertical clasts, shearing and instability (Figure 4.12). The fault zone on the west wall was located approximately 0.5–0.75 m northwards in the trench compared to its location on the east wall, consistent with the strike of the fault trace through the trench and across the paddocks where overall the trench location was within a minor releasing bend along the dextral strike-slip fault. The gravelly sand unit (4a) in the west wall above unit 2 at location 5.5–6 m may correspond to the stratified pebbly sandy gravel (3) in the east wall, however, distinguishing between the fluvial gravel units was difficult due to the saturation and instability of the trench walls. The youngest gravel unit on the west wall (4) was draped across the sheared fault deformation zone and was probably also affected within this zone, however, the bench prevented good sampling of the clast orientation at this stratigraphic level.

Similar to the east wall the clay layer above these gravels graded, across the deformation zone, from a clayey silt (5) north of the fault into a more organic rich clay (5a) south of the fault. Likewise, the topmost peat layer thickened across the fault zone from about 0.3 m on the upthrown side to 0.85 m on the downthrown side. The west wall of the trench had similar stratigraphy on the northern and southern ends beyond the fault zone but time and stability of the walls prevented this being logged in any significant detail.

4.2.3. Tectonic context of trench site and interpretation

Regionally the fault trace across which the trench is located is consistent with the E–W-striking network of re-activated, inherited tear-faults. Based on surface geomorphic mapping the fault is accommodating largely dextral shear, but at the trench site a minor right releasing bend is reflected by extensional (normal) slip. Holocene rupture has created the south-facing topographic scarp, with the downthrown south side towards the Cust River. Similar deformation is reported from the right-bend between the central and western segments of the Greendale Fault (Duffy et al., 2013). The fault offset represents rupture of the eastern end of a fault trace that extends west to Starvation Hill and near Oxford.

The fault footwall is exposed in the north of the trench and the hanging wall in the south of the trench. The hanging wall and footwall are exposed on both east and west trench walls. Although there is clear juxtaposition of older units against younger units on the east wall there is not a complete log of any repeated stratigraphy on the hanging wall therefore absolute displacements cannot be obtained or measured. No strike-slip indicators were able to be measured within the trench. However, at least one faulting event is clearly represented by the juxtaposition, on the east wall, of the oldest large cobbly gravel unit (1) north beside the youngest sandy imbricated pebbly gravel unit (4) south across the fault. The fault zone on the west wall does not lie so clearly between older and younger gravels, however, here the structure and clast characteristics confirm the location of the fault trace.

The extension of this fault trace upwards within the stratigraphy is uncertain although the presence of the clay and peat units above the gravels could represent two events where the first is captured by the deposition of the clayey silt (5) and organic clay (5a) units and the second by the overlying peat unit (7) in different chronological depositional environments. Both the clay-silt/organic clay unit and the peat unit increase in thickness southwards across the projected position of the fault. The colluvial wedge gravel unit (6) on the downthrown side of the fault may be indicative of this second event however, it is inconclusive due to its size and uncertain genesis. Furthermore, buried logs from trees at the boundary of the peat layer and the organic clay layer are located across the fault trace and within the hanging wall of the fault and could also possibly be associated with the most recent faulting event.

4.2.4. Radiocarbon dating

A series of vertically positioned C^{14} dating samples from the youngest gravels, the organic clay and the peat layers within the hanging wall immediately south of the fault location were collected in order to try to determine constraints on the timing of the deposition of these layers (Figure 4.11). Only two samples were subsequently submitted for dating. One was located within the youngest gravel unit (4) and consisted of small samples of wood material. The second was a wood fragment located just above this gravel unit within the organic clay (5a). These samples should give a maximum and minimum age bracketing of the inferred event horizon represented by the contact between the gravel and organic clay unit and therefore constrain the inferred paleo-seismic event that caused this partial unconformity.

The two radiocarbon samples from below and above the colluvial wedge unit were not submitted for sampling due to later interpretation of the trench stratigraphy indicating an uncertain genesis of this gravel wedge, which meant limited constraint was likely from the results in terms of the paleo-seismic history from the trench. A fifth sample for possible C^{14} dating was also obtained from the south end of the trench within the base of the organic clay layer but not submitted.

The age of the sample from within the youngest gravel unit (4) below the organic clay unit (5a) was 5,173 +/- 24 BP while the age of the sample from within the organic clay unit directly above the youngest gravel unit was 6,670 +/- 20 BP. This indicates that the samples may not have been in situ and that perhaps the older age sample incorporated some older carbon possibly due to mixing by tree fall or was part of an older tree from another location. The younger age sample may have been root material from a location above where it was sampled. Therefore, the event recorded by the displaced younger gravel unit (4) is going to be younger than the older age and older than the younger age which places it at around 6,000 years BP.

This age is older than the oldest age determined across the nearby Ashley Fault trace which was 4,785 +/- 255 BP and it was hypothesised that at least two, possibly three, events had occurred since this time on the Ashley Fault (Sisson et al., 2001). Ages have also been obtained from landslide material, thought to be co-seismic with faulting, from the south bank of the Ashley River at a location north of the Mairaki Downs (Cowan, 1992; Cowan & Nicol, 1996). This material gave a date for at least one event having occurred within approximately the last 2,500 years BP and provides some further constraints on the timing of possible co-seismic rupture on the Ashley Fault associated with the growth of the Cust Anticline. Therefore, the event recorded at the Glews Road site in this study may not be the youngest event and the draped stratigraphy of organic clay overlain by peat may be recording at least two events in different depositional environments over the last 6,000 years.

4.2.5. Auger interpretation

Prior to trenching, augering was undertaken along a 24-m transect across the fault scarp at a location 180 m east of the trench site along the edge of a drainage ditch (E1545200, N5206647; Figure 4.13). The stream bank of this ditch was also dug back to ground truth the scarp. On both banks of this drainage ditch draped stratigraphy was visible that clearly showed the top of the gravel layer on the north side of the fault being present just below the soil horizon. On the south

side of the fault the gravel was not visible within the ditch wall but was overlain by increasing depths of peat. Therefore, the overbank silts were draped across gravels which were progressively getting deeper across the south-facing fault scarp and were clearly located below peats on the south side.

The inferred auger profile based on three holes south of the fault trace and five north of the fault trace indicated that there was about 60 cm of soil and clays present before hitting gravels on the upthrown side and about 120 cm of peat and organic clayey silt above the gravels on the downthrown side (Figure 4.14). Although a sand layer is inferred to separate the clay units on the hanging wall this is probably a series of discrete sand lenses of varying thickness but this cannot be distinguished with the limited auger sampling. The presence of organic clayey silt deposits below the peat unit is only observed on the downthrown side. The upper clayey silt unit on the downthrown side most likely has more organics than the upper clayey silt unit on the upthrown side, however, this could also not be determined from the augering. The general characteristics of the auger profile was confirmed in more detail by the trench (Figures 4.11 and 4.12).

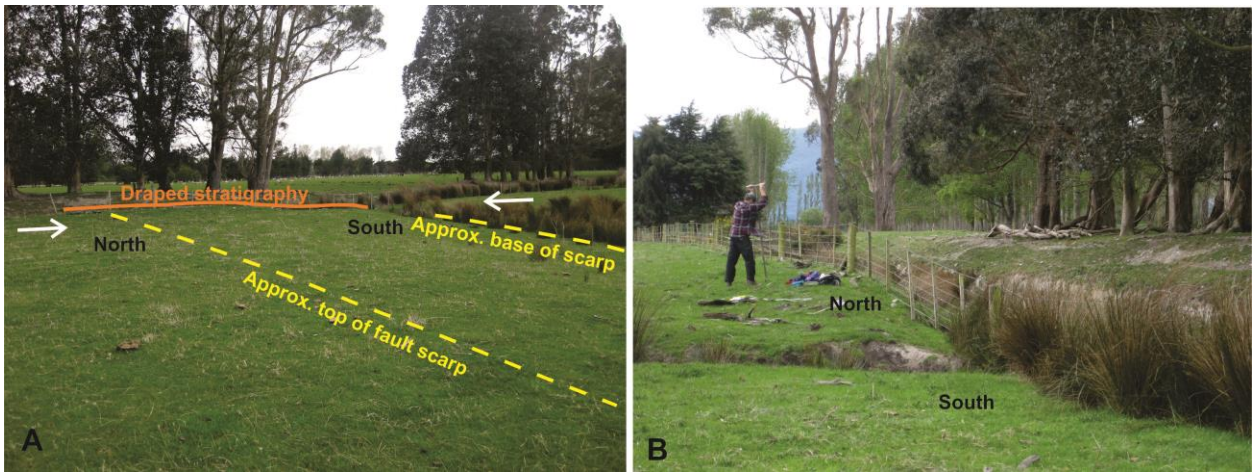

Figure 4.13. Photo of scarp at auger site. A. The auger line across the scarp is indicated between the white arrows. Dashed lines indicate the inferred top and bottom of the scarp. A small drainage channel ran along the bottom of the scarp. Draped stratigraphy consistent with faulting was observed within the ditch running north to south across the scarp. B. The scarp looking northwards.

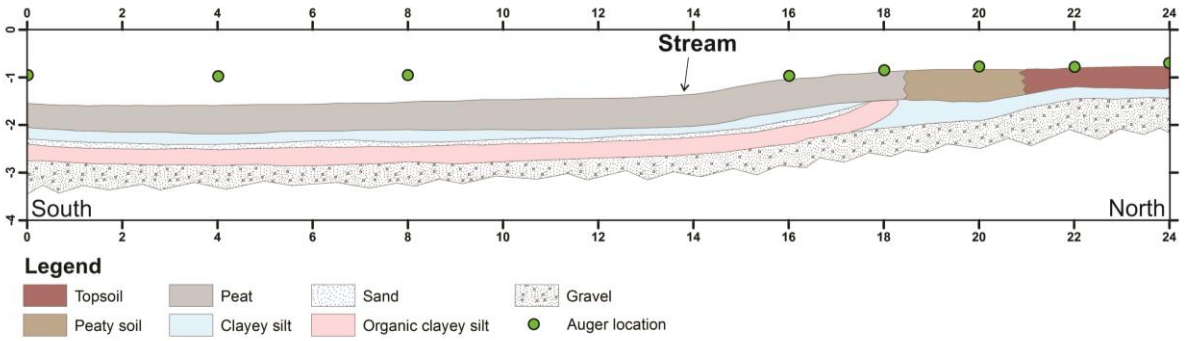

Figure 4.14. Glews Road paleo-seismic site auger profile. Note that while the stratigraphy correlated to a first approximation to the stratigraphy within the trench, due to the limited number of auger locations on the downthrown side of the fault the continuity of layers can only be inferred and may in fact not be continuous as shown.

4.2.6. Ground penetrating radar

A preliminary ground penetrating radar (GPR) survey (E1545845, N5206529) was performed prior to trenching to confirm the scarp located on the LiDAR was likely to be tectonic rather than fluvial. These surveys were carried out using a Sensors and Software PulseEKKO 100 MHz antenna system at a location about 800 m east of the eventual trench site (Figure 4.10). The scarp height at this location was about 1.5 m. The GPR profile indicated some thickening of the upper stratigraphy on the downthrown side of the scarp and increased layering of gravels on the upthrown side of the scarp. The upper stratigraphy also appeared to be draped across a more disrupted zone below the uppermost layers at the steepest angle of the scarp (Figure 4.15).

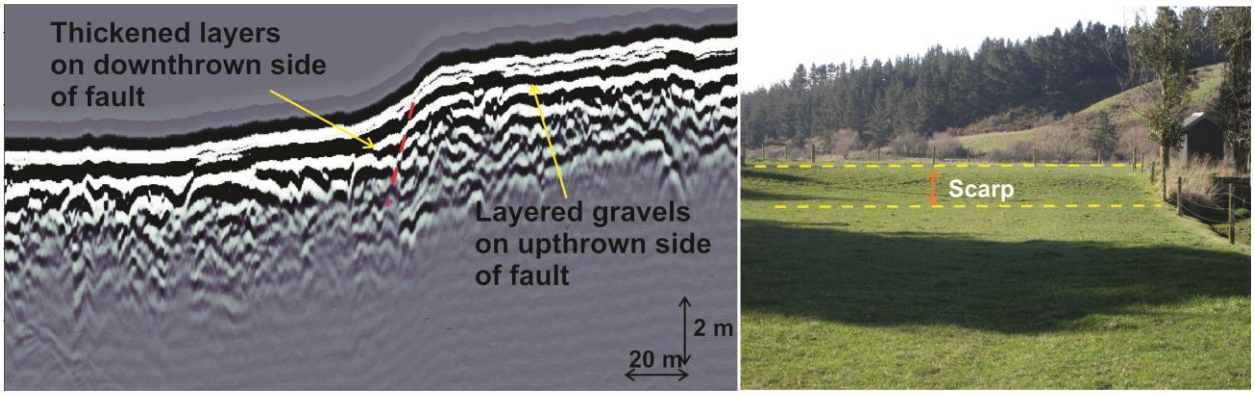

Figure 4.15. Initial GPR profile across Glews Road fault scarp. The profile was obtained about 800 m east of the trench location and confirms the fault deformation zone as well as the thickening of depositional layers above the gravels on the downthrown side of the fault scarp (indicated by dashed red line). Photo indicates the fault trace across the landscape and the subtle nature of its field geomorphic expression.

Ground penetrating radar surveys were carried out post-trenching parallel and perpendicular to the scarp about 250 m east of the trench site to validate the stratigraphy of the trench at a location distance from the trench site (E1545280, N5206611; Figure 4.10). The location for the GPR surveys was a paddock of close cropped grass rather than the swampy environment of the trench

and auger locations. Six surveys were carried out perpendicular to the trench and a representative profile is given in Figure 4.16. Surveys were also carried out parallel, along the top and base, to the scarp. The GPR surveys were carried out using a GSSI shielded 200 MHz antenna system.

The results clearly confirm the stratigraphy of the trench and the auger profile (Figure 4.16). There is draped stratigraphy across the south-facing 1.6-m high scarp in this location. On the upthrown side there are layered gravels immediately below the surface that appear to be offset and deeper below the surface on the downthrown side. On the downthrown side there appears to be a graben-like depression across a 4–5 m wide deformation zone. Within this zone there is non-layered stratigraphy in the upper section which most likely corresponds to the peat and organic clayey silt layers observed in the trench walls. Below this there is disrupted but layered stratigraphy within the deformation zone. The normal fault shear zone, observed in the trench would correspond to the northern side of this graben-like depression. To the south of the deformation zone the layered stratigraphy is less disrupted and again closer to the surface (Figure 4.16).

The GPR surveys parallel to the scarp showed some indication that the gravels were generally thicker and more stratified in the profiles along the top of the scarp and less well defined and variable in the profiles along the base of the scarp.

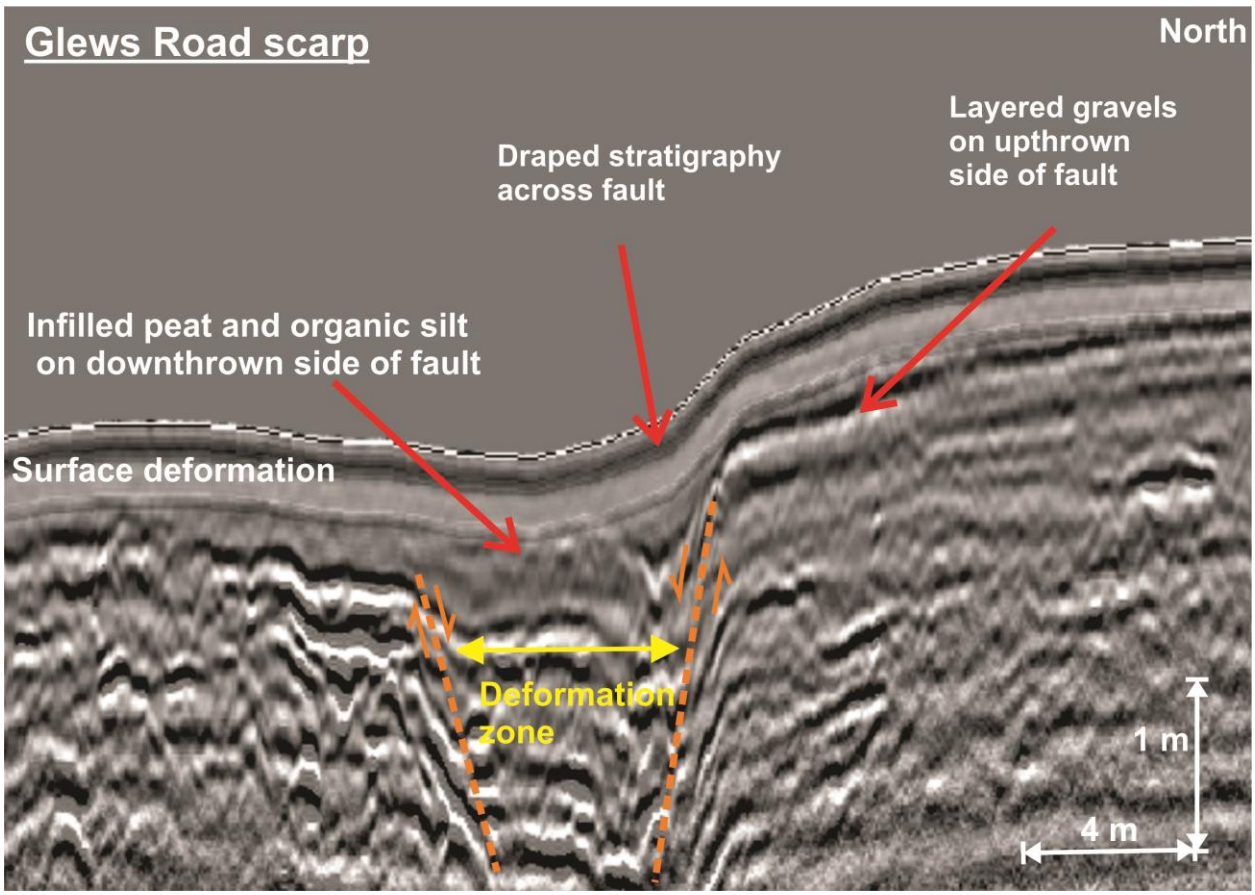

Figure 4.16. GPR profile across Glews Road fault scarp near trench site. The profile was obtained about 250 m east of the trench location and confirms the fault deformation zone as well as the thickening of depositional layers above the gravels on the downthrown side of the fault scarp.

4.2.7. Glews Road trench summary

LiDAR interpretation of this fault trace was instrumental in determining the locations for initial investigation of this site. The initial GPR surveys, although affected by some interference of surrounding reworking provided enough interest to do further investigation by augering at a less disturbed site. The augering profile and nearby excavation across a drainage ditch further indicated the likely presence of a fault trace in the near surface associated with this E–W-striking scarp. The Glews Road paleo-seismic trench confirmed the presence of the fault, beneath the E–W-striking scarp. The fault manifest as a normal fault offset within the near surface gravels consistent with the trench location, which was within a minor right releasing bend along the dextral, oblique-transpressive strike-slip fault, within the present regional stress regime. The trench indicated the presence of at least one and possibly two events within the last 6,000 years.

Chapter 5. Indo-Pacific seismic reflection line interpretation

5.1. Introduction

A large number of exploration seismic reflection lines were undertaken across the Canterbury Plains between 1998–2000 by Indo-Pacific (IP) Energy (Schlumber Geco-Prakla, 1988, 1999, 2000). In the area surrounding the Cust Anticline a total of 12 lines (IP lines 105–111 and IP lines 201–205) and one exploration well (Arcadia-1) were available for interpretation across the study area (Figure 5.1). Although previous interpretations of these lines have been made (Jongens et al., 1999; Bennett et al., 2000; Ghisetti & Sibson, 2012; Jongens et al., 2012) their interpretations were focussed on the deeper subsurface structure and stratigraphy without access to LiDAR surface topography or paleo-seismic trenching. The re-interpretations made from these same lines in this chapter are specifically focussed on the Cust Anticline in relation to the relatively unknown E–W-striking fault relay to the southwest of the Cust Anticline, extending to Starvation Hill and Oxford, and the well-known Ashley structure to the northeast. The aim of this re-interpretation is to compare and relate the surface geomorphology, documented from the LiDAR across the study area (Chapter 3), to the structures displacing the Oligocene marker horizon documented in the seismic reflection data.

The IP lines are of good quality and have well-defined and prominent reflectors down to the top of the basement. Although not all reflectors have good continuity across the entire sections there are generally good reflectors for the top and base of units corresponding to the Quaternary gravels, the Pliocene Kowai Formation, the Miocene, the Oligocene limestone and a Late Cretaceous–Paleogene stratigraphic unit including volcanics (Forsyth et al., 2008). The most continuous and well imaged reflector across the lines in the study area is the Oligocene limestone reflector (ranging from ~100 m to ~800 m below sea-level) which clearly indicates the broad geological structure of faulting, fault block uplift and folding beneath most of the field area. Structure within the younger Quaternary layers is less easily discernible due to the resolution of the seismic in these layers although onlapping relationships are sometimes present. Faulting at deeper levels within the Cretaceous–Paleogene units can also be interpreted in many lines however, the structural interpretation within the basement is more difficult, and is not further considered in this study.

The Arcadia-1 well, which was located very close to line 107, was tied to the seismic reflection lines across the Cust area (Indo-Pacific Energy, 2000). The Arcadia-1 well (elevation 205 m)

provided time-versus-depth conversion information from the well log and this was used to re-check the ties for the seismic reflections before obtaining two-way-travel-time (TWTT) from the Oligocene reflectors for use in the re-interpretations of this study.

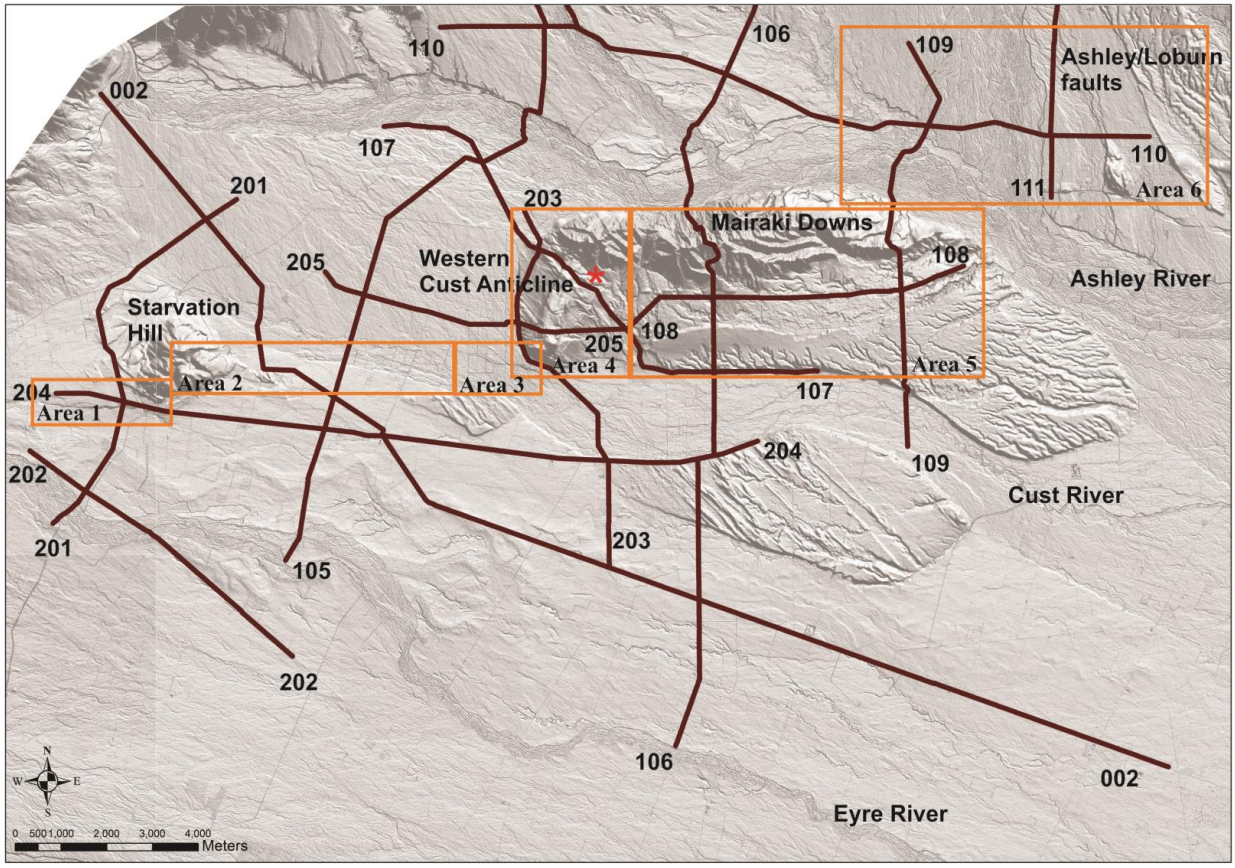

Figure 5.1. Location of the Indo-Pacific seismic reflection lines across the study area. The lines are overlaid on a LiDAR hillshade of the area at a scale of 1:65,000. The six areas of specific LiDAR interpretation (Chapter 3) are indicated across the area. The red star indicates the location of the Arcadia-1 well. Note that line 002 was not available for re-interpretation in this study.

The sequence logged in the Arcadia-1 well was an unusually thick (about 1200 m) Late Cretaceous–Paleogene sequence compared to other parts of the Canterbury Plains region (Jongens et al., 2012). The Arcadia-1 well passed through ~40 m of surface gravels followed by ~144 m of Plio–Pleistocene Kowai Formation gravel. A 111-m section of Starvation Hill basalts were encountered before a thin marker section of Oligocene limestone at about 300 m below ground level. A further 800 m of Paleogene sediments were then logged before Paleogene Broken River Formation with Cretaceous basement greywacke identified at the base of the log which ended at about 1475 m below ground level (Indo-Pacific Energy, 2000).

5.2. Previous interpretation of North Canterbury seismic reflection lines

The initial report based on the Arcadia-1 well and the seismic reflection lines tied to this well concluded that in general the uplift and propagation of thrust dominated structures in the Canterbury Plains appears to have initiated in the Pleistocene with the Cust Anticline initiated in the Early–mid Pleistocene (Jongens et al., 1999). Furthermore, all structures in the contractional domain north and west of Christchurch have formed after deposition of the Kowai Gravels and are active to the present day. Overall northeast-striking reverse faults and fault propagated folds within the Northwest Canterbury Plains are mainly Late Cenozoic structures, however, east-striking faults are often associated with re-activated pre-existing Late Cretaceous normal faults that are now acting as oblique dextral transpressive faults during the Quaternary and Holocene (Jongens et al., 2012).

Re-interpretation of the predominantly N–S seismic reflection lines (IP lines 105, 106 and 109) indicates that the E–W-striking Ashley Fault Zone involves the partial re-activation of Late Cretaceous–Paleogene normal faults, as evidenced by the northward thickening of the Paleogene sequence towards the inferred Ashley Fault location. Although the majority of the deformation associated with the Ashley Fault is interpreted in this study to be transferred south-westward, stepping across beneath the Cust Anticline, a previous interpretation of these seismic lines suggested the possibility that the Ashley Fault extends westwards (north of the Cust Anticline and Ashley River) to the Glentui Fault Zone (Campbell et al., 2012; Jongens et al., 2012).

An extensive analysis of the basement and Late Cretaceous faults and structures within these North Canterbury seismic reflection lines has indicated significant compressional inversion of inherited high-angle E–W-striking normal faults together with some detachment structures below the Neogene cover sequences (Ghisetti & Sibson, 2012). The top of the basement contact surface has a gentle regional southeast dip and is disrupted by a series of east–northeast-striking blind, steeply dipping Late Cretaceous faults that face oppositely from north to south. The location, and surface projection, of some of these re-activated Cretaceous faults is of interest for the interpretation of the surface structures determined from the LiDAR analysis of this study.

The seismic reflection profiles have also been used to interpret the subsurface location of the base of the Quaternary sediments (within the past 2.6 million years) underneath the Canterbury Plains (Jongens, 2011). The structure contours of the Quaternary sediments clearly show the

main faulting and folding within the near surface and that the faulting and folding is more developed closer to the foothills.

The following interpretation of the top of Oligocene surface, in conjunction with the previous analysis of deeper and shallower units within these seismic reflection lines (Jongens, 2011; Ghisetti & Sibson, 2012; Jongens et al., 2012), will be used to better define the geometry and kinematics of active tectonic deformation across the study area. Correlation of structures affecting the top of Oligocene contact surface with the LiDAR analysis may also provide further evidence for the Cust Anticline being a significant structural high developing in the restraining stepover between the Ashley and Loburn faults to the northeast and the E–W-striking structure (confirmed in Chapter 4), extending towards Starvation Hill, to the southwest of the anticline.

5.3. The top of Oligocene contact surface interpretations for this study

The locations and line parameters of the IP seismic reflection lines across the study area are summarised in Table 5.1. The following interpretations describe the main fold and fault structures affecting the marker Oligocene surface, which was the most continuous reflector horizon along the seismic reflection lines across the field area. This reflector was tied to the well log on line 107 and then traced around the lines confirming, at the tie points for the lines across the area, that the TWTT for this reflector was consistent.

The inferred surface location projection of identified structures was determined for monocline steps, flexures and anticline fold axes along this reflector, and also for faults that clearly offset this reflector, in order to correlate and interpret these structures with any evidence for their surface expression in the LiDAR data. The magnitude and direction of uplift or throw of these structures on the top of Oligocene surface was also determined (Table 5.2). The interpreted lines (vertical exaggeration 4.5x), and a description of the lines, from this study are presented in Appendix 1.

Finally, a provisional structure contour map of the top of Oligocene surface was developed using the TWTT across the study area. The TWTT was defined with respect to sea-level with positive values representing depths below sea-level. The contour intervals were determined at 50 ms TWTT and the surface location at which the top of Oligocene reflector crossed the TWTT corresponding to these intervals was determined along each of the lines. These points were then

plotted along the located seismic reflection lines in ArcGIS and the contours determined manually taking into account the determined monocline steps, flexures, anticline folds and fault structures located along these lines.

Seismic line	Length	Direction	Location
105	15 km	SSW to NNE	Eyre River to Ashley River NW of Cust Anticline
106	18 km	S to N	Eyre River across Mairaki Downs to Ashley River
107	12.5 km	WNW to ESE	Across the western arm of the Cust Anticline
108	9 km	W to E	Southern margin of Mairaki Downs (overlaps and continues with line 205)
109	9 km	S to N	Cust River across Mairaki Downs to Ashley River
110	16 km	W to E	Along northern bank of Ashley River
111	16 km	S to N	Ashley River to Whiterock
201	8.5 km	SW to NE	Eyre River to Ashley River west of Starvation Hill
202	7 km	NW to SE	Across the Eyre River
203	8 km	NW to SE	Ashley River around base of Cust Anticline
204	15 km	W to E	Southern margin of Starvation Hill eastward
205	8 km	W to E	Across western arm of the Cust Anticline (overlaps and continues with line 108)
002	24 km	NW to SE	NW–SE across entire study area

Table 5.1. Description of the locations and line parameters of the Indo-Pacific seismic reflection lines across the study area (refer also Figure 5.1 and Appendix 1). Note that line 002 was not available for re-interpretation in this study.

5.4. Structural interpretation of top of Oligocene surface

Figure 5.2 shows an interpretation of the major structures disrupting the top of Oligocene contact surface, including monocline steps and flexures, anticlines and faults. These key structures are summarised in Table 5.2 and interpreted seismic reflection lines are collated in Appendix 1.

The map identifies a series of common structural styles in the study area that have the same underlying structural drivers but vary in the degree of development and expression in the seismic profile (Figure 5.2). The largest fault bounds the northern margin of the E–W-striking Mairaki Downs section of the Cust Anticline and is a steeply south-dipping E–W-striking reverse fault (one of a system of re-activated inherited normal faults) that offsets the Late Cretaceous, Paleogene, and Oligocene strata (line 106, 109). On the south side of the Mairaki Downs Cust Anticline a steeply north-dipping E–W-striking reverse fault offsets the Paleogene strata but not the top of Oligocene contact surface which shows a monocline step above this fault at this location (line 106). Interestingly, the combined throw of the faults south and north of the Mairaki

Downs along line 106 is slightly greater than the total throw of the main fault structure located along line 109, suggesting that the development and elevation of the E–W-trending Cust Anticline is in part a response to the different degrees of re-activation of Late Cretaceous faults associated with the stepover zone from northeast to southwest. Similarly, the left-stepping deformation transfer across to the western arm of the Cust Anticline is attributed to this mechanism. Together these oppositely dipping E–W-striking faults have resulted in the development of the oldest and highest elevated structurally driven culmination in the study area: the E–W-trending Mairaki Downs section of the Cust Anticline.

A similar, younger and less evolved E–W-striking anticlinal structure with very low-relief surface expression has developed between the E–W-striking Ashley and Loburn faults to the northeast, on the north side of the Ashley River (Sisson et al., 2001). Here the E–W-striking Loburn Fault is upthrown to the south and the E–W-striking Ashley Fault is upthrown to the north. However, the seismic reflection lines (lines 109, 110, 111) do not sufficiently cover this region where the Holocene traces have been mapped east of the Okuku River and therefore this structure cannot be clearly confirmed at the depth of the Oligocene (Figure 5.2).

To the southwest of the Cust Anticline the top of Oligocene marker horizon is affected by structural inversion resulting in an elevated section along the top of Oligocene surface, imaged in seismic line 105. There is no surface expression of this structure, but seismic line 105 reveals it extends to the near surface and is below the aggradation surface between the present-day Cust River to the north and Eyre River to the south. The top of Oligocene surface structure is bounded by oppositely-facing monocline steps/flexures in the region between the eastern apex of Starvation Hill and the southwest termination of the Cust Anticline (Figure 5.2). There is no clear evidence for faulting of the top of Oligocene surface at this location along line 105 although there is faulting within the underlying Paleogene strata.

This buried E–W-trending anticlinal structure below the aggradation surface between Starvation Hill and the Cust Anticline is less evolved than that imaged below the Mairaki Downs, where clear surface expression forms the Cust Anticline. However, it is probably more evolved at the top of Oligocene marker horizon than the anticlinal structure below the Ashley and Loburn faults. The top of Oligocene surfaces underlying the E–W-trending Mairaki Downs and the E–W-trending aggradation surface between the Cust and Eyre rivers bound relatively short

northeast-striking faults that left-step between westward extending segments within the overall E–W-striking structural fabric below the study area (Figure 5.2).

Seismic line	Structure	Upthrow	Oligocene offset (m)	Surface elevation	Surface location
105 (S–N)	S-facing monocline step/flexure	North	100	Minimal	1–1.5 km
105 (S–N)	N-facing monocline step/flexure	South	50	Minimal	4.5–5 km
105 (S–N)	S-facing monocline steps/flexures*	North	200*	Minimal*	13–15 km
106 (S–N)	S-facing monocline step/flexure	North	100	Minimal	4 km
106 (S–N)	S-facing monocline step	North	200	150 metres	9.5–10 km
106 (S–N)	S-dipping fault	South	450	150 metres	13.5 km
107 (NW–SE)	NW-facing monocline step/flexure	Southeast	100	Minimal	3.5 km
107 (NW–SE)	Anticline		500 NW	80 metres	5.75 km
			250 SE	80 metres	
108 (S–N)	No structures				
109 (S–N)	S-dipping fault	South	500	80 metres	4.5 km
109 (S–N)	S-facing monocline step/flexure	North	50	Minimal	7.5 km
110 (W–E)	SE-facing monocline step	West	150	Minimal	3 km
111 (S–N)	No structures at start of line				
201 (SW–NE)	Anticlinal structure		150–200	Minimal	2.5–3 km
201 (SW–NE)	NE-facing monocline step	Southwest	150	Minimal	6.5 km
202 (NW–SE)	SE-facing monocline step/flexure	Northwest	50	Minimal	1.5 km
202 (NW–SE)	SE-facing monocline step	Northwest	120	Minimal	4 km
203 (NW–SE)	NW-facing monocline step/flexure	Southeast	100	Minimal	0.5 km
203 (NW–SE)	Anticline		200 W	80 metres	3.25 km
			250 E	80 metres	
204 (W–E)	W-dipping fault	West	220	80 metres	2.5 km
204 (W–E)	E-facing monocline step/flexure	West	100	Minimal	9.5 km
205 (W–E)	Anticline		400 W	80 metres	5 km
			250 E	80 metres	

Table 5.2. Description of the characteristics of the main structures along the Indo-Pacific seismic reflection lines that disrupt the top of Oligocene surfaceacross the study area (also Figure 5.2). * this section of the line involves 2-3 smaller flexural steps.

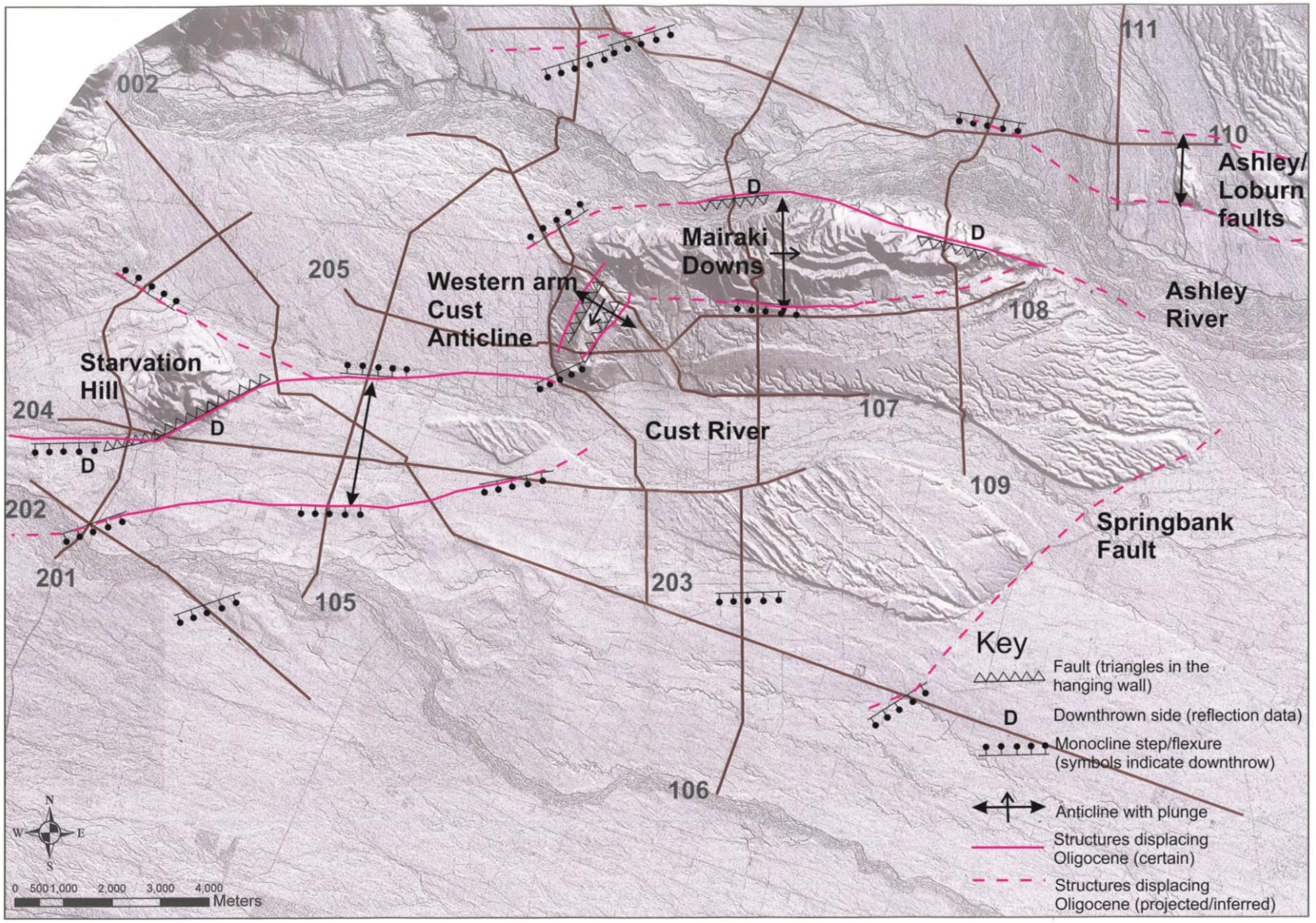

Figure 5.2. Interpretation of the main structures displacing the top of Oligocene surface established from IP seismic reflection lines across the study area.

At the western end of the E–W-trending section of the Cust Anticline the younger less evolved north-northeast-trending anticline has formed in response to north-northeast-striking thrust faulting as part of the present-day regional tectonic stress regime of North Canterbury. Within the seismic profile (line 203) steeply northwest-dipping faults within the Late Cretaceous and Paleogene strata appear to bound the eastern limb of the top of Oligocene anticline structure consistent with thrust propagated folding of the western arm of the Cust Anticline. These faults do not offset the Oligocene marker horizon at this location although there is slight flexural deformation of the top of Oligocene surface. Evidence from the LiDAR indicates that the E–W-striking surface fault trace (Glews Road paleo-seismic site) has greatest expression immediately to the southwest of the anticline with the north side being upthrown however, the seismic profile of line 203 is not optimally oriented or located to confirm a definite subsurface structure for this fault. The asymmetric western arm of the Cust Anticline, and indications for thrust propagated folding, is also clearly indicated in the top of Oligocene horizon within lines 107 and 205 (Figure 5.2).

A northeast-striking surface fault trace is present across the southeast margin of Starvation Hill and is imaged as a west-dipping reverse fault that disrupts the top of Oligocene marker horizon along line 204 below the Starvation Hill location. Here the northeast-striking surface fault trace leads into an E–W-striking trace extending westward from this structural culmination that is imaged beneath the top of Oligocene marker horizon along line 201 (Figure 5.2).

It is reasonable to propose that a similar northeast-striking structure likely exists, creating a left-step relay, between the western location of the Holocene surface trace of the Ashley and Loburn faults at the Okuku River and the plunging eastern termination of the Mairaki Downs Cust Anticline. However, this would be mostly located beneath the present Ashley River floodplain which would extinguish any surface trace and there are no seismic lines in this specific area to confirm a subsurface structure (Figure 5.2).

Finally, monocline steps/flexures of the top of Oligocene contact surface indicate that there are possible west-northwest-trending structures that extend from the Mairaki Downs (lines 105, 110) and Starvation Hill (line 201) structural culminations towards the rangefront (Figure 5.2). These structures are not faulted at the level of the top of Oligocene marker horizon.

Table 5.2 indicates the approximate ground surface elevation (with respect to the Canterbury Plains datum) above the structures (faults, monocline steps/flexures, anticlines) observed displacing the top of Oligocene marker horizon at depth. For monocline steps/flexures of the top of Oligocene horizon with displacement of less than ~150 m there is minimal deformation present at the surface. For monocline steps of the top of Oligocene surface >200 m there appears to be corresponding surface elevation of around 80 m especially if the top of Oligocene surface is offset by faulting. Structures underlying Starvation Hill (line 204) and the Mairaki Downs (line 109) are examples of this (Table 5.2 and Figure 5.2). The highest surface elevation (~150 m), corresponding to the highest elevation along the Mairaki Downs, occurs above the greatest combined throw within the Oligocene surface (line 106). The asymmetric western arm of the Cust Anticline has surface elevation around 60–80 m above the plains however, the top of Oligocene horizon beneath this structural anticline has greater asymmetry and vertical elevation change compared to at the surface (Table 5.2).

5.5. Summary of seismic reflection lines that cross the LiDAR interpretation study areas

Detailed LiDAR interpretation for six areas is presented in Chapter 3. This section highlights the key interpretations of the top of Oligocene contact surface along the seismic lines coinciding with these same areas (Figure 5.1). The lines not presented within the text of this chapter are included in Appendix 1 and the reader is referred to these as appropriate.

5.5.1. Area 1: Oxford to Starvation Hill

This area is crossed by seismic lines 201 and the western end of line 204. The top of Oligocene surface indicates an asymmetric anticlinal fold, along line 201, projected up to a surface location corresponding to the southern margin of Starvation Hill (LiDAR fault F1). Faulting below the Oligocene surface causes uplift, within the crest of this fold, of the top of Oligocene surface below the location of Starvation Hill (Figure 5.3). The ground surface trace (upthrown to the north) is difficult to isolate as being definitely tectonic in origin due to the sub-parallel direction of paleo-channels across these aggradation surfaces. However, the presence of definite fault propagated folding of the top of Oligocene contact at depth is evidence that this E–W-striking surface lineament is most likely a fault trace consistent with a segmented left-step between the E–W-striking fault trace from Starvation Hill to the Cust Anticline and an E–W-striking fault trace between Starvation Hill and Oxford (Figure 5.2).

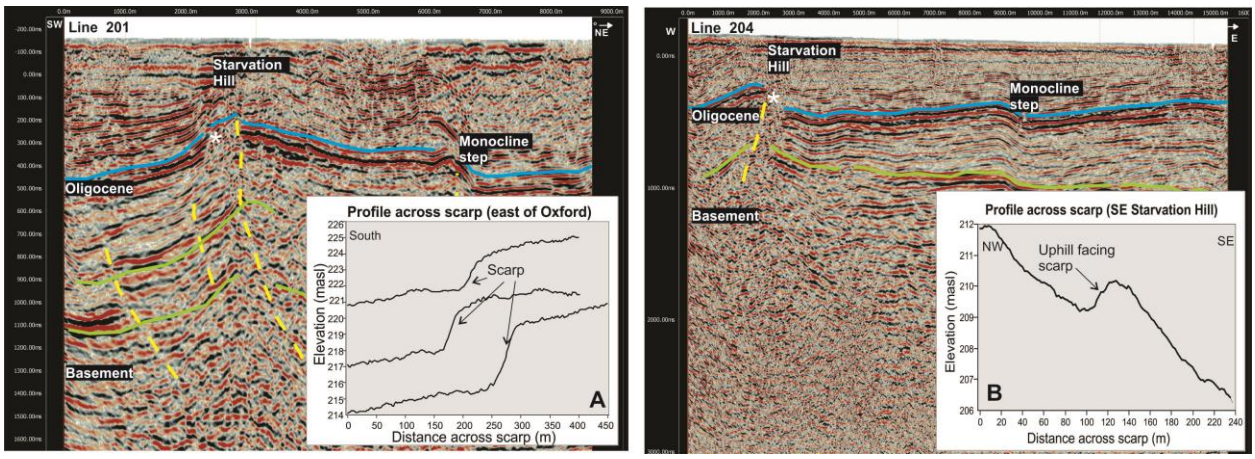

Figure 5.3. Seismic reflection line interpretation of the top of Oligocene contact surface below Starvation Hill. Inset A: LiDAR profile perpendicular across the E–W-striking ground surface scarp between Oxford and Starvation Hill. Inset B: LiDAR profile across the northeast-striking scarp across the southeast slopes of Starvation Hill. The asterisk indicates the approximate projection to the top of Oligocene surface from the ground surface profile.

Line 204 runs sub-parallel to this fault trace, along the southern margin of Starvation Hill. The east-facing limb of the folded top of Oligocene surface along this line, underlain by a steeply west-dipping fault that offsets the top of the Oligocene surface, most likely corresponds to the projected location of the fault trace characterised by back-tilted surfaces across the southeast slopes of Starvation Hill (Figure 5.3). Although, the upthrow direction at depth is not consistent with that of the surface scarp it is consistent with a transpressive hanging-wall fault wedge structure (Eusden et al., 2005). Therefore, this northeast-striking fault (LiDAR fault F2) which connects the E–W-striking trace from the southwest termination of the Cust Anticline with the E–W-striking trace between Oxford and Starvation Hill has an associated structure in the subsurface geology.

5.5.2. Area 2: Starvation Hill to Cust Anticline

This area is crossed by seismic lines 002 and 105 which both run approximately perpendicular to the inferred E–W-striking fault trace between the eastern apex of Starvation Hill and the southwest termination of the Cust Anticline. Although line 002 was not available in this study previous interpretation (May, 2004) has indicated a steeply-dipping thrust fault below the Oligocene surface, with upwarping reflectors on the upthrown south side, at a similar location to the E–W-striking fault trace projecting eastward from Starvation Hill (LiDAR fault F3). This interpretation from line 002 provides confirmation of the extent of the western segment of the trace between these two structural culminations as well as the elevated top of Oligocene surface bounded by the two monoclinal steps/flexures indicated in line 105 (Figure 5.4).

Line 105 also crosses perpendicular to the inferred fault trace between Starvation Hill and the Cust Anticline and indicates a monocline flexure, upthrown to the south, of the top of Oligocene surface at a location corresponding to the Late Quaternary trace on the LiDAR across the aggradation surfaces of the south side of the Cust River (Figures 5.2 and 5.4). Although there are indications on the seismic profile for faulting at depth beneath the elevated top of Oligocene surface it is unclear due to the resolution of the seismic profile as to the presence of faulting higher within the stratigraphy (as might be expected given the LiDAR surface trace). There is very little upwarp of this aggradation surface indicated by LiDAR profiling and no surface indication of active tectonic processes on the south side of this elevated top of Oligocene surface.

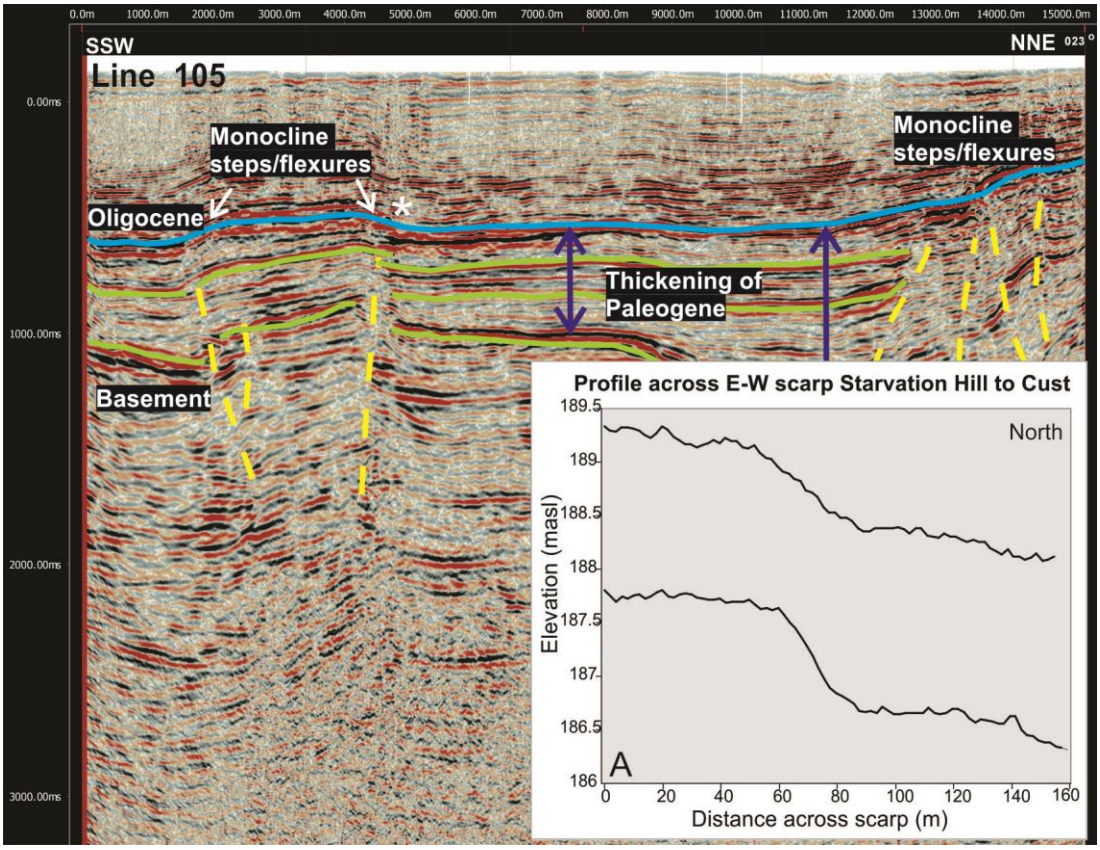

Figure 5.4. Seismic reflection (line 105) interpretation of the top of Oligocene contact surface perpendicular across study area 2. Inset A: LiDAR profile perpendicular across the E–W-striking ground surface scarp between Starvation Hill and the southwest termination of the Cust Anticline. The LiDAR scarp is at a ground surface location equivalent to the north-northeast-facing monocline step/flexure within the seismic line image (indicated by asterisk in the main image).

5.5.3. Area 3: Glews Road paleo-seismic site

This area is crossed by line 203 (Appendix 1) which passes around the base of the anticline and crosses the steeply plunging termination of the western arm of the Cust Anticline on the north side of the Cust River (Figure 5.1). The line confirms that the Cust Anticline is present at the

depth of the Oligocene surface and that it is asymmetric with a steeper vertical elevation change of the Oligocene surface on the eastern limb. The trend of the anticline is approximately at right angles to the seismic line at this location therefore, this asymmetry is most likely because the anticline is an east-facing thrust propagating anticline with the west side up. Steeply northwest-dipping faults within the Late Cretaceous and Paleogene appear to bound the eastern limb of the structure consistent with thrust propagated folding of the western arm of the Cust Anticline.

This seismic line crosses the very tip of the eastern termination of the E–W-striking trace extending to Starvation Hill but is not perpendicular to the trace. Although there does not appear to be any structure at the level of the top of Oligocene surface that corresponds to the eastern termination of this fault from Starvation Hill, the paleo-seismic studies 1 km west of this line confirm the presence of a fault trace in the near surface (LiDAR fault F4).

5.5.4. Area 4: The western arm of the Cust Anticline

The western arm of the Cust Anticline is crossed by lines 107, 205 and 203. Line 107 crosses the northern section and is tied to the Arcadia-1 well, line 205 crosses E–W about 300 m south of the Elliotts Road paleo-seismic site, and line 203 runs around the southern and western base of the hill and was previously discussed in Section 5.5.3., area 3. All three lines confirm the anticlinal structure within the top of Oligocene contact surface and also provide confirmation for the interpretation and the location of the eastern and western crestal scarps (LiDAR faults F5 and F6). The northern seismic reflection line (line 107) indicates that the anticline structure at the level of the top of Oligocene surface is much tighter than it is at the base of the thickened Cretaceous–Paleogene units where there is a broader, flatter block of uplift bounded by monoclinal steps/flexures (Appendix 1, line 107).

Along line 205 the top of the Oligocene marker horizon is folded into an asymmetric anticline with apparent greater vertical elevation change on the west limb compared to the east limb (Appendix 1). There is also evidence for more structural disruption of the east limb compared to the west limb, which is consistent with the LiDAR profile across the anticline surface at this location (Figure 5.5). The top of Oligocene marker horizon is clearly offset between the north-northeast-striking crestal fault scarps along this line, creating a structural depression across the anticline fold axis, which is also confirmed in the field at the surface. It is difficult to unequivocally determine from the seismic profile if these structures are thrust/reverse or normal

faults, however, at a low vertical exaggeration ratio it appears that the top of Oligocene offsets are controlled by thrust faults on its eastern limb and also on the western limb although within the resolution of the line the dip of the western limb fault is less apparent (Figure 5.5). While the foregoing is the preferred interpretation the possibility that the surface faults are non-seismogenic oppositely dipping normal or reverse faults still exists given the resolution of the seismic lines within the Quaternary strata above the top of Oligocene reflector although the paleo-seismic evidence also suggests thrust faulting is controlling these scarps at depth.

Furthermore, underlying the Cust Anticline structure there is clearly a shallow west-dipping thrust/reverse fault detachment present at the base of the Paleogene sequence that influences the continuing uplift of this structure during the Quaternary (Appendix 1, line 205). Steeply east-dipping inferred faulting within the Late Cretaceous below the Paleogene may also be present, however, fault offsets and present-day activity at this deeper level is not as easily determined and further analysis is beyond the scope of this project.

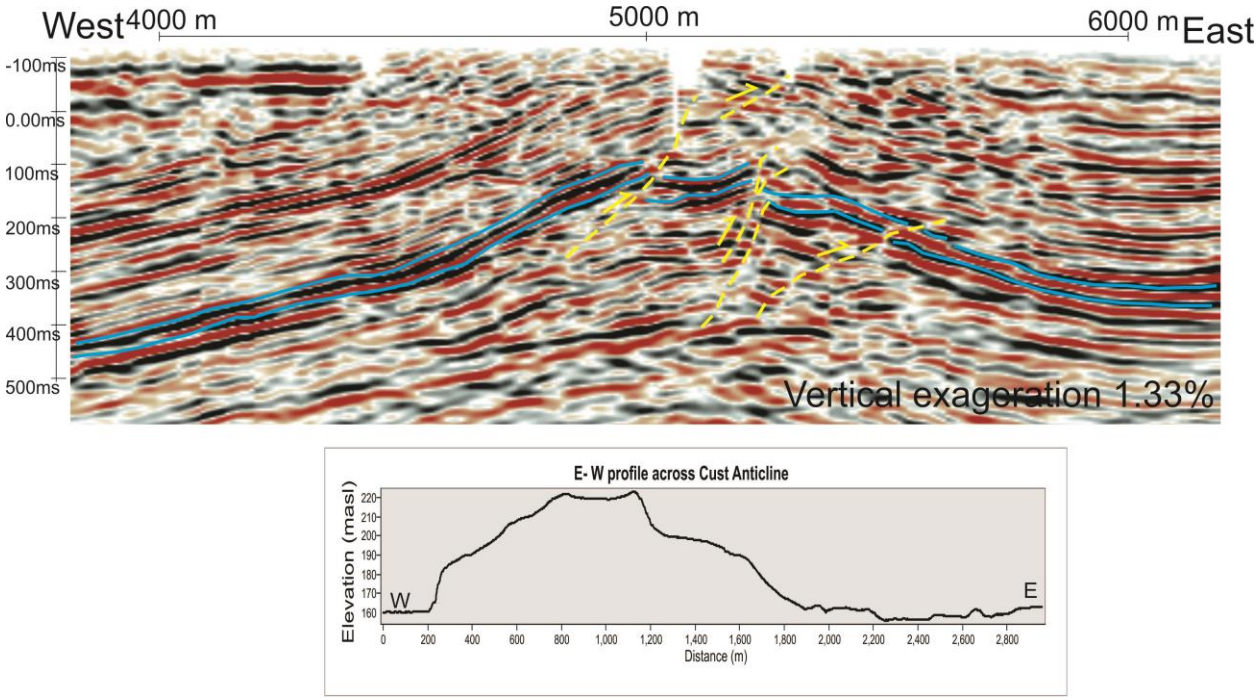

Figure 5.5. Seismic line 205 with minimal vertical exaggeration. This figure represents only the top 500 ms TWTT between the surface locations of 4–6 km along the line (the full seismic line with interpretation is shown in Appendix 1). It shows the top of Oligocene surface (blue) below the western arm of the Cust Anticline with the preferred interpretation of faults (dashed yellow lines). The W–E ground surface LiDAR profile across this section of the line is shown below for comparison, however, this profile has significant vertical exaggeration and corresponds to the elevated surface above the Canterbury Plains datum (0.00ms) which on the seismic profile is represented above 0.00 ms.

5.5.5. Area 5: E–W Cust Anticline - Mairaki Downs

This area is crossed by N–S seismic lines 106 and 109, which run perpendicular to the Mairaki Downs, and line 108 that runs parallel to the southern edge of the Mairaki Downs (Figure 5.1 and Appendix 1). There is no indication on line 108 for the inferred E–W-striking fault trace along the southern edge of the Mairaki Downs (LiDAR fault F8) although if this line did cross this fault it would be at a very oblique angle. However, the presence of this E–W-striking fault is clearly confirmed along line 106 by the south-facing monocline step, upthrown to the north, within the top of Oligocene marker horizon underlying the Cust Anticline south of the Mairaki Downs (Figures 5.2 and 5.6).

Line 109 indicates a steeply dipping fault (upthrown to the south) across the plunging eastern termination of the Cust Anticline. This is the most significant structure in terms of vertical offset across the entire study area (Appendix 1, line 109). The exact location of this structure with respect to any surface geomorphology is difficult to determine due to the highly dissected topography although it is probably close to the northern margin of the Mairaki Downs. However, it is clearly a bounding structure to the formation of the Cust Anticline and is likely to connect at depth with other E–W-striking Late Cretaceous faults (i.e. the E–W-striking fault south of the Mairaki Downs line 106). This structure is clearly related and confidently correlated to the similarly large fault offset north of the Mairaki Downs on line 106 (Figure 5.6).

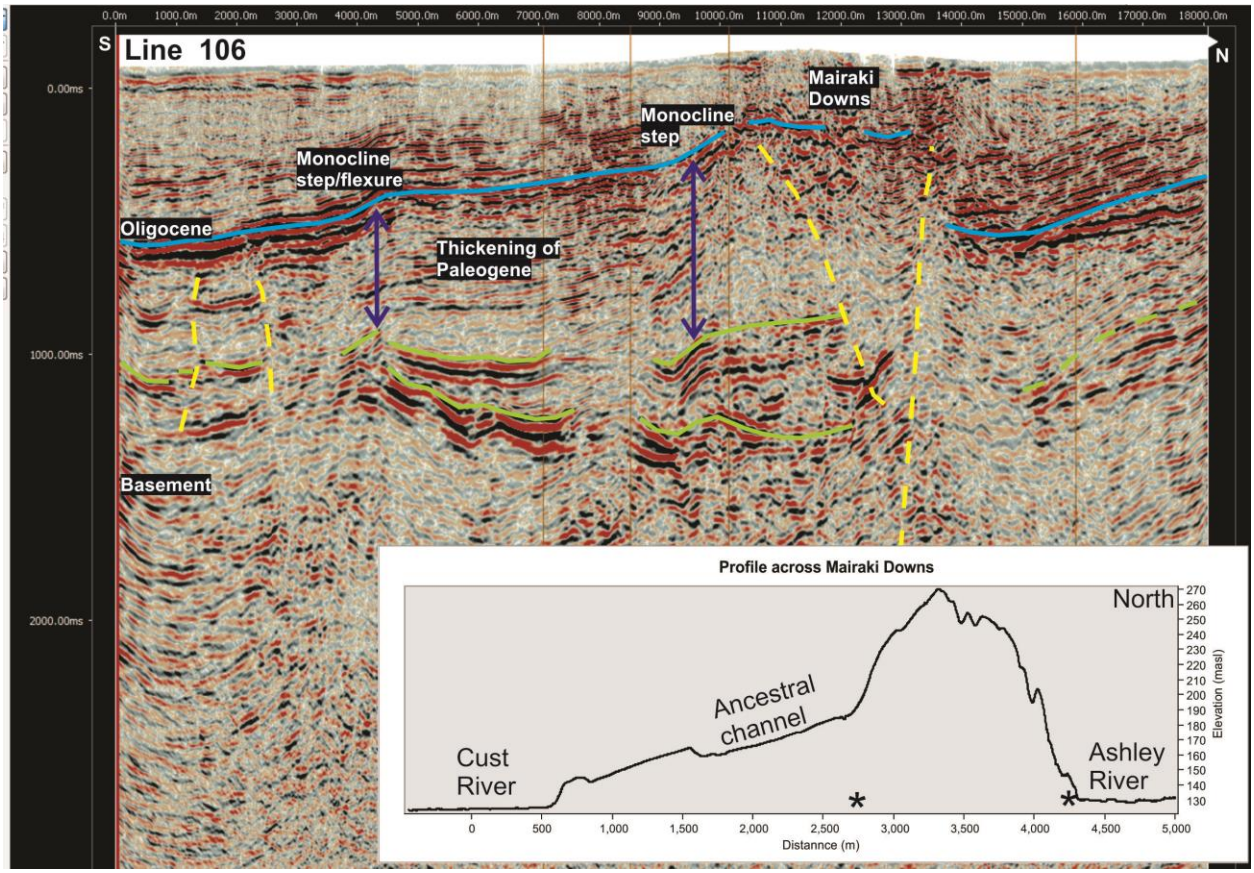

Figure 5.6. Seismic line 106 indicating the top of the Oligocene surface below the E–W Mairaki Downs section of the Cust Anticline. Inset: The N–S ground surface LiDAR profile across the Mairaki Downs. The approximate surface location of the faults either side of the Mairaki Downs are indicated by an asterisk.

5.5.6. Area 6: Northeast of the Cust Anticline

The seismic reflection lines 109, 110 and 111 are present in this area and have been previously interpreted for the Ashley and Loburn faults (Jongens et al., 2012; Ghisetti & Sibson, 2012). Interestingly, at the northern end of line 109 on the downthrown side of the major fault discussed in area 5, a structural depression of the Oligocene surface is apparent west of the location of the Holocene trace of the Ashley and Loburn faults north of the Ashley River. This is confirmed by line 110 which indicates that the top of Oligocene surface dips to the southeast and is at its structurally lowest level along line 110 west of the Okuku River (Appendix 1).

5.6. Top of Oligocene surface two-way-travel-time structure contour map

A provisional TWTT structural contour map of the top of Oligocene surface across the study area, encompassing the significant fault and fold structures disrupting the Oligocene surface, has been developed (Figure 5.7). This map indicates the top of Oligocene structural culminations and basins, which underlie both the low-relief aggradation surfaces and the structural highs that have

developed, due to active tectonics in the Late Quaternary, across this section of the Northwest Canterbury Plains.

The top of Oligocene surface is significantly uplifted underneath the western arm of the Cust Anticline which is also reflected by the uplift expressed at the surface by this structure. The closeness of the contours also indicates that the asymmetric western arm of the Cust Anticline is characterised by steep limbs. The top of Oligocene contours derived from the seismic reflection profiles also confirm the steep plunge at the southern termination of the anticline, and does not indicate any projected continuation of this anticline south of the Cust River. Here the top of Oligocene surface appears to flatten into the E–W-trending monocline bounded structure that extends westward to Starvation Hill (Figure 5.7). With respect to the E–W-trending Mairaki Downs section of the Cust Anticline the top of Oligocene contours representing the south limb of this anticline gradually dip southwards via a series of monocline steps/flexures towards the Eyre River in comparison to the fault terminated north limb of the Mairaki Downs. The north limb has been eroded by the present-day Ashley River which may be trapped in a fault angle depression as a result of the fault along the northern margin of the Mairaki Downs (Figure 5.7).

Interestingly, there is a basin-like depression of the top of Oligocene surface to the northwest of the Cust Anticline between the Ashley River and the Cust River (Figure 5.7). This depression is therefore northwest of the left-step restraining stepover fault relay driving the growth of the complex Cust Anticline between E–W-striking segments of a large basement fault system. A similar but smaller top of Oligocene surface lowpoint is present, north of the Ashley River and west of the Okuku River, west of the Loburn and Ashley fault surface traces. This is to the northwest of the inferred left-step between the Ashley Fault to the eastern termination of the Cust Anticline. Although, the Ashley/Loburn structure is much less evolved than the Cust Anticline structure, this similarity may provide further evidence for the Ashley/Loburn structure undergoing a left-step via a northeast-striking fault onto the Cust Anticline.

The top of Oligocene surface structure contours also indicate that there is a gradual southeast dip of the Oligocene surface across the region both north of the Ashley River and south of the Eyre river, to the north and south of the Cust Anticline structure respectively. This regional dip is also present in the Late Cretaceous (Ghisetti & Sibson, 2012).

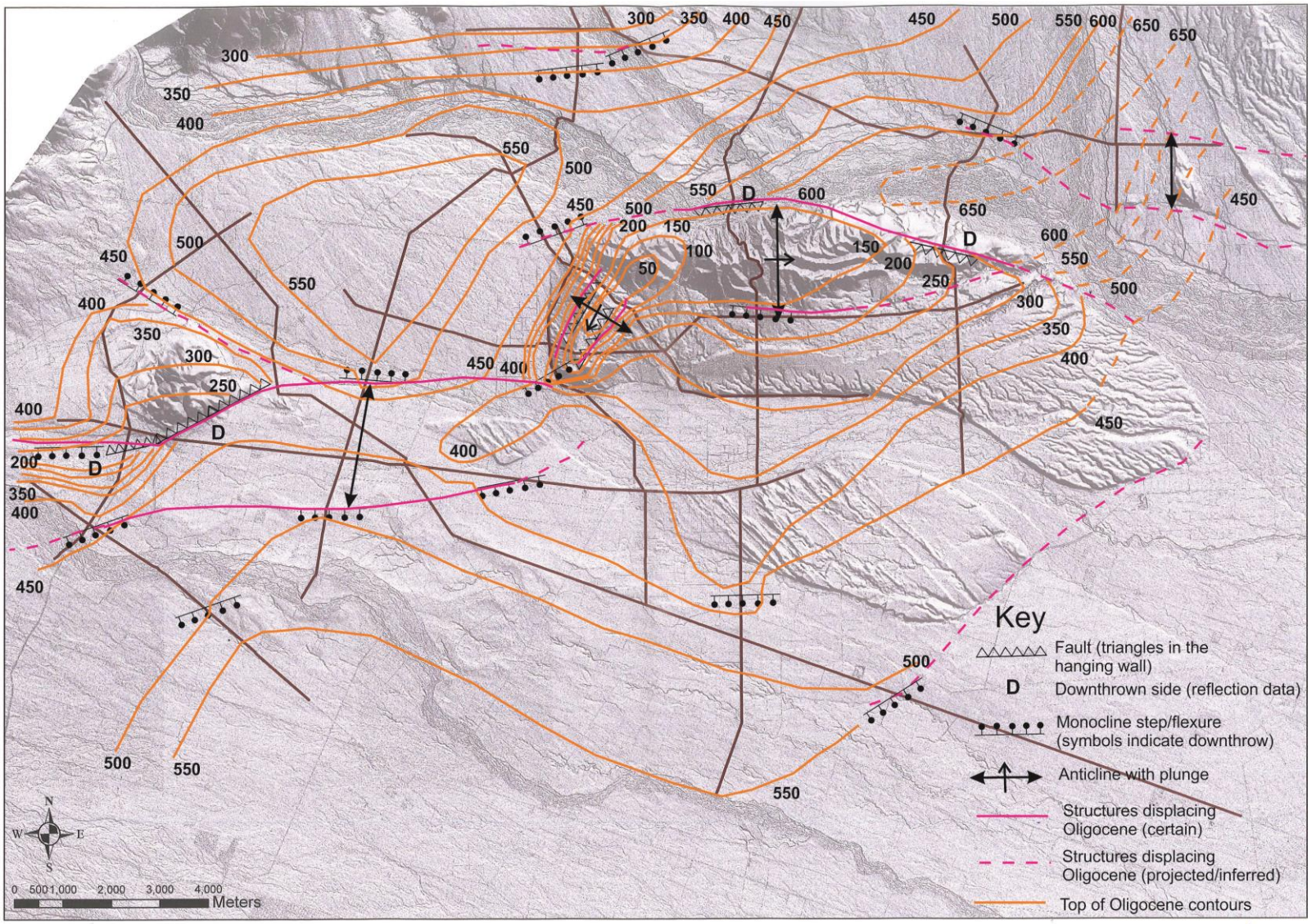

Figure 5.7. Top of Oligocene surface determined by two-way-travel-time contouring across the study area. The two-way-travel-times were defined with respect to sea-level with positive values representing depths below sea-level.

5.7. Summary of seismic interpretation

Structures disrupting the top of Oligocene surface (Figure 5.2) identified in industry seismic reflection lines beneath the study area correlate with the following surface-mapped active structures interpreted from the LiDAR data (Chapter 3, Figure 3.12) and also from the paleo-seismic investigations (Chapter 4):

- An E–W-striking fault southwest of Starvation Hill (LiDAR fault F1).
- A northeast-striking reverse fault across the southeast slopes of Starvation Hill (LiDAR fault F2).
- An inferred E–W-striking fault trace east of Starvation Hill and across the Cust River floodplain (LiDAR fault F3).
- An E–W-striking fault at the southwestern termination of the Cust Anticline within the northern Cust River floodplain (LiDAR fault F4).
- Asymmetric uplift of the western arm of the Cust Anticline with a structural depression across the anticline axis bounded by two north-northeast-striking thrust faults along the crest (LiDAR faults F5 and F6).
- An E–W-striking fault trace on the south side of the Mairaki Downs in line with the termination of the north-northeast-striking faults of the western Cust Anticline (LiDAR fault F8).

The top of Oligocene surface also indicates that across the study area there is (Figure 5.7):

- A gradual dip of the Oligocene reflector W–E both to the southwest of the anticline (lines 202, 204) and north of the anticline (line 110).
- An E–W-trending elevated top of Oligocene surface between Starvation Hill and the southwest termination of the Cust Anticline (line 105).
- Confirmation that this E–W structure between Starvation Hill and the western arm of the Cust Anticline is linked by the tightly folded north-northeast-trending western arm of the Cust Anticline to the older and much more evolved E–W-trending Mairaki Downs section (lines 107, 205, 203).
- A top of Oligocene surface structural basin-like depression west of the region where there is a change in strike of the Cust Anticline (lines 105, 107, 201) and a similar structural depression of the top of Oligocene surface west of the ground-surface location of the emerging low-relief anticline between the Loburn and Ashley faults (lines 109, 110, 111).

- The largest fault within the study area corresponds with the E–W-striking structure on the northern side of the Mairaki Downs and across the plunging eastern termination of the Cust Anticline (line 106, 109).

The overall interpretation of the structures in the seismic profiles, as quantified using the top of Oligocene surface (and correlated with the ground surface LiDAR interpretation), confirms a series of left-stepovers, between E–W-striking (inherited and re-activated) faults, through various structural culminations across the study area. These left-stepovers, are facilitated by a complex relay of northeast-striking thrust faults and thrust propagated anticlines and cross-faults. This mesh of active tectonic structures extends between the E–W-striking Ashley Fault to the northeast via the E–W-striking faults on the north and south sides of the Mairaki Downs. It then continues by left-stepping across the western arm of the Cust Anticline to the E–W-striking Glews Road fault southwest of the Cust Anticline (as confirmed by the paleo-seismic studies) and its extension across to Starvation Hill. Finally, a left-stepover around Starvation Hill links to the likely E–W-striking fault trace from Starvation Hill to the rangefront.

A similar interpretation, beneath the Mairaki Downs, has been previously suggested through an analysis of the Late Cretaceous structures within these seismic lines (Ghisetti & Sibson, 2012) where their F4 fault corresponds to a partially re-activated Late Cretaceous E–W-striking structure north of the Mairaki Downs and their F5 fault corresponds to a partially re-activated Late Cretaceous E–W-striking structure south of the Mairaki Downs. Re-activation of these Late Cretaceous structures was greatest westward along their identified faults corresponding to the elevated culmination of the Cust Anticline. In the above discussion, as well as the LiDAR interpretation (Chapter 3) and paleo-seismic discussion (Chapter 4), significant further detail of these E–W-striking and northeast-striking structures has been provided suggesting a series of common structural relays across the area that have the same underlying characteristics but different degrees of expression.

Chapter 6. Discussion and conclusions

6.1. Structural and tectonic synthesis

At a regional level the structural styles of active earth deformation observed across the Northwest Canterbury Plains are characterised by complex interactions of re-activated, inherited E–W-trending faults, now accommodating oblique strike-slip, with newly developed relays of northeast-striking thrust faults and associated thrust propagated anticlines (e.g. Campbell et al., 2012). Within this framework the geomorphic expression of structural culminations within the study area for this project has evolved in response to Late Quaternary tectonic activity. Across the intervening aggradation surfaces of the plains the ongoing fluvial and aeolian deposition has also been overprinted by active tectonic movements. However, the geomorphology and expression of active tectonic related landforms across the plains is masked by the highly active depositional environments of the large fan surfaces, river erosion and by the fact that activity on many of these structures is not frequent.

A review of the available industry seismic lines across the study area has emphasised the presence of a series of common structural styles that have the same underlying structural drivers but vary in the degree of development and expression both in the seismic profiles and in surface elevations across the study area. The structural interpretations based on the subsurface geology are consistent with the proposed structural mesh of interacting E–W-striking oblique strike-slip and northeast-striking reverse/thrust faults across the area and also provide constraints on the locations of faults with respect to the evolving structural culminations. The LiDAR digital terrain maps provided for a more detailed analysis of individual fault and fold surface expression. They also indicated previously unrecognised active fault traces, with surface expression, across the low-relief aggradation surfaces that are consistent with the subsurface geology and with predictions based on the structural mesh of interacting faults across the region. Paleo-seismic studies were able to confirm the location, and structural style, of tectonic structures both across the crest of the western arm of the Cust Anticline and immediately to the southwest of the steeply plunging Cust Anticline termination. This is an area, where the western arm of the Cust Anticline has formed due to interaction between its underlying north-northeast-striking faults with the E–W-striking fault projection between the Cust Anticline and Starvation Hill to the southwest and the E–W-striking faults on the north and south side of the Mairaki Downs that project eastward towards the Ashley Fault. This area, which stretches ~35 km east-northeast from Oxford is subsequently referred to as the Oxford–Cust–Ashley Fault System.

The Cust Anticline and Starvation Hill represent contractional pop-up structures, with complex styles of deformation driving different surficial expression, at restraining stepovers within this newly evolving dextral shear system exploiting the inherited, re-activated basement fault zone. The oldest E–W-trending section of the Cust Anticline (Mairaki Downs) is bounded to the north by a re-activated E–W-striking fault with the largest subsurface offsets, revealed from the seismic reflection profiles, within the study area (Figure 6.1). The strike of this fault extends sub-parallel along the northern boundary of the anticline and has significant throw (>500 m) along this margin where there is clear topographic surface elevation. However, this throw quickly reduces westward to insignificant amounts where the E–W-striking Cust Anticline interacts with the younger north-northeast-striking western arm of the Cust Anticline. Similarly, an inherited, Late Cretaceous–Paleogene E–W-striking fault of opposite throw bounds the southern limb of the Mairaki Downs however, the eastward extent of this structure, although present, is less precisely confirmed. The large spatial overlap of these two E–W-striking structures, observed in the seismic reflection data, has resulted in the topographic elevation of the high-relief E–W-trending section of the doubly plunging Cust Anticline due to significant re-activated, strike-slip driven inversion of the inherited, oppositely-dipping transpressive E–W-striking faults.

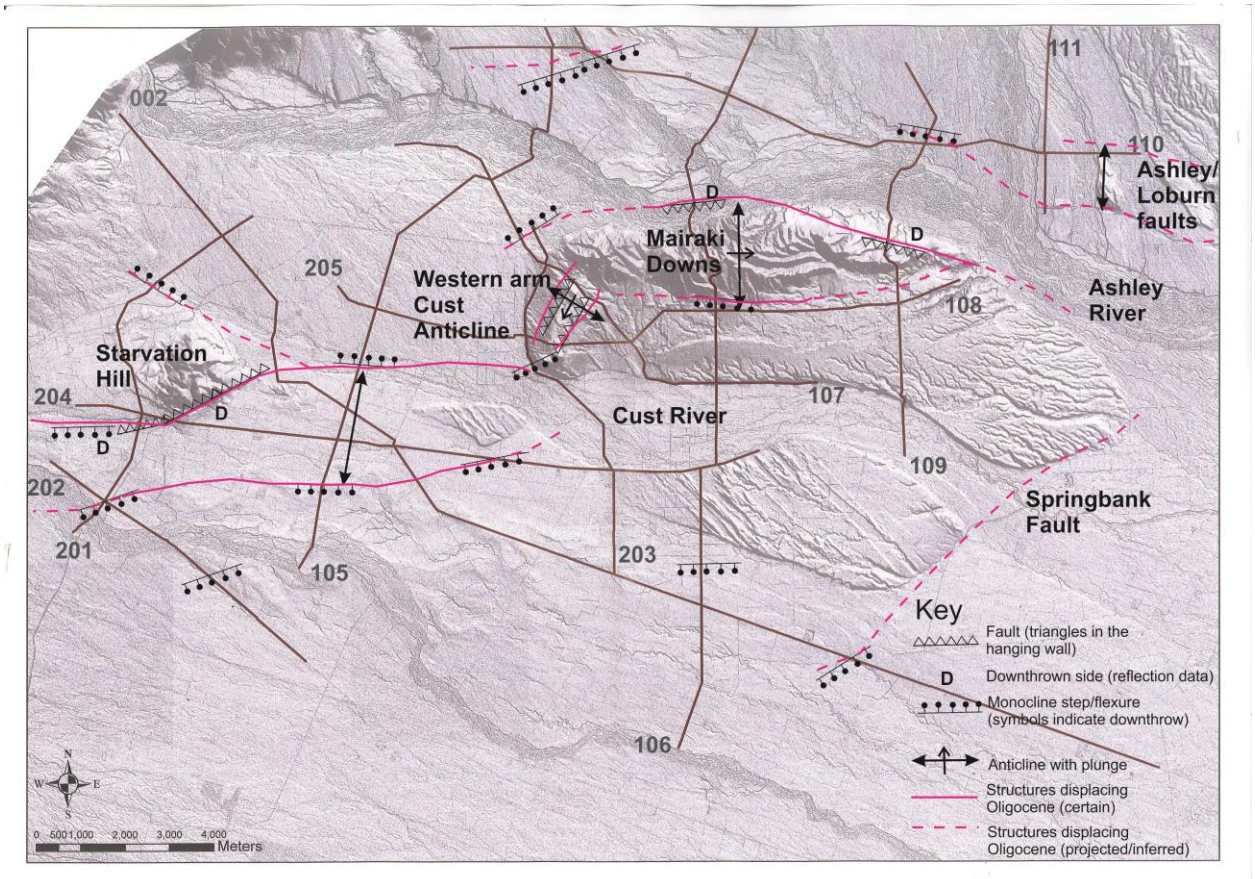

Figure 6.1. Interpretation of the main structures displacing the top of Oligocene surface, established from industry seismic reflection lines, across the study area as discussed in Chapter 5.

Interaction of the Mairaki Downs bounding, E–W-striking, faults with younger north-northeast-striking thrust faults underlying the western arm of the Cust Anticline creates cross-folded interference resulting in the L-shape anticline structure. At this junction the fault underlying the southern margin of the Mairaki Downs terminates and dextral-slip is dissipated through the western Cust Anticline restraining stepover structure. This forms a strike-slip fault relay, within the present-day tectonic stress regime, between the fault to the north of the Mairaki Downs and the E–W-striking fault (Glews Road site) southwest of the anticline extending to Starvation Hill (Figure 6.2).

Starvation Hill is complexly folded with two interfering fold axes indicative of the interaction of more than one active fault, of different strike and slip sense, during its formation and which is confirmed on the seismic reflection profiles. The throw of the E–W-striking faults southwest of both the Cust Anticline and Starvation Hill is north side up which is consistent with these faults acting as tear-fault structures at these locations due to the continued emergence of these structural culminations.

6.2. Fault zones forming the Oxford–Cust–Ashley Fault System

The following fault zones are defined, from southwest to northeast across the study area, based on LiDAR surface mapping and the preliminary re-analysis of industry seismic reflection data.

6.2.1. Starvation Hill Fault Zone

This fault zone consists of E–W-striking faults to the northeast and southwest of Starvation Hill connected by a northeast-striking relay fault (Figure 6.2). Similar structures are also found within the Cust Fault Zone to the east-northeast. The LiDAR indicated three faults that bound Starvation Hill: an E–W-striking fault between Oxford and the southern apex of Starvation Hill (F1), a northeast-striking fault across the southeast slopes of Starvation Hill (F2) and an E–W-striking, discontinuous fault trace (F3) from Starvation Hill towards the southern termination of the Cust Anticline. Structures within the seismic reflection profiles are present for all three traces. Starvation Hill is in the hanging wall of a west-dipping fault, observed in the seismic, that projects to a surface location across the southeast-facing slopes. Surface expression along the E–W-striking fault traces is subtle with minimal surface folding, although there is greater surface expression on the trace southwest of Starvation Hill. There is no apparent overlap of the tips of the E–W-striking faults to the northeast or southwest of Starvation Hill as determined from the

LiDAR surface mapping or the presently available seismic across this area (Figure 6.2). However, recently acquired high resolution seismic reflection surveys around Starvation Hill may provide new insight into these subsurface structures but the data is not available at this time.

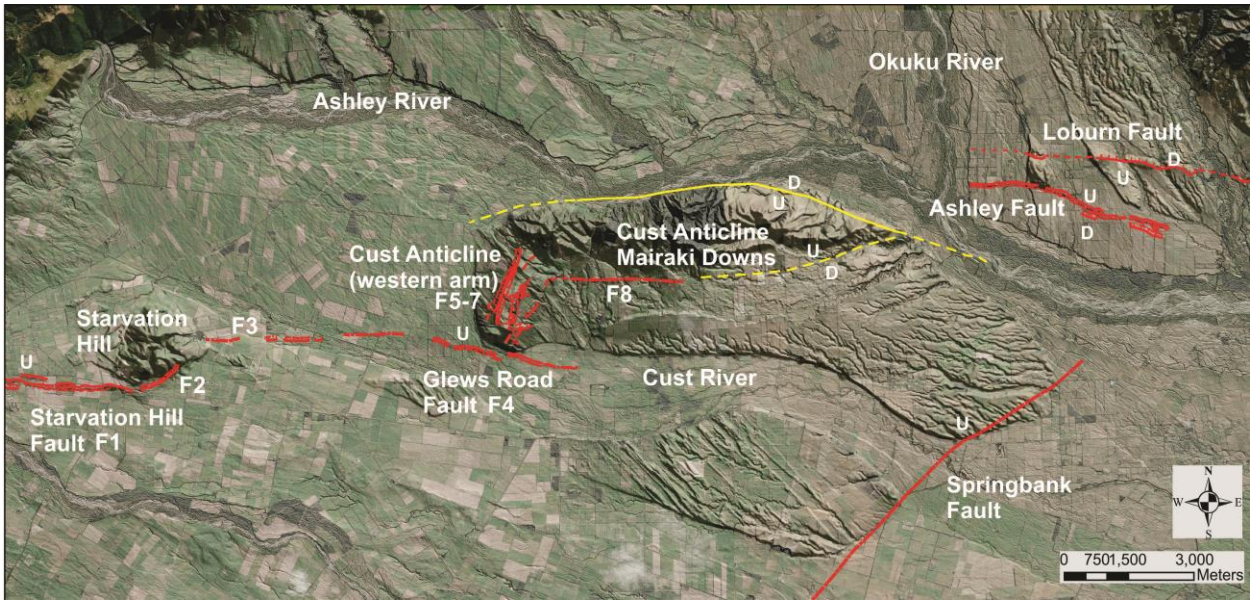

Figure 6.2. Summary of fault traces determined from the LiDAR analysis and the re-interpretation of industry seismic reflection lines across the study area. LiDAR image at scale of 1:100,000. The main LiDAR interpreted fault segments referenced in the text are labelled F1–F8 and are indicated in red. The faults, not observed on the LiDAR, but based on re-interpretation along the top of Oligocene marker horizon of industry seismic reflection lines are indicated in yellow.

6.2.2. Cust Fault Zone (western arm of the Cust Anticline)

This fault zone includes both the north-northeast-trending western arm of the Cust Anticline and the area of the Cust River floodplain immediately to the southwest of the plunging tip of the Cust Anticline (Figure 6.2). The LiDAR has clearly detailed the geometry of the two north-northeast-striking crestal faults (western fault F5; eastern fault F6) and the asymmetric, plunging anticline structure was confirmed within the seismic lines. Although the kinematics of faulting in the Quaternary and cover sequence strata was not able to be unequivocally confirmed the preferred option from this study is for northwest-dipping thrust faults controlling fault propagated folding of both the eastern and western limbs. Included in this fault zone is the E–W-striking fault (LiDAR fault F4) immediately southwest of the Cust Anticline which was first recognised in this study and for which detailed paleo-seismic and geophysical results are presented in Chapter 4 (Section 4.2; Glews Road site). Therefore, faulting indicates that the north-northeast-trending western arm of the Cust Anticline is a ramp inversion structure between E–W-striking faults to the north and south of this restraining stepover. The overlap between the western tip of the structure imaged in seismic reflection profiles along the Ashley River, north of the Mairaki Downs, and the eastern tip of the Glews Road Fault, obtained from LiDAR surface expression is

between 2–3 km (Figure 6.2). The E–W-striking Glews Road fault probably acts syn-kinematically with the north-northeast-striking faults, however, this was not confirmed from the paleo-seismic dating results.

6.2.3. Mairaki Downs Fault Zone

The Mairaki Downs section of the Cust Anticline is formed within the upthrown hanging wall of the transpressively re-activated E–W-striking, south-dipping (inherited normal) fault along the northern margins of this structural high. The elevation of the Mairaki Downs is clearly a result of activity along this fault (Figure 6.2). This fault appears to extend the length of the E–W-trending Cust Anticline as documented on the seismic reflection profiles and is around 10–11 km in length with a throw of ~500–600 m of the top of Oligocene surface. Industry seismic also reveals a re-activated E–W-striking, north-dipping (inherited Late Cretaceous normal) fault along the south margin of the Mairaki Downs that coincides with an inferred E–W-striking surface fault trace (LiDAR fault F8) that extends westwards towards the location of the change in trend of the L-shaped Cust Anticline (Figure 6.2). This fault is probably an antithetic back-thrust off the main E–W-striking fault bounding the northern edge of the Mairaki Downs and overlaps the northern limb fault by ~6–7 km providing the greatest degree of overlap between any two E–W-striking faults, associated with the structural culminations within the study area.

6.2.4. Ashley Fault Zone

This zone has been previously identified east of the Okuku River based on field mapping and paleo-seismic studies of the E–W-striking component faults including the Ashley Fault and Loburn Fault (Sisson et al., 2001) as well as more recently using LiDAR (Barrell & Van Dissen, 2014). These two faults overlap for around 3.5 km east of the Okuku River, creating a low-relief anticline (structural inversion) between oppositely dipping E–W-striking faults with the less active Loburn Fault located north of the more active Ashley Fault (Figure 6.2). The surface traces of the Ashley and Loburn faults appear to terminate westward near the Okuku River. Although the Ashley Fault Zone (incorporating both faults) has been inferred to extend west of the Okuku River (Campbell et al., 2012; Ghisetti & Sibson, 2012; Jongens et al., 2012) its surface expression there is equivocal. Therefore, the overlap between the Ashley and Loburn Fault Zone with the large fault, on the south side of the Ashley River, bounding the north margin of the E–W-trending Mairaki Downs, is not well constrained. Furthermore, the detail of how deformation transfers through this fault relay, from the Ashley Fault Zone west-southwest across

to the L-shaped Cust Anticline, is not clearly documented although the Ashley River most likely occupies a structural depression (Figure 6.2).

6.3. Explanations for tectonic structures within the study area

Transpressional uplifts across restraining bends or stepovers are integral to strike-slip fault zones and form areas of anticlinal uplift, commonly with doubly plunging fold formations of limited strike extent (e.g. Christie-Blick & Biddle, 1985; McClay & Bonora, 2001). Antiformal pop-up structures (that have both positive structural and topographic relief) developed above restraining stepovers/bends in offset strike-slip fault systems have been simulated using sandbox models (e.g. McClay & Bonora, 2001). Restraining bend geometry is dependent on the stepover angle and the stepover width between the controlling strike-slip fault segments. In plan view restraining bends and stepovers form lozenge-shaped popups across underlapping stepovers and sigmoidal antiform pop-ups for more overlapping restraining step-overs (McClay & Bonora, 2001). The pop-up structures are often asymmetric and rotation of the uplifted region increases with the amount of overlap of the controlling strike-slip faults. The formation of cross-cutting faults and anastomosing synthetic and antithetic shears is also dependent upon the geometry of the stepover faults with a decrease in the width of the stepover resulting in narrower pop-ups with more complex internal structures (McClay & Bonora, 2001; Dooley & Schreurs, 2012).

The hybrid tectonic deformation across North Canterbury is fundamentally associated with dextral transpressive strike-slip structures that extend from offshore below Pegasus Bay onshore across to the Southern Alps foothills (e.g. Barnes et al., 2011). It also involves crustal shortening on northeast-striking upper plate thrust fault blocks with southeast-facing faults propagating from a basal décollement at the frontal edge as a result of an inferred ductile mid-crustal detachment below the Canterbury Plains (e.g. Reyners et al., 2013). The Oxford–Cust–Ashley Fault System is within one of these upper plate thrust fault blocks. However, the extent of re-activation of the E–W-striking faults is controlled by segmentation, thus not involving the entire length of individual faults (Ghisetti & Sibson, 2012). Characteristically, slip deformation is transferred across relays of E–W-striking faults linked by northeast-striking thrust faulting repeatedly forming restraining stepovers across the region.

Restraining bend/stepover structures of similar dimensions to those linking across the Ashley/Loburn faults, the Cust Anticline and Starvation Hill have been documented along the

San Andreas Fault strike-slip system in California (e.g. Brown & Sibson, 1989; Brown et al., 2001). Restraining bend slip transfer has also been documented in many other similar tectonic settings around the world (e.g. McClay & Bonora, 2001; McCalpin, 2009; Dooley & Schreurs, 2012) as well as in New Zealand (e.g. Campbell et al., 2012).

Although the seismic reflection data indicate similar structures underlying the structural culminations within the study area the surface expression of these culminations and the fault and fold driven geomorphology as detailed from the LiDAR is more variable. Three factors to explain the varying expression of these structural culminations segmenting the E–W-striking faults across the study area are: (i) the amount of inversion on the inherited E–W-striking Late Cretaceous faults; (ii) the potential fault length, and (iii) the overlap of the segmented E–W-striking fault structures either side of the structural restraining stepover culminations. A first-order qualitative summary of this evidence is provided based on the LiDAR and seismic data within the resolution available in these datasets.

The E–W-trending Mairaki Downs section of the Cust Anticline is bounded by a subsurface fault that extends up to 11 km sub-parallel to the northern margin of this structure and has the greatest amount of inversion (up to 500–600 m throw) of any fault within the study area. This fault appears to overlap by up to ~6–7 km with an E–W-striking fault on the south side of this anticline (Figure 6.2). Therefore, this region is bounded by E–W-striking faults with significantly greater inversion, in terms of both throw and strike-length, and greater overlap than either of the structural culminations to the southwest or northeast. The length of the north-northeast-striking faults along the western arm of the Cust Anticline is up to two kilometres with significant structural uplift of the anticline observed in the Quaternary reflectors on the seismic profiles. There is only between 2–3 km of overlap of the E–W-striking faults located north and south of the western arm of the Cust Anticline; the intervening E–W-striking trace south of the Mairaki Downs appears to be truncated by the tips of the north-northeast-striking faults (Figure 6.2 and Figure 6.3).

The overlap of the E–W-striking structures bounding Starvation Hill is minimal and the length of the northeast-striking relay fault is less than the north-northeast-striking faults of the western arm of the Cust Anticline. There is also less uplift of the subsurface structure documented in the seismic reflection profile data. Interestingly, seismic structures that disrupt the top of Oligocene reflector horizon with throws of >150–200 m appear to result in significant positive topographic

elevation consistent with that present at Starvation Hill and the Cust Anticline. Finally, although there is overlap of the Loburn and Ashley faults to the northeast there is only a very low-relief anticline forming between these structures which may reflect a lower degree of inversion associated with these fault traces.

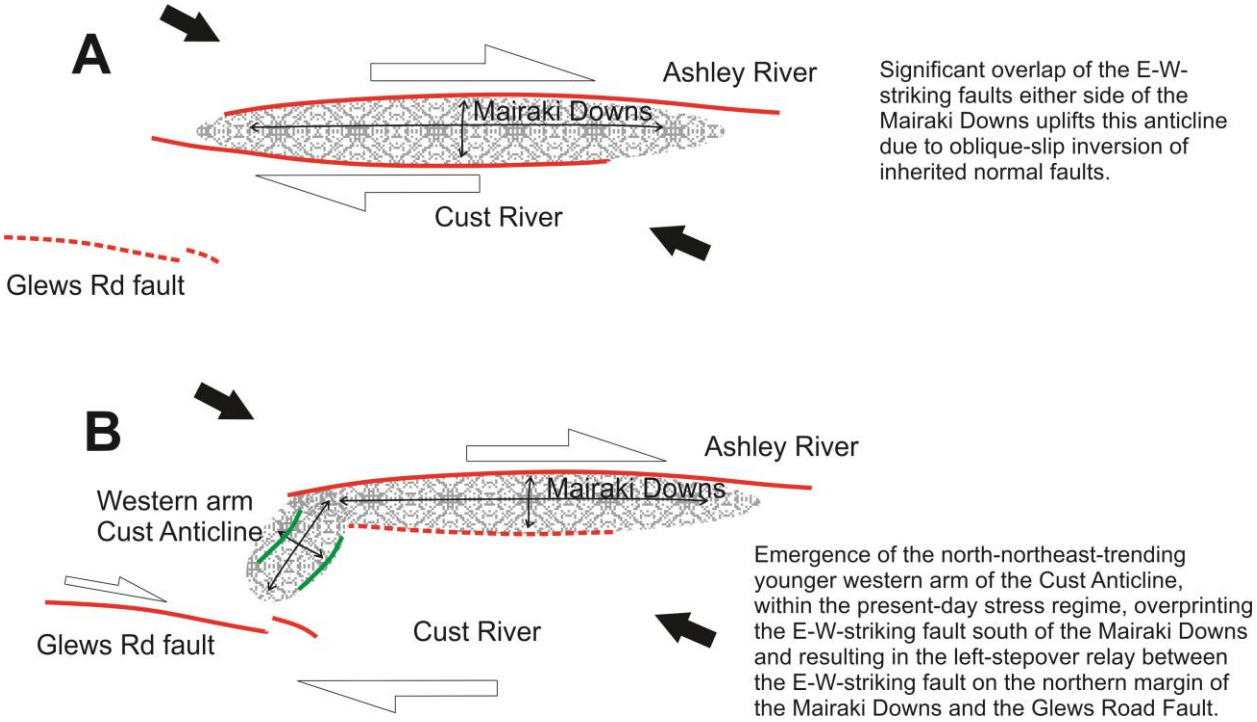

Figure 6.3. Schematic model for the evolution of the L-shaped Cust Anticline and the restraining stepover through the western arm of the Cust Anticline due to associated structural inversion of E–W-striking, inherited Late Cretaceous normal faults. Note how the width of the restraining stepover increases with emergence of the north-northeast-trending western arm of the Cust Anticline, within the present-day contractional stress regime, due to selective termination and re-activation of E–W-striking faults. Thrust faults controlling the western arm of the Cust Anticline are indicated in green and E–W-striking faults are indicted in red. Dashed lines indicate overprinted faults or faults not related to the development of the structure described. The regional maximum compressive stress direction (115°) is indicated by large black arrows.

Positive fault inversion has recently been studied and documented within the Taranaki Basin to determine factors that may affect the degree of inversion expected across a region (Reilly et al., submitted). The amount of normal displacement prior to inversion as well as the length of the previous extensional faults is important for determining the amount and length of the re-activated faults. In the Taranaki Basin, faults with vertical displacement >600 m and lengths >9 km were more likely to show significantly greater inversion. These longer inverted faults are also likely to accommodate more of the total strain budget during deformation and might work to accommodate displacement in preference to smaller faults. This is consistent with the first-order seismic interpretation of structures, in terms of the throw and fault lengths of re-activated, inherited normal faults, across the field area (i.e. Mairaki Downs versus the Starvation Hill

structural culminations). However, the re-activation of faults in North Canterbury involves transpresional strike-slip compared to the reverse re-activation in Taranaki therefore more significant correlations cannot be justified at this stage.

Therefore, the significant structural development of the Cust Anticline compared to other structural culminations might be representative of, and reflect the pre-inversion tectonics of the Late Cretaceous faults. The emergence of the restraining stepover structures is further enhanced by the degree of interaction with younger northeast-striking thrust faults in the present-day stress regime. In other words the larger the pre-inversion displacements and fault lengths the greater the post-inversion tectonic effects which are likely enhanced by greater amounts of pre-existing heterogeneities in regions as a result of the pre-inversion activity. Interestingly, fault inversion and re-activation only occurs across a small percentage of an initial normal fault system and an analysis of the Late Cretaceous faults beneath the Cust Anticline has indicated greater inversion westward, but not complete inversion along the entire length, of some of these E–W-striking faults (Ghisetti & Sibson, 2012). Other factors that may have an influence on which fault segments may show re-activation might include the relative orientation of the inherited faults with respect to the present compressional stress regime, the fault dip and fluid overpressure.

6.4. Future work

1) Targeted high resolution seismic reflection lines across some of the above established structures would be useful to determine more detail, with respect to fault growth and structural style of deformation, within the shallower level stratigraphy.

i) A high resolution line across the crest of the western arm of the Cust Anticline could determine if the structural characteristics documented in the north-northeast-striking eastern scarp (Elliotts Road trench) are similar across the western scarp. It may also determine how close to daylighting these faults are and provide evidence for reverse or alternatively shallow aseimogenic normal faults bounding the structural anticlinal depression of the western arm of the Cust Anticline. This may reconcile potential disparities, due to poor resolution, between the seismic reflection profiles above the Oligocene horizon and the surface expression of the faults.
ii) A high resolution seismic reflection line across the southeast limb of the western arm of the Cust Anticline (along Elliotts Road) may determine whether flexural-slip type faulting occurs in this location.

iii) A high resolution seismic reflection line across the E–W-striking fault established immediately to the southwest of the steeply plunging Cust Anticline could determine deeper characteristics of this structure (Glews Road trench).

iv) Further lines south of IP line 111, southeast of IP line 110 and east of IP line 109 and 108 cold establish subsurface structures related to the Ashley Fault and faults at the eastern termination of the Mairaki Downs.

2) Further OSL dating of the Late Pleistocene gravels within the crestal zone of the western arm of the Cust Anticline. In particular to establish an age constraint from material or loess within gravels that are definitely related to the onset of uplift of the paleo-aggradation surface as opposed to loess layers draping across the underlying strata. An age from the base of the paleo-dune structures could also be a useful indicator to constrain the onset of uplift. Obtaining an age of the vertically tilted units could also better determine uplift and folding rates of this structure but might require other techniques than OSL to extend back further in time (possibly cosmogenic burial).

3) A detailed analysis of the inferred E–W-striking fault trace across the highpoint at the southern end of the western arm of the Cust Anticline would be informative to understand the complexity of faulting and folding across the restraining stepover structure and exactly how displacement transfer is being accommodated. This might need to involve drilling to determine the amount of loess and gravels below this structure.

4) Field mapping of the inferred E–W-striking trace on the south side of the Mairaki Downs and its projected trace westwards towards the northern termination of the north-northeast-striking crestal faults along the western arm of the Cust Anticline would be informative to ground truth the LiDAR and determine if there are sites for further investigation of this fault. The landowner did not provide permission for access during this study.

6.5. Final conclusions

There is a repetitive structural pattern across North Canterbury that extends beneath the plains away from the more evolved structures closer to the foothills. This structural sequence of northeast-striking contractional faults linked by re-activated, inherited Late Cretaceous E–W-striking faults acting as transpressive dextral strike-slip structures underlies the active tectonic culminations that have emerged within the Late Quaternary. The 2010–2012 Canterbury Earthquake Sequence showed many similarities (determined by aftershock patterns, DInSAR, LiDAR, field mapping and GPS-derived ground deformation data) to the established structural pattern outlined across the study area for this project, albeit with different range of scales (e.g.

Beaven et al., 2102., Elliott et al., 2012., Duffy et al., 2013). The Oxford–Cust–Ashley Fault System therefore provides a more evolved analogue of the recently intensely studied Greendale Fault network involved in the 2010–2012 Canterbury Earthquake Sequence (e.g. Quigley et al., 2012).

The 2010–2012 Canterbury Earthquake Sequence involved synchronous faulting on several interconnected structures and triggering events up to 8–10 km north of the E–W-striking surface trace of the Greendale Fault. Furthermore, thrust fault focal mechanisms were associated with the initial triggering of each of the main earthquake events which then involved aftershock series that were dominated by strike-slip focal mechanisms. Such combined fault ruptures propagating both spatially and temporally through a fault network highlights how a structural mesh of oblique strike-slip E–W-trending faults and northeast-striking thrust faults operates within the active tectonic setting of the present-day transpressional plate boundary margin.

Compared to the Greendale Fault network, which does not have any significantly elevated structural culminations above the plains (but shows a similar pattern of fault rupture and left stepovers), the Oxford–Cust–Ashley Fault System is very clearly segmented by intervening structural culminations (i.e. Starvation Hill, Cust Anticline). The Oxford–Cust–Ashley Fault System has therefore evolved during the Late Quaternary into a new transpressional fault zone that relays through faults linked across contractional restraining stepovers. Interestingly, DInSAR and GPS-derived ground deformation patterns indicated very subtle anticlinal warping and uplift parallel to the faults, and that also coincided with some of the more linear aftershock clustering, of the Canterbury Earthquake Sequence (e.g. Beaven et al., 2012). This is further evidence for the structural similarity between the Canterbury Earthquake Sequence and the documented Oxford–Cust–Ashley Fault System as outlined in this study.

The initial earthquake event of the Canterbury Earthquake Sequence, involving the daylighting Greendale Fault, was across a fault zone about 35–40 km E–W and about 8–10 km N–S, with the E–W Greendale Fault segments themselves being around 30 km in length (e.g. Quigley et al., 2012). The similarly dimensioned study area is also about 35–40 km E–W and about 8–10 km N–S, however, the E–W-striking segments across the study area are shorter at ~6–7 km between the rangefront and Starvation Hill, ~6–7 km between Starvation Hill and the Cust Anticline and ~11–12 km between the western arm of the Cust Anticline and the Holocene trace of the Ashley and Loburn faults east of the Okuku River which can then be traced ~4–5 km further east.

Therefore, the Oxford–Cust–Ashley Fault System has a similar spatial extent to the Greendale Fault location. However, the E–W-striking faults, between the rangefront and the Ashley/Loburn fault traces appear to be more segmented compared to those further southeast across the plains where the development of any structural culminations associated with the more dominant northeast-striking thrust faulting has not become apparent above the surface elevation. This will be a function of the structural geometry associated with the inherited fault fabric, the arrangement of contractional structures interacting with the Greendale Fault and the relative strain rates of structures closer to the foothills versus further southeast across the plains. The N–S separation across the restraining left-stepovers between each of the E–W-striking faults across the study area is around 1.5–2 km.

The greater segmentation closer to the foothills may be due to the influence of more established Late Quaternary rangefront fault systems, such as the Porters Pass–Amberley Fault Zone, on the structural mesh underlying the Canterbury Plains. Although the Cust Anticline is closer to the rangefront there could also be a greater influence, in North Canterbury, from the opposing propagation onshore of effects from the southern Hikurangi subduction margin resulting in greater inversion and emergence of structures in North Canterbury compared to structures south of the Waimakariri River. Furthermore, the development of restraining bend structural culminations within the present-day transpressional fault setting are dependent upon the overlap of E–W-striking bounding structures as well as the amount of inversion and the length of the E–W-striking fault segments accommodating the inversion.

The underlying structural control across the study area therefore indicates how significant structural culminations develop at restraining bend/stepovers and form fault network linkages between the dextral transpressive inherited faults. Although these structural culminations appear to segment the E–W-striking re-activated faults into smaller lengths it is likely that this network of multiple fault segments will be seismogenically linked and earthquake rupture within the Oxford–Cust–Ashley Fault System will likely involve the spatial extent of the system in relative close temporal succession during a protracted earthquake sequence. Furthermore, E–W-striking fault re-activation is preferentially associated with the more dominant northeast-striking thrust faults within the present-day stress regime and therefore activity of E–W-striking active fault traces is closely associated with the location of thrust faults and associated emerging anticlines. The E–W-striking faults acting effectively to accommodate complex displacement transfer between the shorter linking thrust faults.

For instance the E–W-striking Glews Road Fault (LiDAR fault F4 and Chapter 4) is acting as a tear-fault that breaks the surface, showing mapable younger displacement, due to the ongoing emergence of the western arm of the Cust Anticline. This fault is in close association with the north-northeast-striking thrusts and the visible trace terminates very close to the projected termination of the north-northeast-trending steeply plunging anticlinal fold. Therefore, in more evolved regions of the mesh of intersecting faults the daylighted E–W-striking traces are more likely to have surface expression closer to these northeast-striking faults where elsewhere these E–W-striking fault traces are more likely to remain hidden beneath the aggradation surfaces or be masked by ongoing fluvial processes, despite their activity.

Finally, the importance of identification and characterization of presently-hidden fault sources and the understanding of fault network linkages is a critical issue in light of the 2010–2012 Canterbury Earthquake Sequence. Improved understanding of potentially-interactive fault sources and the potential for combined initial fault rupture and spatial and temporal rupture propagation within the Oxford–Cust–Ashley Fault System, immediately north of the Waimakariri River, in future large earthquake events is important given its proximity to Christchurch and other regional centres such as Rangiora, Kaiapoi and Oxford. The results of this study will improve constraints on earthquake source potential in North Canterbury and can be used in probabilistic seismic hazard analysis which is essential for the suitability and sustainability of future social and economic development across the region.

References

Alloway, B. V., Lowe, D. J., Barrell, D. J. A., Newnham, R. M., Almond, P. C., Augustinus, P., et al. (2007). Towards a climate event stratigraphy for New Zealand over the past 30 000 years (NZ-INTIMATE project). *Journal of Quaternary Science, 22*, 9-35.

Anderson, H., Beanland, S., Blick, G., Darby, D., Downes, G., Haines, J., et al. (1994). The 1968 May 23 Inangahua, New Zealand, earthquake: an integrated geological, geodetic, and seismological source model. *New Zealand Journal of Geology and Geophysics 37,* 59-86.

Bannister, S., Thurber, C., & Louie, J. (2006). Detailed fault structure highlighted by finely relocated aftershocks, Arthur's Pass, New Zealand. *Geophysical Research Letters, 33,* L18315, doi: 10.1029/2006GL027462.

Barnes, P. M. (1994). Inherited structural control from repeated Cretaceous to Recent extension in the North Mernoo Fault Zone, western Chatham Rise, New Zealand. *Tectonophysics, 237,* 27-46.

Barnes, P. M., de Lepinay, B. M., Collot, J. M., Delteil, J., & Aeudru, J. C. (1998). Strain partitioning in the transition area between oblique subduction and continental collision, Hikurangi margin, New Zealand. *Tectonics, 17(4),* 534-557.

Barnes, P., Sutherland, R., & Delteil, J. (2005). Strike-slip structure and sedimentary basins of the southern Alpine Fault, Fiordland, New Zealand, *Geological Society of America Bulletin, 117(3/4),* 411-435.

Barnes, P. M., Castellazzi, C., Gorman, A., & Wilcox, S. (2011). Submarine faulting beneath Pegasus Bay, offshore Christchurch. Short-term Canterbury Earthquake Recovery Project 2: offshore faults. National Institute of Water & Atmosphere (NIWA) Client Report WLG2011–28, 46 p.

Barrell, D. J. A. (2013). Glaciations: Late Quaternary of the Southwest Pacific Region. In: S. A. Elias (Ed.), *Encyclopaedia of Quaternary Science,* (pp. 202-215). New York, NY, Elsevier.

Barrell, D. J. A., & Begg, J. G. (2013). General distribution and characteristics of active faults and folds in the Waimakariri District, North Canterbury. GNS Science Consultancy Report 2012/325, 52 p.

Barrell, D. J. A., & Van Dissen, R. J. (2014). Assessment of active fault ground deformation hazards associated with the Ashley Fault Zone, Loburn, North Canterbury. GNS Science Consultancy Report 2013/173, 62 p.

Barth, N. C., Toy, V. G., Langridge, R. M., & Norris, R. J. (2012). Scale dependence of oblique plate-boundary partitioning: new insights from LiDAR, central Alpine fault, New Zealand. *Lithosphere, 4(5),* 435-448.

Beavan, J., Tregoning, P., Bevis, M., Kato, T., & Meertens, C. (2002). Motion and rigidity of the Pacific Plate and implications for plate boundary deformation, *Journal of Geophysical Research,* 107(B10), doi: 10.1029/2001JB000282.

Beavan, J., Motagh, M., Fielding, E., Donnelly, N., & Collett, D. (2012). Fault slip models of the 2010-2011 Canterbury, New Zealand, earthquakes from geodetic data, and observations of post-seismic ground deformation. *New Zealand Journal of Geology and Geophysics (Special issue: Canterbury, New Zealand, 2010-2011 earthquake sequence), 55(3),* 207-221.

Bennett, D., Brand, R., Francis, D., Langdale, S., Mills, C., Morris, B., & Tian, X. (2000). Preliminary results of exploration in the onshore Canterbury Basin. New Zealand Petroleum Conference Proceedings.

Berger, G. W., Pillans, B. J., & Tonkin, P. J. (2001). Luminescence chronology of loess-paleosol sequences from Canterbury, South Island, New Zealand. *New Zealand Journal of Geology and Geophysics, 44(4),* 501-516.

Berryman, K. R., Beanland, S., Cooper, A. F., Cutten, H. N., Norris, R. J., & Wood, P. R. (1992). The Alpine Fault, New Zealand: variation in Quaternary style and geomorphic expression. *Annales Tectonicae, 6,* 126-163.

Bradley, B. A. (2012). Strong ground motion characteristics observed in the 4 September 2010 Darfield, New Zealand earthquake. *Soil Dynamics and Earthquake Engineering, 42,* 32-46.

Bradshaw, J. D. (1989). Cretaceous geotectonic patterns in the New Zealand region. *Tectonics, 8,* 803-820.

Brown, N. H., &, Sibson, R. H. (1989). Structural geology of the Octillo Badlands antidilational fault jog, Southern California. In: D. P. Schwartz, & R. H. Sibson (Eds.), *Fault Segmentation and Controls of Rupture Initiation and Termination, US Geological Survey Open File Reports 89–315,* (pp. 94–110).

Brown, N. H., & Sibson, R. H. (1991). Paleomagnetism of the Octotillo Badlands, Southern California, and its implications for slip transfer through an antidilational fault jog. *Earth and Planetary Science Letters, 102,* 277-288.

Brown, L. J., & Wilson, D. D. (1988). Stratigraphy of late Quaternary deposits of the northern Canterbury Plains. *New Zealand Journal of Geology and Geophysics, 31,* 305-335.

Browne, G. H., & Field, B. D. (1985). The lithostratigraphy of Late Cretaceous to early Pleistocene rocks of northern Canterbury, New Zealand. *New Zealand Geological Survey Record, 6,* 63 p.

Browne, G. H., Field, B. D., Barrell, D. J. A., Jongens, R., Bassett, K. N., & Wood, R. A. (2012). The geological setting of the Darfield and Christchurch earthquakes, New Zealand. *Journal of Geology and Geophysics,* 55(3), 193-197, DOI:10.1080/00288306. 2012.682654.

Burbank, D. W., & Anderson, R. S. (2011). *Tectonic geomorphology*. Hoboken, NJ, John Wiley & Sons.

Campbell, J., Pettinga, J., & Jongens, R. (2012). The tectonic and structural setting of the 4th September 2010 Darfield (Canterbury) Earthquake sequence, New Zealand. *New Zealand Journal of Geology and Geophysics, 55(3),* 155-168.

Carpentier, S. F. A., Green, A. G., Doetsch, J., Dorn, C., Kaiser, A. E., Campbell, F., et al. (2012). Recent deformation of Quaternary sediments as inferred from GPR images and shallow P-wave velocity tomograms: Northwest Canterbury Plains, New Zealand. *Journal of Applied Geophysics, 81,* 2-15.

Cowan, H. A. (1990). Late Quaternary displacements on the Hope Fault at Glynn Wye, North Canterbury. *New Zealand Journal of Geology and Geophysics, 33(2),* 285-293.

Cowan, H., Nicol, A., & Tonkin, P. (1996). A comparison of historical and paleoseismicity on a newly formed fault zone and a mature fault zone, North Canterbury, New Zealand. *Journal of Geophysical Research*, 101(B3), 6021-6036.

Cowan, H. A. (1992). Structure, seismicity and tectonics of the Porters Pass–Amberley fault zone, North Canterbury, New Zealand. PhD thesis, University of Canterbury, 181 pp.

Cox, S. C., & Barrell, D. J. A. (2007). Geology of the Aoraki Area: Institute of Geological and Nuclear Sciences Geological Map 15: GNS Science, Lower Hutt, New Zealand scale 1:250,000, 1 sheet and 71 p.

Cox, S. C., & Sutherland, R. (2007). Regional geological framework of South Island, New Zealand, and its significance for understanding the active plate boundary. *American Geophysical Union Geophysical Monograph, 175*, 19-46.

Christie-Blick, N., & Biddle, K. T. (1985). Deformation and basin formation along strike-slip faults. In K. T. Biddle & N. Christie-Blick (Eds.), Strike-slip deformation, basin formation, and sedimentation. *Society of Economic Palaeontologists and Mineralogists Special Publication, 37,* 1-35.

Davis, J. L., & Annan, A. P. (1989). Ground penetrating radar for high resolution mapping of soil and rock stratigraphy. *Geophysical Prospecting, 37,* 531-551.

Davy, B., Stagpoole, V., Barker, D., & Yu, J. (2012). Subsurface structure of the Canterbury region interpreted from gravity and aeromagnetic data. *New Zealand Journal of Geology and Geophysics, 55(3),* 185-191.

DeMets, C., Gordon, R. G., & Argus, D. (2010). Geologically current plate motions. *Geophysical Journal International, 181,* 1-80, doi:10.1111/j.1365-246X.2009.04491.x.

Dooley, T. P., & Schreurs, G. (2012). Analogue modelling of intraplate strike-slip tectonics: A review and new experimental results. *Tectonophysics, 574-575,* 1-71.

Dorn, C., Carpentier, S., Kaiser, A. E., Green, A. G., Horstmeyer, H., Campbell, F., et al. (2010a). First seismic imaging results of tectonically complex structures at shallow depths beneath the northwest Canterbury Plains, New Zealand. *Journal of Applied Geophysics, 70(4),* 317-331.

Dorn, C., Green, A. G., Jongens, R., Carpentier, S., Kaiser, A. E., Campbell, F., et al. (2010b). High-resolution seismic images of potentially seismogenic structures beneath the northwest Canterbury Plains, New Zealand. *Journal of Geophysical Research B: Solid Earth, 115(11),* B11303, doi:10.1029/2010JB007459.

Duffy, B., Quigley, M. C., Barrell, D., Van Dissen, R., Stahl, T., Leprince, S., et al. (2013). Fault kinematics and surface deformation across a releasing bend during the 2010 M_W 7.1 Darfield, New Zealand, earthquake revealed by differential LiDAR and cadastral surveying. *Geological Society of America Bulletin, 125(3-4),* 420-431.

Eberhart-Phillips, D., Reyners, M., Bannister, S., Chadwick, M., & Ellis, S. (2010). Establishing a versatile 3D seismic velocity model for New Zealand. *Seismological Research Letters, 81,* 992-1000.

Eberhart-Phillips, D., & Reyners, M. (2012). Imaging the Hikurangi Plate interface region, with improved local-earthquake tomography. *Geophysical Journal International, 190,* 1221-1242.

Ehlers, J., Gibbard, P. L., & Hughes, P. D. (2011). *Quaternary glaciations-extent and chronology: a closer look*. New York, NY, Elsevier.

Elliott, J. R., Nissen, E. K., England, P. C., Jackson, J. A., Lamb, S., Li, Z., et al. (2012). Slip in the 2010 and 2011 Canterbury earthquakes, New Zealand. *Journal of Geophysical Research, 117(B3),* B03401, doi:10.1029/2011JB008868.

Estrada, B. (2003). Seismic hazard associated with the Springbank Fault, North Canterbury Plains. Geology MSc thesis, University of Canterbury, 193 pp.

Eusden, J. D., Pettinga, J. P., & Campbell, J. K. (2005). Structural collapse of a transpressive hanging-wall fault wedge, Charwell region of the Hope Fault, South Island, New Zealand. *New Zealand Journal of Geology and Geophysics, 48*, 295-309.

Finnemore, M. (2004). The application of seismic reflection surveying to the characterisation of aquifer geometry and related active tectonic deformation, North Canterbury. PhD thesis, University of Canterbury, 202 pp.

Fossen, H. (2010). *Structural Geology*. Cambridge, Cambridge University Press.

Forsyth, P. J., Barrell, D. J. A., & Jongens, R. (2008). Geology of the Christchurch area. Institute of Geological and Nuclear Sciences Geological Map 16. GNS Science, Lower Hutt, New Zealand, 1 sheet + 67 p.

Ghisetti, F. C., & Sibson, R. H. (2012). Compressional reactivation of E-W inherited normal faults in the area of the 2010-2011 Canterbury earthquake sequence. New Zealand. *Journal of Geology and Geophysics (Special issue: Canterbury, New Zealand, 2010-2011 earthquake sequence). 55(3),* 177-184.

Gledhill, K., Ristau, J., Reyners, M., Fry, B., & Holden, C. (2011). The Darfield (Canterbury, New Zealand) Mw 7.1 earthquake of September 2010: a preliminary seismological report. *Seismological Research Letters, 82,* 378-386.

Gold, R. D., Stephenson, W. J., Odum, J. K., Briggs, R. W., Crone, A. J., & Angster, S. J. (2013). Concealed Quaternary strike-slip fault resolved with airborne lidar and seismic reflection: The Grizzly Valley fault system, northern Walker Lane, California. *Journal of Geophysical Research: Solid Earth, 118(7),* 3753-3766.

Gold, R.D., Briggs, R.W., Personius, S.F., Crone, A.J., Mahan, S.A., & Angster, S.J. (2014). Latest Quaternary paleoseismology and evidence of distributed dextral shear along the Mohawk Valley fault zone, northern Walker Lane, California. *Journal of Geophysical Research: Solid Earth, 119(6),* 2014JB010987.

Holbrook, J., & Schumm, S. A. (1999). Geomorphic and sedimentary response of rivers to tectonic deformation: a brief review and critique of a tool for recognizing subtle epeirogenic deformation in modern and ancient settings. *Tectonophysics, 305*, 287-306.

Holden, C., Beavan, J., Fry, B., Reyners, M., Ristau, J., Van Dissen, R., et al. (2011). Preliminary source model of the M_W 7.1 Darfield earthquake from geological, geodetic and seismic data. *Ninth Pacific Conference on Earthquake Engineering, Building an Earthquake-Resilient Society,* Paper 164. New Zealand Society for Earthquake Engineering, Auckland, New Zealand.

Howard, M. (2001). Holocene surface-rupturing earthquakes on the Porters Pass Fault. Geology PhD thesis, University of Canterbury, 165 pp.

Howard, M., Nicol, A., Campbell, J., & Pettinga, J. R. (2005). Holocene paleoearthquakes on the strike-slip Porters Pass Fault, Canterbury, New Zealand, New Zealand. *Journal of Geology and Geophysics, 48(1),* 59-74. DOI: 10.1080/00288306.2005.9515098.

Hudnut, K. W., Borsa, A., Glennie, C., & Minster, J. B. (2002). High-Resolution topography along surface rupture of the 16 October 1999 Hector Mine, California, Earthquake (M_W 7.1) from airborne laser swath mapping. *Bulletin of the Seismological Society of America, 92(4),* 1570-1576.

Indo-Pacific Energy (2000). Arcadia-1 well completion report PEP 38256. Ministry of Economic Development Petroleum Report Series PR2561, 27 p. http://www.nzpam.govt.nz.

Jaedicke, C. (2003). Snowmass quantification and avalanche victim search by ground penetrating radar. *Surveys in Geophysics, 24,* 431-445.

Jongens, R., Pettinga, J. R., & Campbell, J. K. (1999). Stratigraphic and structural overview of the onshore Canterbury Basin. Ministry of Economic Development Petroleum Report Series, PR 4067, 33 p. http://www.nzpam.govt.nz.

Jongens, R. (2011). Contours for the base of Quaternary sediments under the Canterbury Plains between the Ashley and Rakaia rivers. GNS Science Consultancy Report 2011/132. 17 p.

Jongens, R., Barrell, D. J. A., Campbell, J. K., & Pettinga, J. R. (2012). Faulting and folding beneath the Canterbury Plains identified prior to the 2010 emergence of the Greendale Fault. *New Zealand Journal of Geology and Geophysics (Special issue: Canterbury, New Zealand, 2010-2011 earthquake sequence), 55(3),* 169-176.

Kerr, J., Nathan, S., Van Dissen, R., Webb, P., Brunsdon, D., & King, A. (2003). Planning for development of land on or close to active faults: A guideline to assist resource management planners in New Zealand. Ministry for the Environment, ME Number: 483; also identified as Institute of Geological and Nuclear Sciences Client Report 2002/124. Accessible at the Ministry for the Environment www.mfe.govt.nz.

Lambeck, K., & Chappell, J. (2001). Sea level change through the last glacial cycle. *Science 292(5517),* 679-686.

Langridge, R. M. J., Campbell, N. L., Hill, V., Pere, J., Pope, J., Pettinga, J., et al. (2003). Paleoseismology and slip rate of the Conway Segment of the Hope Fault at Greenburn Stream, South Island, New Zealand. *Annals of Geophysics, 46(5),* 1119-1139.

Langridge, R. M., Ries, W. F., Farrier, T., Barth, N. C., Khajavi, N., & De Pascale, G. P. (2014). Developing sub 5-m LiDAR DEMs for forested sections of the Alpine and Hope faults, South Island, New Zealand: Implications for structural interpretations. *Journal of Structural Geology, 64(0),* 53-66.

Lebrun, J., Lamarche, G., & Collot, J. (2000). Abrupt strike-slip fault to subduction transition: The Alpine Fault-Puysegur Trench connection, New Zealand. *Tectonics, 19(4),* 688-706.

Litchfield, N. J., Campbell, J. K., & Nicol, A. (2003). Recognition of active reverse faults and folds in North Canterbury, New Zealand, using structural mapping and geomorphic analysis, New Zealand. *Journal of Geology and Geophysics, 46(4),* 563-579. DOI: 10.1080/00288306.2003.9515030.

Litchfield, N. J., Van Dissen, R., Sutherland, R., Barnes, P. M., Cox, S. C., Norris, R., et al. (2014). A model of active faulting in New Zealand. *New Zealand Journal of Geology and Geophysics, 57(1),* 32-56. DOI: 10.1080/00288306.2013.854256.

McCalpin, J. (2009). *Paleoseismology* (2nd ed.). New York, NY, Academic Press.

McClay, K. R., & Bonora, M. (2001). Analog models of restraining stepovers in strike-slip fault systems. *American Association of Petroleum Geologists Bulletin, 85,* 233-260.

May, B. D. (2004). Comparative geomorphology of two active tectonic structures, near Oxford, North Canterbury. MSc thesis, University of Canterbury, 165 pp.

Milsom, J. J., & Eriksen, A. (2011). *Field geophysics (4th ed).* Hoboken, NJ, John Wiley & Sons.

Mortimer, N., & Campbell, H. (2014). *Zealandia: our continent revealed*. New York, NY, Penguin.

Nicol, A., Alloway, B., & Tonkin, P. (1994). Rates of deformation, uplift, and landscape development associated with active folding in the Waipara area of North Canterbury, New Zealand. *Tectonics, 13(6),* 1327-1344.

Nicol, A. (1993). Haumurian (c.66-80 Ma) half-graben development and deformation, mid Waipara, north Canterbury, New Zealand. *New Zealand Journal of Geology and Geophysics, 36(1),* 127-130.

Nicol, A., & Nathan, S. (2001). Folding and the formation of bedding-parallel faults on the western limb of Grey Valley Syncline near Blackball, New Zealand. *New Zealand Journal of Geology and Geophysics, 44(1),* 127-135.

Nicol, A., & Campbell, J. K. (2001). The impact of episodic fault-related folding on late Holocene degradation terraces along Waipara River, New Zealand. *New Zealand Journal of Geology and Geophysics, 44(1),* 145-156.

Nicol, A., & Van Dissen, R. (2002). Up-dip partitioning of displacement components on the oblique-slip Clarence Fault, New Zealand. *Journal of Structural Geology, 24,* 1521-1535, doi:10.1016/S0191-8141(01)00141-9.

Nicol, A., Mazengarb, C., Chanier, F., Rait, G., Uruski, C., & Wallace, L. (2007). Tectonic evolution of the active Hikurangi subduction margin, New Zealand, since the Oligocene. *Tectonics 26, TC4002,* http://dx.doi.org/10.1029/2006TC002090.

Nobes, D. C. (2011). Ground penetrating radar measurements over glaciers. In: V.P. Singh, P. Singh, & U. K. Haritashya (Eds.), *Encyclopaedia of Snow, Ice and Glaciers*, (pp. 490-503). New York, NY, Springer.

Norris, R., Koons, P., & Cooper, A. (1990). The obliquely-convergent plate boundary in the South Island of New Zealand: implications for ancient collision zones. *Structural Geology, 12 (5-6),* 715-725.

Norris, R. J., & Cooper, A. F. (2001). Late Quaternary slip rates and slip partitioning on the Alpine Fault, New Zealand. *Journal of Structural Geology, 23,* 507–520. doi: 10.1016/S0191-8141(00)00122-X.

Norris, R. J. & Toy, V. G. (2014). Continental transforms: A view from the Alpine Fault. *Journal of Structural Geology, 64,* 3-31.

Pettinga, J. R., & Wise, D. U. (1994). Paleostress adjacent to the Alpine fault: Broader implications from fault analysis near Nelson, South Island, New Zealand. *Journal of Geophysical Research: Solid Earth, 99(B2),* 2727-2736.

Pettinga, J. R., Cowan, H. A., Nicol, A., Quigley, M., Jongens, R., & Campbell, J. K. (2014). Structural styles of transpressional deformation along the margin of the New Zealand Plate Boundary: The Porters Pass-Amberley fault zone and 2010-12 Canterbury Earthquake sequence. In: *Geological Society of America Annual Meeting,* Vancouver, British Columbia.

Pettinga, J. R., Yetton, M., Van Dissen, R., & Downes, G. (2001). Earthquake Source Identification and Characterisation for the Canterbury Region, South Island, New Zealand. *Bulletin of the New Zealand Society for Earthquake Engineering, 34(4),* 282-317.

Pettinga, J. R., Chamberlan, C. G., Yetton, M. D., Van Dissen, R. J., & Downes, G. (1998). Earthquake source identification and characterisation. CRC Publication number U98/10.

Prentice, C. S., Crosby, C. J., Whitehill, C. S., Arrowsmith, J. R., Furlong, K. P., & Phillips, D. A. (2009). Illuminating Northern California's Active Faults. *EOS, Transactions American Geophysical Union, 90(7),* 55.

Quigley, M. C., Van Dissen, R., Litchfield, N., Villamor, P., Duffy, B., Barrell, D., et al. (2012). Surface rupture during the 2010 M_W 7.1 Darfield (Canterbury) earthquake: implications for fault rupture dynamics and seismic-hazard analysis. *Geology, 40(1),* 55-58.

Reilly, C., Nicol, A., & Walsh, J. (2015). Importance of size for the evolution of an inverted fault system. (submitted for review, *Geological Society Special Publications*).

Reyners, M., & Cowan, H. (1993). The transition from subduction to continental collision: crustal structure in the North Canterbury region, New Zealand. *Geophysical Journal International, 115(3),* 1124-1136.

Reyners, M., & Webb, T. (2002). Large earthquakes near Doubtful Sound, New Zealand, 1989-93. *New Zealand Journal of Geology and Geophysics, 45,* 109-120.

Reyners, M., & Robertson, E. (2004). Intermediate depth earthquakes beneath Nelson, New Zealand and the southwestern termination of the subducted Pacific plate. *Geophysical Research Letters, 31,* doi: 10.1029/2003GL019201.

Reyners, M., Eberhart-Phillips, D., & Bannister, S. (2011). Tracking repeated subduction of the Hikurangi Plateau beneath New Zealand. *Earth Planetary Science Letters, 311,* 165-171.

Reyners, M., Eberhart-Phillips, D., & Martin, S. (2013). Prolonged Canterbury earthquake sequence linked to widespread weakening of strong crust. *Nature Geoscience, 7,* 34-37.

Ristau, J., Holden, C., Kaiser, A., Williams, C., Bannister, S., & Fry, B. (2013). The Pegasus Bay aftershock sequence of the Mw 7.1 Darfield earthquake (Canterbury), New Zealand *Geophysical Journal International, 195,* 444-459. doi: 10.1093/gji/ggt222.

Roering, J. J., Mackey, B. H., Marshall, J. A., Sweeney, K. E., Deligne, N. I., Booth, A. M., et al. (2013). 'You are HERE': Connecting the dots with airborne lidar for geomorphic fieldwork. *Geomorphology, 200,* 172-183.

Schlumberger Geco-Prakla, (1998). Seismic survey, PEP 38256, onshore Canterbury, IP256-98 lines. Operator: Indo-Pacific Energy (NZ) Limited. New Zealand unpublished petroleum report PR2391. Ministry of Economic Development, Wellington. 417 p. 5 enclosures. http://www.nzpam.govt.nz.

Schlumberger Geco-Prakla, (1999). PEP 38256, Canterbury Basin seismic survey. Operator: Indo-Pacific Energy (NZ) Limited. New Zealand unpublished petroleum report PR2424. Ministry of Economic Development, Wellington. 516 p. 15 enclosures. http://www.nzpam.govt.nz.

Schlumberger Geco-Prakla, (2000). IPE00-256 Seismic Survey. Canterbury PEP 38256. Operator: Indo-Pacific Energy (NZ) Limited. New Zealand unpublished petroleum report PR2480. Ministry of Economic Development, Wellington. 300 p. 18 enclosures. http://www.nzpam.govt.nz.

Sibson, R. (1989). Earthquake faulting as a structural process. *Journal of Structural Geology, 11(1/2),* 1-14.

Sibson, R., Ghisetti, F., & Ristau, J. (2011). Stress control of an evolving strike-slip fault system during the 2010–2011 Canterbury, New Zealand, earthquake sequence. *Seismological Research Letters, 82(6),* 824-832.

Sisson, R. (1999). Paleoseismic investigation of the Ashley Fault, North Canterbury, New Zealand. BSc Hons thesis, University of Canterbury, 124p.

Sisson, R. J., Campbell, J., Pettinga, J., & Milner, D. (2001). Paleoseismicity of the Ashley and Loburn faults, North Canterbury, New Zealand. EQC Research Project 97/237. University of Canterbury/Earthquake Commission Research Foundation, Wellington.

Smith, E. G. C., & Davey, F. J. (1984). Joint hypocentre determination of intermediate depth earthquakes in Fiordland, New Zealand. *Tectonophysics, 104,* 127-144.

Stern, T., Okaya, D., Kleffmann, S., Scherwath, M., Henrys, S. & Davey, F. (2007). Geophysical exploration and dynamics of the Alpine Fault Zone. In: D. Okaya, T. Stern, F. Davey, (Eds.), A Continental Plate Boundary: Tectonics at South Island, New Zealand, *Geophysical Monograph Series, 175. American Geophysical Union,* Washington DC, (pp. 207-233).

Stirling, M., Pettinga, J., Berryman, K., & Yetton, M. (2001). Probabilistic seismic hazard assessment of the Canterbury region, New Zealand. *Bulletin of the New Zealand Society for Earthquake Engineering, 34(4),* 318-334.

Stirling, M. W., McVerry, G. H., & Berryman, K. R. (2002). A new seismic hazard model for New Zealand. *Bulletin of the Seismological Society of America, 92,* 1878-1903.

Stirling, M., Gerstenberger, M., Litchfield, N., McVerry, G., Smith, W., Pettinga J., & Barnes P. (2008). Seismic hazard of the Canterbury region, New Zealand: new earthquake source

model and methodology. *Bulletin of the New Zealand Society for Earthquake Engineering. 41(2),* 51-67.

Stirling, M. W., McVerry, G. H., Gerstenberger, M. C., Litchfield, N. J., Van Dissen, R. J., Berryman, K. R., et al. (2012). National seismic hazard model for New Zealand: 2010 update. *Bulletin of the Seismological Society of America 102,* 1514-1542.

Sutherland, R., Berryman, K., & Norris, R. (2006). Quaternary slip rate and geomorphology of the Alpine fault: Implications for kinematics and seismic hazard in southwest New Zealand. *Geological Society of America Bulletin, 118(3-4),* 464-474.

Syracuse, E. M., Thurber, C. H., Rawles, C. J., Savage, M. K., & Bannister, S. (2013). High-resolution relocation of aftershocks of the Mw 7.1 Darfield, New Zealand, earthquake and implications for fault activity. *Journal of Geophysical Research: Solid Earth. 118,* 1-12.

Wallace, L., Beavan, J., McCaffrey, R., Berryman, K., & Denys, P. (2007). Balancing the plate motion budget in the South Island, New Zealand using GPS, geological, and seismological data. *Geophysics Journal International, 168,* 332-352.

Wallace, L. M., Barnes, P., Beavan, J., Van Dissen, R., Litchfield, N., Mountjoy, J., et al. (2012). The kinematics of a transition from subduction to strike-slip: An example from the central New Zealand plate boundary. *Journal of Geophysical Research, 117. B02405,* doi:10.1029/2011JB008640.

Wilson, D. (1985). Erosional and depositional trends in rivers of the Canterbury Plains, New Zealand. *Journal of Hydrology, 24(1),* 32-44.

Wilson, D. (1989). Quaternary geology of the northwestern Canterbury Plains 1: 100 000. *New Zealand Geological Survey Miscellaneous Series, 14.* Department of Scientific and Industrial Research, Wellington, New Zealand.

Yeats, R. S., Sieh, K., & Allen, C. (1997). *The geology of earthquakes.* Oxford, Oxford University Press.

Yeats, R. S. (2000). The 1968 Inangahua, New Zealand, and 1994 Northridge, California, earthquakes: Implications for northwest Nelson, New Zealand. *Journal of Geology and Geophysics, 43(4),* 587-599.

Appendix 1. IP seismic reflection profiles and geological interpretation notes

Notes on structural deformation of the top of Oligocene surface interpreted from IP seismic profiles

The following notes provide a description of the IP seismic reflection lines across the study area. The main interpretations relevant to this study are provided in Chapter 5. Figures of the study area and each labelled individual interpreted line are to be found at the end of the text to this appendix. Each interpreted line has a vertical exaggeration of 4.5x. Inferred faults are indicated in yellow and the top of Oligocene horizon is indicated by blue. Other prominent reflectors below the Oligocene and above the top of the Basement are indicated by dashed green lines and surface structures are indicated as required.

Line 105 (SSW to NNE)

There is a south-facing monocline step/flexure that projects to a surface location along the line at about 1–1.5 km from the SSW end of the line. This is controlled by a north-northeast-dipping reverse fault resulting in uplift to the north with throw of about 100 m on the top of Oligocene surface. A similar north-facing monocline step/flexure, with a surface location around 4.5–5 km, is controlled by a steeply south-dipping reverse fault with resultant uplift to the south and a throw of about 50 m. Combined, these two monoclinal steps/flexures form a 3–4 km wide elevated section displacing the top of Oligocene marker horizon.

At the surface these monocline steps/flexures correspond to the north and south limbs of an inferred E–W-trending structure between the Cust Anticline and Starvation Hill (Forsyth et al., 2008). This area is overlain by the aggradation surface between the Cust River to the north and the Eyre River to the south. Surface expression for this uplifted Oligocene surface from the LIDAR interpretation is minimal with only 1–2 m of warping of the aggradation surface between these two rivers. However, the surface expression of the inferred E–W-striking fault trace across the Cust River floodplains, interpreted on the LiDAR between the Cust Anticline and Starvation Hill (Chapter 3, LiDAR fault F3), is consistent with the location of the north-facing monocline step/flexure.

North of this structure the top of Oligocene surface is flat before upwarping to the north via a series of flexures north of the Ashley River (13–15-km line location). There is a total throw of

the top of Oligocene surface across these flexural steps of about 200 m. At depth, northward thickening of the underlying Paleogene sequence also occurs along this line.

Line 106 (S to N)

There is a gradual rise of the top of Oligocene surface northwards for the first 4 km of this line. Reverse faults in the Paleogene sequence below the top of Oligocene reflector result in offsets of the lower units but no resolved offsets of the top of Oligocene surface. At a surface location of around 4 km from the southern end of the line there is a monocline flexure in the gradually rising top of Oligocene surface, uplifted to the north with a throw of about 100 m. The presence of steeply dipping faults within the Paleogene unit is difficult to interpret at this location. The top of Oligocene surface continues rising beyond this monocline flexure, and the Paleogene unit thickens northwards towards the fault zone underlying the Mairaki Downs.

At a location of 9.5–10 km a monocline step in the top of Oligocene surface is upthrown to the north with a throw of about 200 m. The reflector is also slightly offset at this location and the south-dipping top of Oligocene surface changes beyond this location to very gently north-dipping. The surface location of this step corresponds to the south margin of the Mairaki Downs where an E–W-striking fault, which projects westward towards the northern termination of the north-northeast-striking faults of the western arm of the Cust Anticline, is inferred from the LiDAR interpretation (Chapter 3, LiDAR fault F8). A steeply south-dipping reverse fault (re-activated Late Cretaceous inherited normal fault), upthrown to the south, with a throw of about 450 m, offsets the top of Oligocene surface north of the Mairaki Downs. The monocline step on the south side of the Mairaki Downs is likely controlled by a north-dipping back-thrust off the major fault to the north of the Mairaki Downs.

The uplifted block bounded by thrust faults elevates the top of Oligocene marker horizon between surface locations around 10–14 km, indicating that the Mairaki Downs section of the Cust Anticline is much wider than its present surface extent and that much of the northern limb of the surface anticline has been eroded by the Ashley River. The direction of throw on the fault on the northern margin of the Mairaki Downs is consistent with the direction of uplift across a monoclinal step/flexure at a similar N–S location on line 107 further west (northwest of the western arm of the Cust Anticline), although the amount of uplift on line 107 is significantly

less. The amount and direction of throw of this fault is similar to observations on line 109 further east.

Line 107 (WNW to ESE)

The top of Oligocene surface is slightly upwarped for the first 3 km of this line across the plains northwest of the Cust Anticline. The main anticline structure is present along the top of Oligocene surface between 4 and 8 km along the line. A monocline step/flexure (uplift of about 100 m), at a surface location of around 3.5 km, forms a break in the slope of the top of Oligocene surface at the edge of the northwest limb of the anticlinal structure. There is a possible southeast-dipping fault within the Paleogene below this step but no surface expression of this feature on the LiDAR.

The top of Oligocene surface is at a depth of around 250–300 m, below ground level, on the Oligocene anticline crest. However, there is no obvious downdropping of the top of Oligocene surface across the anticline crest along this line, compared to that seen on lines 205 and 203. Although fault-controlled folding is likely to have occurred in the Oligocene and younger overlying strata, the resolution of this line cannot determine this. Uplift across the anticline is asymmetric with about 500 m vertical elevation on the northwest limb and about 250 m vertical elevation on the southeast limb. Therefore, the apparent depth of the top of Oligocene surface is shallower on the southeastern side of the anticline by about 250 m and continues eastward, without any obvious faulting, at a constant depth. However, there is evidence for Paleogene faults and northwest-dipping Late Cretaceous faults along the southeast section of the line, although these do not offset the top of Oligocene surface. Interestingly, the Paleogene unit is thickest across the anticline crest, as was also indicated in the well log report (Jongens et al., 1999) and remains thicker on the southeast compared to the northwest side.

Line 108 (W to E)

The top of Oligocene surface rises over the first three kilometres from the west end of this line, which corresponds to the northeast trend of the seismic line, sub-parallel to the dip of the top of Oligocene surface, at this location. The top of Oligocene surface is essentially flat as it continues along the eastward projection of the seismic line on the south side of the Mairaki Downs. At the eastern end of the line an inferred west-dipping reverse fault extends from the Late Cretaceous through the Paleogene package up to the top of Oligocene surface. This fault projects to the

surface at the very end of the seismic line and could potentially correspond to the east-southeast extension, at the plunging eastern termination of the Cust Anticline, of the major fault along the north side of the Mairaki Downs (line 109). However, the seismic data does not extend far enough along line 108 into this area. There is no indication for a fault corresponding to the E–W-striking fault south of the Mairaki Downs along this line, however, if the line did cross this fault it would be at a very oblique angle. There is thickening of the Paleogene strata along this line.

Line 109 (S to N)

The top of Oligocene surface rises northwards until a wide zone of disruption bounded by a steeply south-dipping reverse fault at a surface projection around 5 km north along the line. The south side of this fault is upthrown around 400–500 m. This structure has the largest throw of any of the structures indicated on the seismic lines within the field area and is the same direction and similar throw of a structure, located slightly northwest within the Ashley River bed, on line 106. An inferred north-dipping fault is indicated which could correspond to a splay off the main fault representing the fault trace on the south margin of the Mairaki Downs. A much smaller monocline flexure (throw of about 50 m) occurs at a surface location (~8 km) on the north side of the Ashley River. An inferred steeply dipping fault within the Paleogene unit at this location does not offset the top of Oligocene reflector.

Line 110 (W to E)

The top of Oligocene surface very gently rises for the first 3 km of the line, from the west end, before an east-facing monocline step with uplift to the west and a throw of about 150 m. The surface then gradually dips eastward for about 8 km towards a structural lowpoint along the line. The top of Oligocene surface is around 300 m deeper at the eastern end of the line compared to the western end. There is no clear evidence for faulting within or below the continuous top of Oligocene surface. Interestingly, the base reflector of the underlying Paleogene package shows an anticlinal structure, rather than a monocline step, at the western end of the line, with thickening of the Paleogene section eastwards. The dip of the top of Oligocene horizon to the east along this line is similar to the east-southeast dip along lines 202 and 204 to the southwest of the Cust Anticline.

Line 111 (S to N)

Only the first 3 km of this line is relevant for this study area. The top of Oligocene surface gently dips to the north in the first 2 km of this line and is then flat at a similar depth to that of line 110 up to a surface location around 8 km. The Ashley Fault would intersect the southern end of this line therefore the slightly southwards upwarping of the top of Oligocene surface is suggestive of this structure.

Line 201 (SW to NE)

The top of Oligocene surface shows an asymmetric anticlinal structure with the crest at a surface location between 2.5 and 3 km along the line from the south-southwest end. Interestingly, Quaternary reflectors above this Oligocene structure are not as significantly folded. The Oligocene anticlinal structure is steeper on the south-southwest limb compared to the north limb, although this could be due to obliqueness of the seismic line with respect to the axis of the structure. There is evidence in the seismic profile for steeply dipping faults controlling the south-southwest and north limbs of this Oligocene structural high. The surface location above the south-southwest limb of this Oligocene anticlinal structure corresponds to the location of the inferred fault trace between Oxford and Starvation Hill (Chapter 3, LiDAR fault F1) which has surface expression upthrown to the north, consistent with that indicated along the top of Oligocene surface. The top of Oligocene reflector dips gradually northeast for the rest of the seismic line with a monocline step, upthrown to the southwest with a throw of about 150 m, north of Starvation Hill. At this location, a steeply southwest-dipping reverse fault is inferred, which could be an antithetic backthrust from the fault, south-southwest of Starvation Hill, below the Oligocene anticlinal structure.

Line 202 (NW to SE)

There are two monocline steps/flexures along the top of Oligocene surface, which gradually dips southeast. These steps are both upthrown to the northwest and have a throw of about 50 m and 120 m respectively. The throw direction across the steps is similar to the throw of the top of Oligocene surface across the monocline steps of line 204. The Paleogene unit below the Oligocene also appears to thicken southeast along this line.

Line 203 (NW to SE)

This line does not cross the surface topography of the western arm of the Cust Anticline but follows around the base of the anticline crossing the steeply plunging southwest termination of the anticline on the Cust River floodplain. At the start of the line, to the northwest of the surface anticline, there is a monocline step/flexure upthrown to the southeast with a throw of about 100 m. This is consistent with the monocline step/flexure on line 107 at this location. The Paleogene sequence does not thicken along this line.

The top of Oligocene surface clearly shows at depth an anticlinal structure, consistent with the surface of the western arm of the Cust Anticline. However, the structure has less vertical elevation compared to the anticlinal structure shown on lines 205 and 107, which do cross the topography of the western arm of the Cust Anticline. The vertical elevation change of the top of Oligocene surface along this line is about 200 m for the western limb and 250 m on the eastern limb, the western limb having a shallower slope compared to the eastern limb. The top of Oligocene surface also appears to be slightly offset at the crest by a steeply northwest-dipping fault. A similar inferred northwest-dipping fault is located below the eastern limb however expression of these faults in the shallower units is unclear. This seismic line crosses the very eastern tip of the Glews Road fault trace (Chapter 3, LiDAR fault F8); however, no evidence for this fault can be seen in the seismic line.

Line 204 (W to E)

There is an east-facing monocline step upthrown to the west with a throw of 200 m, at a surface location ~2.5 km along the line from the west end, that is disrupted by a steeply west-dipping reverse fault within the top of Oligocene surface. The surface projection of this fault trace corresponds with the surface fault trace across the southeast-facing slopes of Starvation Hill that is upthrown to the west (Chapter 3, LiDAR fault F2).

The top of Oligocene surface is essentially flat eastward from this location except for an east-facing monocline step/flexure (throw about 100 m) at a surface location around 9.5 km along the line. The Paleogene sequence slightly thickens eastward across this monocline step. There is no clear evidence of faulting of the top of Oligocene surface east of Starvation Hill. This line runs parallel to the axis of the uplifted Oligocene surface seen on line 105 and is consistent with the dip and monocline steps indicated along line 202 to the southwest.

Line 205 (W to E)

The western arm of the Cust Anticline structure is clearly present within the top of Oligocene surface of this line and there is no indication of faulting of this reflector until the anticline crest. The top of Oligocene surface is downdropped in the centre of the anticline structure, and folding has occurred within both the Oligocene and the overlying younger strata. The top of Oligocene reflector indicates a fault on the west and the east side of the anticline crest (Chapter 3, LiDAR faults F5 and F6). The eastern fault is west-dipping, however, the dip of the western fault is more difficult to determine at this vertical exaggeration, although the preferred interpretation for this fault is also west-dipping (Chapter 5). The resolution of the data above the top of Oligocene horizon does not allow interpretation of the faults in the overlying strata. Interestingly, there is a décollement style fault at the base of the Paleogene and an inferred Cretaceous east-dipping reverse fault structure below this.

The anticline is asymmetric along the top of Oligocene surface, which is consistent with the LiDAR surface profile across this section, with uplift across the anticline of around 400 m for the western limb and around 250 m for the eastern limb. The upward dip of the top of Oligocene horizon further east corresponds to the dip seen on line 108, which overlaps this line.

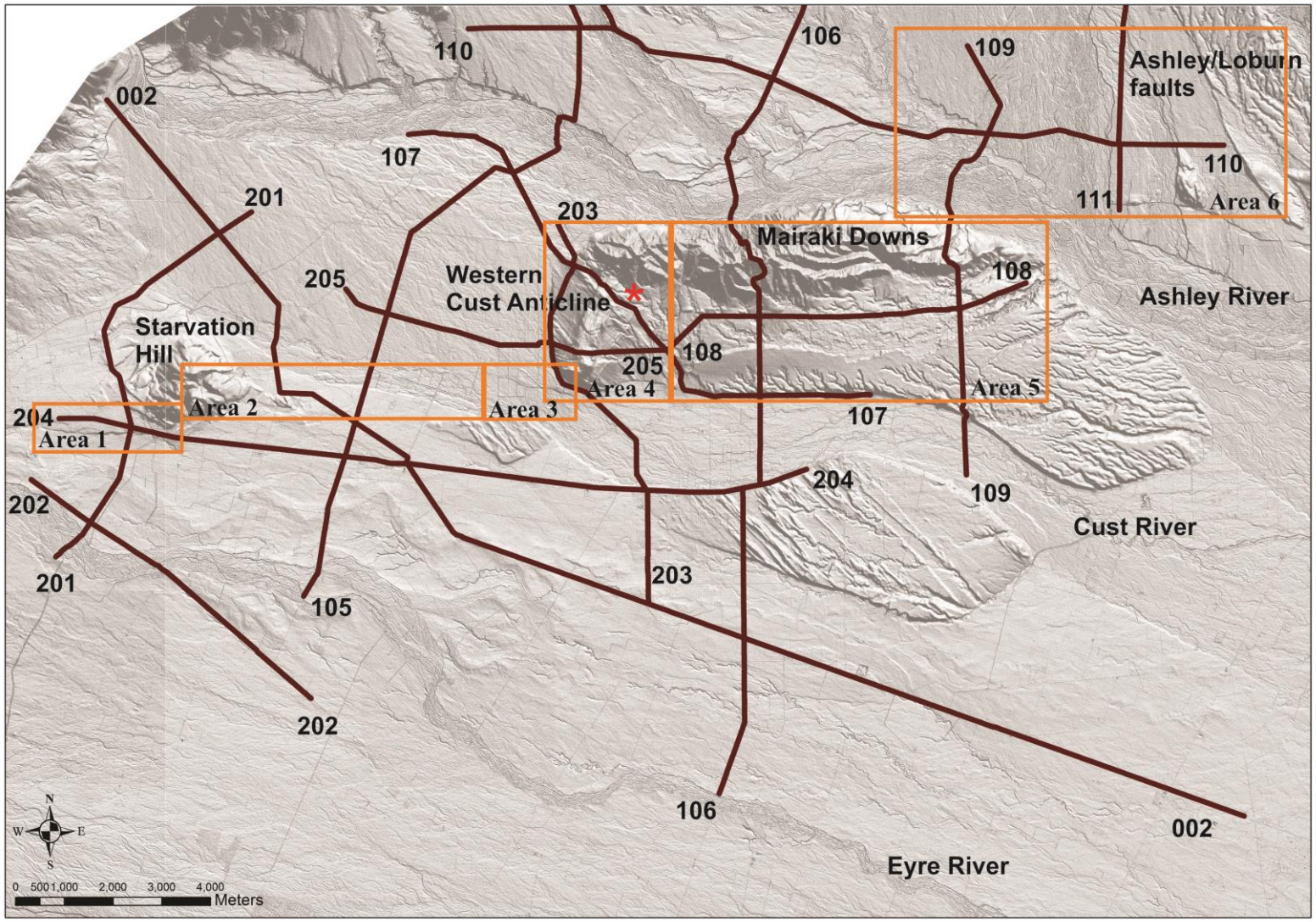

Location of the Indo-Pacific seismic reflection lines across the study area. The lines are overlaid on a LiDAR hillshade of the area at a scale of 1:65,000. The six areas of specific LiDAR interpretation (Chapter 3) are indicated across the area. The red star indicates the location of the Arcadia-1 well. Note that line 002 was not available for re-interpretation in this study.

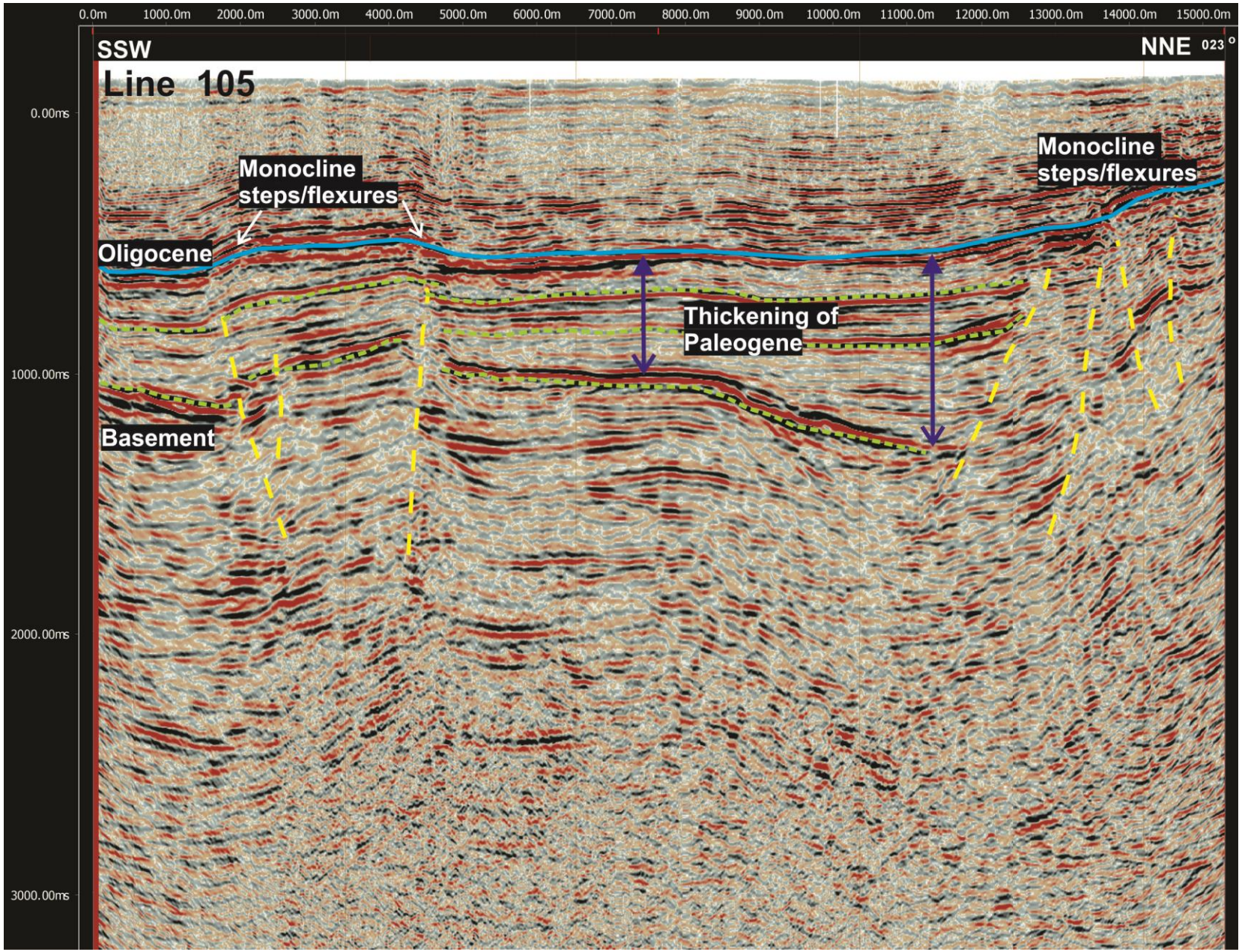
0.0m
1000.0m
2000.0m
3000.0m
4000.0m
5000.0m
6000.0m
7000.0m
8000.0m
9000.0m
10000.0m
11000.0m
12000.0m
13000.0m
14000.0m
15000.0m
SSW
NNE 023 °
Line 105
0.00ms
1000.00ms
2000.00ms
3000.00ms
Monocline steps/flexures
Monocline steps/flexures
Oligocene
Thickening of Paleogene
Basement

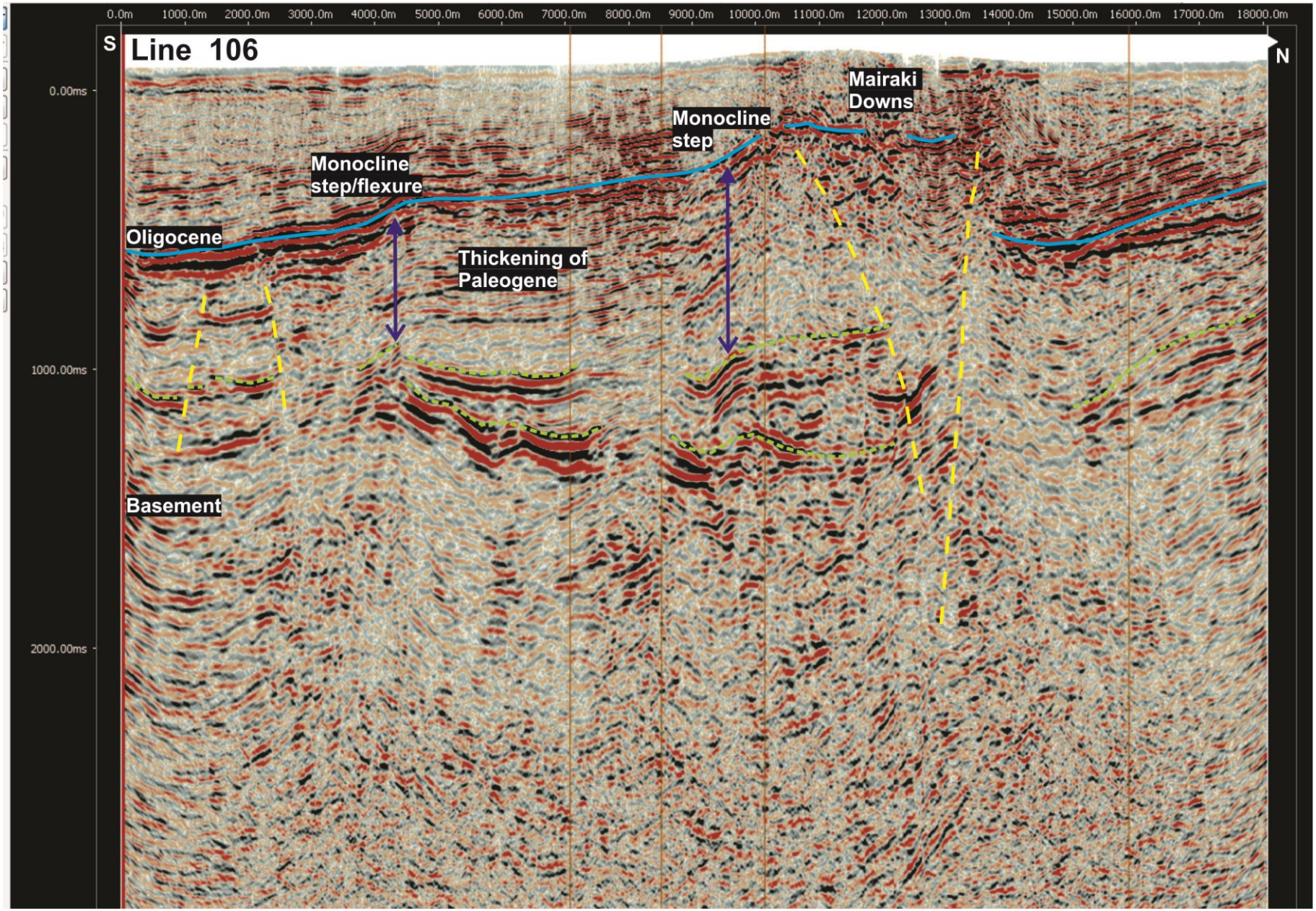
0.0m
1000.0m
2000.0m
3000.0m
4000.0m
5000.0m
6000.0m
7000.0m
8000.0m
9000.0m
10000.0m
11000.0m
12000.0m
13000.0m
14000.0m
15000.0m
16000.0m
17000.0m
18000.0m
S
Line 106
N
0.00ms
1000.00ms
2000.00ms
Mairaki Downs
Monocline step
Monocline step/flexure
Oligocene
Thickening of Paleogene
Basement

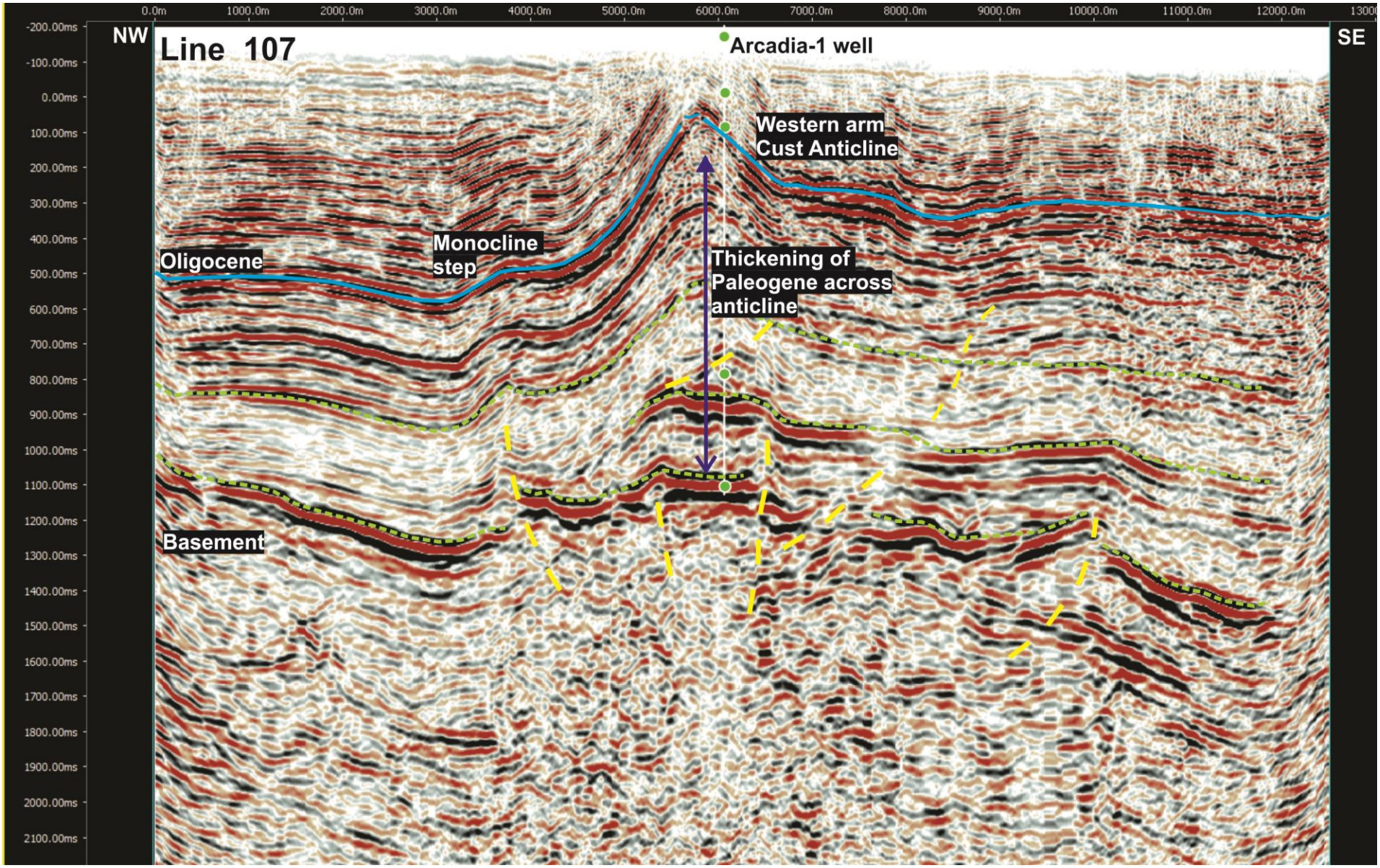
NW
SE
Line 107
Arcadia-1 well
Western arm
Cust Anticline
Monocline
step
Oligocene
Thickening of
Paleogene across
anticline
Basement
0.0m
1000.0m
2000.0m
3000.0m
4000.0m
5000.0m
6000.0m
7000.0m
8000.0m
9000.0m
10000.0m
11000.0m
12000.0m
-200.00ms
-100.00ms
0.00ms
100.00ms
200.00ms
300.00ms
400.00ms
500.00ms
600.00ms
700.00ms
800.00ms
900.00ms
1000.00ms
1100.00ms
1200.00ms
1300.00ms
1400.00ms
1500.00ms
1600.00ms
1700.00ms
1800.00ms
1900.00ms
2000.00ms
2100.00ms

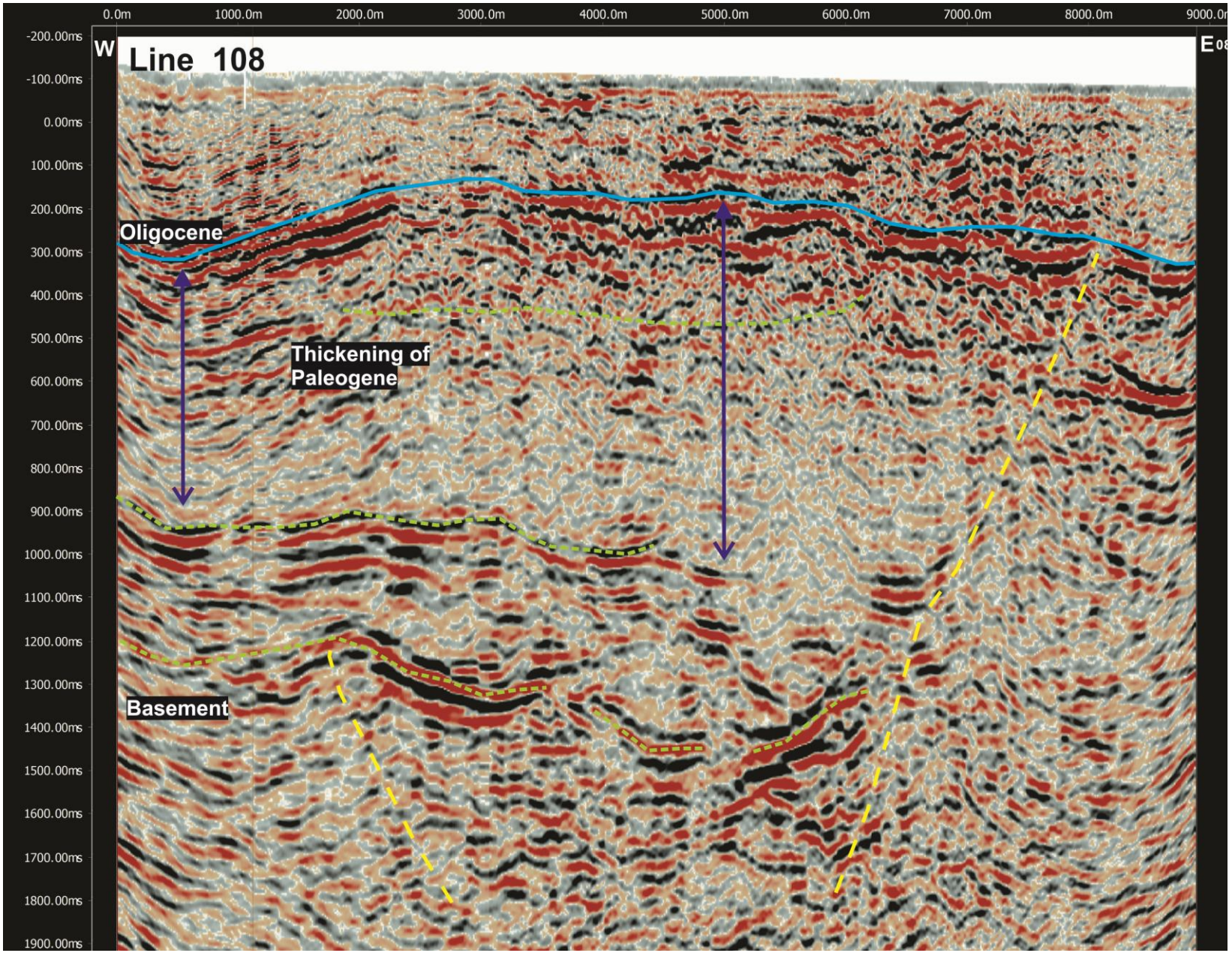
0.0m
1000.0m
2000.0m
3000.0m
4000.0m
5000.0m
6000.0m
7000.0m
8000.0m
9000.0m
-200.00ms
-100.00ms
0.00ms
100.00ms
200.00ms
300.00ms
400.00ms
500.00ms
600.00ms
700.00ms
800.00ms
900.00ms
1000.00ms
1100.00ms
1200.00ms
1300.00ms
1400.00ms
1500.00ms
1600.00ms
1700.00ms
1800.00ms
1900.00ms
W
Line 108
E
Oligocene
Thickening of Paleogene
Basement

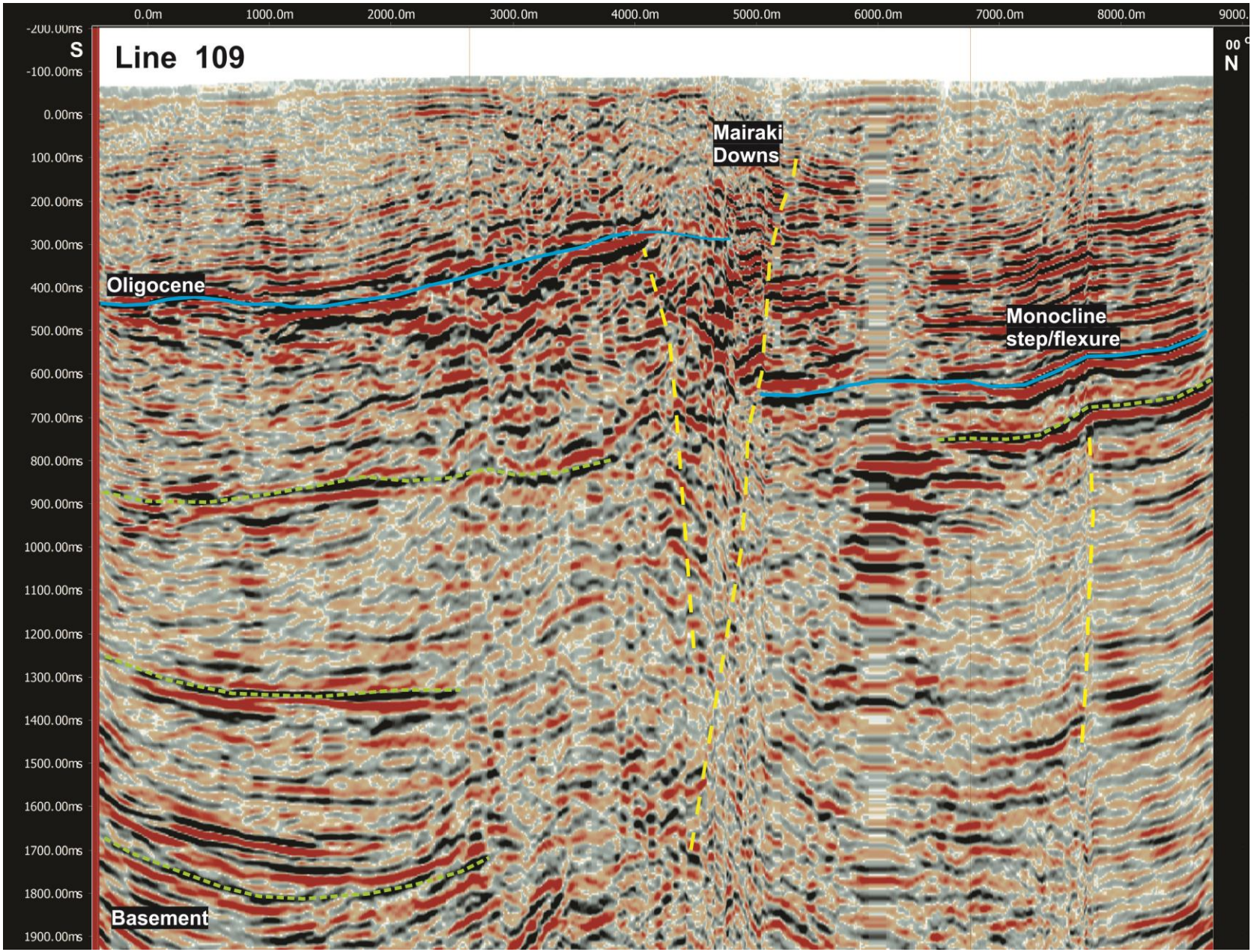
Line 109
S
N
0.0m
1000.0m
2000.0m
3000.0m
4000.0m
5000.0m
6000.0m
7000.0m
8000.0m
-100.00ms
0.00ms
100.00ms
200.00ms
300.00ms
400.00ms
500.00ms
600.00ms
700.00ms
800.00ms
900.00ms
1000.00ms
1100.00ms
1200.00ms
1300.00ms
1400.00ms
1500.00ms
1600.00ms
1700.00ms
1800.00ms
1900.00ms
Mairaki Downs
Oligocene
Monocline step/flexure
Basement

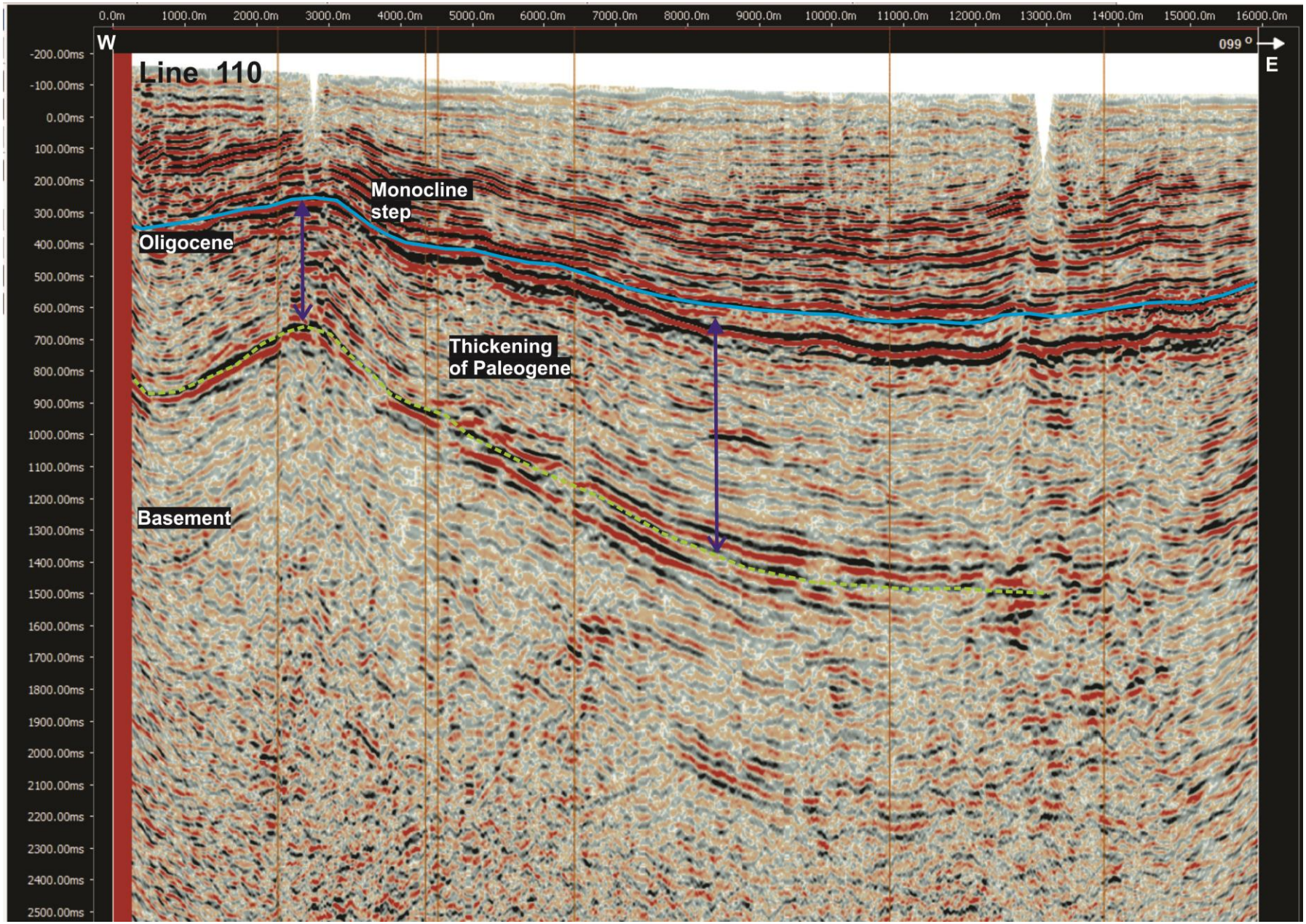
0.0m
1000.0m
2000.0m
3000.0m
4000.0m
5000.0m
6000.0m
7000.0m
8000.0m
9000.0m
10000.0m
11000.0m
12000.0m
13000.0m
14000.0m
15000.0m
16000.0m
W
099 °
E
Line 110
-200.00ms
-100.00ms
0.00ms
100.00ms
200.00ms
300.00ms
400.00ms
500.00ms
600.00ms
700.00ms
800.00ms
900.00ms
1000.00ms
1100.00ms
1200.00ms
1300.00ms
1400.00ms
1500.00ms
1600.00ms
1700.00ms
1800.00ms
1900.00ms
2000.00ms
2100.00ms
2200.00ms
2300.00ms
2400.00ms
2500.00ms
Monocline step
Oligocene
Thickening of Paleogene
Basement

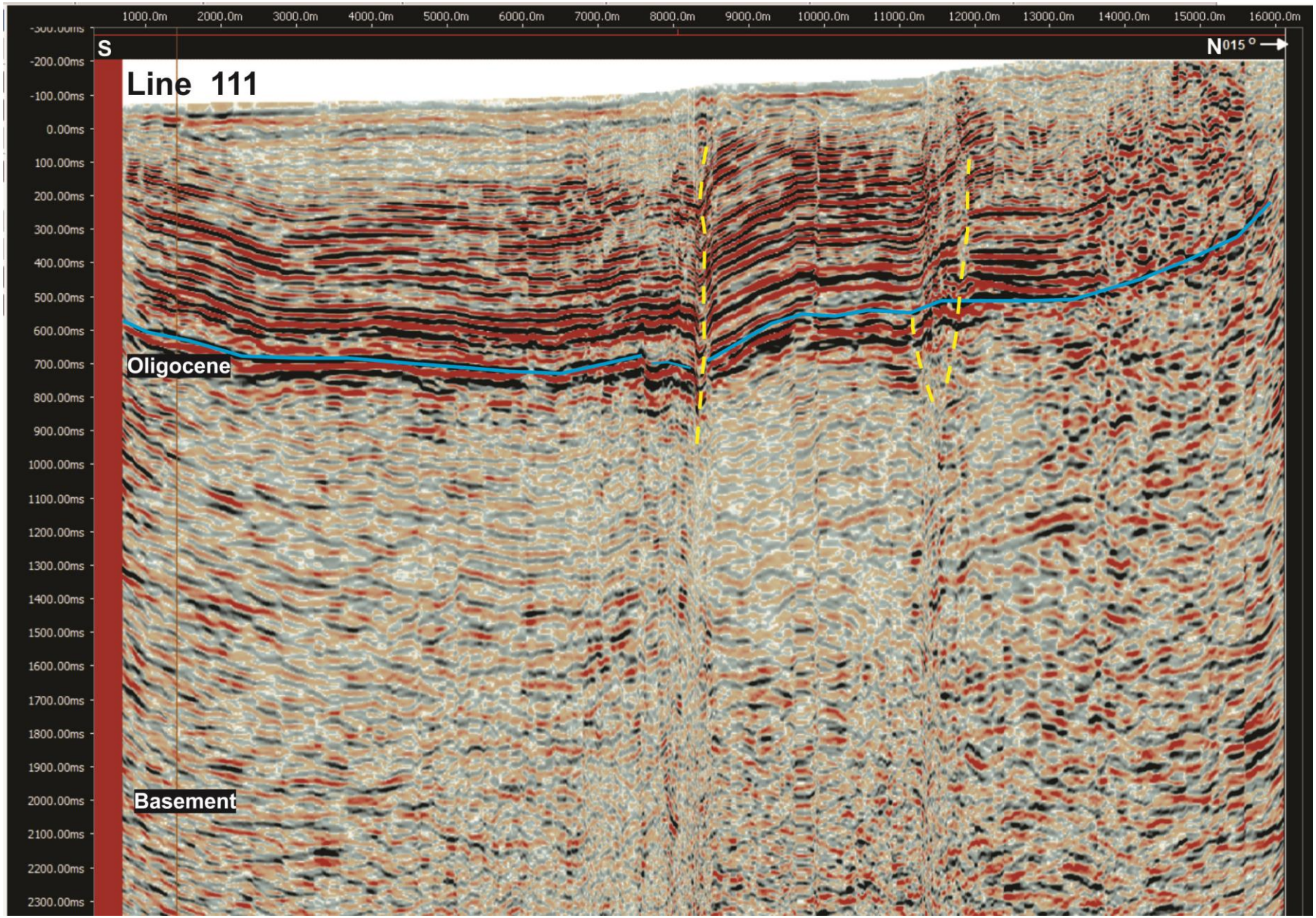
1000.0m
2000.0m
3000.0m
4000.0m
5000.0m
6000.0m
7000.0m
8000.0m
9000.0m
10000.0m
11000.0m
12000.0m
13000.0m
14000.0m
15000.0m
16000.0m
S
N015°
Line 111
-200.00ms
-100.00ms
0.00ms
100.00ms
200.00ms
300.00ms
400.00ms
500.00ms
600.00ms
700.00ms
800.00ms
900.00ms
1000.00ms
1100.00ms
1200.00ms
1300.00ms
1400.00ms
1500.00ms
1600.00ms
1700.00ms
1800.00ms
1900.00ms
2000.00ms
2100.00ms
2200.00ms
2300.00ms
Oligocene
Basement

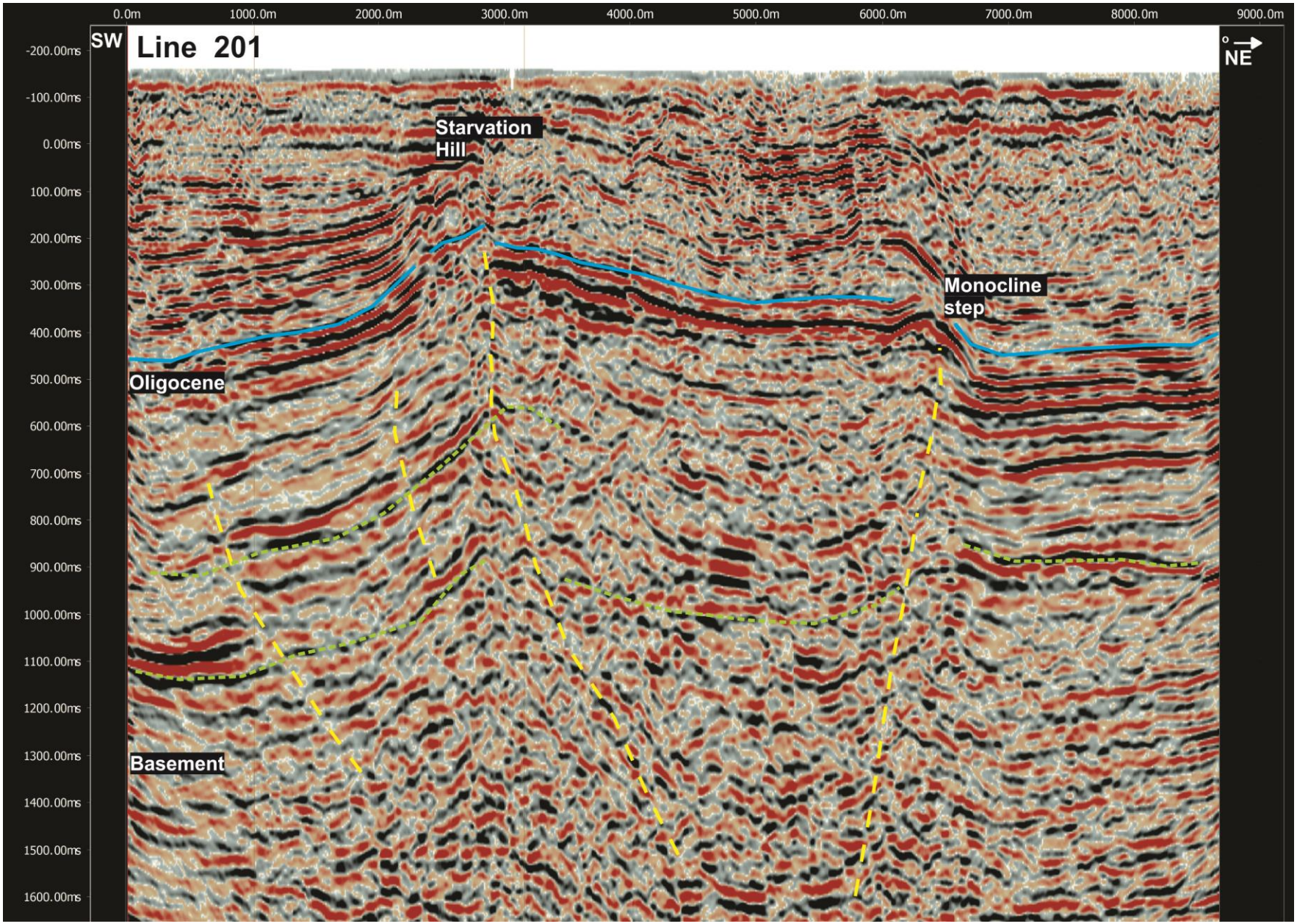
0.0m
1000.0m
2000.0m
3000.0m
4000.0m
5000.0m
6000.0m
7000.0m
8000.0m
9000.0m
SW
Line 201
NE
-200.00ms
-100.00ms
0.00ms
100.00ms
200.00ms
300.00ms
400.00ms
500.00ms
600.00ms
700.00ms
800.00ms
900.00ms
1000.00ms
1100.00ms
1200.00ms
1300.00ms
1400.00ms
1500.00ms
1600.00ms
Starvation Hill
Monocline step
Oligocene
Basement

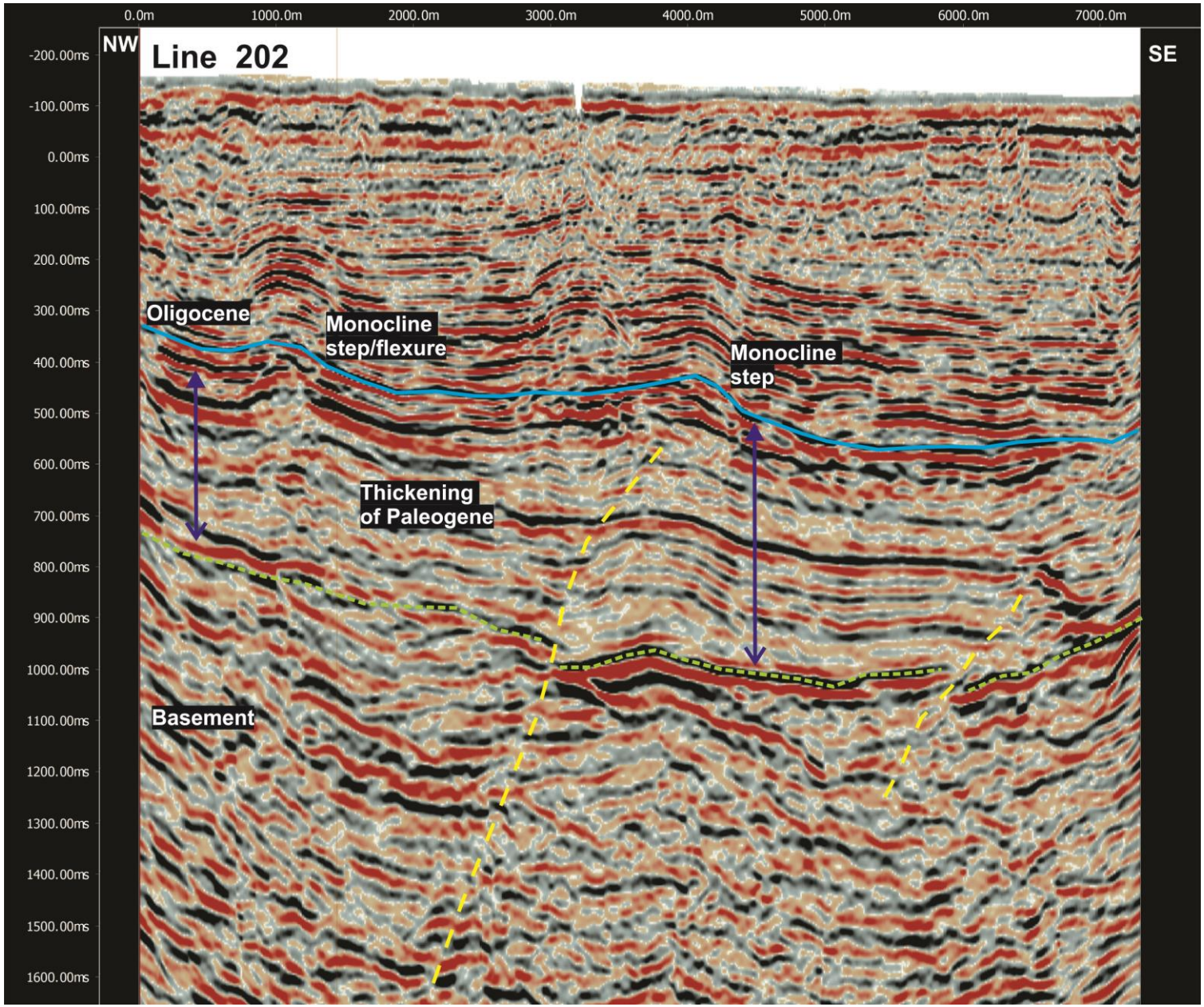
0.0m
1000.0m
2000.0m
3000.0m
4000.0m
5000.0m
6000.0m
7000.0m
NW
Line 202
SE
-200.00ms
-100.00ms
0.00ms
100.00ms
200.00ms
300.00ms
400.00ms
500.00ms
600.00ms
700.00ms
800.00ms
900.00ms
1000.00ms
1100.00ms
1200.00ms
1300.00ms
1400.00ms
1500.00ms
1600.00ms
Oligocene
Monocline step/flexure
Monocline step
Thickening of Paleogene
Basement

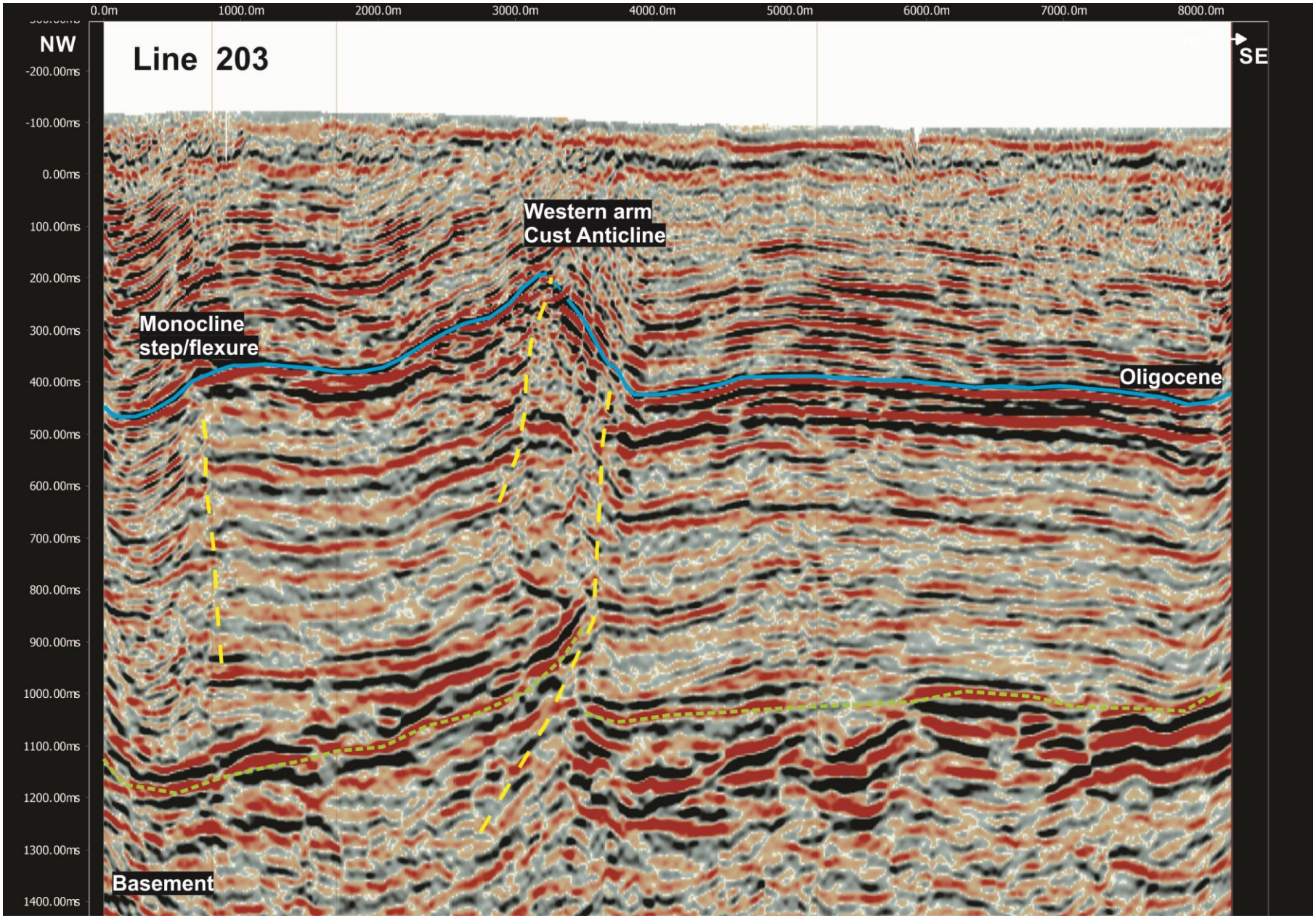
0.0m
1000.0m
2000.0m
3000.0m
4000.0m
5000.0m
6000.0m
7000.0m
8000.0m
NW
SE
Line 203
-200.00ms
-100.00ms
0.00ms
100.00ms
200.00ms
300.00ms
400.00ms
500.00ms
600.00ms
700.00ms
800.00ms
900.00ms
1000.00ms
1100.00ms
1200.00ms
1300.00ms
1400.00ms
Western arm
Cust Anticline
Monocline
step/flexure
Oligocene
Basement

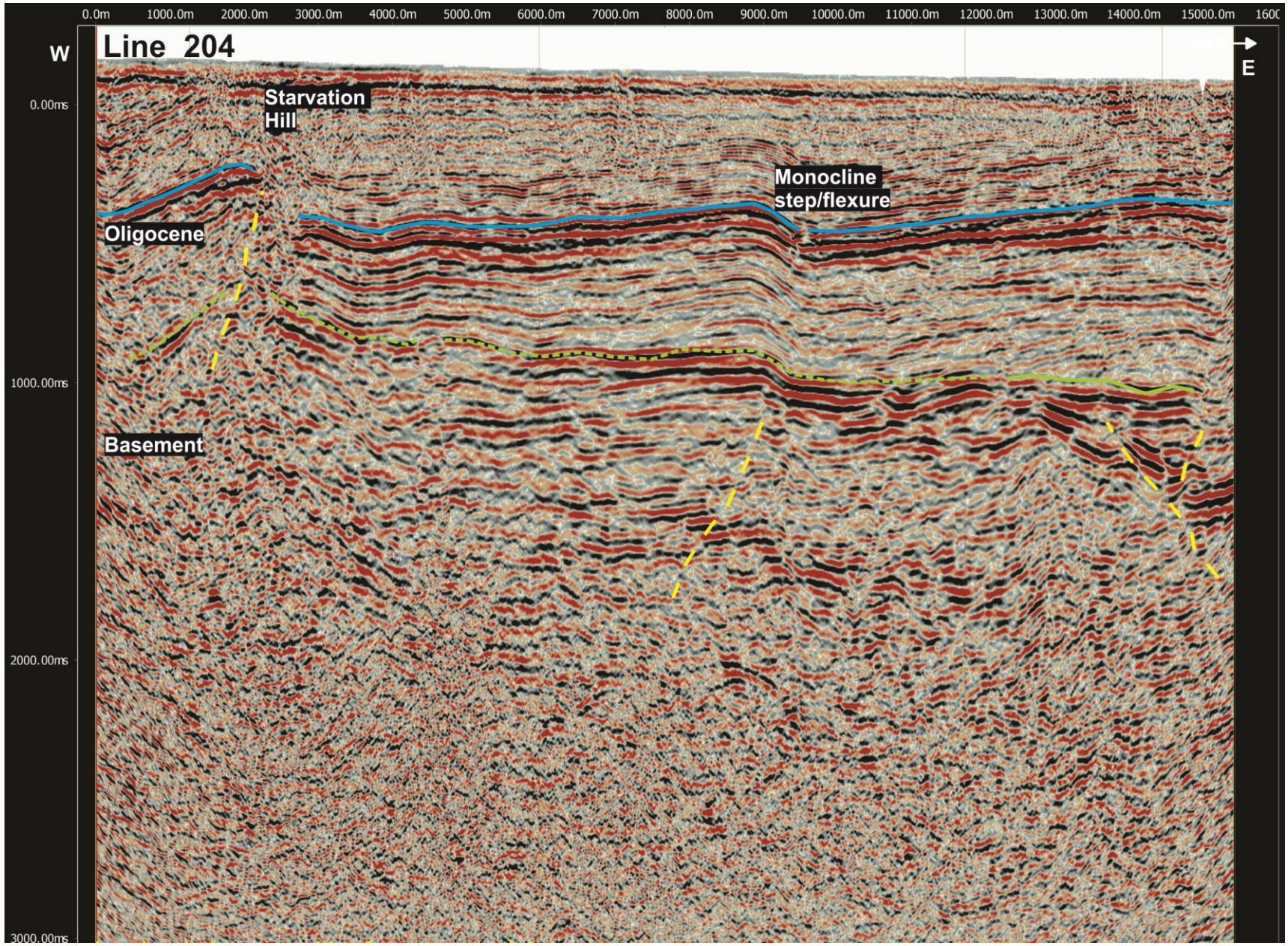
0.0m
1000.0m
2000.0m
3000.0m
4000.0m
5000.0m
6000.0m
7000.0m
8000.0m
9000.0m
10000.0m
11000.0m
12000.0m
13000.0m
14000.0m
15000.0m
W
E
Line 204
0.00ms
1000.00ms
2000.00ms
3000.00ms
Starvation Hill
Monocline step/flexure
Oligocene
Basement

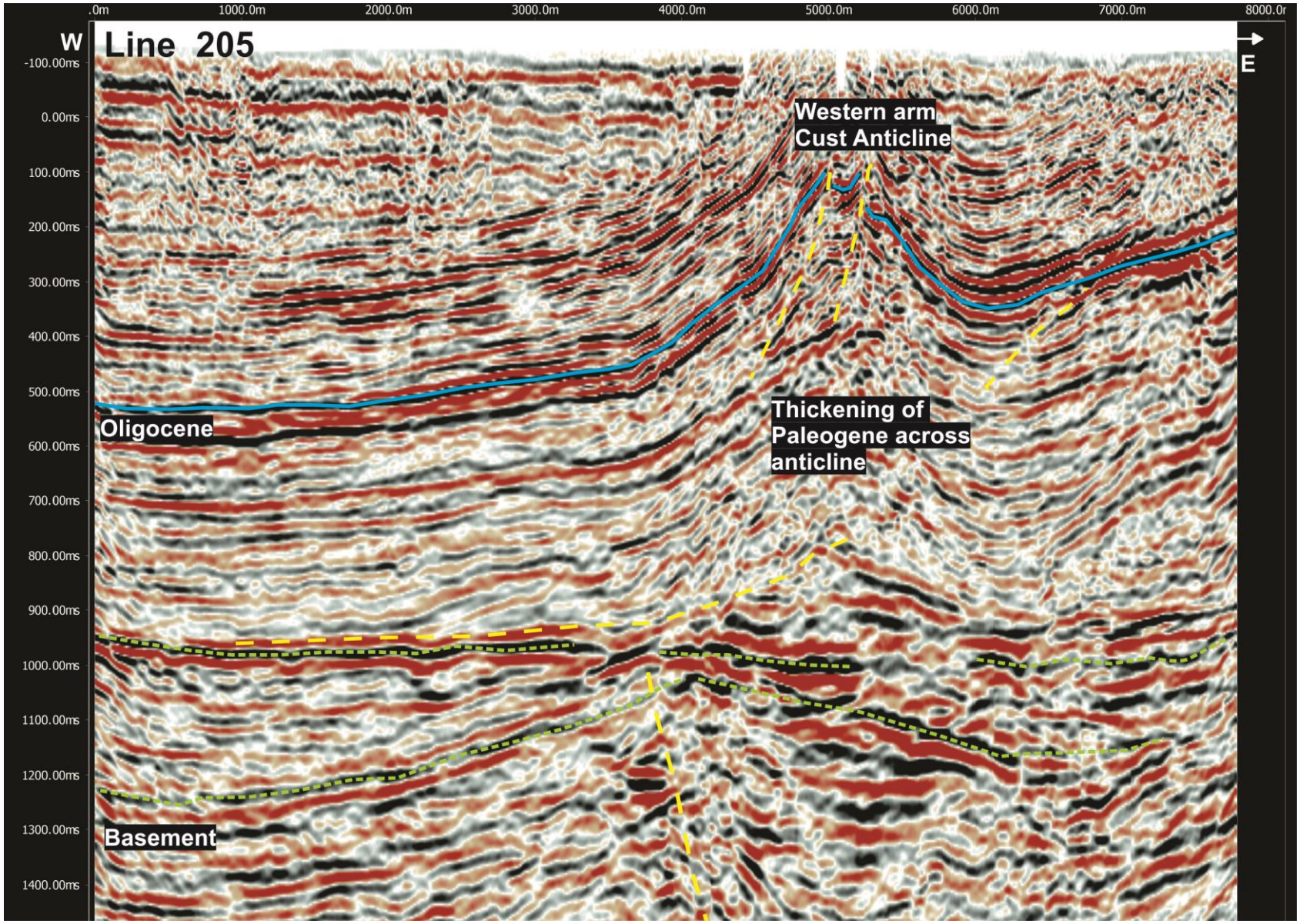
.0m
1000.0m
2000.0m
3000.0m
4000.0m
5000.0m
6000.0m
7000.0m
8000.0r
W
Line 205
E
-100.00ms
0.00ms
100.00ms
200.00ms
300.00ms
400.00ms
500.00ms
600.00ms
700.00ms
800.00ms
900.00ms
1000.00ms
1100.00ms
1200.00ms
1300.00ms
1400.00ms
Western arm
Cust Anticline
Thickening of
Paleogene across
anticline
Oligocene
Basement

Appendix 2. Chapmans Boundary Road seismic reflection survey

Seismic reflection surveys are an effective way of imaging layered subsurface geology using acoustic energy sound waves transmitted through vibration of the rock mass and near surface unconsolidated deposits (Milsom & Eriksen, 2011). A comprehensive series of industry seismic surveys were run in North Canterbury, by Indo-Pacific, during 1998–2000 (Jongens et al., 1999) and are detailed in Chapter 5 and Appendix 1. Limited shallow seismic surveys have also been run north and south of the Waimakariri River west of Darfield and while giving useful results of the subsurface geology, highlighted the significant challenges in processing seismic reflections given the low signal-to-noise ratios of the raw seismic data (Finnemore, 2004; Dorn et el., 2010a; 2010b). The thickness of the Quaternary sediments above the basement and cover geology across the Canterbury Plains are not suitable to conventional paleo-seismic investigations in many places except for targeted sites with clear evidence for tectonic activity from other sources, such as LiDAR surface mapping (Chapters 3 and 4). Ground penetrating radar (GPR) and other very shallow geophysical techniques are limited for similar reasons although GPR surveys in conjunction with seismic lines add to interpretations (Carpentier et al., 2012). Therefore, despite the cost, time and processing difficulties shallow, high frequency seismic reflection surveys are useful in assessing tectonic structures beneath the topographically starved Canterbury Plains (Dorn et al., 2010a). Although single survey lines are useful the most comprehensive data comes from comparing many lines, forming part of a grid, across a region.

LiDAR analysis of the study location

LiDAR analysis indicated an E–W-striking, south-facing scarp extending ~4 km from Earlys Road to east of Chapmans Boundary Road (Figure A2.1). The trace is upthrown to the north. The scarp location would be consistent with an E–W-striking tear-fault structure at the southern termination of the northeast-striking Springbank Fault. Geomorphically it is difficult to determine if this scarp is due to Quaternary fluvial erosion processes or is tectonic in origin. Fluvial processes can degrade and mask active tectonic processes across the Canterbury Plains and will have affected the Eyre River aggradation surfaces. However, the paleo-channel directions are sub-parallel across the scarp in a southeast direction and show some evidence of increased sinuosity on the higher scarp surface and less sinuosity on the lower scarp surface indicating that the scarp possibly displaces the drainage (Figure A2.1, bottom). Although initial GPR along Chapmans Boundary Road was inconclusive it was decided to run a shallow seismic reflection survey to investigate this structure as the location of the southern termination of the Springbank Fault has remained unresolved from previous studies (Estrada, 2003).

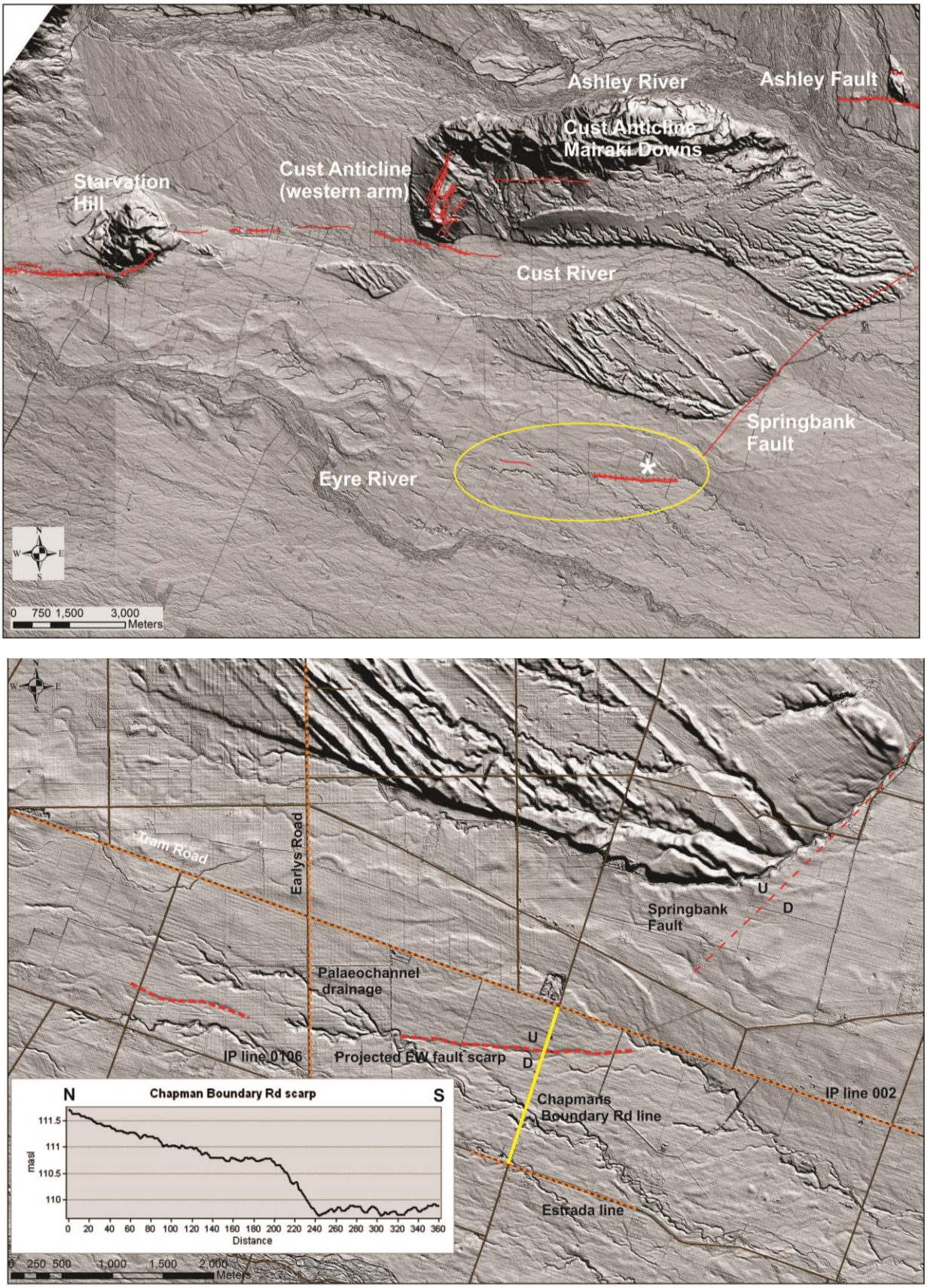

Figure A2.1. Top: LiDAR image of the main faults mapped across the study area with the location of the HRR seismic reflection line indicated by the asterisk within the yellow ellipse. Bottom: Detailed LiDAR image across the potential E–W-striking fault south of Tram Road at the southern termination of the inferred Springbank Fault. The scarp profile indicates the low relief of this feature within the overall landscape. The seismic line for this study is indicated in yellow and other nearby seismic lines are indicated in orange with labels of origin.

Further justification for running this seismic line

- Evidence on IP seismic reflection line 98-002 for the Springbank Fault along Tram Road (Estrada, 2003).
- No evidence for the continuation of the northeast-striking Springbank Fault south of Tram Road on a shallow seismic reflection line on North Eyre Road (parallel but 1.5 km south of Tram Road; Estrada, 2003).
- If the potential southern termination of the Springbank Fault is abrupt it may relay to another structure south of Tram Road and north of the Eyre River, and it was considered possible that there might be an E–W transfer tear-fault at this location.
- The wavelength of the regional tectonic fabric of the Northwest Canterbury Plains suggests potentially unresolved blind structures in this area (Campbell et al., 2012).
- The Springbank Fault is bounded to the north by the Ashley-Loburn fault zone (Estrada, 2003). South of the Waimakariri River northeast-striking faults (i.e. View Hill, Springfield and Hororata Faults) project into this area but are discontinuous with the structures north of this area.
- Bedform analysis of the Eyre River (Estrada, 2003) indicates an anomaly, east of Eyreton at the 160 m contour, that potentially projects to the trace of this E–W projection identified on the LiDAR.
- Very subtle gentle tilting to the south and to the north of the aggradation surface between the Eyre and the Cust rivers extends from the southern edge of the Cust Anticline to Starvation Hill and may indicate a greater degree of warping at depth due to the presence of blind faults. The top of Oligocene marker horizon reflects this through an uplifted surface bounded by oppositely facing monocline steps/flexures (Chapter 5).
- The projection of the Kaiapoi Fault onshore would extend into this area further suggesting that there may be blind structures underlying the Eyre River area.
- IP line 98-106 along Earlys Road about 2.5 km west of Chapmans Boundary Road shows evidence of possible fault traces, within the Late-Cretaceous, that project to monoclinal flexures within the Oligocene–Miocene strata.

Survey design

The seismic line was run from south to north along Chapmans Boundary Road starting at the North Eyre Road intersection and continuing for 1.4 km (12 cables) north to near the intersection with Tram Road. The line was not continued to Tram Road due to traffic management issues and also noise from the significant amount of traffic along this main road.

The data was recorded using two seismographs: a Geometrics 48-channel Stratavisor seismograph (channels 1-48) and a 24-channel Geometrics Geode seismograph (channels 49-72). The records were combined after data acquisition before processing the line. Therefore, the records consisted of 72 channels each channel having a record length of 1000 ms, sample rate of 0.5 ms and a recording gain of 48 dB. The spread-type was asymmetrical with a saw tooth movement (Excel Geophysical processing report). The 30 Hz geophones were placed at 5 m intervals along the seismic survey line on the west roadside boundary. The shot offset was ~2 m from the geophone placements. The seismic source was a 25 kg accelerated weight drop operated with a -0.05 s pre-trigger. The dogbox, containing the data recording system, and weight drop operator were within visual and radio contact to co-ordinate the operation. A total of six weight drops to produce six stacks were performed at each shot location.

The survey design consisted of the 'dogbox' being located with 2 cables (48 geophones) connected in series south and one cable (24 geophones) connected north of the 'dogbox'. Shots were performed adjacent to each geophone beginning one cable length from the 'dogbox' and shooting north through to the 'dogbox'. The 'dogbox' was then moved forward one cable length, the geophones and seismograph channels reconnected and the line continued. A total of 12 cables were laid with cable 1 and cable 12 forming the tails of the line. The geophone locations were mapped using GPS to subsequently obtain elevation data from the LiDAR for processing.

Data processing

The data was initially processed using ReflexW software to join the two seismograph records into one supergather of 72 channels. The records were edited for reversed traces and bad traces and the time window altered to a reasonable value. The first 158 records were flipped before joining the seismographs because they were recorded on the 48 channel Strata Visor as 1-48 from the 'dogbox' instead of 48-1. The set-up was altered in the field at record 158 when this was realised (personal communication from Mike Finnemore SGL). The data was sent to Excel Geophysical Services Ltd (Wellington) for processing by Meredith Ross. The processing steps were as follows:

- Geometry information compiled in ProMAX and crooked line binning performed.
- Geometry definition and trace edit for noisy, dead and reversed traces.
- Time delay correction (-50 ms was applied to all shots).

- Gain recovery (T^1 was applied to correct for amplitude decay with time).
- Elevation statics corrections (replacement velocity of 2500 m/s to a 150 m datum used).
- A prestack minimum phase bandpass filter applied (frequency limits:30-45-180-250 Hz.)
- Surface consistent deconvolution (trace by trace predictive deconvolution was applied with a single design window, gap of 1 ms and operator length of 80 ms).
- Spectral whitening: time invariant spectral whitening was applied using 6 filter panels automatically calculated between the following frequencies: 40-50-140-150 Hz.
- Airwave attenuation (velocity 331 m/s to attenuate noise).
- A surgical mute was interactively picked to remove aliased ground roll from the near traces of all shots.
- Velocity analysis and residual statics: three iterations of velocities and residual statics calculations were performed. Interactive velocity picks were made using 9 cdp super-gathers on constant velocity stacks for initial analysis at an interval of 150 m, referenced to a floating datum. Iterative stack power surface consistent residual statics were calculated and applied between each pass of velocity analysis. The final velocity analysis was picked at an interval of 75 m.
- EITHER: Dip Moveout correction: Data were passed through two migration flows, resulting in two separate stacks. DMO was performed in the TX domain using common shot gathers and final stacking velocities.
- OR: Pre-stack time migration: The pre-stack Kirchhoff time migration (PSTM) was performed in the offset domain using final smoothed stacking velocities.
- NMO correction and interactive mute applied
- Pre-stack balance (automatic gain applied with operator length of 500 ms for all lines).
- CMP stack (stack data and move traces to a final 150 m datum).
- Bandpass filter (post stack filter applied: 50-70-130-180 Hz).
- Wiener Levinson FX deconvolution applied to DMO stack to suppress random noise on final section (window: 15 traces; filter length: 5 samples; time window: 500 ms).
- Automatic Gain (operator length of 500 ms for all lines).
- SEG-Y output: The final stacks and velocity files were written in SEG-Y format.

Dorn et al., 2010a outline the many significant challenges in processing shallow seismic reflection data obtained across the Canterbury Plains and how custom processing may provide better quality images than standard processing procedures. However, the processing of the line was not able to be subjected to such rigour due to time and expertise required within the scope of

this project. Nevertheless it took significant effort and innovation by Excel Geophysics Ltd to be able to obtain a reflective signal in the final product even though signal appeared to be present on the initial processing of the raw shots.

The significant ground roll was aliased in the shot traces and therefore regular signal processing to attenuate this noise was generally ineffective. Furthermore, a coherent signal was not visible during velocity analysis on the constant velocity stacks and a clear velocity function could not initially be determined (Meredith Ross pers. comm., 2014). The reflective horizons become more visible on the stacks and in the velocity analysis when a surgical mute was interactively picked on all shots to remove as much ground roll as possible while maintaining the signal. This was an essential part of the processing for this survey. However, there was still a loss of horizon amplitudes across the final stacks due to use of this surgical mute processing technique in combination with the acquisition method and the reasons for this were not able to be determined.

Interpretation of the seismic line

A series of strong reflectors are present between a depth of about 220–450 m. Although these reflectors have a loss of horizon amplitude approximately every 50 cdp (i.e. every 25 stations or one cable length) the reflectors can still be traced across the seismic section (Figure A2.2). The reflectors are labelled as Kowai Formation based on depth interpretations for seismic lines near this location (Jongens et al., 1999; Estrada, 2003). The surface topography of the line was very subtle and varied by <2 m along the line. The scarp, as located on the LiDAR image was between 1000–1300 m from the start of the line (represented by CDP locations 400–500).

No obvious fault is observed offsetting the reflectors across the scarp location or elsewhere along the line. However, the reflectors dip towards the south along the profile length and dip increases with reflector depth. The low-value dip angle almost doubles from the top of the strong reflectors to the bottom of the reflectors although without any tectonic structures present along the line no obvious interpretation for this is apparent. The dip direction is consistent with that observed in the IP seismic line 106 (located ~2.5 km west of this line). Interestingly, in line IP-106 small south-facing monoclinal flexures are present along the top of Oligocene marker horizon at a depth of ~500 m which is just below the depth of data obtained in this survey line.

Therefore, this seismic line does not confirm the presence of an E–W-striking tear-fault, as was potentially indicated by the LiDAR geomorphology. However, the dipping reflectors could indicate a steeply dipping fault at greater depth (which would not be visible in this shallow seismic survey), most likely within the Late Cretaceous basement consistent with the depth of E–W-striking re-activated Late Cretaceous faults elsewhere within the Northwest Canterbury Plains (Ghisetti & Sibson., 2012; Campbell et al., 2012; Chapter 5 this study). Evidence from this line and others (Estrada, 2003) suggest that the southern tip of the Springbank Fault either terminates very abruptly to the south of Tram Road or that it changes strike significantly at this location. If this seismic line is crossing the Springbank Fault structure at quite an oblique angle the likelihood of observing reflections associated with a fault might be reduced. Therefore, it cannot be equivocally determined that this geomorphic feature represents a Holocene scarp from co-seismic rupture associated with the Springbank Fault. Alternatively, it could simply be a more defined fluvial terrace feature that has remained geomorphologically dominant in this section of the landscape and the Springbank Fault termination might in fact be north of Tram Road.

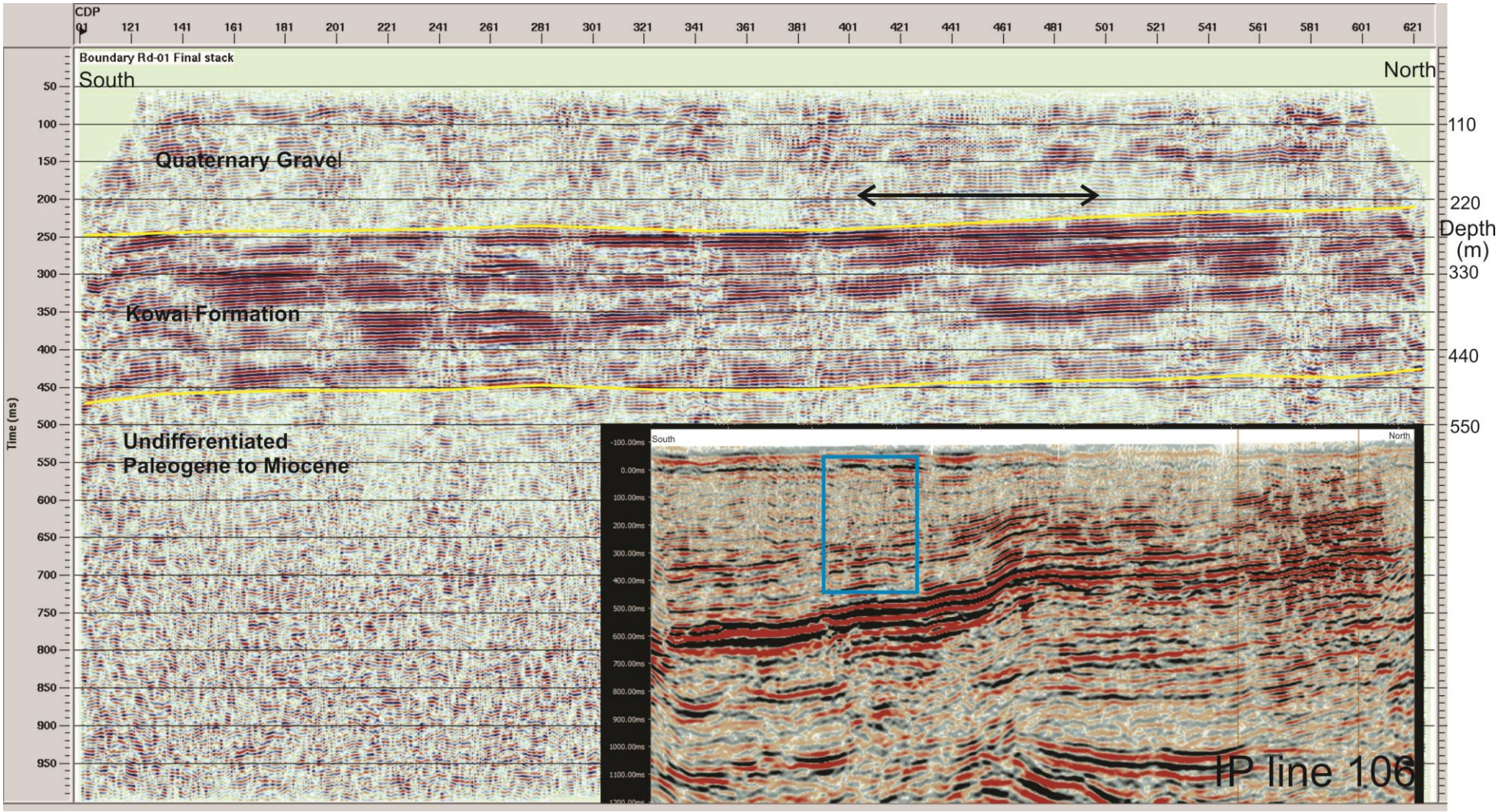

Figure A2.2. Interpretation of Chapmans Boundary Road shallow seismic reflection line. Main image indicates the strong reflectors most likely associated with the Kowai Formation gravels (between the yellow lines). The location of the scarp is within the area indicated by the black arrow. Inset: Indo-Pacific line 106 run along Earlys Road about 2.5 km west. The blue box indicates the approximate position and depth of the Chapmans Boundary line (main image) with respect to this industry line.